28

THE STRATIGRAPHY AND STRUCTURAL EVOLUTION OF THE LATE PROTEROZOIC GARIEP BELT IN THE SENDELINGSDRIF - ANNISFONTEIN AREA NORTHWESTERN CAPE PROVINCE

by

MARK WOLTER VON VEH

Thesis submitted in fulfilment of the requirements for the degree of Doctor of Philosophy in the Faculty of Science of the University of Cape Town

Department of Geology

1988

ABSTRACT

The Stratigraphy and Structural Evolution of the Late Proterozoic Gariep Belt in the Sendelingsdrif - Annisfontein Area, northwestern Cape Province

A geological investigation of the Port Nolloth metasediments in the central external parts of the Gariep Belt has led to a re-interpretation of their lithostratigraphy and Pan-African geotectonic evolution.

During the rifting stage of passive continental margin evolution, the basal clastic Stinkfontein Sequence was deposited in an alluvial fan environment. Fluviatile conglomerates and quartz arenites (Lekkersing Formation) interfinger with feldspathic arenites and minor volcanics (Vredefontein Formation), and prograde into marginal marine clastics and carbonates (Gumchavib Formation). Rift faulting produced local grabens into which mass-flow sediments (Kaigas Formation) and volcaniclastics (Rosh Pinah Formation) were shed. During the sea-floor spreading stage, a shallow-water carbonate-clastic unit, the Hilda Sequence, was deposited. Conglomerates, quartzites, and schists with resedimented gravity-flow characteristics (Wallekraal Formation) are sandwiched between lower and upper platform carbonates (Pickelhaube and Dabie River Formations). The Hilda is unconformably overlain by the Numees Sequence, consisting of a widespread glaciogenic diamictite (Sendelingsdrif Formation) and a near-basal banded iron formation (Jakkalsberg Formation). A deep-water clastic unit, the Holgat Sequence, was laid down during the early stage of the lower Nama transgression.

Several generations of deformational features formed during a single SE- to SSE-directed tectonic event. A transpressive phase, D_1, produced NNW-trending basement-involved thrust faults, mesoscopic ENE-facing F_1 folds, and a penetrative S_1 transposition foliation. A southward decrease in the wrench shear/thrust shear ratio is recorded by the structural fabrics and strain markers. The D_1 structures were coaxially refolded by non-cylindrical WSW-facing F_2 shear folds during a sinistral plane wrenching phase, D_2. A late left-lateral transtensive phase (D_3-D_5) coincided with the emplacement of the Kuboos-Swartbank plutons and produced westerly-cascading gravity folds and east-west to WNW-ESE trending tensional features.

The mineral parageneses and microtextures indicate that D_1 was accompanied by regional lower greenschist facies M_1 metamorphism, culminating in post-kinematic biotite porphyroblast growth. The later deformational phases are mostly associated with retrograde effects, although a local thermal metamorphic event, M_2, reached amphibolite facies conditions during the Kuboos pluton intrusion.

The stratigraphic, structural and metamorphic evidence is in agreement with a plate tectonic model involving the growth and oblique closure of a proto-Atlantic ocean. The southeastward obduction of the leading edge of a subduction complex onto the west facing margin of the Kalahari craton, prior to or during final closure of the intracrustal arm of the Damara Orogen, was followed by the continued SSE-ward migration of the uncollided part of the subduction zone parallel to the western margin of the craton.

TABLE OF CONTENTS

ABSTRACT		i
1 INTRODUCTION		1
1.1 Regional setting		1
	1.1.1 Port Nolloth Assemblage	3
	1.1.2 Marmora Terrane	3
	1.1.3 Geochronology	5
	1.1.4 Physiography of the field area	7
1.2 Previous research		8
1.3 Present study		9
1.4 Acknowledgements		11
2 STRATIGRAPHY		13
2.1 Introduction		13
2.2 Basement Complex		13
	2.2.1 Field relationships and lithologies	16
2.3 Stinkfontein Sequence		17
	2.3.1 Field relationships, distribution, and stratigraphy	17
	2.3.2 Lithology and petrography	26
	2.3.3 Depositional environment	31
2.4 Hilda Sequence		32
	2.4.1 Field relationships, distribution, and stratigraphy	33
	2.4.2 Lithology and petrography	39
	2.4.3 Depositional environment	41
2.5 Numees Sequence		42
	2.5.1 Field relationships, distribution, and stratigraphy	43
	2.5.2 Lithology and petrography	45
	2.5.3 Depositional environment	45
2.6 Holgat Sequence		46
	2.6.1 Field relationships, distribution, and stratigraphy	47
	2.6.2 Lithology and petrography	51
	2.6.3 Depositional environment	51

3 STRUCTURE 52

3.1 Introduction 52

3.1.1 Previous work 52
3.1.2 Research method 53

3.2 Geometrical analysis 53

3.2.1 Fabric elements 54
3.2.2 Structural domains 69

3.3 Kinematic analysis 93

3.3.1 Transpressive phase 93
3.3.2 Plane wrenching phase 105
3.3.3 Transtensive phase 108

4 METAMORPHISM 110

4.1 General aspects 110

4.2 The regional metamorphic event (M_1) 111

4.2.1 Mineral paragenesis 111
4.2.2 Temperatures 112
4.2.3 Pressures 112
4.2.4 Relationship to D_1 113

4.3 The contact metamorphic event (M_2) 114

4.3.1 Characterization 114
4.3.2 Timing 115

5 CONCLUSIONS 117

5.1 Geodynamic synthesis 117

5.1.1 Oceanic opening 118
5.1.2 Oceanic closure and collision 120

5.2 Summary 124

5.2.1 Stratigraphy 124
5.2.2 Structure 125
5.2.3 Metamorphism 127
5.2.4 Geodynamics 127

REFERENCES CITED 128

APPENDICES 144

I A computerized system for structural domain analysis 144

II A computerized system for finite strain analysis 164

PLATES 170

ANNEXURES

I Geological map of the western Richtersveld and environs

II Geological map of the northwestern Richtersveld

III Microfiches of software coding and structural orientation and location data

1 INTRODUCTION

1.1 Regional setting

The Gariep Belt is an arcuate north-south trending tectonic unit straddling the Orange River along the South Atlantic coast in the northwestern Cape Province of South Africa and in southern SWA/Namibia. It is considered to be a subprovince of the extensive Damara Orogenic Province, which formed during the Upper Proterozoic/Lower Palaeozoic Pan-African event (Clifford, 1967; Stowe et al., 1984; Fig. 1). The Gariep Belt links up with the southern subprovince of the Damara Belt in the Lüderitz area to the north (Kröner & Jackson, 1974), and strikes out to sea to the south, so that its link with the Saldania Belt of the southwestern Cape Province is buried beneath Mesozoic-Cenozoic continental shelf deposits.

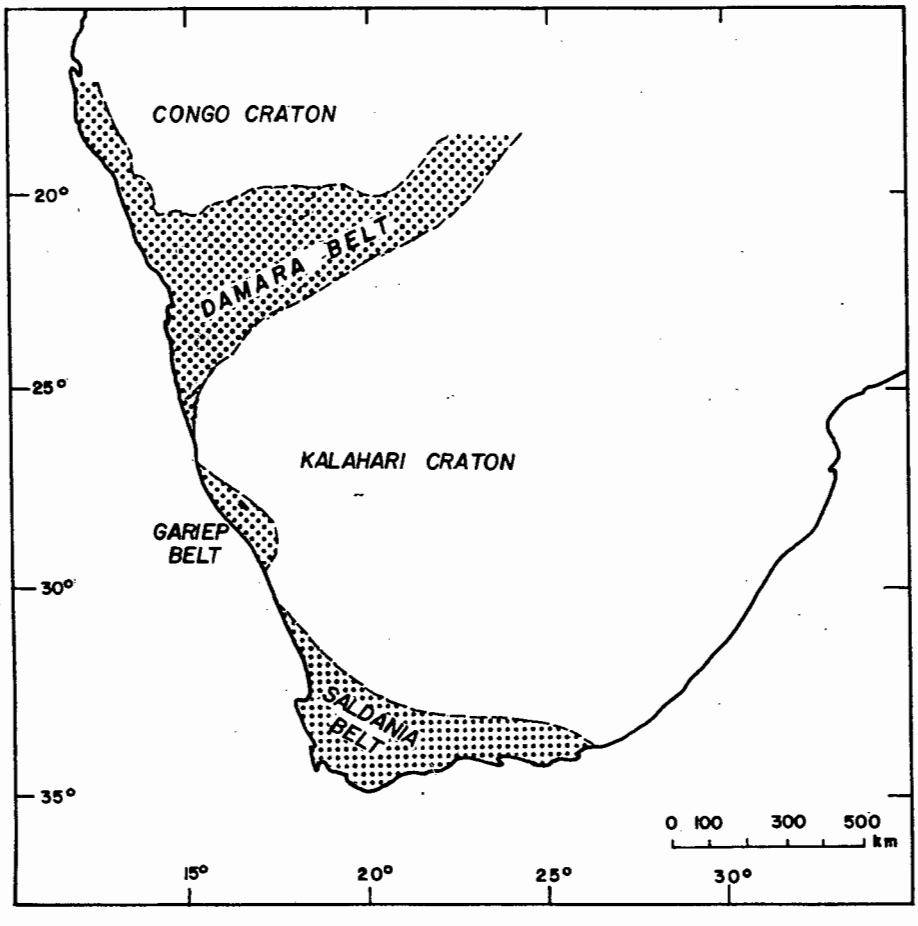

Fig. 1 : Generalized map of the Damara Orogenic Province.

It is bounded to the east by an eastward-tapering tectonic domain of low-grade supracrustal rocks, the Richtersveld Subprovince of the Namaqua Province. The Richtersveld Subprovince is made up of metavolcanics (De Hoop and Haib Subgroups) and metasediments (Rosyntjieberg Formation) of the early Proterozoic (Kibaran-age) Orange River Group (De Villiers & Söhnge, 1959; Ritter, 1978, 1980; Blignault, 1977; Reid, 1977). The Orange River Group was formerly known as "Kheis System", but was renamed to avoid an implied correlation with the Kheis sequence in the eastern parts of the Namaqua Province (Blignault, 1974). The metavolcanics are intruded on a large scale by the cogenetic ~1900-1730 Ma Vioolsdrif Granitoid Suite (Blignault, 1977; Reid, 1977, 1979, 1982). The Richtersveld Subprovince is bounded by complexly deformed suites of granites and gneisses of higher metamorphic grade belonging to the Bushmanland and Gordonia Subprovinces of the Namaqua Province.

The Gariep Belt cover rocks have in the past been described as a geosynclinal assemblage, the "Gariep Group", in which a distinction could be made between an eastern "miogeosyncline" and a western "eugeosyncline" (Martin, 1965; McMillan, 1968; Kröner, 1972, 1974, 1975), but it has recently been realized that this highly deformed suite is not a lithostratigraphic group in the formal sense so that new tectonostratigraphic nomenclature, such as "Gariep Complex" (South African Committee for Stratigraphy (SACS), 1980), "Gariep Arc" (Davies & Coward, 1982), and "Gariep Province" (Tankard et al., 1982) has appeared. A subdivision of the belt into an eastern "Port Nolloth Terrane" separated by a major tectonic discontinuity, the Schakalsberg fault, from a western "Marmora Terrane" (Fig. 2) was recognized (Stowe et al., 1984; Hartnady et al., 1985). The names of the terranes were derived from the "Port Nolloth Beds" (Rogers, 1915) between Port Nolloth and the Orange River, and the "Marmora Beds" of the Bogenfels area in southern SWA/Namibia (Martin, 1965). The term "terrane", defined by Beck et al. (1980) as "a fault-bounded entity characterized by a distinctive stratigraphic sequence and/or structural history differing markedly from its neighbours", has not been adopted here for the eastern unit as it is para-autochthonous in places. The term Port Nolloth Assemblage (PNA) is used in its place to refer to all the rocks lying between the Schakalsberg fault to the west, and the discontinuity at the base of the Gariep rocks to the east.

A clastic-carbonate deposit of Late Precambrian-Cambrian age, the Nama Group, is present in a foreland basin to the east. The Nama Group is divided from the base upwards into the Kuibis, Schwarzrand, and Fish River Subgroups (Germs, 1972, 1974). According to Martin (1965) and McMillan (1968), the Nama conformably overlies the PNA in the area west of Witputs in SWA/Namibia. Germs (1983) considers the Nama Group and the Gariep Belt to have been deposited during one major geotectonic cycle, with deposition of the upper Schwarzrand and Fish River Subgroups occurring during uplift associated with the Damaran orogeny.

A number of pre-, syn- and posttectonic intrusions occur in the Gariep Belt. The Richtersveld Igneous Suite, consisting of a large batholith and two smaller plutons of granite and leucogranite, and the Gannakouriep dykes, comprising a 100 km wide swarm of northeast-trending mafic and ultramafic dykes (De Villiers & Söhnge, 1959; Middlemost, 1964; Kröner & Blignault, 1976;

Reid, 1979a), are intrusive into the basement complex and basal cover rocks. Some syntectonic stocks, dykes and sills have been reported from the central internal parts of the Gariep Belt (Kaiser, 1926; De Villiers & Söhnge, 1959). The two southernmost plutons of a northeast-trending Kuboos-Bremen line of intrusives, the Swartbank and Kuboos plutons, intrude deformed cover rocks (Van Biljon, 1939; Söhnge & De Villiers, 1948). A late set of aplite, granite porphyry, basic and bostonite dykes of early Phanerozoic age cut the plutons (Kröner & Hawkesworth, 1977).

Superficial surface deposits of silcrete, calcrete, gravel and sand conceal some of the Gariep rocks to the west. A Tertiary to Recent age is indicated for them from the occurrence of marine fossils in the gravels south of Alexander Bay and from vertebrate fauna in the Arrisdrif gravels (Corvinus & Hendey, 1978; Hendey, 1978).

1.1.1 Port Nolloth Assemblage

The PNA forms an extensive NNW-SSE trending belt running from Kleinzee in the south to Lüderitz in the north. South of the Orange River, a thick variable succession of arenites, rudites, carbonates, diamictite, and minor volcanics is subdivided into the Stinkfontein, Hilda, Numees, and Holgat Sequences (Chap. 2). In SWA/Namibia, a lower sedimentary-volcanic and an upper volcaniclastic succession, the Rosh Pinah (or Kapok) Formation, underlies and interfingers with grits, quartzite, phyllite, diamictite, and dolomitic limestone of the Hilda Sequence in the restricted diamond area known as the Sperrgebiet (McMillan, 1968; Page & Watson, 1976; Page & Kindl, 1978). Numerous carbonate-rich outcrops of the Bogenfels Formation occur further to the north.

The PNA is deformed and tectonically dismembered by numerous thrust faults and folds, notable amongst which are the Klipneus-Black Hills fault, the Annisfontein-Gumchavib anticlinorium, and the Sendelingsdrif synclinorium (Fig. 2).

1.1.2 Marmora Terrane

The Marmora Terrane consists of two stratigraphic units in the Orange River region (SACS, 1980):

- The Grootderm Suite is composed mainly of metabasaltic "greenstone" belonging to the basalt family, but ranging from tholeiitic through to alkaline types (Smith & Hartnady, 1984). A pinkish dolomite with abundant cherty intercalations (the "Gais" dolomite) overlies the greenstone at a conformable or interfingering contact (Joubert et al., 1986). Kröner (1974, 1975, 1979) proposed that the metavolcanics originated as oceanic seamounts or

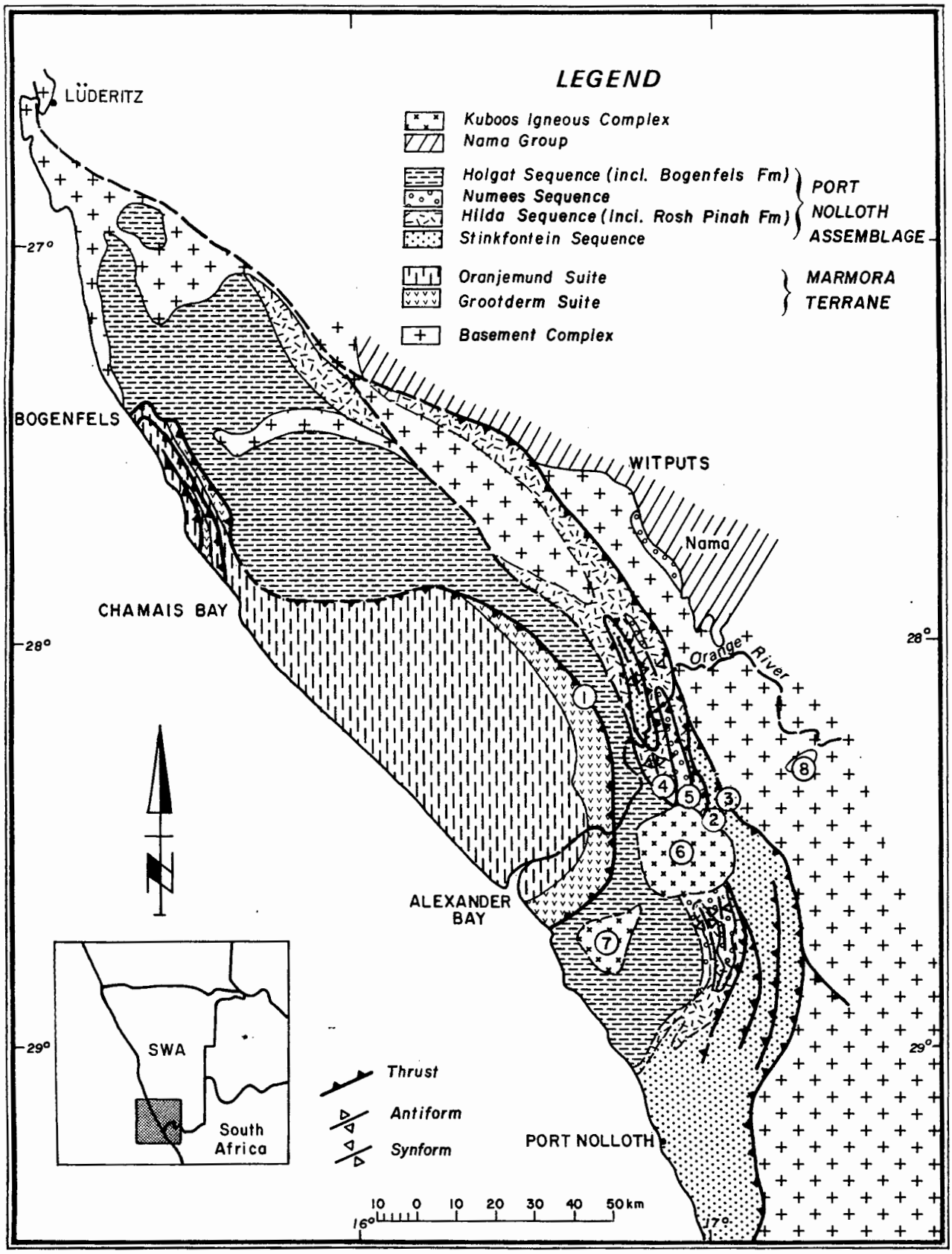

Fig. 2 : Simplified map of the general structure which defines the Gariep Belt (1) Schakalsberg fault; (2) Klipneus-Black Hills fault; (3) Vandersterrberg fault; (4) Annisfontein-Gumchavib anticlinorium; (5) Sendelingsdrif synclinorium; (6) Kuboos pluton; (7) Swartbank pluton; (8) Tatasberg plutons. Compiled from the maps of De Villiers & Söhnge (1959), Martin (1965), SACS (1980), Davies & Coward (1982), Tankard et al. (1982).

guyots, now incorporated in a relict subduction complex, and that the dolomitic carapace was an oceanic reef deposit capping the guyots. Geochemical work on the greenstones supported an intraplate oceanic ridge/ plateau or ocean island origin (Smith & Hartnady, op. cit.).

- The overlying Oranjemund Suite, made up of a suite of phyllites, schists and minor quartzite, is lithologically similar to the Holgat Sequence in the PNA. A greywacke with turbiditic characteristics is present around Alexander Bay.

The Grootderm and Oranjemund Suites are believed to correlate northwards with the metavolcanics and associated metasediments in the Chamais Bay area (Davies & Coward, 1982; Fig. 2). The latter rocks were formerly thought to unconformably underlie the Bogenfels Formation of the PNA (Kaiser, 1926; Knetch, 1937; Martin, 1965; SACS, 1980).

1.1.3 Geochronology

The Gannakouriep dyke swarm and the Richtersveld Igneous Suite give a lower age limit for the PNA. The dykes have yielded equivocal ages from 1200 Ma to 200 Ma ($^{40}Ar/^{39}Ar$; Reid, 1977; 1979), and often falling in the range 500-550 Ma (543±15 Ma in De Villiers, 1968; 542±4 Ma in Onstott et al., 1986). These late ages correspond in time to the Pan-African metamorphic overprint, so that the 878±41 Ma age obtained by Snelling (in De Villiers, 1968) is probably a closer reflection of the true age of many of the dykes. The two Richtersveld Suite granites in the basement gave a U-Pb zircon concordia intercept age of 920±10 Ma and a Rb-Sr whole-rock isochron of 911±39 Ma, while the intrusive Lekkersing granite yielded a U-Pb zircon age of 780±10 Ma (Allsopp et al., 1979). Burger & Coertze (1973) quoted an age of 920±30 Ma for the Richtersveld granites.

Allsopp and his coworkers noted the presence of xenoliths of quartzite and lava in the older Richtersveld intrusives that resemble the Stinkfontein lithologies, implying that the Stinkfontein may be older than ~920 Ma, but this is an unreliable indicator because the Orange River Group lithologies are quite similar to those in the Stinkfontein.

The 719±28 and 686±32 Ma Rb-Sr ages obtained by Welke (in De Villiers, 1968) and Allsopp et al. (1979) for the Rosh Pinah felsites may be primary ages, thereby placing some control on the age of the interfingering Hilda Sequence (Table 1). The Numees diamictite was deposited at around 670 Ma if its correlation with the widespread Varangian Glacial Episode is correct (Harland, 1983; Hambrey & Harland, 1985). The apparent absence of any fossils in the overlying beds suggests that PNA deposition ended during the early stages of the Vendian (750-570 Ma).

Table 1 : Summarized interpretation of the chronological evolution of the Gariep Belt.

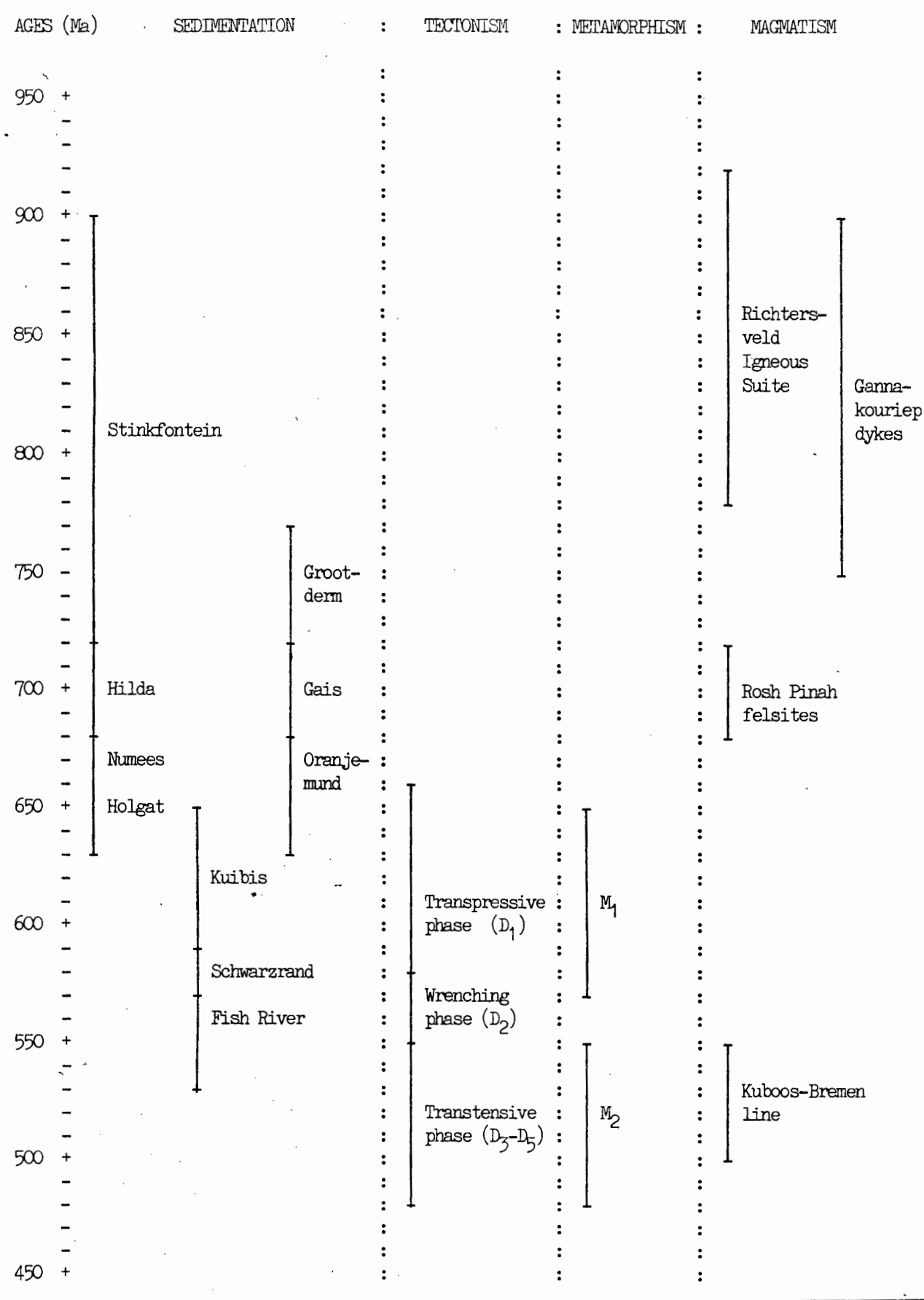

The uplift associated with the Pan-African tectonism is believed by Germs (1983) to have been responsible for the Late Vendian Nomtsas unconformity in the Nama basin, implying that the main phase of deformation (D_1) is "somewhat older than 570 m.y." (op. cit., p. 110). Detrital muscovite ages ranging from 670 to 570 Ma were determined from the upper Nama molasse by Horstmann (1987) and related to a metamorphic alteration event during the Damaran orogeny (M_1). Since the lower Nama contains representatives of an Ediacaran fauna of probable Vendian age (Germs, 1972, 1983; Germs et al., 1986), the main phase of deformation must already have been active during its deposition.

The late-tectonic Kuboos-Bremen line provides minimum ages for the deformation. The southwestern Kuboos pluton has been dated at 550±20 Ma (De Villiers & Burger, 1967) and 525±60 Ma (Allsopp et al., 1979). The post-Nama Bremen Suite further east has yielded ages of 506±10 and 518±15 Ma (Burger & Coertze, 1973; Allsopp et al., op. cit.).

The occurrence of a late thermal event (M_2) from ~ 550-480 Ma is indicated from age determinations cited by De Villiers (1968), Ahrendt et al. (1978), Onstott et al. (1986), and Horstmann (1987), amongst others. Ages of 495±30 Ma for Bogenfels shales in the Sperrgebiet area (Kröner & Welin, 1973), 501±19 Ma for the Rosh Pinah felsics and 481±20 Ma for the Numees shales (Allsopp et al., 1979), and 503±36 Ma for one of the "Rooilepel" bostonite intrusives in the Grootderm Suite (Kröner & Hawkesworth, 1977) have been ascertained.

1.1.4 Physiography of the field area

The present research project focussed on the central portions of the PNA in an area known loosely as the Richtersveld. Detailed field mapping was restricted to a well exposed and easily accessible ~750 km^2 tract of land between the Orange River and the Kuboos pluton within the rectangle bounded by longitudes 16° 45'E and 17° 05'E and latitudes 28° 05'S to 28° 30'S. Some reconnaissance work was done further afield to reconcile the current work with that of previous research.

The area is mostly a dissected desert mountain land, forming an escarpment which drops rapidly in elevation westward towards a coastal plain. The elevation varies from a maximum of 1365 m at Vandersterrberg in the east to less than 20 m at Arrisdrif in the west.

Road access has improved greatly in recent years. The gravel roads leading from Alexander Bay to the alluvial diamond diggings at Arrisdrif, Bloeddrif and Reuning (formerly known as Octha) are regularly maintained. Many of the local nomadic Nama inhabitants now have motorized transport so that a criss-crossing network of passable tracks for sturdy vehicles is in existence and four-wheel drive capability is rarely required. The availability of water has also improved with the drilling of numerous boreholes to furnish supplies for their livestock: the Orange River has a perennial flow but surface water is

otherwise scarce.

The area hosts an extraordinary diversity of flora and fauna which is being placed under increasing pressure from livestock overgrazing and human land usage. Proclamation of the Richtersveld as a nature and recreational reserve was recommended by the S.A. Working Group of the International Biological Programme in 1972 and is currently under consideration by the National Parks Board of Trustees (Botha, 1986).

1.2 Previous research

Geological interest in the western Richtersveld dates back to the 19th century when a number of prospecting expeditions were undertaken in search of rumoured rich mineral deposits (Alexander, 1838; Wyley, 1857; Dunn, 1872). In 1913 Dr. A.W. Rogers made a reconnaissance survey of the area and was able to establish an account of the stratigraphic succession (Rogers, 1915). His report dispelled the rumours of mineral wealth. Interest in its economic potential was renewed with the outbreak of the 2nd World War. During the years 1943-1945, Drs. J. de Villiers and P.G. Söhnge of the Geological Survey mapped a major portion of the western Richtersveld and wrote a comprehensive report on its geology (De Villiers & Söhnge, 1959). In a preface to this report, Dr. F.C. Truter commented that their work had substantiated that "the region does not offer immediate economic prospects", but that "it is of considerable importance from the purely geological point of view" (op. cit., p. iii).

Since the Precambrian Research Unit (PRU) was established at the University of Cape Town in 1963 for the specific purpose of advancing knowledge of crustal evolution in the southwestern part of the African continent (Martin, 1965), it is to be expected that much academically motivated attention would have been directed within it towards the study of the Gariep Belt. Prof. H. Martin, founding Director of the PRU, published a synthesis and summary of the Gariep geology in 1965 (op. cit., p. 71-83). Dr. M. McMillan was compiling a map and report on the Witputs-Sendelingsdrif area at the time (McMillan, 1968). The geology of the western Richtersveld and adjacent coastal geology were revised by Dr. A. Kröner in 1969-1970 (Kröner, 1974, 1975) and a number of papers on particular aspects were published (Kröner & Germs, 1971; Kröner & Rankama, 1972; Kröner, 1972, 1977, 1977a; Kröner & Welin, 1973; Kröner & Jackson, 1974; Kröner & Blignault, 1976; Kröner & Hawkesworth, 1977; Kröner et al., 1980). Work on Gariep-basement contact relationships and metamorphic overprinting effects was undertaken by Drs. U. Ritter and H.F. Theart in the eastern and southern Richtersveld respectively (Ritter, 1978, 1980; Theart, 1980). The geochemistry of the Grootderm volcanics was analysed by Smith & Hartnady (1984). The far southwestern Sperrgebiet north of the Orange River, officially known as Diamond Area 1, was mapped by Dr. C.J.H. Hartnady for the purposes of compiling a 1:250000 scale geological map of the Alexander Bay Sheet (sheet 2816) for the Geological Survey. A final compilation with a report was

recently completed (Joubert et al., 1986). Two associates of the PRU, Dr. A. E. Shimron of the Israel Geological Survey, and Mr. P. Booth of the University of Port Elizabeth are presently involved in studies of the basement geology immediately adjacent to the Gariep Belt.

Excursions were organized by the PRU through the area following the July 1984 conference on Middle to Late Proterozoic Lithosphere Evolution held in celebration of its 21st anniversary (Hartnady et al., 1984), and the Alex L. Du Toit Golden Jubilee Conference on Tectonostratigraphic Terrane Analysis in October 1987 (Von Veh, 1987).

1.3 Present study

Although the previous research workers established a regional geological framework for the Gariep Belt, the large areas that needed to be covered precluded detailed sedimentological and structural investigations. There has been a growing awareness in recent years of the importance of overthrusting in its structural development and the possible implications for assumed stratigraphic relationships (Joubert & Kröner, 1972; Theart, 1980; Davies & Coward, 1982). A re-examination of a small, critical area, using a conventional stratigraphic investigation complemented by a detailed structural analyses is thus warranted. Many recent advances have been made in interpreting thrust-and-fold belts (e.g. Dahlström, 1969; Boyer & Elliott, 1982, Elliott, 1976, Elliott & Johnson, 1980; Butler, 1982, 1985; Butler & Coward, 1984; Price, 1981, 1986; Suppe, 1983) and modern computing developments have greatly simplified the task of employing a "geometrical approach" to structural analysis.

The Sendelingsdrif-Annisfontein area was an obvious choice as a study area because it is well-exposed and had not as yet been mapped in detail, whereas the geology of the adjacent Namibian outcrops was reasonably well understood from the mapping of McMillan (1968) and Iscor geologists from the Rosh Pinah Pb-Zn-Cu mine (Page & Watson, 1976; Page & Kindl, 1978; Van Vuuren, 1986). Indications that the area had been tectonically disrupted by thrust faulting and nappe formation came from the disparity in thickness between the relatively undeformed PNA beds underlying the Nama beds east of Witputs (McMillan, 1968) and those in the study area, the lateral and vertical interleaving of lithofacies (De Villiers & Söhnge, 1959; Kröner, 1974), and the reports of extensive thrust faults in the Rosh Pinah area (Davies and Coward, 1982).

The objectives that the study attempts to address are manifold:

(i) to resolve stratigraphic relationships from field mapping and structural studies - What are the major stratigraphic units and what are their unifying lithological features? Are lower rank lithofacies present? What are the

boundary relationships between units? Can tectonic repetition or alternatively "loss-of-ground" be recognized?

(ii) to interpret the palaeo-environments of units from their compositional make-up and bedding plane and internal sedimentary structures;

(iii) to characterize the physical and geometrical properties of structural elements - Can a sequence of tectonic styles related to distinct phases of deformation be recognized? In what respects do structures in the study area differ from those of adjacent areas? To what extent has the subjacent basement been affected by the Pan-African deformation?

(iv) to build up a picture of the mesoscopic structure of the study area from an analysis of domains that are homogeneous with respect to fabric elements;

(v) to reconstruct the kinematic history - What are the transport vectors as deduced from the orientations of fabric elements? Can the translations associated with the major thrusts be quantified? What internal strains are recorded in deformed markers and what is the regional palaeo-strain pattern?

(vi) to place constraints on metamorphic grades and timing of metamorphism - How many metamorphic events are recorded and what are the associated mineral assemblages? What is the microtextural relationship of metamorphic minerals to deformational fabrics?

(vii) to develop a geodynamic model for the evolution of the PNA that is consistent with the sedimentological, structural and metamorphic evidence.

The computing facilities available to research workers in the PRU at the beginning of this study were in need of upgrading to effectively undertake a geometrical and kinematic analysis (c f. Hartnady, 1978a). As a result, a major task of this project was to design and implement a comprehensive graphics-based structural and strain analysis software package for which much of the methodology was already available (e.g. Whitten, 1969, 1981). Certain programming standards as defined in the initial prospectus for such a package (Hartnady, 1978a, 1983) were met: the programs have a high degree of portability or "device-independence", they are "user-friendly" and can be operated with minimal preparatory training, and the principles of structured programming are adhered to. The emphasis in the software development was placed on the formal design and implementation of system components that would:

(i) enable structural orientation and location data of structurally homogeneous domains to be processed and displayed;

(ii) allow for the rapid determination of finite strains from deformed elliptical objects.

The field mapping was undertaken over a 12 month period during the 1983-1985 winter months. Mapping was done on plastic overlays on 1:36 000 aerial photographs (Job 525, Trigonometric Survey, Cape Town). Use was made of 1:6 000 magnifications in complex areas. Field information was transferred manually onto the official 1:50 000 topographical sheets supplied by the Trigonometrical Survey of South Africa (sheets 2816BB Sendelingsdrif, 2816BD Khubus, and 2817AC Vandersterrberg).

Annexure I is a regional 1:150 000 scale map of the Gariep Belt from latitudes 16° 30'E to 17° 15'E and from longitudes 27° 55'S to 29°S, compiled using the field maps, reconnaissance mapping of adjacent areas, and the maps of previous workers. (Much geological detail was omitted from this map as it can be found on the official map of the Richtersveld, sheets 256 and 257, published by the Geological Survey of South Africa in 1958.) Annexure II is a detailed 1:50 000 geological map of the Sendelingsdrif-Annisfontein area.

Structural orientation data readings were measured with a Zeiss COCLA compass. The orientation data is presented in the text as strike and dip for planar data and trend and plunge for linear data. The right-hand convention is used throughout. Trend azimuth refers to the down-plunge direction and all readings are relative to true north. The magnetic declination for the western Richtersveld is presently about 22° west of true north. The fabric elements are plotted on equal area lower hemisphere stereographic projections (Schmidt net). Planar fabrics are presented as π-diagrams. A listing of the structural data is presented in microfiche form in Annexure III. The geographical location of sample numbers cited in the ensuing text can be read from the locality data listing.

Appendices I and II contain descriptions of the developed computer software, the coding of which is also given in microfiche form in Annexure III. The listed programs are presently operational on an HP1000 microcomputer running under RTE-6/VM Real-Time Executive. The coding is written in a version of the FORTRAN language referred to as the "ANSI 77 standard". All graphics tasks are performed using the Hewlett Packard DGL (Device Independent Graphics) library.

1.4 Acknowledgements

I am greatly indebted to numerous individuals and organizations for providing the opportunity to undertake this study.

Sincere thanks are extended to Prof. P. Joubert, director of the PRU until his retirement in December 1986, for arranging financial support. Grants awarded by the Council for Scientific and Industrial Research (C.S.I.R) and the GENCOR Corporation are gratefully acknowledged. Shell Metals and Namex (Pty.) Ltd. allowed access into areas in which they hold prospecting options. The generous

hospitality of the management and staff of the Octha Diamond Mine was much appreciated during field trips.

Prof. C.J.H. Hartnady, the current director of the PRU, supervised the project since its inception in March, 1983. During his sabbatical leave from August 1985 to July 1986, Dr. A. E. Shimron acted in an unofficial capacity as supervisor. I owe a debt of gratitude to them both for their constructive guidance. Numerous field and petrological problems were also clarified by discussions with colleagues in the Department of Geology, particularly Drs. C. Stowe and D. Waters, and Messrs. R. Harris, C. Schlegel, and C. Hoffman. A PRU departmental technician, Mr. C. Steyl, kindly assisted in implementing the G/ASTRA software. The existence of the package is due to a large extent to the numerous research workers in several countries who freely provided source listings of their computer programs; in particular Prof. H.A.K. Charlesworth, and Drs. D.J. Gendzwill, M.R. Stauffer, G. Oertel and N.S. Mancktelow.

On the production side, I would like to thank Ms. R. Kovats and Ms. P. Eloff for their professional drafting of the figures in the text and the annexures, Mr. C. Basson who processed the photographic plates, and Messrs. H. Hendricks, R. Olivier, and D. Davids who prepared the thin sections.

Grateful thanks are also due to my wife, Anna, for her love, support, and companionship.

2 STRATIGRAPHY

2.1 Introduction

The Sendelingsdrif-Annisfontein area is underlain by a diverse assemblage of basement and cover sedimentary, metamorphic and igneous rocks, but the PNA metasediments are volumetrically the most important. Their stratigraphic classification has been a matter of much debate because of complications caused by faulting and folding and numerous schemes have been put forward (Table 2a, 2b).

A revision of the most recent formal classification scheme (SACS, 1980) was found to be necessary because of new data obtained during mapping. The chronological order of rock entities was found to be partly incorrect, and evidence for duplication of stratigraphy across thrust faults, in particular the Klipneus-Black Hills fault, was recognized. Many of the units designated as formations and members in the SACS publication consist of heterogeneous mixtures of rock types with few unifying lithological characteristics. By mapping at a more detailed scale it was possible to define the boundaries of smaller sub-units, so that the ranks of units needed to be raised.

A tectonostratigraphic terminology has been adopted, with the term "sequence" being used to define rock units bounded by major unconformities or faults (Table 2b). The geographic names of sequences have not been changed since they are firmly entrenched in the Gariep literature (in accordance with the recommendations of the South African Place Names Committee (SACS, 1977)), although they are for the most part inappropriate: the village of Stinkfontein has undergone a change of name to Eksteenfontein and the Hilda trigonometrical beacon and Numees copper prospect are not type area localities. Note also that the village of Kuboos is now referred to as Khubus (1:50 000 topographic sheet, 2816BD Khubus). Because of the complex history of correlations of the various lithostratigraphic units, consideration should be given in the future to a complete revision of the Gariep nomenclature.

2.2 Basement Complex

The basement rocks of the Richtersveld Subprovince have been described in detail by a number of research workers, including De Villiers & Söhnge (1959), Blignault (1974, 1977), Ritter (1978, 1980), Reid (1977, 1979), and are the subject of current investigations (Shimron, 1987; Booth, 1987). This section is therefore restricted to a few brief comments and observations about the units immediately underlying the PNA cover rocks.

Table 2a : Past and present classification schemes for the Gariep Belt (pre-1965; after Kröner, 1974; SACS, 1980).

Rogers (1915, 1929)	De Villiers & Söhnge (1959)	Haughton (1961, 1963)	Martin (1965)
			Kuboos Granite
	NAMA SYSTEM	NAMA SYSTEM	Numees Formation with Kaigas Substage (belonging to NAMA SYSTEM)
	Kuboos Igneous Complex		
Kuboos Granite	Numees Formation		Stinkfontein Formation
Grootderm Series	Kaigas Formation	Numees Formation	
			Grey gneiss, etc.
Numees Series	Stinkfontein Formation	Holgat Series	
~~ ~~~~ ~~~~ Western		Hilda-Kaigas Series GARIEP	Holgat Series GARIEP
? ? folded	Grey gneisses, etc.	Black Hills Series SYSTEM	Hilda Series SYSTEM
NAMA		Stinkfontein Series	Black Hills Series
Kaigas Series	Grootderm Series		Grootderm Series
	Holgat Series GARIEP SYSTEM		
Stinkfontein Series	Hilda Series		
	Black Hills Series		
Ancient gneisses	KHEIS SYSTEM	KHEIS SYSTEM (Grootderm Series?)	

Table 2b : Past and present classification schemes for the Gariep Belt (post-1965).

Kröner (1974)	SACS (1980), Tankard et al. (1982)		Von Veh (1987a, this work)	
	Miogeosynclinal facies	Eugeosynclinal facies	Port Nolloth Assemblage	Marmora Terrane
Kuboos Igneous Complex				
NAMA GROUP	NAMA GROUP		Kuboos-Bremen line Nama Group	
			Holgat Sequence	
Numees Formation	Numees Formation			
Helskloof Formation			Numees Sequence: Sendelingsdrif Formation	
Oranjemund Formation			Numees Sequence: Jakkalsberg Formation	
Hilda Formation = GARIEP	Hilda Suite	Holgat Suite	Hilda Sequence: Dabie River Formation	
Holgat Formation GROUP			Hilda Sequence: Wallekraal Formation	
			Hilda Sequence: Pickelhaube Formation	
Grootderm Formation		Oranjemund Suite		Oranjemund Suite
	Stinkfontein Formation	Grootderm Suite	Kaigas Formation	
Stinkfontein Formation			Stink-fontein Sequence: Gumchavib Formation	
			Stink-fontein Sequence: Vredefontein Formation	Grootderm Suite
Basement Complex			Stink-fontein Sequence: Lekkersing Formation	
			Basement Complex	

2.2.1 Field relationships and lithologies

2.2.1.1 De Hoop Subgroup

The De Hoop metavolcanics are exposed in northwest-trending belts to the east of Numeesberg and in the hanging-wall of the Klipneus fault. A Namaqua-age thrust fault duplicates the volcanics south of Numees Peak (Annexure II). Recent mapping in the Omsberge and Tswaies mountains has shown that the De Hoop volcanics unconformably underlie the quartzites of the Rosyntjieberg Formation, but that they are tectonically imbricated with them (Shimron, 1987).

The volcanics consist of a fine-grained grey feldspar-quartz-sericite schist, or less frequently a dark blue-green biotite-chlorite schist containing quartz and feldspar porphyroclasts. Positive identification of an extrusive origin for the schists was not possible because of their complete reconstitution, but original volcanic textures of acid to intermediate lavas, tuffs, and welded tuffs have been identified from less deformed exposures further to the east (Ritter, 1978, 1980; Blignault, 1977).

2.2.1.2 Rosyntjieberg Formation

Various stratigraphic subdivisions of the Rosyntjieberg quartzites have been made in the past. De Villiers & Söhnge (1959) described their Kaaien Series, as this sequence was previously known, as an alternation of cross-bedded and ripple-marked orthoquartzite interbedded with chloritic and ferruginous schist. Ritter (1980, p. 25) proposed a six-fold subdivision for a reference section along the Orange River on the basis of colour and stratification of the quartzites and interbedding of mafic volcanics. Shimron (1987) excluded the volcanics from the Rosyntjieberg Formation, and suggested a four-fold subdivision, consisting of a lower orthoquartzite, a ferruginous quartzite, a feldspathic quartzite and an upper orthoquartzite. This subdivision is readily apparent in traverses through the Rosyntjieberg beds of the Klipneus sheet.

The Rosyntjieberg quartzite is often poorly distinguishable from the Stinkfontein quartzite. A number of quartzites in the Khubusberge and Numeesberge were remapped as Stinkfontein on the basis of a paucity of iron-rich psammites and pelites, greater abundance of conglomerates, presence of iron-rich inclusions along laminations, and absence of pre-Gariepian structural fabrics. Subangular pebbles occur in both units, so that the rounding of pebbles is a poor discriminator between them. Pre-Gariepian tectonic fabrics are often difficult to recognize because of their sub-parallelism with the Pan-African trend along the contact (p. 54-55).

2.2.1.3 Vioolsdrif Suite

The Vioolsdrif granitoids (the grey gneissic granite of De Villiers & Söhnge, 1959) was shown by Blignault (1977) and Reid (1977, 1979b, 1982) to consist

of numerous intrusions of variable composition which have an order of emplacement from basic to acid. Only the intermediate to acid members, in the form of grey-brown medium-grained granodiorite or granite with occasional rounded mafic inclusions, are found in the northwestern Richtersveld. A thin-sectioned sample of a porphyritic granite from Mehlberg (locality 563) consisted of plagioclase (35 per cent), K-feldspar (microcline- microperthite; 31 per cent), quartz (29 per cent), and biotite (4 per cent), with secondary sericite and epidote, and accessory apatite, zircon, and opaques.

The contacts between the Vioolsdrif granitoids and the De Hoop volcanics are faulted and abrupt in the Klipneus sheet outcrops, but further north near Five Sisters the relationships are intrusive and the granitoids grade into a quartz-feldspar porphyry.

2.3 Stinkfontein Sequence

The Stinkfontein Sequence consists of a thick clastic unit at the base of the Gariep cover succession. Its age relationship to the other PNA beds was the subject of much debate in the older literature. De Villiers & Söhnge (1959) interpreted their Stinkfontein Formation as being entirely younger than a mixed sedimentary sequence, the Gariep System (Table 2a). This conclusion, which was based largely on a critical outcrop below the Hilda beacon in the southwestern Richtersveld, was refuted by most subsequent workers. Haughton (1961, 1963) pointed out that the Gannakouriep dykes intrude the Stinkfontein beds but not the Gariep System and that members of the Gariep System are absent in places where basement and Stinkfontein are in proximity to one another. A dolomitic sequence with the appearance of the overlying beds was found below the Stinkfontein in the area south of Eksteenfontein during the current work, but structural relationships showed that it occupies a higher stratigraphic position (see pp. 58-59). A basal tectonic breccia consisting of highly stretched angular gneissose and pegmatitic blocks in a mylonitic matrix locally resembles the overlying diamictites. Kröner (1974) showed that the tilloidal rock underlying the Stinkfontein at Hilda beacon has a chemical affinity with the basement granite-gneisses and schists.

2.3.1 Field relationships, distribution, and stratigraphy

The Stinkfontein was subdivided by Van Biljon (1939) into four members:

Vetberg quartzites and schists
Klein Dwarsberg quartzites
Gelykwerf grits, quartzites and thin conglomerates
Dwarsberg group of quartzites with alternating schists

Söhnge & De Villiers (1946) excluded the lowermost Dwarsberg member in the Rosyntjiebos Mountains (the Rosyntjieberg Formation) and proposed a four-fold subdivision based on the coarseness of the sediments:

Upper quartzites and sandstones
Upper conglomerates and grits
Lower quartzites and grits
Lower conglomerates and grits

This distinction was noted to be only practicable south of Fielding's Prospect in the central Richtersveld where the upper conglomerate is present. Joubert & Kröner (1972, p. 48) argued for repetition of the sequence by a strike fault and proposed a two-fold subdivision based on lithological differences:

Upper Stinkfontein Formation, consisting of red and brown-weathering feldspathic quartzites, arkoses, and minor volcanics
Lower Stinkfontein Formation, comprising grey and white flaggy quartzites underlain by boulder conglomerates in places.

Kröner (1974, p. 7) stated that this subdivision could not be applied successfully to the Stinkfontein Formation in the north and the proposal was intended as an informal one. Because the extent of the units are defined in the maps of De Villiers & Söhnge (1959) and Kröner (1974), the SACS publications (1977, 1980) gave them member status, naming them the Lekkersing and Vredefontein Members. They are referred to here as the Lekkersing and Vredefontein Formations in line with the upgrading of the ranks of units.

The Vredefontein was shown by Kröner to have an interbedded relationship with an overlying diamictite-dolomite unit, the Kaigas Member, at the Ione River northeast of Hilda beacon. De Villiers & Söhnge (1959) included the beds north of Annisfontein in their Kaigas Formation, but these were subsequently correlated with the Hilda (Martin, 1965; Kröner, 1974). The upper dolomite-phyllite unit west of the Kaigas River is lithologically indistinguishable from the Hilda dolomite in the hanging-wall of the Black Hills fault and should also be excluded from the Kaigas.

It will be argued below that the Kaigas Formation has a much more widespread distribution, consisting of all the diamictite-grit units immediately overlying the Lekkersing and Vredefontein Formations and the basement complex. The Numees Prospect diamictite and the diamictite in the immediate hanging-wall of the Klipneus-Black Hills fault are thus included in the Kaigas. As a result of this redefinition, the enigmatic multiple repetition of diamictite-dolomite of previous stratigraphic columns falls away and only one duplication remains. It is noteworthy that only two diamictite units are reported from the Khomas Belt of the Damara Orogen (the Varianto/Blaubeker

Formations at the top of the Nosib Group and the Chuos Formation in the Khomas Subgroup (Kröner & Rankama, 1972; Miller, 1983)) and from several other Upper Proterozoic "Varangian" deposits world-wide (Harland, 1983; Hambrey & Harland, 1985).

Although the upper Vredefontein beds resemble the Kaigas diamictite in places, and the contact in the Ione River is gradational (see Kröner, 1974, Fig. 4), the basal Kaigas contact is mostly unconformable. The contact east of Hilda beacon, which Kröner (1974, p. 18) claimed to be gradational, was found to be faulted. Fault imbrication is also at least partly responsible for the alternation of diamictite and quartzite in the Kook River valley.

A clastic unit in the core of the Annisfontein anticlinorium is recognized as a fourth formation of the Stinkfontein Sequence, the Gumchavib Formation. It is named after the beacon north of the Orange River where it has its maximum development.

For the purposes of description, the Stinkfontein outcrops along the eastern margin of the Gariep Belt are subdivided into the Nanoas, Khubusberge, Numeesberge, Numees Prospect, and Kodas beds, and the Gumchavib Formation south of the Orange River is referred to as the Daberas beds (Fig. 3).

2.3.1.1 Nanoas beds

The Nanoas beds thin progressively northwards from ~2500 m at Nanoas to ~1800 m at Helskloof Pass. The rugged Vandersterrberge to the east are underlain by the Lekkersing Formation, which undergoes a gradational sedimentary change upwards into the Vredefontein Formation. The areas underlain by the Vredefontein can be distinguished by a relatively more subdued relief, improved vegetation cover, darker outcrops and exfoliation weathering effects. An extensive andesitic lava band displaying sedimentary relationships with the bounding quartzites can be traced northwards from Nanoas to the Helskloof Pass, the Numees Prospect inlier, and into the Numeesberge.

2.3.1.2 Khubusberge beds

The Lekkersing and Vredefontein strata are duplicated in the hangingwall of the Klipneus fault between Swartberg and Khubus. A thin discontinuous sliver of the lava is also found here. The northward interfingering of these beds with Kaigas diamictite and Hilda schist appears to be of tectonic origin because of intense shearing in the area.

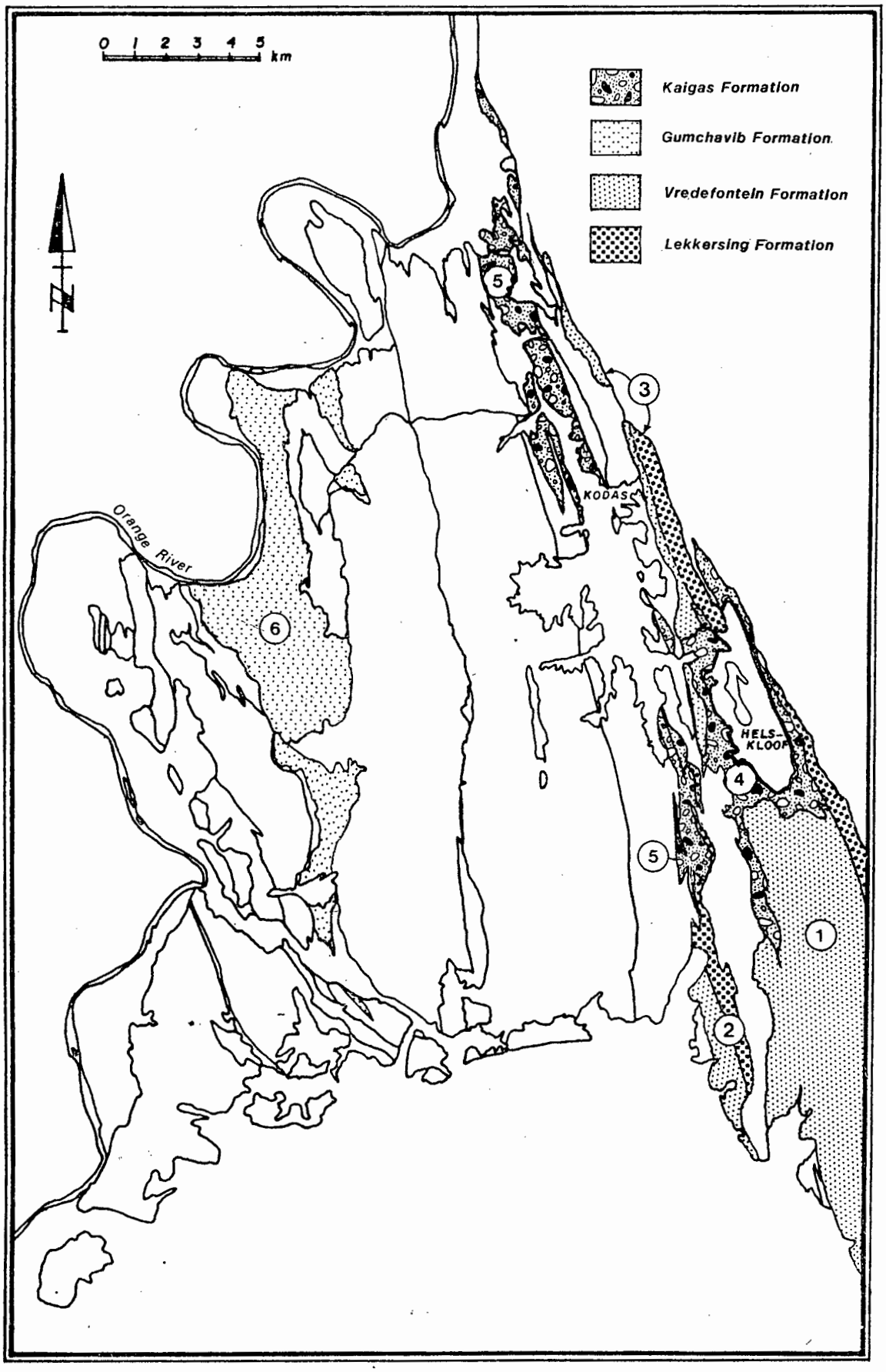

Fig. 3 : Distribution of the various formations in the Stinkfontein Sequence. (1) Nanoas beds, (2) Khubusberge beds, (3) Numeesberge beds, (4) Numees Prospect beds, (5) Kodas beds, (6) Daberas beds.

2.3.1.3 Numeesberge beds

The distinction between the Lekkersing and Vredefontein beds becomes poorer as the Stinkfontein thins out northwards. Two discontinuous bands of lava, volcanic breccia, and tuff are interbedded with the Stinkfontein in the up-faulted strip at the mouth of the Numees valley and in the Numeesberge. Thin strips of Stinkfontein conglomerate and quartzite were found along the northward continuation of the Klipneus fault and along the basement/cover contact near Mehlberg (Fig. 4).

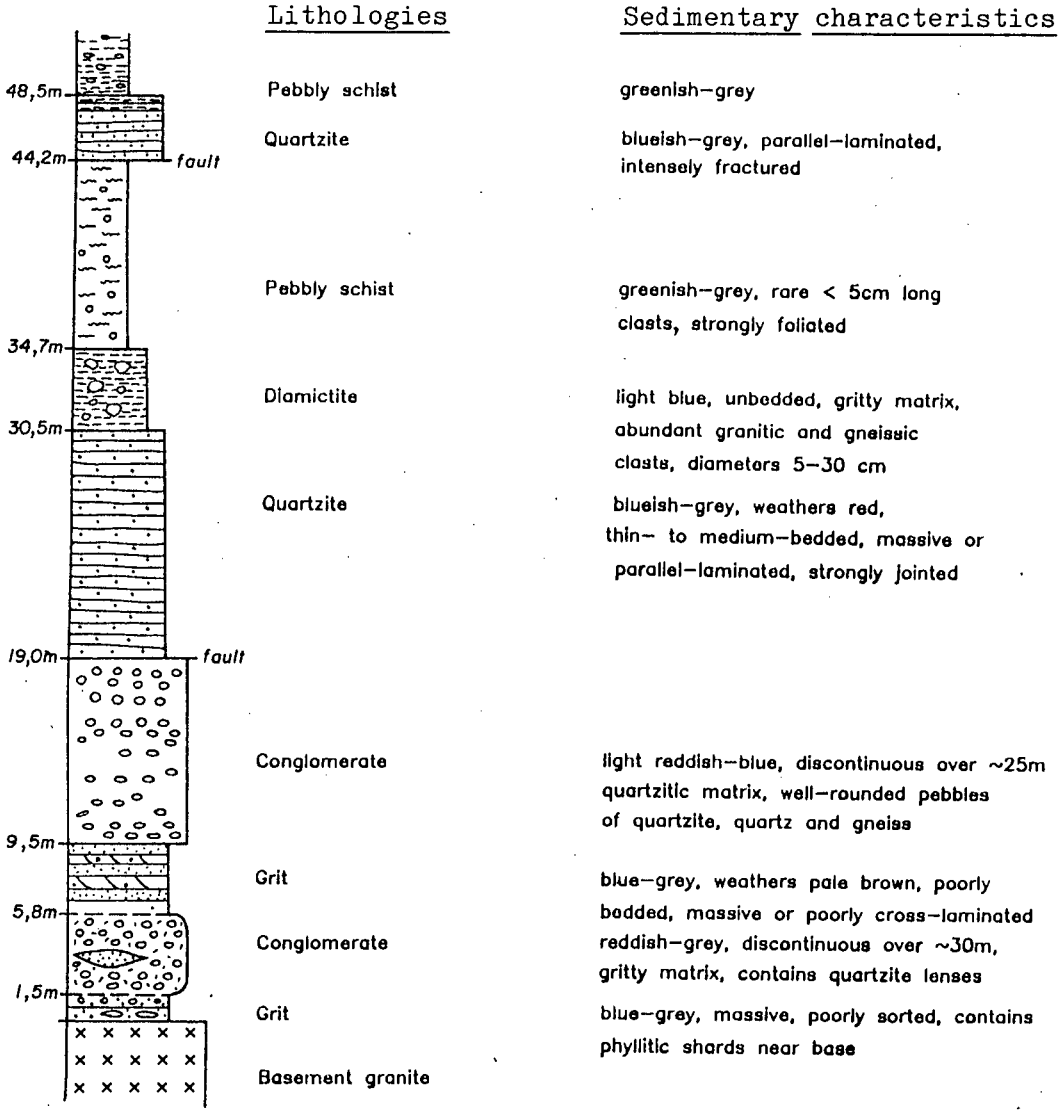

Fig. 4 : Section through the basal conglomerates at Grasvlakte (locality 475).

2.3.1.4 Numees Prospect beds

The stratigraphic position of the diamictite beds surrounding Numees Prospect has been a matter of contention amongst field workers because of their isolated occurrence and lithological similarity to other formations. Rogers (1915) distinguished between a lower "Numees Series" tillite and an upper "Kaigas Series" limestone. De Villiers & Söhnge (1959) assigned the entire sequence to the Numees Formation. They recognized a four-fold subdivision with all zones following conformably on each other:

Upper stage	Upper dolomite Arkoses, grits, etc. Lower dolomite
Lower stage	Tillite

Kröner (1974, p. 39,44) opted for the establishment of an independent "Helskloof Formation" of uncertain correlation, although he favoured a correlation with the main Numees Formation exposure in the Sendelingsdrif synclinorium. The placing of his Helskloof Formation in an intermediate position between the Hilda and Numees in the stratigraphic column on his map is contradictory however since he maintains that the Hilda passes conformably into the Numees. The proposal for a name change was rejected by the South African Commission for Stratigraphy (SACS, 1980, p. 441) and the beds were retained as the type area for the Numees Formation.

A correlation of the Numees Prospect diamictite with the Sendelingsdrif-Numees diamictite is considered to be incorrect for a number of reasons:

- Although both units have unconformable basal contacts (see Plates 1 and 2), the former beds rest on basement rocks and Stinkfontein quartzites, whereas the latter are everywhere underlain by Hilda sediments;
- The Numees Prospect diamictite is interbedded with grit, arenite and phyllite, while the Sendelingsdrif diamictite is largely unbedded and massive;
- The Numees Prospect beds do not contain a near-basal iron formation or ferruginous zone (the Jakkalsberg Formation);
- Carbonate erratics are conspicuously absent in the Numees Prospect diamictite, but are present in the Sendelingsdrif beds;
- The overlying beds do not resemble each other (pp. 37, 50).

A correlation with the Kaigas diamictite in the type area is favoured because:

- The two units lie along strike from each other in structurally similar positions in the footwall of the Klipneus-Black Hills fault;
- They are both laterally discontinuous;
- They rest unconformably on the Stinkfontein quartzites with the basal unconformity becoming progressively more discordant in a northerly direction;
- The type area diamictite is also interbedded with phyllite, greywacke and

grit. The stratigraphic similarities between these units become more readily evident if it is borne in mind that many of the thick quartzite units in the type area sequence are tectonically interleaved;
- The overlying beds have comparable lithologies (p. 37).

The Numees Prospect basin is bounded by major faults. The depositional floor is exposed as an even, smooth surface in a number of valleys in the area south and southeast of the Helskloof summit and in inliers in the Numees and Helskloof valleys. Thin slivers of diamictite are faulted against basement granite and the Stinkfontein Formation north and northwest of Numees Prospect and south of Mehlberg.

A ~117 m thick measured section in the Numees Prospect valley (Fig. 5) was found to consist of a lower diamictite unit (NP1), a middle phyllite-siltstone unit (NP2), and an upper diamictite unit (NP3). In the Helskloof Pass valley, NP1 is intercalated with greywackes and grits and NP3 pinches out. The southern and northern extensions of the basin consist predominantly of massive diamictite. A maximum thickness of ~280 m is attained in the northern extension.

2.3.1.5 Kodas beds

The diamictite and pebbly schist occurrences to the west of Numees Peak and west of Kodas Prospect were regarded by De Villiers & Söhnge (1959, p. 146) as a part of their Numees Formation, resting unconformably on and over-folding Hilda grits, conglomerates and schists, but Kröner (1974, p. 23) showed them to be underlying and interfingering with the Hilda strata. They are interpreted here as a duplication of the Kaigas Formation in the footwall of the Klipneus fault.

The ~1000 m thick Kodas beds intertongue with Hilda carbonates (the Five Sisters and Driegratberg dolomites) and extend northwards towards Rosh Pinah.

2.3.1.6 Daberas beds

The basal clastic unit in the Annisfontein anticlinorium is interpreted as part of the main Stinkfontein Sequence for a number of reasons:

- It is directly underlain by basement rock in the Obib mountains (Welke et al., 1979);
- It bears a lithological affinity to the Stinkfontein beds, consisting of a relatively monotonous sequence of massive or cross-bedded grits, arkoses and calcareous quartzites;
- The substantial thickness of the Stinkfontein Sequence suggests that it could extend for some distance in a basinward direction;
- The map of McMillan (1968) shows several north-south trending amphibolite dykes intruding this formation northeast of the Obib waterhole (Fig. 6). The dykes are possibly related to the Gannakouriep swarm which cuts the Stinkfontein, but is absent from younger rocks.

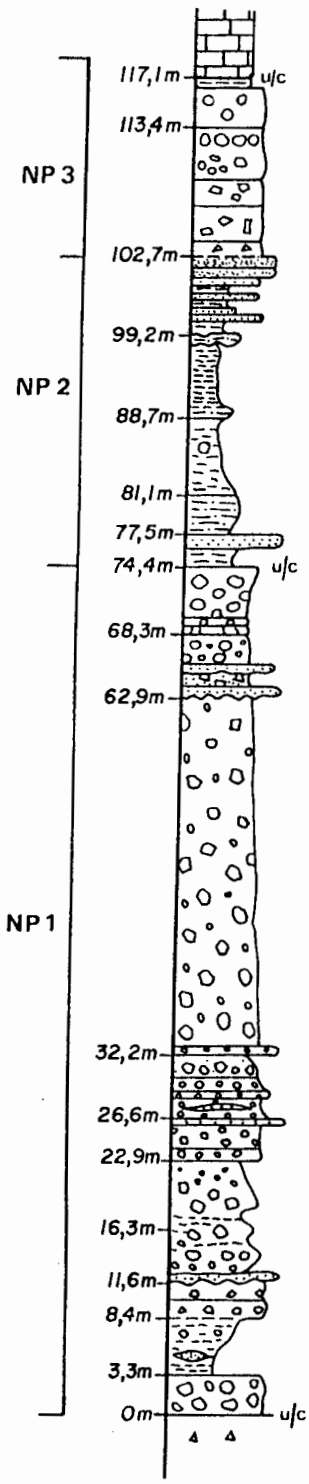

Lithologies	Sedimentary characteristics
Limestone	(Hilda)
Graphitic schist	Dark blue-grey; highly foliated and folded.
Pebbly schist	Blue-grey.
Diamictite	Blue-grey; sub-angular clasts; bimodal sizes; large (<2,5 m) clasts near top; forms cliff. Gradational contact.
Arenite	Ochre; medium-thick bedded; massive.
Phyllite/arenite	Olive-grey to ochre; thin-medium bedded;
Greywacke	very variable thicknesses; graded.
Phyllite	Strongly foliated; graded silty laminations.
Greywacke	Pale blue;planar-parallel laminated; isolated
Phyllite	70 cm granite boulder.
Greywacke	Grey-blue; thin-bedded, cross-laminated, graded.
Grit	Brown; Alt. thin grit/greywacke; sharp contacts.
Phyllite	Blue-grey;strongly foliated; upward coarsening; wavy-parallel laminated; forms ledge.
Diamictite	Blue-grey, weathers ochre; Large (<1 m) clasts near top.
Grit	Brown-grey; graded, diffuse lower contact.
Diamictite	Purple-grey, weathers ochre-red; massive; mostly small (<3 cm), sub-rounded granite and quartz clasts; Low clast/matrix ratio; muddy-silty matrix; forms steep slope.
Grit	Symmetrical grading;parallel-lamin. at contacts.
Pebbly schist	Small, rare clasts; load-casted arenite lenses.
Grit	Dark brown; discontinuous; load casts.
Diamictite	Brown-grey; bimodal clast sizes (1-5 cm and 20-30 cm); slope breaker.
Diamictite	Grey-purple; clasts upward fining; bimodal clast sizes; massive matrix; some silty inter-beds with flame structures.
Grit	
Pebbly schist	Grey-blue; gritty matrix; small, rare clasts.
Phyllite	Grey; parallel-wavy laminated; grit lenses; load casting and ripples.
Diamictite	Brown-grey; abundant, poorly sorted clasts.
Volcanics	(Stinkfontein)

Fig. 5 : Section through the Numees Prospect beds of the Kaigas Formation taken on the ridge immediately south of the prospect.

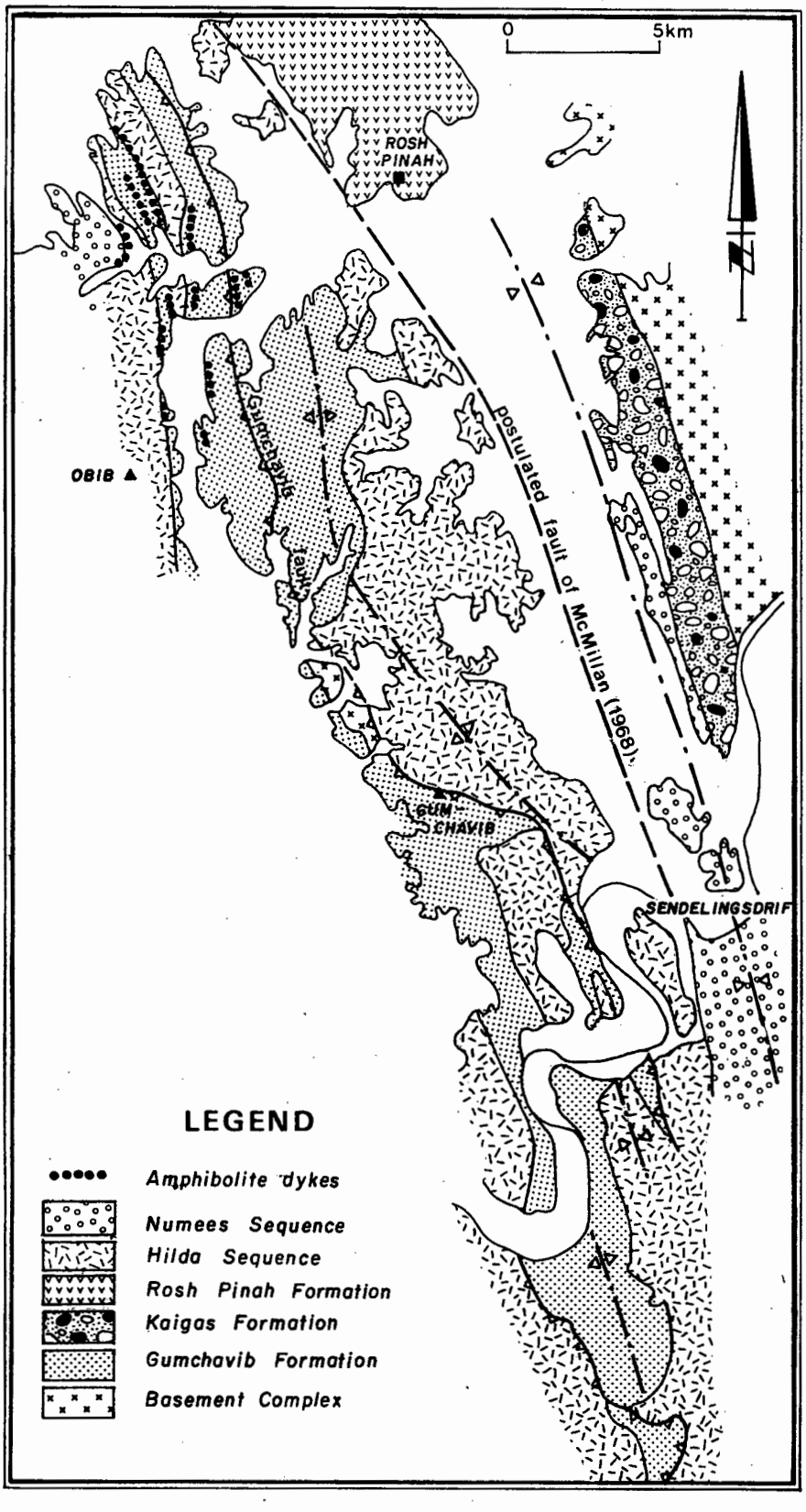

Fig. 6 : Simplified map of the relationship between lithological units north of the Orange River (after McMillan, 1968).

The relationship of the Daberas beds to the composite beds around Rosh Pinah (the Rosh Pinah Formation of SACS (1980)) is complicated by a lack of continuity but the structural evidence suggests that the former is older:

- The beds of the Gumchavib Formation occupy the cores of anticlines whereas the Rosh Pinah strata are located along strike from the Sendelingsdrif synclinorium. McMillan's (1968) map shows matching of dolomitic and volcanic stratigraphy across the extrapolated axis of the synclinorium north of Rosh Pinah (the NuCd1, G2G1 and KL1 units);

- an older age for the Gumchavib calcareous quartzite (McMillan's G2Qc2 unit) can be inferred from the fact that it is thrust over the Hilda strata by the Gumchavib fault, and the contact between the Rosh Pinah and Hilda strata is gradational (Davies & Coward, 1982). A gradational northward facies change from quartzite and feldspathic grit to dolostone-bearing arkose and pebbly schist is readily apparent in the Jakkalsberg area. There is no direct field evidence for McMillan's (1968) postulated fault extending from Trekpoort to Jakkalsberg which separates Hilda (his G2G1 unit) from Rosh Pinah strata (Fig. 6).

Field mapping by Dr. C.J.H. Hartnady (pers. commun., 1984) has indicated that the Gumchavib fault may be duplicating the Gumchavib Formation in the central Obib mountains so that McMillan's G2Qc2 unit is probably equivalent to his G2Qc1 unit.

South of the Orange River, the Daberas beds attain a thickness of ~260 m. The Annis fault exposes a ~70 m thick arcuate strip further south between the Gorab River and Anniskop.

2.3.2 Lithology and petrography

2.3.2.1 Lekkersing Formation

The bulk of the Lekkersing Formation is made up by a pale cream to blue-grey quartz arenite. The arenite is medium bedded (~5-40 cm) with sharp, straight bedding planes defined by partings. Erosional channels are frequent. Continuous to discontinuous, thin, straight-laminated beds alternate with planar cross-beds and massive beds. Isolated well-rounded granitoid pebbles up to 30 cm in length were found at one locality southwest of Numees Peak (locality 650). Widely dispersed palaeocurrent directions from the east or southeast are suggested from cross-bed foreset to bedding plane relationships. Occasional reversals in the cross-bedding inclination results from the presence of antidune structures.

The mineral constituents are quartz, feldspar and muscovite with accessory calcite, chlorite, biotite, zircon, apatite, and detrital and authigenic ore minerals (sample 388; Table 3). The grains range in size from ~0,1-0,5 mm with a median of ~0,15 mm, but polygonization has obscured the original sizes and shapes.

Table 3 : Estimated modal compositions of samples from the Lekkersing Formation.

Sample locality	quartz	plagio-clase	K-feldspar	white micas	biotite	opaques	others
388	80	3	7	6	<1	1	Ap,Zc,Ca,Chl
611	65	6	8	6	11	3	Ca,Zc,Chl
615	68	17	13	1	<1	<1	Sn,Ap,Chl
3002	70	4	7	17	<1	<1	Sn,Ap,Chl

Abbreviations are: Ap - apatite Ca - Calcite Chl - chlorite
Sn - sphene Zc - zircon

The arenite is sparsely intercalated with blue-grey or pale brown conglomerate, comprising subrounded to well rounded ellipsoidal pebbles in a quartzitic or gritty matrix. A few thin near-basal conglomerate lenses occur in the Numeesberg and behind the Octha terraces (Fig. 4), and conglomerates with angular to subangular pebbles outcrop at the base of the Paradys and Numees Peak exposures. Changes in pebble size and packing may define a crude horizontal stratification. The pebble assemblage consists of laminated orthoquartzite (~40 per cent), vein quartz and chert (~40 per cent), gneisses and granites (~15 per cent), and grit and schists (~5 per cent).

Pinkish-grey feldspathic grit becomes important in the upper parts of the formation. Bedding planes and internal structures are fairly indistinct in the grit, but a crude horizontal or tabular cross-lamination may be discernible. The constituent grains are made up of quartz, plagioclase (oligoclase-andesine), K-feldspar (microcline, perthite), muscovite, biotite, and rock fragments. The matrix consists of muscovite, sericite, quartz, feldspar, biotite, and opaque ores (samples 611, 615, 3002; Table 3). The grains are angular to subrounded and range in size from 0,4-3,0 mm.

2.3.2.2 Vredefontein Formation

The most abundant rock type in the Vredefontein is a blue-grey to reddish-brown, medium-bedded feldspathic arenite. Internal sedimentary structures are well preserved and accentuated by heavy mineral concentrations along laminations. Cross-bedding, of low angle wedge, tabular planar, or trough type, alternates with parallel-laminated bedding (Figs. 7a, 7b). Cross-bedding sets vary in thickness from ~5-20 cm and cosets attain thicknesses of up to several metres. Bedding plane structures are rare, apart from some small scale asymmetrical ripple marks with linguoid and cuspate crests. Bedding appears to be fairly continuous along strike with few crosscutting erosional structures.

Palaeocurrent directions are from the east or southeast. The parallel-laminated zones consist of medium to thick alternations of finer and coarser material with sharp to gradational transitions. Soft sedimentary deformation of internal structures takes the form of recumbent folds with a down-current direction of overturn near the tops of cross-sets, (Fig. 7c), oversteepened cross-laminae, convoluted laminae (Fig. 7d), disrupted and ripped-up clasts (Fig. 7e), and "flame" structures.

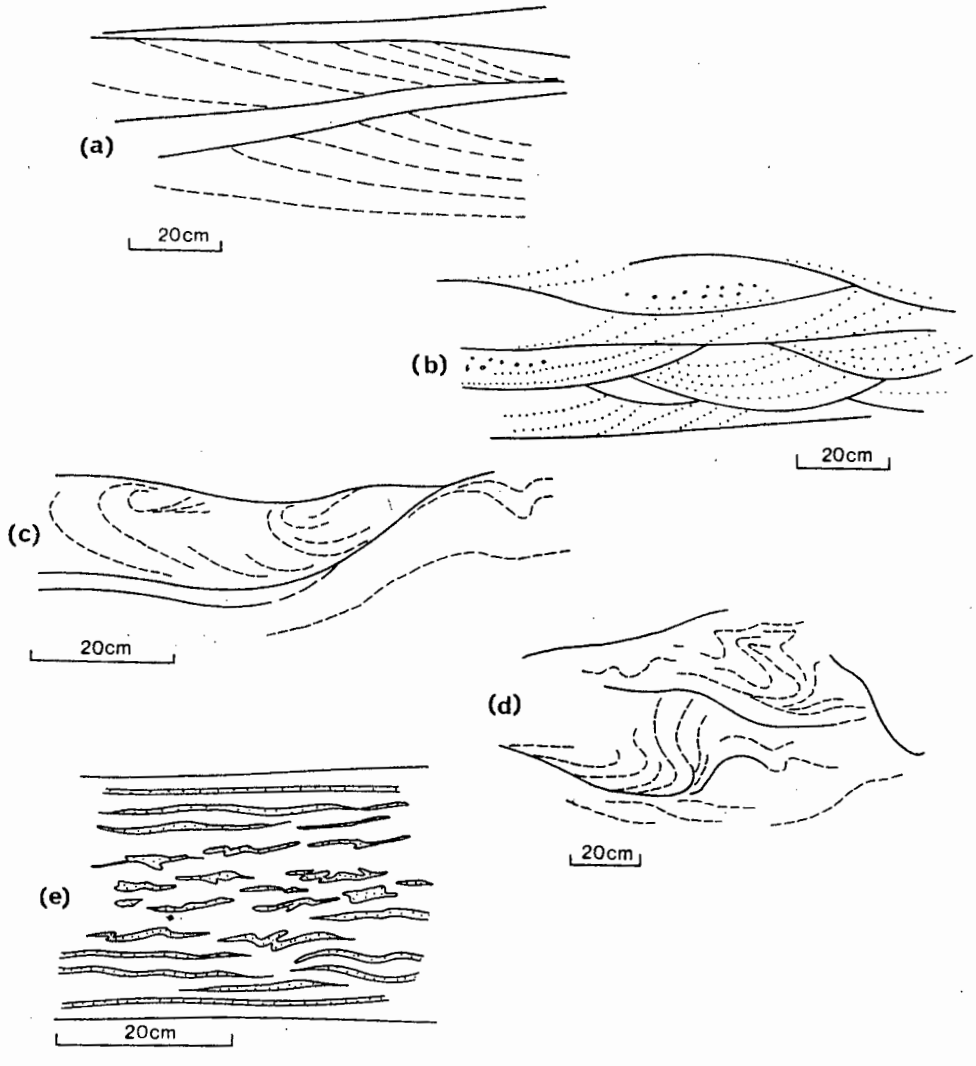

Fig. 7 : Field sketches of sedimentary structures in the Vredefontein beds.

The arenite consists of quartz, plagioclase, K-feldspar, muscovite, biotite, chlorite, opaques, and trace amounts of apatite, zircon, and epidote (Table 4). Grain sizes vary from 0,06-0,8 mm. The quartz grains are subangular and sutured and the feldspar grains are subrounded.

Table 4 : Estimated modal compositions of samples from the Vredefontein Formation.

Sample locality	quartz	plagio-clase	K-feldspar	white micas	biotite	opaques	others
306	73	13	6	5	<1	2	Ap, Zc, Ep
475	70	8	8	10	<1	1	Chl, Ap

Abbreviations are: Ap - apatite Chl - chlorite
Ep - epidote Zc - zircon.

The volcanics have been studied in depth by Rogers (1915, p. 85-86), De Villiers & Söhnge (1959, p. 121-124) and Middlemost (1966, p. 92-94) and are described as being mostly rhyolites and quartz latites with subordinate latites, trachytes, and andesites.

Sandy or gritty breccia, composed of angular to subrounded pebbles of vein quartz, granitoid, microgranite, gneiss, orthoquartzite, calcareous grit, and felsic volcanics, in a massive or indistinctly cross-bedded feldspathic grit matrix, occurs towards the top of the Vredefontein. The pebbles vary in size up to several centimetres and make up 30-45 per cent of the rock. In a weathered state the breccia may resemble the Kaigas diamictite.

2.3.2.3 Kaigas Formation

The diamictite consists of an association of subangular to subrounded pebbles, cobbles, and boulders of granite, gneiss, quartzite, vein-quartz, chert, and greenstone, in a blue-grey to ochre-buff mudstone or silty mudstone groundmass. The term "diamictite" (Flint et al., 1960) is used in preference to "mixtite", "pebbly schist", or "tilloid", as it well-established and non-committal as to clast or matrix grain size or genesis.

The rock has an unbedded massive appearance, but careful inspection of cliff faces reveals bedding planes defined by partings and mudstone interbeds at intervals of up to several metres. The thicknesses of the beds appear to be related to the sizes of the clasts which range in diameter from less than 1 mm to several metres, averaging ~10 cm. Tectonic effects have destroyed evidence for primary preferred orientations or sedimentary striations in the clasts. The matrix comprises variable proportions of angular quartz, K-feldspar, plagioclase, and interstitial micas, and is partly a pseudo-matrix formed by crushing and recrystallization of rock fragments (samples 556, 636, 657).

The diamictite is interdigitated with continuous, parallel-sided, pale brown to green-blue grit, quartzite, greywacke, and mudstone. The grit and

arenite are medium-bedded and massive, but normal, reverse, and symmetrical grading are also present. The greywacke exhibits a variety of turbiditic features including normal grading, ripple cross-laminations, rip-up clasts, load and flute casts, and sinuous ripple marks. The cross-laminations indicate palaeocurrent directions from the east or southeast. The mudstone is thin to medium-bedded, with a massive or straight-laminated internal structure.

2.3.2.4 Gumchavib Formation

The main rock-type of this formation is a light grey-brown or red-brown, coarse-grained feldspathic quartzite or arkose. The sedimentary structures are generally obliterated by a strong foliation, but medium bedding (~5-50 cm) with straight bedding planes is discernible from grading and compositional variations. Rare ripple-cross laminations and small-scale channels indicate a palaeocurrent direction from the southeast.

In thin-section, subrounded to rounded grains of quartz and feldspar with a diameter of 1,5 mm occur in a matrix made up of ~0,1-0,2 mm thick grains of quartz, feldspar, muscovite, biotite, and opaques (Table 5). The grains in the matrix are mostly angular and comprise 60-75 per cent of the rock. The textural inversion is partly a secondary feature caused by grain size reduction.

Table 5 : Approximate modal compositions of wackes from the Gumchavib Formation.

Sample locality	quartz	plagio-clase	K-feldspar	white micas	biotite	opaques	others
321	65	13	10	8	2	1	Ap, Chl
322	73	13	8	4	1	1	Ap, Zc, Chl, Ca

Abbreviations are: Ap - apatite, Ca - calcite, Chl - chlorite, Zc - zircon

Calcareous and feldspathic arenite and phyllite become interbedded to the north, and blue-grey dolomitic limestone is present towards the top of the sequence. A discontinuous ~1 m thick pebbly schist with angular banded gneiss and quartzite clasts in a gritty matrix outcrops near Xoboep Daberas (locality 311).

2.3.3 Depositional environment

The Stinkfontein sediments are widely regarded as having been deposited as an alluvial fan or as broad coalescing fans at the foot of an uplifted region to the east (Fig. 8; Middlemost, 1966; De Villiers & Söhnge, 1959; Tankard et al., 1982). The association of conglomerate and gravel interbeds, antidune structures, planar bedforms with horizontal laminae, and erosional channels in the Lekkersing is typical of the upper flow regime, which is present in sub-aerial or very shallow water environments. The coarse angular conglomerates near the base of the formation would initially have been dumped in the upper fan region, while stream flows in the mid-fan region deposited the more rounded and sorted conglomerates, gravels, and arenites.

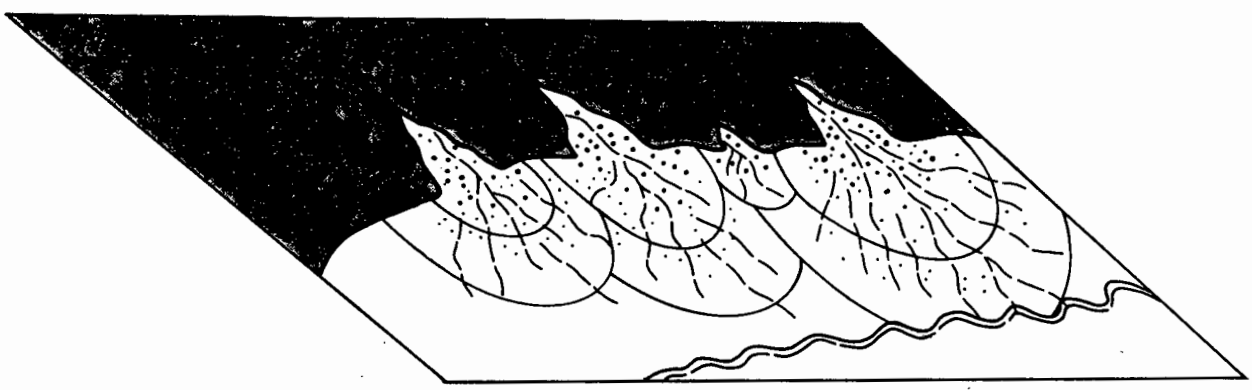

Fig. 8 : Schematic alluvial fan depositional model for the Stinkfontein Sequence.

A gradual change to more moderate flow conditions during Vredefontein deposition is inferred by the greater continuity of bedding, abundance of trough cross-bedding, decrease in matrix grain size and maturity, and poorer sorting. A distinction between a fluvial and a nearshore marine setting cannot readily be made since cross-bedding is common in both environments, although trough-cross stratification tends to be better developed in a fluvial environment (McKee, 1982, pp. 249-250). A continental environment is favoured by the absence of carbonates, paucity of fine-grained mudstone, and poor sorting. The penecontemporaneous deformational structures indicate unstable slopes with fairly rapid rates of deposition. Intermittent nearby volcanic activity covered the fan deposits with volcanic and volcaniclastic material. The decrease in sorting and coarsening of the sediments at higher stratigraphic levels points to a late transition from current-flow to mass-flow deposition.

The pinching out of the Lekkersing and Vredefontein beds in a northward direction appears to be a primary sedimentary feature related to a westward swing of the depositional basin and an increase in distance from the main depocentre. The volcanic bands are time markers that can be traced across the area from the Vredefontein into the Lekkersing zones, and show that deposition of the marginal Lekkersing beds in the north was synchronous with the more "distal" Vredefontein beds to the south. The poor development and small clast size of the conglomerate in comparison to the central Richtersveld is indicative of a northward decrease in relative proximality of the depositional basin.

The Kaigas diamictite in the type area and Numees Prospect was regarded by the early researchers as glacial deposits. De Villiers & Söhnge (1959, pp. 130, 149-154) interpreted the tillite as morainic debris interbedded with glacial outwash deposits. Kröner & Rankama (1972, p. 14) and Kröner (1974, pp. 16, 42-43) claimed that it lacked the characteristics of continental till, and suggested a glaciomarine, fluvial glacial, or even a fluvial origin on the basis of the partial stratification, roundness of clasts, and high proportion of fine-grained material. Evidence for some contribution by melt-out glacial debris comes from clasts that penetrate and deform underlying laminations (Kröner, 1974, p. 41), bimodal clast distributions, and outsized erratics in shaly beds.

A debris flow depositional mechanism can be inferred for most of the Kaigas beds from their limited geographic distribution, the sharp upper and lower bedding contacts, their massive internal structure, correlations between clast sizes and bedding thicknesses, and a rapid westward decrease in clast sizes. The intercalated grit, greywacke, and shale exhibit turbidity and bottom current depositional features. The presence of gravity flow deposits overlapping onto a basement foreland suggests a phase of marine transgression with rapid deposition of immature sediments into restricted basins. Fault scarp deposition is suggested by the normal fault relationships at Paradys and south of Numees Peak. Uplifted horsts along the margins of the basins may have been the sites of mountain glaciers which contributed some glacial material.

The absence of conglomerate, scarcity of cross-bedding, presence of thin bedding, and high carbonate-content of the Gumchavib arenites indicate quieter, submerged conditions such as can be expected in the distal parts of a fan complex. Some of the clastic beds may represent turbidites and minor debris flow deposits.

2.4 Hilda Sequence

The Stinkfontein Sequence is overlain by the Hilda Sequence, a mixed succession of limestone, dolomite, schist, quartzite, grit, and conglomerate. The first appearance of extensive carbonates marks a fundamental break in the PNA stratigraphy.

2.4.1 Field relationships, distribution, and stratigraphy

Despite the rapid lateral and vertical lithological variations, a three-fold subdivision into a lower carbonate unit, a mixed rudite-argillite unit, and an upper dolomite unit is readily apparent in the northern Richtersveld. These units will be referred to as the Pickelhaube, Wallekraal, and Dabie River Formations, after the localities where they are best developed.

The two diamictite levels that have been reported from within the Hilda (SACS, 1980, p. 441) are interpreted as correlatives of the underlying Kaigas and overlying Numees beds (Fig. 9). In the central Richtersveld, the lower diamictite (the Black Hills tillite of De Villiers & Söhnge, 1959, p. 49) is situated in the immediate hanging-wall of the Black-Hills-Klipneus thrust fault. A correlation with the Kaigas Formation is favoured by its location opposite the footwall occurrences, the comparable lithologies, and the sporadic presence of Stinkfontein quartzite at its base. The upper Billingham's diamictite is situated within Hilda schists, phyllites, and carbonates, but is assigned to the Numees Sequence because it contains a characteristic near-basal ferruginous quartzite and its upper contact is faulted. This poorly exposed thrust fault duplicates Stinkfontein quartzite and Hilda dolomite at the Holgat River (Annexure I).

In the northwestern Richtersveld, the lower Kodas diamictite is correlated with the Helskloof diamictite and assigned to the Kaigas Formation (p. 23). The upper Bloeddrif diamictite belongs to the Numees Sequence as it joins up with the main Sendelingsdrif-Numees diamictite around the nose of the Annisfontein anticlinorium (Annexure II). It is duplicated by faulting further to the west.

As a result of these reinterpretations, the Hilda Sequence is defined here to have a more limited distribution, consisting of four separate exposures (Fig. 10) :

(i) The Anniskop beds in the Annisfontein anticlinorium. Excluded from these beds are the basal arenites (a part of the Stinkfontein Sequence), the diamictite along its western limb (the Numees Sequence), and the upper dolomitic beds in the Sanddrif area (the Holgat Sequence);
(ii) The Khubus beds on the eastern limb of the Sendelingsdrif synclinorium. The underlying diamictites (the Kodas beds of the Kaigas Formation) are excluded from them;
(iii) The Helskloof Pass beds south of Numees Prospect; and
(iv) the Hakiesdoringhoek beds east of Khubus.

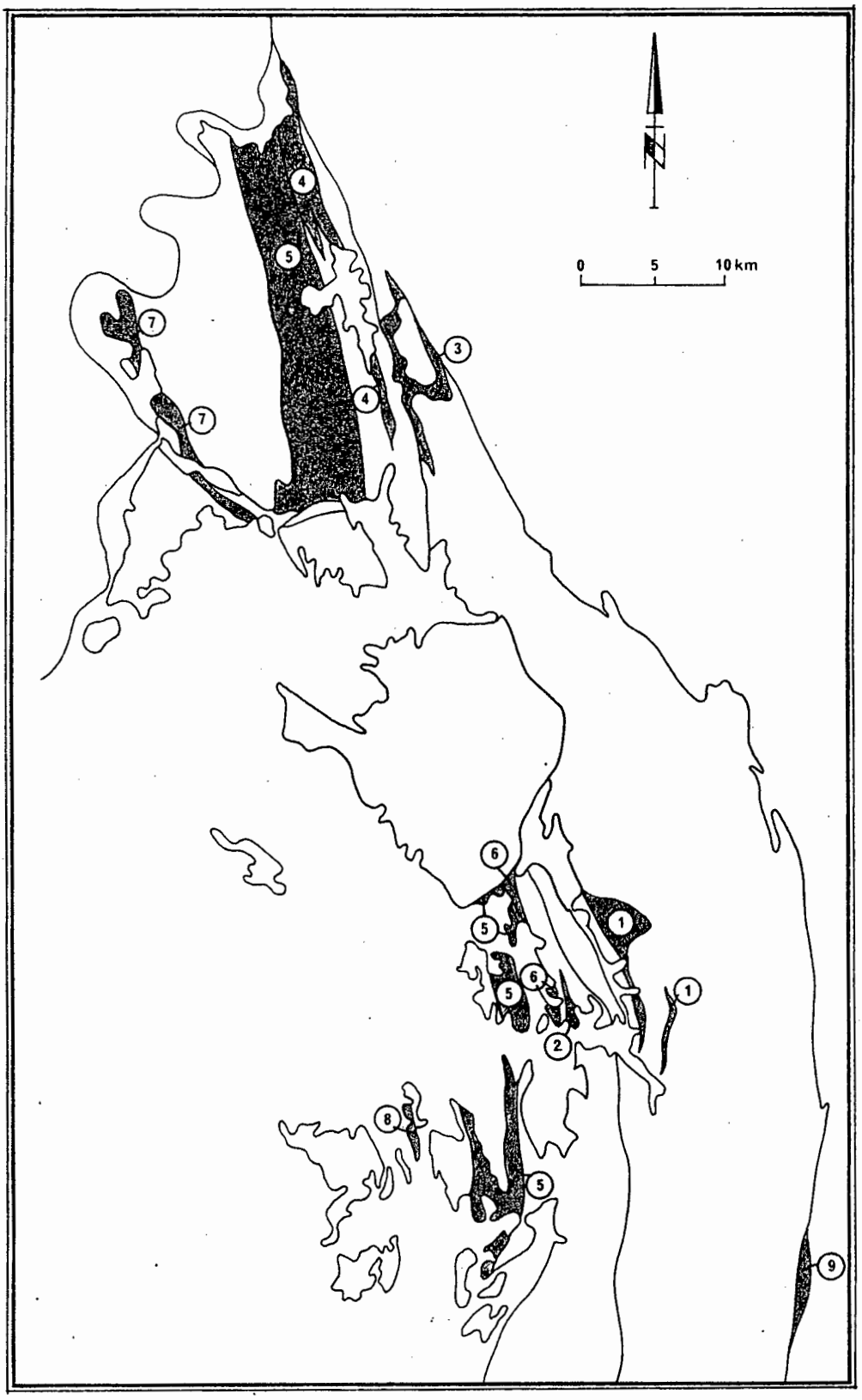

Fig. 9 : Distribution of the various diamictites. Included in the Kaigas Formation are: (1) Kaigas diamictite, (2) Black Hills diamictite, (3) Helskloof diamictite, and (4) Kodas diamictite. The Numees Sequence includes: (5) Sendelingsdrif-Hogsback diamictite, (6) Billingham's diamictite, (7) Bloeddrif diamictite, (8) Goms diamictite, and (9) Eksteenfontein diamictite.

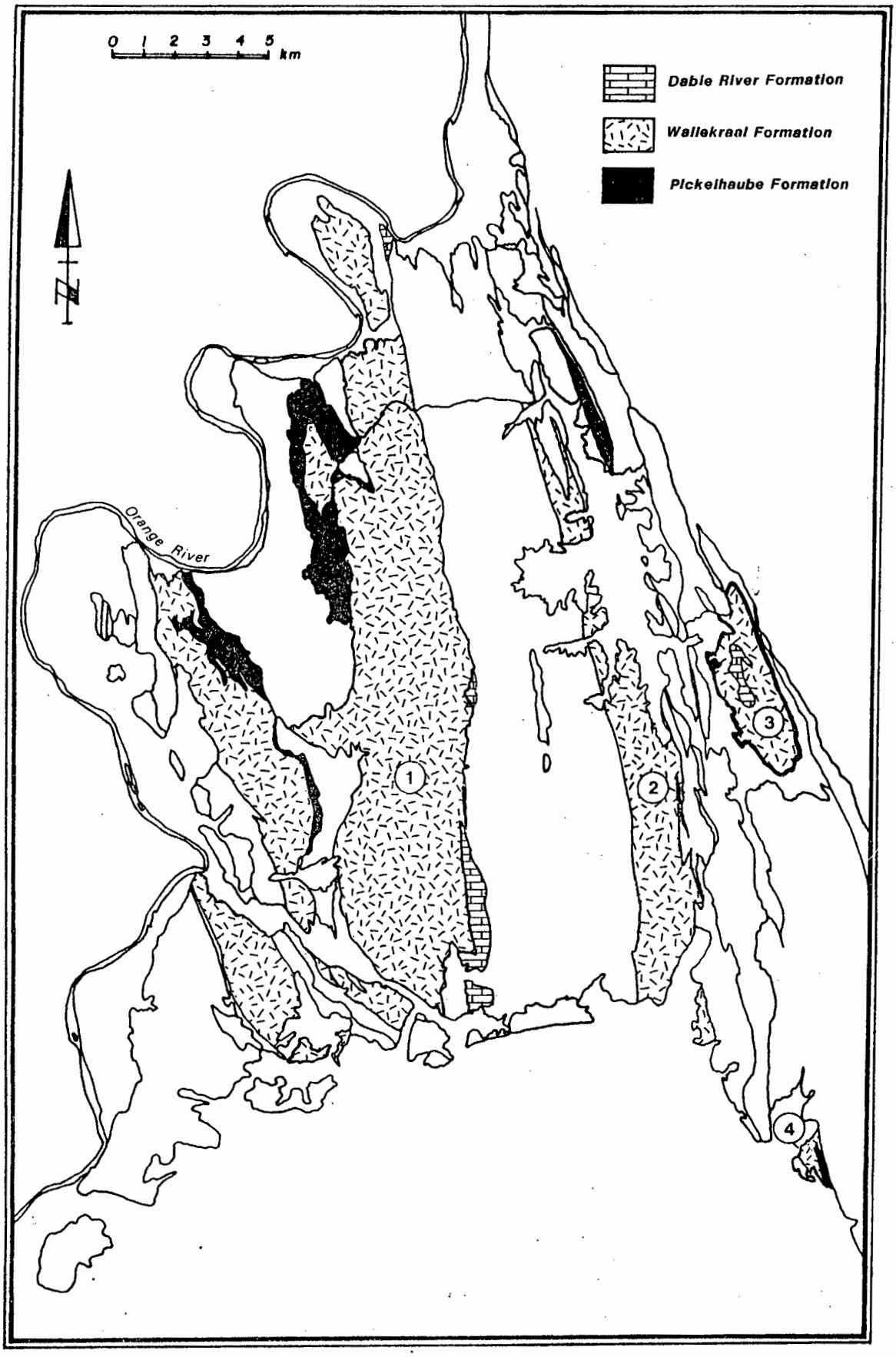

Fig. 10 : Distribution of the Hilda Sequence in the northwestern Richtersveld.
(1) Anniskop beds, (2) Khubus beds, (3) Helskloof Pass beds,
(4) Hakiesdoringhoek beds.

Outside the study area, a number of exposures are redefined as Hilda correlatives:

- The carbonates and schists in the Dolomite Peaks area. They were previously assigned to the upper Numees Formation, but were found to underlie the Hogsback-Numees diamictite. They occupy the cores of anticlinal structures and are surrounded by poorly developed basal ferruginous quartzite beds of the Numees Sequence;
- The "upper Kaigas" carbonate-phyllite beds in the footwall of the Black Hills fault in the Kaigas River valley; and
- Some schist, phyllite, and dolomite in a synclinal fold south of Eksteenfontein (pp. 58, 59).

2.4.1.1 Anniskop beds

In the Annisfontein anticlinorium, the dolomitic limestone beds of the Pickelhaube Formation rest conformably on and interfinger with the Gumchavib Formation arenite. The Pickelhaube Formation attains a thickness of ~90 m at Xoboep Daberas, but it thins rapidly southwards and is almost absent at the Gorab River closure.

The overlying Wallekraal Formation is made up of a ~1400 m thick sequence of arenite and rudite alternating with mica-schist and phyllite. Carbonates are poorly developed. Textural variations indicate a northerly source region. In the Jakkalsberg area, conglomerates and grits with numerous large embedded carbonate boulders intertongue with pebbly schists and diamictite. Further south, conglomerates are less abundant and the clast sizes and packing densities decrease. South of the Kuboos pluton, fine-grained schists and phyllites comprise the dominant rock type.

The Dabie River dolomite has an erratic distribution. Thin, fairly continuous lenses with transitional lower contacts occur along the western flank of the anticlinorium, in contrast to the eastern flank where discontinuous pods up to 320 m thick are found. Kröner (1974, p. 4) interpreted these extreme thickness variations and the interleaving with Numees beds west of the Nabab River in terms of contemporaneous biohermal reef deposition. A tectonic origin involving attenuation and thickening is preferred because of small-scale structural evidence for intense shearing along the basal contacts and because the Numees ferruginous quartzite also becomes interleaved with the dolomite just south of the Gorab River. In the hinge of the anticlinorium, the dolomite has been smeared out along the Hilda-Numees structural discontinuity, so that it appears as if the dolomite is resting unconformably on the Wallekraal beds and is conformably overlain by the Numees diamictite.

2.4.1.2 Khubus beds

In the eastern limb of the Sendelingsdrif synclinorium, the Pickelhaube Formation is represented by a thin marble to the east and northwest of Khubus. The Five Sisters dolomite which interfingers with the Kaigas diamictite at Kodas Prospect is a possible time equivalent of the Pickelhaube. The Wallekraal Formation contains several laterally discontinuous quartzite, grit, conglomerate, and dolomite zones of mappable thickness. The conglomerate zones undergo a gradational facies change into diamictite west of Kodas Prospect. The Dabie River Formation is not represented in these beds.

2.4.1.3 Helskloof Pass beds

A correlation of the upper Helskloof strata with the Hilda Sequence is supported by its three-fold subdivision into lower and upper dolomite units separated by a mixed arenite unit (Fig. 11).

The lower Pickelhaube dolomite (H1) progressively overlaps the underlying Helskloof-Kaigas diamictite eastwards until it is in contact with Lekkersing quartzite south of the track to the Gannakouriep prospects. The dolomite also outcrops for some distance along the Klipneus fault contact east of Rupping's Prospect. Thicknesses are very variable up to ~60 m.

The overlying grit and arkose differ in some respects from the Wallekraal lithologies in the type area, but this is not unexpected in view of the marked facies variations within the formation. At Numees Prospect, thick-bedded feldspathic arenites (H2) are overlain by a coarsening upward sequence of medium-bedded arkose with some thin interbedded shale and limestone (H3) and thick-bedded grits (H4).

The upper Dabie River dolomite (H5) comprises a ~40 m thick sequence of thin-bedded dolomitic limestone intercalated with calcareous grit and dolomite. The beds have undergone syn-sedimentary disruption into plastically deformed shards of variable size. Dolomites with a similar appearance, but which also contain granitic and gneissose clasts and interbedded graphitic schist, are found immediately below the Numees Sequence east of Billingham's Prospect.

2.4.1.4 Hakiesdoringhoek beds

A thick coarse-grained grey marble occurs to the southeast of Khubus and is overlain by a poorly exposed sequence of blue-grey schist and phyllite with interbedded graded arkose. The Klipneus fault has truncated these beds and thrust Rosyntjieberg and Stinkfontein quartzites over them.

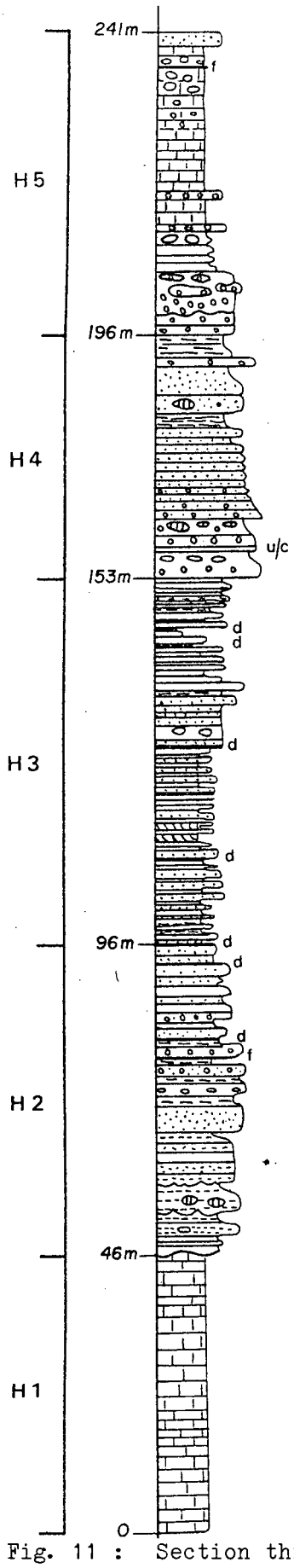

	Lithologies	Sedimentary characteristics
H5	Limestone, dolomite, feldspathic quartzite	Pale blue; brecciated and contorted bedding, alternating with straight-laminated beds. Some arkosic interbeds.
	Alternating calcareous grit limestone	Grey to blue-grey; Contorted and boudinaged grit layers; brecciated limestone shards.
H4	Grit, arkosic quartzite	Grey-blue; thick-bedded, massive or graded. Some dolomite and shale clasts.
H3	Arkosic quartzite, shale, dolomite	Light reddish-brown; medium-bedded; upward-coarsening; normal grading, small-scale dykes, shales parallel-laminated or cross-laminated, some ripple marks; dolomite markers.
H2	Arkosic grit, minor shale	Grey-blue, weathers ochre; grits thick-bedded and massive; discontinuous beds; wavy bedding planes, flame structures; shales contain wavy silty laminations, rarely contorted.
H1	Dolomitic limestone	Blue-grey to grey; straight laminated.

Fig. 11 : Section through the Hilda Sequence on the southeastern side of the Numees Prospect valley.

2.4.2 Lithology and petrography

2.4.2.1 Pickelhaube Formation

The Pickelhaube dolomitic limestone is a fine-grained blue-grey rock containing thin to medium straight laminations. Thin lenses of grey to reddish-brown arkose and grey-white phyllite are occasionally interbedded and quartz and calcite veins are abundant. The Five Sisters dolomite is partly oolitic. The Pickelhaube beds consist of calcite and dolomite with variable minor amounts (<10 per cent) of graphite, muscovite, biotite, quartz, and plagioclase (samples 323, 573, 620).

2.4.2.2 Wallekraal Formation

The Wallekraal conglomerate is composed of a variety of well-rounded boulders and pebbles in a light-coloured gritty or quartzitic groundmass. The larger-pebble varieties have thicker beds, greater lateral extent, and more clearly defined bedding planes. Bedding thicknesses range from ~20-60 cm. The beds are usually massive, but normal grading is locally observed. Clast rock types include vein-quartz (~45 per cent), gneissic granite and granodiorite (~23 per cent), quartzitic sandstone (~13 per cent), grit (~7 per cent), mica-schist and phyllite (~5 per cent), and dolomite (~2 per cent). The groundmass consists of quartz, feldspar, and mica grains and rock fragments, set in a quartz, calcite, and sericite cement (samples 617, 619).

The intercalated feldspathic grits and arenites are beige-brown in colour, becoming reddish-blue to dark grey in the northern and northwestern parts. They are generally thick-bedded and massive to poorly graded. Bedding plane features include local unconformities, scour structures, load casts, sand dykes, flame structures, and rip-up shale clasts (Fig. 12). Short, narrow en-echelon dykes with a gritty fill occur in the Helskloof arenites (Fig. 12c). The arenites and grits consist of 70-82 per cent quartz, 10-15 per cent feldspar, and 2-3 per cent muscovite. The interstitial matrix contains quartz, sericite, calcite, and oxides. The grains are subangular to subrounded and have an average size of 0,8-2,0 mm (samples 436, 608, 610).

Isolated subrounded lenses of massive dolomite ranging in size up to 10's of metres are found throughout the Wallekraal beds (and to a lesser extent in the underlying and overlying sequences). They are often associated with the conglomerate and arenite.

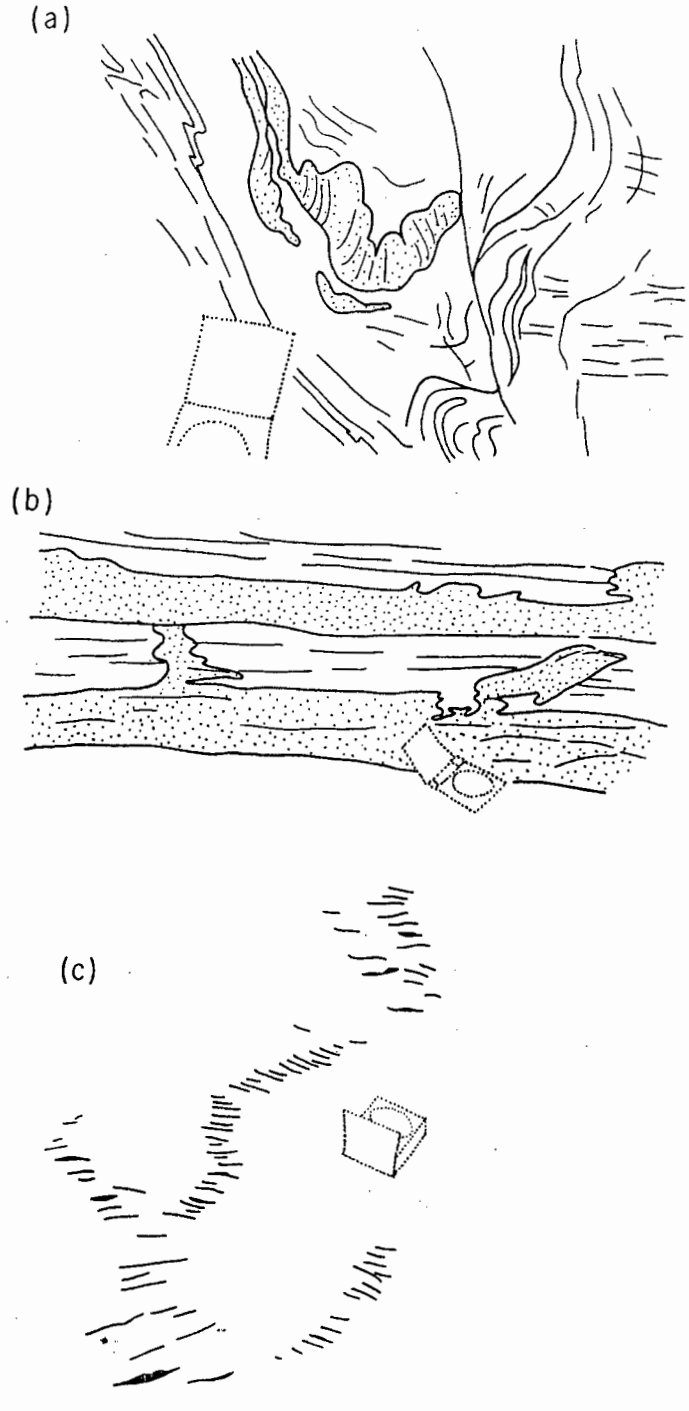

Fig. 12 : Sketches of bedding features in the Hilda arenites:
a) load cast structures (tectonically inverted)
b) sand dykes in the Gorab Peak area
c) sand dykes in the Helskloof Pass area (view oblique to bedding plane).

The Wallekraal quartz-mica schist is fine- to medium-grained, silvery blue-grey to green-grey, and contains fine straight laminations. It alternates locally with siltstone and calcareous schist. Modal compositions of some thin-sectioned samples are shown in Table 6. Accessory minerals are apatite, epidote, sphene, and zircon. Grain sizes range between 0,03-0,15 mm.

Table 6 : Estimates of modal proportions of quartz-mica schist from the Wallekraal Formation.

Sample	quartz	muscovite	biotite	chlorite	feldspar	calcite	opaques
341	77	12	<1	2	7	-	1
358	72	15	10	1	1	-	1
526	50	35	3	8	1	1	2
597	38	20	2	5	2	30	2
606	65	20	12	2	-	-	1

2.4.2.3 Dabie River Formation

The Dabie River dolomite and dolomitic marble beds are laterally discontinuous, massive, medium grained, and grey to blue-grey in colour. The dolomite beds north of Annisfontein exhibit rare stromatolite mats with elongated "dome and basin" upper surfaces and rounded apices. The cone wavelengths range from 10 cm to 15 cm in the long axis direction and their amplitudes are less than 2 cm. At numerous other localities, minor non-cylindrical en-echelon folds and wavy laminations that converge onto lower parallel laminations could represent deformed Conophyton-like forms. The brecciation of the dolomites in the Helskloof Pass area appears to have been due to an "in situ" disruption as boudinaged clasts can often be followed along strike to join up with coherent beds.

2.4.3 Depositional environments

A carbonate shelf palaeo-environment is inferred for the Pickelhaube Formation. The calcitic composition of the carbonates (undersaturated in Mg^{++}), the lateral persistence of bedding, presence of parallel laminations, absence of stromatolites, and relatively high argillaceous and graphitic content indicate moderately deep water conditions. The complex contact relationships with the underlying Stinkfontein Sequence (the dolomite is interbedded with the Kaigas diamictite at Five Sisters and Driegratberg, whereas relationships are disconformable in the Helskloof area) is attributed to continuous carbonate deposition during and after the Kaigas transgression. The locus of carbonate deposition probably migrated eastwards as water depths increased.

The lithologies and sedimentary features of the Wallekraal Formation are consistent with deposition in a submarine fan environment. High energy gravity flow processes are indicated for the conglomerate, grit, and arenite by their interfingering relationship with the Kaigas diamictite, the coarseness of pebbles and matrix, the paucity of internal sedimentary structures, and the types of bedding plane features. The lateral discontinuity of the conglomerate and quartzite units suggests deposition in channels in the upper fan or in suprafan lobes in the mid fan region. Low energy turbidity current deposition on channel levees or abandoned lobes is inferred for the fine grained beds from the parallel, even laminations and normal grading.

The depth of deposition is poorly constrained, but the good rounding of pebbles, the isolated dolomite pods, and the dominance of gravity flow mechanisms indicates resedimentation from a shallower-water platform or shelf environment. A moderate to deep water euxinic environment is suggested by the preservation of the fine-grained sediments and the presence of graphite in the mica-schist.

A shallow water carbonate platform environment, such as a barrier bar or shelf lagoon, is indicated for the Dabie River Formation from the low argillaceous content of the dolomite and the presence of stromatolites. Some dessication cracks were observed in the dolomite southeast of Hogsback in the southern Richtersveld. Cyclical emergence and submergence may have produced the interbedding of limestone and dolomite in the Helskloof Pass beds. The extraneous basement material in the dolomite breccia at Billingham's Prospect was probably transported by carbonate debris flows and deposited in erosional channels. The brecciation at Helskloof may have resulted from gravitational slumping, dissolution of interstratified evaporites, or ice-push and freeze-thaw associated with the succeeding Numees glacial event.

2.5 Numees Sequence

The Numees diamictite, which unconformably overlies the Hilda, is a distinctive unit that has attracted the attention of many geologists. Previous descriptions have grouped an upper dolomitic unit with it, but because of evidence that the diamictite is overlain by the dolomitic Holgat Sequence (pp. 47, 48), the Numees is redefined here as consisting only of the lower diamictite unit. The term "sequence" is used in preference to "formation" because of the interbedding of iron formation and other rock types of dissimilar depositional origin.

2.5.1 Field relationships, distribution, and stratigraphy

Because of the exclusion of the upper dolomites, and the type area and Kodas diamictites, the redefined Numees Sequence consists only of the main diamictite exposure in the Sendelingsdrif synclinorium (the Nabab River beds) and the beds which join up with it around the hinge of the Annisfontein anticline (the Bloeddrif beds; Fig. 13).

In the central Richtersveld, the Numees includes the Hogsback diamictite, the previously unmapped Goms diamictite on the western side of the Khubus-Lekkersing road, and the diamictite strip south of Eksteenfontein (Fig. 9).

These Numees occurrences are characterized by the presence of a poorly developed near-basal iron formation. The diamictite unit is referred to below as the Sendelingsdrif Formation, and the iron formations as the Jakkalsberg Formation. Both names are derived from well-known landmarks along the Orange River where their respective lithologies are well-exposed.

2.5.1.1 Nabab River beds

The Nabab River beds have a maximum thickness of ~700 m. The basal contact is markedly unconformable along the western flank of the Sendelingsdrif syncline, a feature that is clearly visible in aerial photographs of the Gorab Peak area. A divergence in strike is less apparent along the eastern flank, where bedding has undergone extensive flattening and rotation towards parallelism with the contact. Kröner's (1974, 1975) assertion that the contacts are conformable and gradational was based partly on a misinterpretation of tectonic interleaving of Hilda dolomite for contemporaneous growth of dolomite reefs, and the inclusion of the Jakkalsberg ferruginous quartzite in the Hilda Sequence (op. cit., pp. 24, 31, 33). The unconformity may however have an entirely tectonic origin as the basal contact is paraconformable where it is unfaulted north of Khubus.

The Jakkalsberg banded ironstone and iron-rich quartzite and schist beds are located a few metres above the unconformity. They are well-developed along the eastern flank of the Sendelingsdrif synclinorium in the Orange River region where they are duplicated by faulting and folding.

2.5.1.2 Bloeddrif beds

The Numees Sequence thins rapidly in a westerly direction and is less than 100 m thick along the western flank of the Annisfontein fold structure. These Bloeddrif beds, which are para-conformable with the underlying beds, become extensively imbricated to the north with the overlying dolomite. The Jakkalsberg iron formation is absent here, but a grey graphitic schist or schistose quartzite is often found in its place.

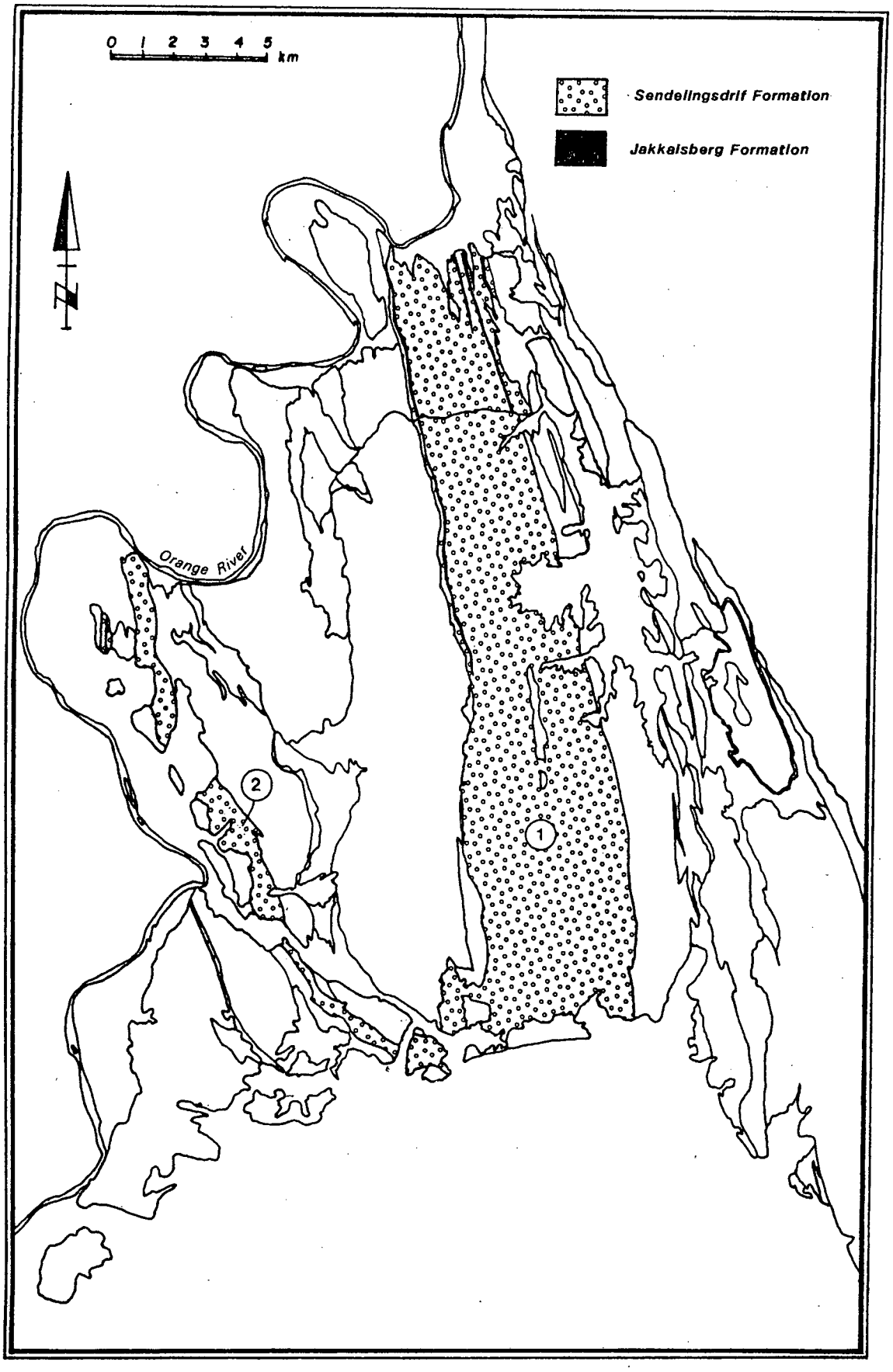

Fig. 13 : Distribution of the Numees diamictite in the northwestern Richtersveld. (1) Nabab River beds, (2) Bloeddrif beds.

2.5.2 Lithology and petrography

2.5.2.1 Sendelingsdrif Formation

The Sendelingsdrif Formation consists predominantly of a massive or very poorly bedded, light grey to blue-grey diamictite. Very subordinate, thin-bedded, graded quartzite or ripple-laminated shale interbeds define straight, sharp lower contacts and sharp or gradational upper contacts. The diamictite contains sparsely scattered, subrounded clasts of the basement pegmatite, leucogranite, and gneiss (70-85 per cent) and intrabasinal quartzite, schist, and carbonate (15-30 per cent). The clast size distribution is polymodal, ranging from small granules to large boulders (2 mm-10 m in long dimension), but averaging less than 20 cm. The clasts are extensively rotated into parallelism with the tectonic fabric. The matrix is made up of fine- to medium-grained subangular muscovite, quartz, feldspar, biotite, and iron oxides (samples 382, 484, 613, 630). A decrease in clast and grain size and matrix competency from the bottom to the top of the formation is reflected in the decrease in topographic elevation towards the central parts of the main belt.

2.5.2.2 Jakkalsberg Formation

The iron formation consists of an interbedded sequence of magnetite-quartzite, and iron-rich and iron-poor schist, arkose and diamictite. Contacts with the adjacent diamictite are sharp or gradational. Polymict lonestones having the appearance of dropstones are abundant (Fig. 14).

The magnetite-quartzite is comprised of medium laminated alternations of fine- to medium-grained magnetite and quartz. The iron-rich schist consists of fine-grained interlaminated bands of quartz, haematite, chlorite, amphibole (actinolite, grunerite), and carbonate, with accessory plagioclase, apatite, and biotite (samples 324, 587), or large muscovite and magnetite grains in a fine-grained chloritic schist (sample 632).

2.5.3 Depositional environment

A glacial origin for the diamictite has been favoured by most workers, including Rogers (1915), De Villiers & Söhnge (1959), Martin (1965), McMillan (1968), and Tankard et al. (1982), although Kröner & Rankama (1972, p. 14) advocated a subaqueous setting where glaciogenic material became partly incorporated into turbidites through processes of reworking. Davies & Coward (1982) suggested that the diamictite could even be a molasse-type deposit formed during contemporaneous overthrusting. The uncertainties that surround interpretations of its origin and the origin of other Damaran diamictites (Hoffman, 1983, Martin et al., 1985, Henry et al., 1986) result from the fact that many of the commonly cited criteria for distinguishing between ice-laid,

ice-derived, and non-glacial diamictites are ambiguous (Kruger & Marcussen, 1976; Kruger, 1979; Crowell, 1983; Visser, 1983; Dreimanis & Schluchter, 1985). A glaciogenic origin, involving deposition of material adjacent to a glaciated continental margin by processes of settling from suspension and ice-rafting, is nevertheless favoured by an association of the following features:

- The extensive lateral distribution and relative textural homogeneity implies that sediment was being supplied along an entire slope region rather than from point sources (Hoffman, 1983). An easterly provinence area is indicated by the similarity of the clast assemblage to the metamorphic and plutonic basement rocks of the eastern Richtersveld, the rapid westward thinning of the Numees Sequence, and sporadic cross-lamination palaeocurrent indicators;
- Evidence for continuous settling of suspended sediment rests on the massive, generally unbedded nature of the diamictite. The paucity of turbidites or other sedimentary intercalations suggests a very quiet moderate to deep water environment. Traction-current activity is observed in the coarser lower parts of the sequence where a stratification is locally preserved;
- Mass-movement depositional indicators, such as soft-sediment folds, slump breccia, intraformational unconformities and load structures are rare, but they may have been obliterated by the penetrative foliation.
- Ice-rafting processes are indicated by the presence of outsized extrabasinal lonestones and clusters of clasts of a particular lithology in groups. These clusters, which were noted by De Villiers & Söhnge (1959, p. 150), may have resulted from icebergs suddenly releasing large quantities of debris from their upper surfaces by processes of tilting and fragmentation (Ovenshine, 1970).

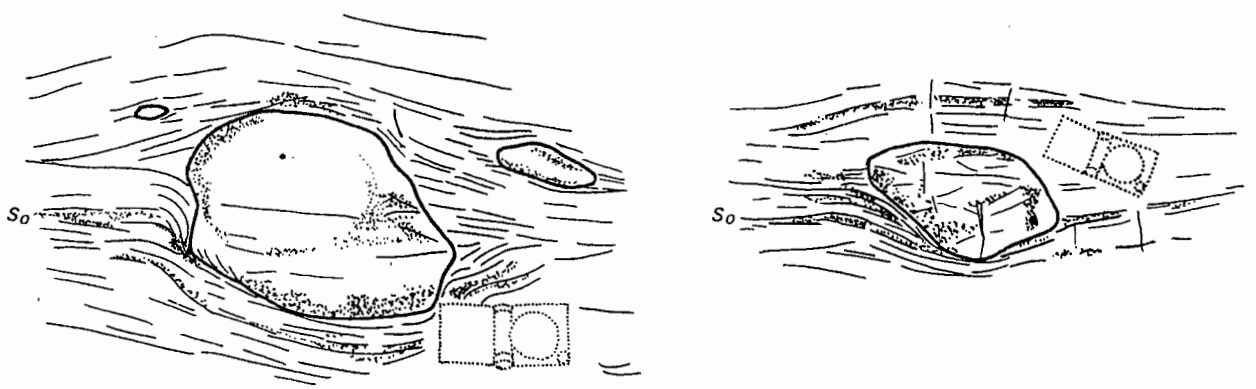

Fig. 14 : Outsized clasts deflecting and piercing bedding planes in the iron formation.

The occurrence of carbonates and other chemical sediments in diamictite has been cited as being incompatible with glaciogenic deposition, as modern chemical deposits tend to to be found in warm-water environments (Schemerhorn, 1974). The Numees beds are underlain and overlain by carbonates, but rapid palaeoclimatic changes or low latitude glaciations are not necessarily implied because of the evidence for tectonic juxtaposition of these sediments. Some carbonate lenses occur within the formation, but their abrupt subrounded terminations suggests that they are reworked detrital clasts rather than penecontemporaneous reefs.

The association of iron formation with glaciogenic rocks occurs in several other Late Precambrian localities, including the Rapitan Group in the Yukon Territory of Canada (Young, 1976; Eisbacher, 1978; Yeo, 1978), the Jacadigo Series in Brazil and Bolivia (Dorr, 1973; Gross, 1973), and the Chuos iron formation of the Damara Orogen (Breitkopf & Maiden, 1986). The development of these Algoma-type deposits has been ascribed to leaching of volcanic rocks by hydrothermal activity (Kimberly, 1978; Yeo, 1978). The precipitation of iron and silica has been attributed to the admixture of cold oxygenated water or to convective overturn related to tidewater glaciers (Young, 1982, p. 733).

2.6 Holgat Sequence

The clastic-carbonate beds on the western side of the Gariep Belt are an enigmatic group of rocks. Their relation to the other PNA sequences and their lithostratigraphy has been poorly constrained in the past because of their poor exposure and intensely deformed character. Evidence was however found to indicate that they overlie the Hilda and Numees sequences.

2.6.1 Field relationships, distribution, and stratigraphy

The Holgat beds were interpreted by De Villiers & Söhnge (1959) as overlying the Hilda strata. They postulated an unexposed SSE trending fault extending from Arrisdrif to Rooisands which thrust Holgat strata over both their younger Kaigas Series north of Annisfontein and older Hilda Series. The Kaigas beds were subsequently correlated with the Hilda (Martin, 1965; Kröner, 1974). Kröner (op. cit., p. 47-48) favoured a facies change between the Hilda and Holgat across the Hogsback synform.

In the area east of the Goms and Omkeer trigonometrical beacons, a thin horizon of Numees diamictite containing the characteristic near-basal ferruginous quartzite was found to underlie the Holgat beds (Annexure I).

The Numees and Holgat beds have a shallow west or northwest dip here, rather than a steep easterly dip as shown in Kröner's (1974, Fig. 13) section. The Hilda and Numees beds pinch out in a southwesterly direction so that the Stinkfontein is directly overlain by Holgat strata along the coast near Cliff Point.

A dark grey feldspathic grit unit that underlies the Numees diamictite at the Hogsback beacon was described by De Villiers & Söhnge (1959, p. 54) as part of their Holgat Series, but remapped by Kröner (1974) as belonging to the Hilda. It is situated between the uppermost Hilda dolomite and the Numees diamictite and is tentatively included in the Jakkalsberg Formation.

As mentioned previously, in the northwestern Richtersveld the Nabab River diamictite of the Numees Sequence joins up with the Bloeddrif diamictite around the Annisfontein anticline, so that the sequence on the western side of the Bloeddrif-Annisfontein road overlies the Numees. The lower part of this sequence is a tectonic duplication of the underlying Hilda and Numees beds, but the greywacke, grit, and dolomite that are exposed at higher stratigraphic levels closely resemble the Holgat lithologies in the type area.

The reinterpretation of the Holgat as overlying the Numees has an important bearing on Holgat-Nama relationships, since the Numees is generally considered to be directly overlain by the Nama Group (De Villiers, 1945). McMillan (1965) and Martin (1965, p. 105) considered the basal Kuibis feldspathic quartzite of the Nama Group to lie conformably on the Numees beds in the Witputs area of SWA/Namibia, although Kröner & Germs (1971) found an angular unconformity between Numees diamictite, siltstone and quartzite, and Nama conglomerate and quartzite at an outlier near Aussenkjer in the eastern Richtersveld.

A Holgat-lower Nama correlation is favoured by the substantial thickness of the Holgat Sequence in the western Richtersveld, the absence of any known Nama beds here, and the continuity of structures northwards to the Witputs area. Recent geochronological data of Horstmann (1987) points to an early lower Nama age for the Holgat. His data shows that the molasse that was being shed from the Damaran Orogen into the upper Nama basin had undergone a metamorphic alteration from 670 to 570 Ma, suggesting that the Gariep tectonic phase was already proceeding while the lower Nama was still being lain down to the east (the lower Nama is dated from fossil evidence at 650-570 Ma; Germs, 1972, 1983).

Three carbonate-bearing exposures are correlated with the Holgat Sequence in the study area (Fig. 15). The beds to the far west (the Sanddrif beds) can be traced eastwards to join up with the 'upper Numees' beds along the downwarped northern margin of the Kuboos pluton (the Annisfontein beds), and are correlated with a small outlier in the core of the Sendelingsdrif synclinorium (the Remhoogte Peak beds).

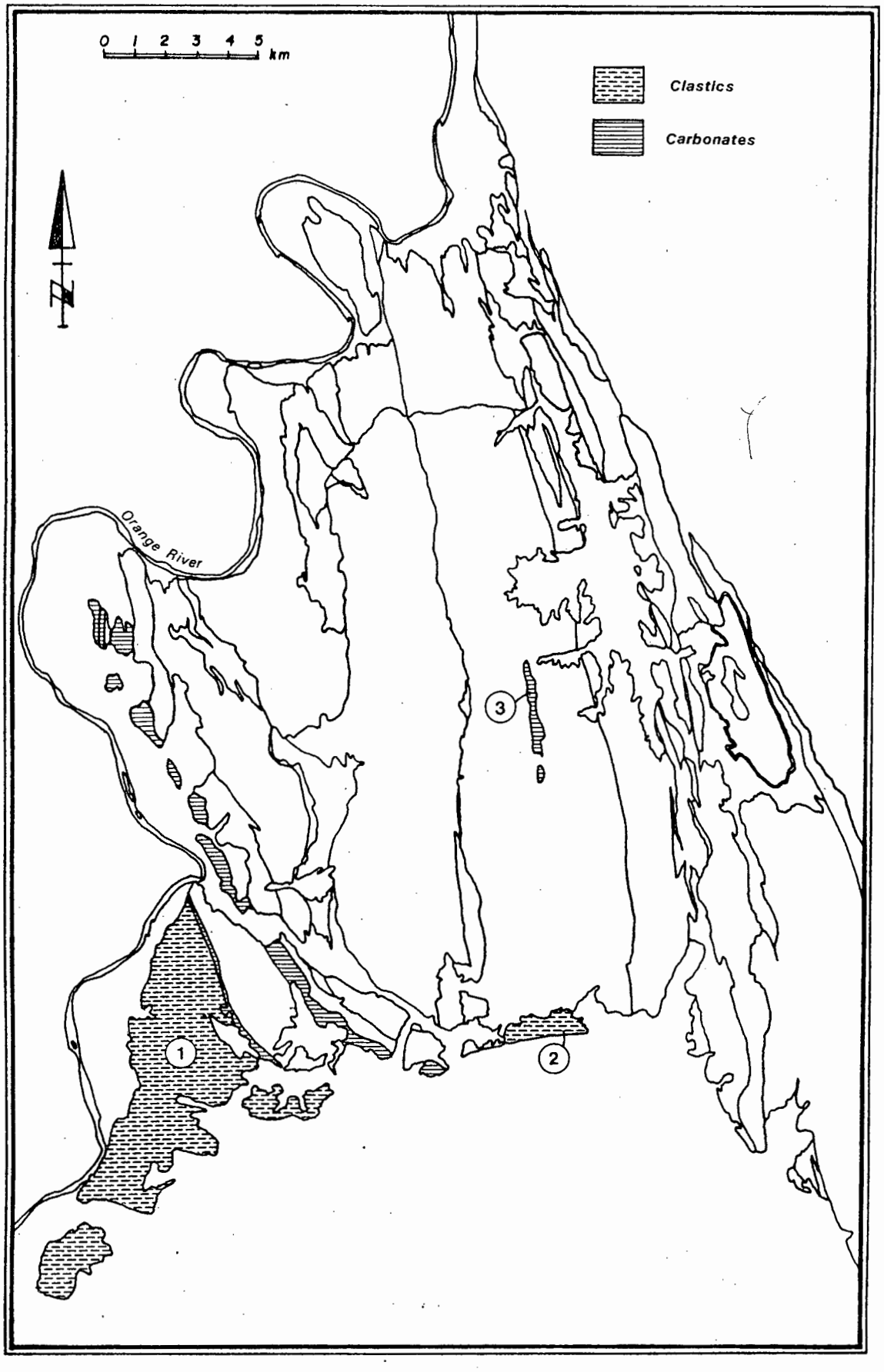

Fig. 15 : Distribution of the Holgat Sequence. (1) Sanddrif beds, (2) Annisfontein beds, (3) Remhoogte Peak beds.

2.6.1.1 Sanddrif beds

The ~3500 m thick Sanddrif beds consist of a basal dolomite, a lower zone of chloritic and calcareous schist, greywacke, arkose, grit and thin carbonate interbeds, and an upper zone of quartz mica-schist and phyllite, with discontinuous carbonate and quartzite lenses. The beds are metamorphosed to hornfels and marble in the Kuboos pluton aureole.

2.6.1.2 Annisfontein beds

The ~350 m thick sequence along the down-bent Kuboos pluton contact to the east of Annisfontein is made of dark grey schistose hornfels and slate and subordinate calc-silicate. A discontinuous thin-bedded marble outcrops along the eastern side.

2.6.1.3 Remhoogte Peak beds

The beds at the western approach to the Remhoogte Pass have a distinctive stratigraphy (Fig. 16):

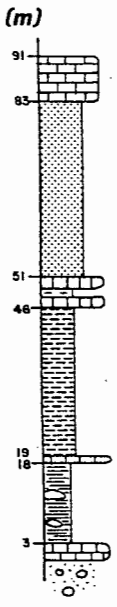

Lithologies

Dolomite marker

Arkose, greywacke, calcareous schist

Dolomite marker, interbedded with calcareous schist

Calcareous schist, greywacke, limestone

Graphitic phyllite, partly calcareous, with a few limestone lenses

Dolomitic limestone, grey-black

Numees diamictite

Fig. 16 : Measured section from the central parts of the Remhoogte Peak outcrop.

Thicknesses of the Remhoogte Peak beds vary considerably along strike. The basal limestone thickens to the south and becomes interbedded with the overlying phyllite, while the lower dolomite marker thins out.

2.6.2 Lithology and petrography

The arkose, greywacke and schists are light blue-grey to brown-grey in colour. They generally have a massive unbedded appearance because of the intense deformational imprint. The affects of the Kuboos pluton contact metamorphism are reflected in the high biotite, muscovite (sericite), and cordierite modal proportions (Table 7). Grains are subangular and have average diameters of 0,02-0,25 mm.

Table 7 : Modal analysis of thin-sectioned clastic samples from the Holgat Sequence.

Sample	Quartz	Biotite	Muscovite	Feldspar	Chlorite	Calcite	Cordierite	Opaques
68	19	15	42	24	-	-	-	-
456	25	25	8	7	-	35	-	-
462	27	17	14	25	-	-	15	<1
463	48	22	7	13	-	8	-	1
466	20	57	15	5	-	-	-	3

The **dolomitic limestone** and **calcareous marble** is grey to blue in colour, and massive or parallel-laminated. Dolomitization occurs in irregular patches and along fractures subparallel to bedding. The carbonates consist of anhedral grains of calcite and dolomite with accessory talc, tremolite, biotite, and opaques (sample 337). Grain sizes are in the order of 0,2-1,3 mm.

2.6.3 Depositional environment

A turbiditic origin can be inferred for the greywacke from their composition, texture, and thick development, implying resedimentation from a more elevated region. The interbedding of fine-grained micaceous quartzites and schists, and the impersistent occurrence of carbonates and coarse clastics indicate a moderate to deep water slope or basin environment.

Because the interval of time between deposition of the Numees and the onset of Pan-African tectonism appears to have been brief, it is likely that some of the Holgat sediments were derived as molasse from an advancing orogenic front to the west, at the same time as the lowermost Nama sediments to the east were being supplied with sediment from an easterly source. As the deformation proceeded, the depositional basin became closed to the west and north, but sediment transport from these directions only appeared in the east during upper Nama times.

3 STRUCTURE

3.1 Introduction

3.1.1 Previous work

Although many impressive structural geological features are displayed in the hilly and poorly vegetated countryside of the northwestern Richtersveld, relatively little attention has been directed by previous workers towards their description and interpretation. Rogers (1915) commented briefly on structural complications in the Numees and other areas. De Villiers & Söhnge (1959, pp. 197-208) dealt at length with major structures but presented no details about the nature and orientation of small-scale features. They were impressed by the parallelism of structures of widely different ages, and interpreted the tectonic evolution in terms of seven repeated cycles of geosynclinal deposition, orogenesis, and magmatism along identical structural trends. Kröner (1974) adopted the "tectogene" model of geosynclinal subsidence in which "geosynclinal development accompanied by gravity folding and subsequent compressional deformation of the trough contents is a continuous process of crustal evolution" (op. cit., p. 63). He recognized two tectonic domains: an eastern miogeosynclinal basin within which gravity deformation occurred simultaneously with deposition, and a western eugeosynclinal pile in which deformation was of a compressional type.

Many of the field criteria cited by Kröner (1974) for penecontemporaneous gravity deformation are open to question. Tankard et al. (1982, p. 283-284) noted that his example of distorted trough cross-bedding indicates an eastward up-current sense of movement. Most of his inferred synsedimentary structures (Figs. 20, 22, 24, 25, 26) are deforming an existing metamorphic foliation. This is a definitive criterion for distinguishing between synsedimentary and tectonic deformation. Other features which he mentioned, such as asymmetric folding, variable orientation of fold axes, isolated horizons of folding, truncation of folds, disruption of bedding, and decollement, can be attributed to postsedimentary deformation, and are in fact frequently described from thrust-faulted terranes.

Joubert & Kröner (1972) and Kröner (1974, 1975) recognized four distinct Pan-African deformational events in the southern Richtersveld:

F_1 - An early phase of syn-sedimentary gravity sliding tectonics that resulted in small folds with moderate westward plunges;
F_2 - A main folding phase characterized by "mainly symmetrical" folding associated with a penetrative axial planar foliation;
F_3 - A cataclastic phase producing long westerly dipping faults and mild

north-south trending monoclinal folds;
F_4 - A late phase associated with east- or southeast-striking transverse features, including breccia-faults, joints, kink-folds, and minor crenulations.

This subdivision into early ductile and late brittle phases has not been supported by later studies. Because of the large contrasts in sediment ductility, early detachment faults duplicating the original stratigraphic sequence are to be expected. Major overthrust faults with a southeasterly transport direction were for example reported by Davies & Coward (1982) from the Chamais Bay and Witsputs-Rosh Pinah areas. Aerial photographic interpretations and limited field checking in the Obib Hills area of SWA/Namibia has indicated that the extent of early low-angle faulting is still greatly underestimated here (Dr. C.J.H. Hartnady; pers. commun., 1985). Evidence for thrust imbrication of basement quartzites and volcanics in the northeastern Richtersveld, at least some of which appears to be of Pan-African age, has also been documented (Shimron, 1987).

3.1.2 Research method

The method used for building up a picture of the order of deformational events was to document local structures and to correlate them throughout the area. The standard tools for correlation are overprinting relationships, characteristic "styles" and patterns of orientations of structures, and relationship to metamorphic minerals and assemblages (cf. Turner & Weiss, 1963; Hobbs et al., 1976; Williams, 1985).

The important overprinting criteria of minor structures are:

- Late folds affecting earlier folds to form refolding interference patterns;
- Late cleavages affecting early ones to form strain-slip cleavages;
- Late cleavages overprinting across the hinge zones of early folds; and
- Late folds having an earlier cleavage folded around their hinge.

3.2 Geometrical analysis

The physical and geometrical properties of fabric elements associated with the three pre-Gariepian (D_1^b, D_1^n, D_2^n) and five Pan-African (D_1-D_5) deformational generations that were recognized in the basement and cover rocks of the northwestern Richtersveld are described below. The Namaqua-age basement structures are dealt with in a somewhat cursory fashion as they are peripheral to the main theme of the present work and are currently under

investigation by other research workers (Shimron, 1987; Booth, 1987). Particular emphasis is placed on the D_1 overthrusting and D_2 backfolding events as they were responsible for the formation of most of the structures and penetrative fabrics.

3.2.1 Fabric elements

3.2.1.1 Basement fabrics

(a) D_1^b

An early (> 1900 Ma) tectonic event, the Orange River Orogeny (D_1^b), that folded the De Hoop volcanics along NNW trends prior to or during emplacement of the Vioolsdrif intrusive Suite, has previously been recognized (Bertrand, 1976; Ritter, 1978, 1980). Shimron (1987) showed that D_1^b predates the deposition of the Rosyntjieberg Formation. Since the primary fabrics in the metavolcanics along the basement-cover interface have effectively been obliterated by the Namaquan and Gariepian orogenic events , the only remaining evidence for D_1^b are local remnants of a folded schistosity in the main basement cleavage.

(b) D_1^n

The ~ 1200 Ma Namaqua Orogeny (D_1^n) produced shear belts concentrated along the northeastern and southern margins of the Richtersveld Subprovince (Blignault, 1974, 1977; Bertrand, 1976; Theart, 1980; Booth, 1987). Mineral lineations plunge in a northeasterly direction indicating that they are southwest-directed thrusts. In the central parts of the Richtersveld Subprovince, the deformational structures related to D_1^n (e.g. the Mike Nappe in the Rosyntjieberg Formation; Ritter, 1980, p. 107) have transport vectors directed towards the NNE (Shimron, 1987). This reversal in the transport direction appears to be related to the development of a backthrust (the Mount Erebus fault) which has placed the Vioolsdrif granitoids and the Windvlakte metavolcanics of the southeastern Richtersveld over the Rosyntjieberg Formation (Von Veh & Shimron, 1987; Fig. 17). The backthrust probably developed because of the impediment of forward motion on a basal detachment flooring the Richtersveld Subprovince. Continued underwedging of the northern parts of the subprovince was probably responsible for the development of the large-scale anticlinorium in the northeastern Richtersveld (the Richtersveld anticline of Ritter, 1980).

The thrust faults in the Armmanshoek-Omsberge area which imbricate the De Hoop volcanics and Rosyntjieberg quartzites have been interpreted as Pan-African features (Shimron, 1987), but several lines of evidence suggest that their Gariepian signature is due to reactivation of existing structures with similar trends, and that they formed during the backthrusting event:

- Many of the fault imbricates strike slightly obliquely to the Pan-African cover faults, and terminate against the basement-cover contact. In the Klipneus sheet, these faults cut up-section in a NNW direction, whereas the Pan-African faults generally have southeast-directed slip vectors;
- In several instances, the Gannakouriep dykes show surprisingly little displacement across the faults. Geochronological data indicates that the dykes were mostly intruded between the Namaquan and Pan-African events;
- The cover rocks near the basement-cover interface are relatively unfaulted in comparison to the adjacent basement rocks, and there is not much imbrication between basement and cover;
- The dextral swing in strike of the basement fabrics as the Gariep Belt is approached is incompatible with the predominantly sinistral sense of movement associated with the Pan-African. This feature can be related to downflexuring of bedding into the southwestern limb of the Richtersveld anticline during the backthrusting event.

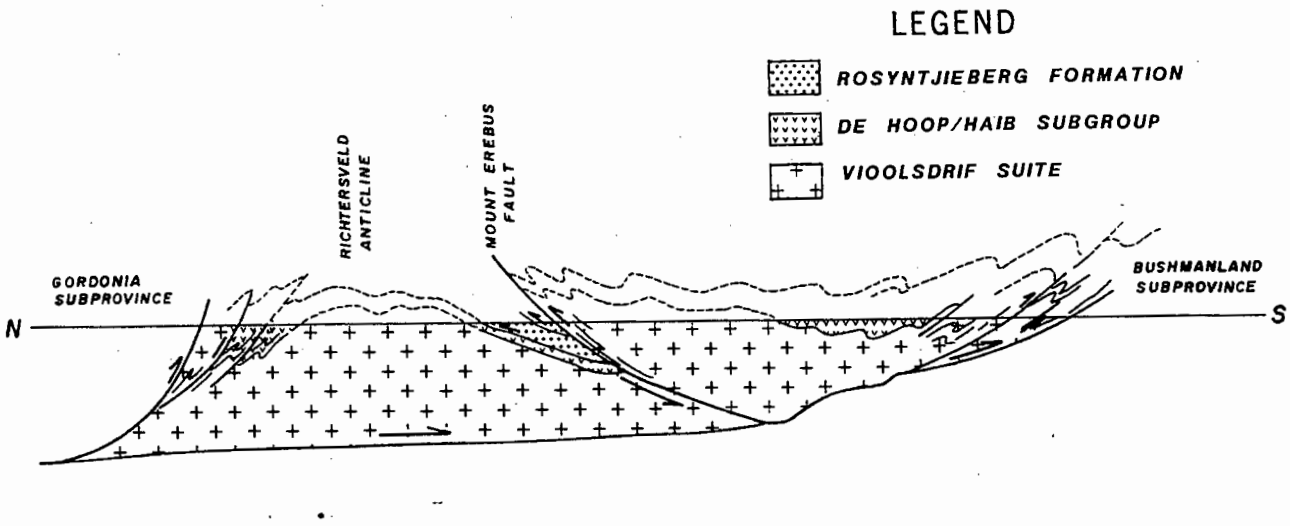

Fig. 17 : Synoptic north-south section through the Richtersveld Subprovince.

(c) D_2^n

A set of north- to NNE-trending dextral shears is often developed in the basement rocks. The Gannakouriep dykes are located along some of these shears, and they are sinistrally offset by the Pan-African thrusts. The Devilscastle and Black Face Mountain shears, which Ritter (1980) claimed were of pre-Gariepian age, may be D_2^n faults that were reactivated during Pan-African times.

3.2.1.2 Cover fabrics

(a) Faults and planar discontinuities

(i) Synsedimentary normal faults

Examples of penecontemporaneous normal faults occur at the base of the Kaigas diamictite at Paradys and near Swartberg. Small listric normal faults, fractures, and en-echelon tension gashes of syn-depositional origin are also found in the Stinkfontein quartzite (Fig. 18; see also Kröner, 1974, p. 70, Fig. 19). The faults generally die out towards the margins of the beds, but may extend across and displace bedding planes. Some of the faults have been reactivated by later movements to cut across the main (S_1) cleavage.

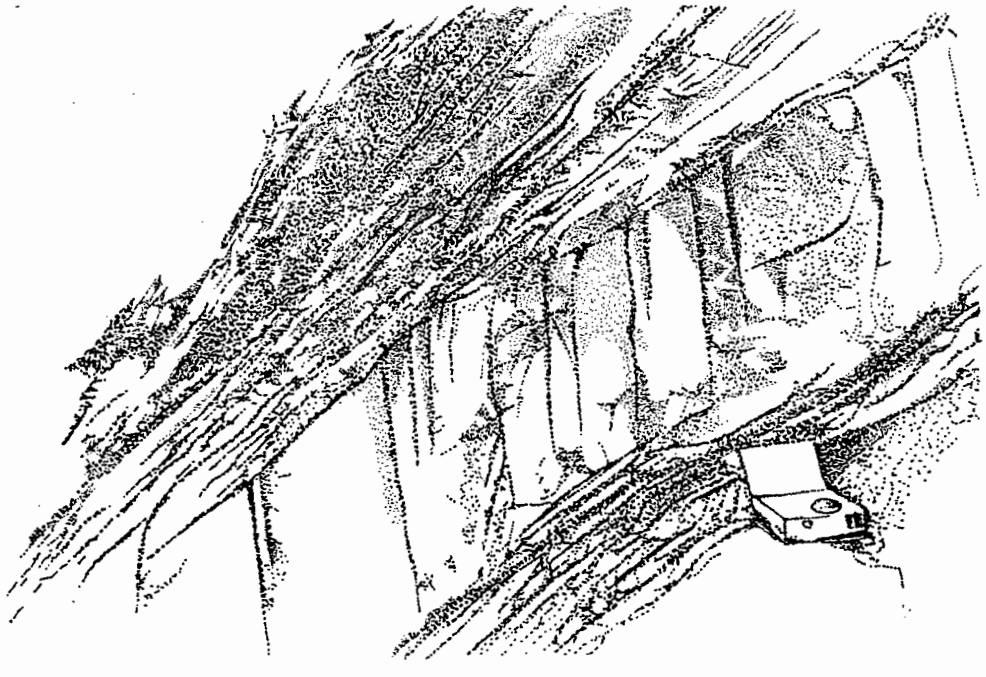

Fig. 18 : Small westward dipping normal faults in massive quartzite in the Numeesberg.

(ii) Reverse faults (D_1)

Most of the faults in the present area are thrust or reverse faults related to the D_1 phase of deformation. The faults trend northwest-southeast in southern SWA/Namibia, NNW-SSE in the northwestern Richtersveld, and north-south in the western central parts of the Richtersveld. They have shallow-moderate westerly dips to the west, but steepen to the east and northeast and dip eastwards north of the Orange River. The faults formed prior to, during, and after the formation of the F_1 folds, so that some of them are bedding-parallel and folded, while others cut through the folds.

In the fine-grained ductile units (limestone, schist, phyllite, diamictite), the faults are characterized by an intense schistosity and an abundance of tight, asymmetrical, recumbent, and curvilinear folds. Resistant beds and veins are usually broken up, boudinaged and folded, and the original fabric is often completely destroyed. In the coarser-grained units (arenite, rudite, dolomite) the faults are more discrete, displaying minor brittle fracturing, jointing, and microfaulting of the wallrock. Faulted contacts are often silicified and dolomitized, and minor concentrations of manganese, iron, and copper may be present. The faults formed under relatively low confining pressures since open-space fillings in sigmoidal tension gashes, joints, and veins are frequent, while higher pressure and temperature indicators, such as microbreccias and mylonites, are rare.

(iii) Syn-intrusive faults (D_4)

A few crosscutting faults are related to the Kuboos pluton emplacement, the most prominent of which is the east-west striking thrust fault west of the Five Sisters Hills. It mimics the pluton contact and duplicates and displaces the hinge of a major fold at Gorab Peak.

(iv) Late- to post-intrusive planar faults (D_5)

A late east-west to WNW-ESE striking set of planar features, ranging from extensive faults, fractures, and dykes to localized joints and tension gashes, cut through the Kuboos granite and country rocks. The faults make up horsts and grabens with appreciable displacements in the core of the Sendelingsdrif synclinorium. Tension fractures, gashes, and joints are profuse in resistant rocks which become broken up into regular blocks. The gashes contain quartz or calcite vein material and some copper and tungsten mineralization (e.g. at Rupping's and Wallekraal Prospects). The dykes consist of a variety of rock-types including granite-porphyry, aplites, bostonites, camptonites and kersantites (Van Biljon, 1939, p. 190-198; De Villiers & Söhnge, 1959, p. 168-172). A NNW-SSE striking Karroo dolerite dyke cuts the northern part of the Numeesberge.

(b) Folds

(i) F_1

Most of the folds in the area have NNW-trending axes and cannot be separated on the basis of orientation (Fig. 19). The large-scale folds are interpreted as F_1 structures because the S_1 cleavage has an axial planar relationship to them. They conform to the fold form types commonly found in thrust terranes (cf. Suppe & Medwedeff, 1984; Boyer, 1986; Jamison, 1987).

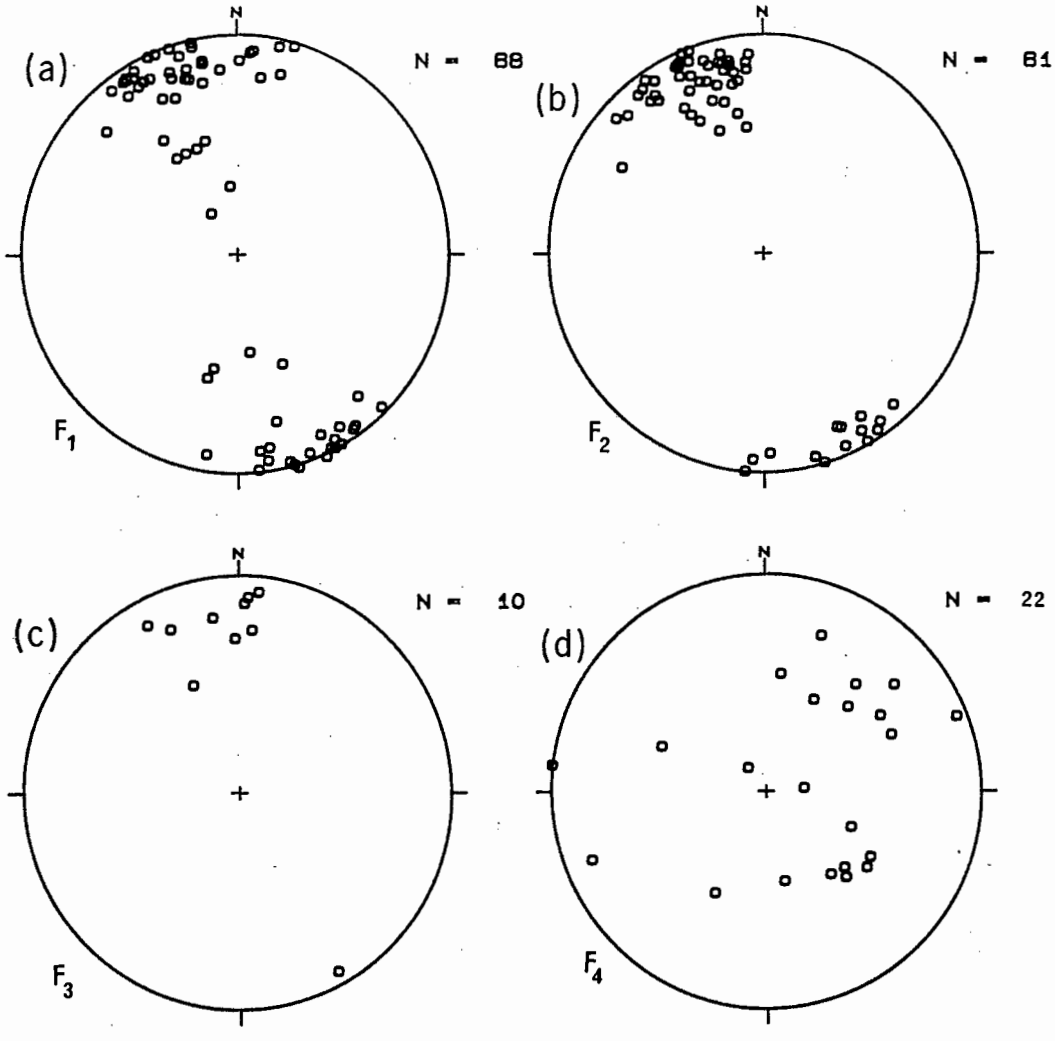

Fig. 19 : Equal-area stereonets of fold axes associated with the various deformational pulses.

An impressive example of a fault-propagation fold occurs along the basement-cover contact south of Eksteenfontein. The marginal Stinkfontein beds are overturned for a distance of several 100 m from the contact and a tight synclinal fold containing the unconformably overlapping Hilda and Numees strata is preserved along the contact (Figs. 20a, 20b). The fold is bounded by forelimb and backlimb thrusts which shear out the stratigraphically lower parts of the western limb and the higher parts of the eastern limb. Because of its double-plunge, only the lower parts of the structure (the eastern limb) are exposed at the northern and southern ends of the outcrop. A later fault transects the fold and displaces the hinge. Two adjacent synclinal remnants of Hilda strata with a sheared out intervening anticline occur further south (Figs. 20c, 20d).

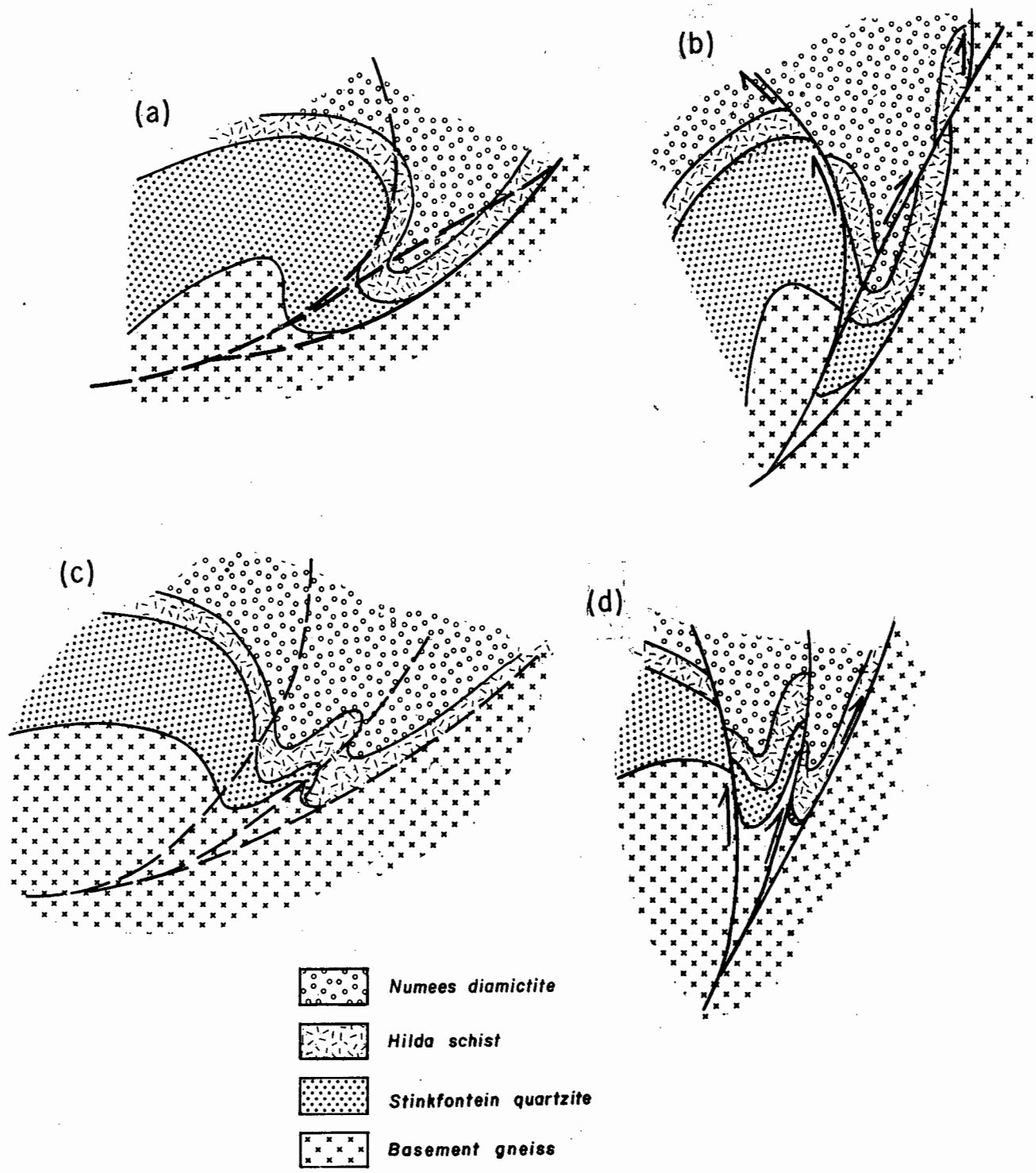

Fig. 20 : Generalized cross-sections showing the development of faults and folds along the basement-cover contact south of Eksteenfontein. See text for details.

Small-scale F_1 folds are infrequent, although their presence may be obscured by transposition, shearing out of fold hinges and paucity of younging indicators. S_0 is normally the only fabric to be folded in the hinge. The folds are often refolded by later folds but they do not deform earlier ones (Plates 7, 8 and 10). Two distinctive fold styles are evident (Fig. 21):

- Asymmetric folds with ENE-directed vergences ranging from open warps and monoclinal bends to overturned or recumbent structures (Fig. 21a);
- Strongly curvilinear or "sheath" folds with NNW-SSE trending axes lying in the plane of the regional S_1 foliation (Fig. 21b). These folds are found in proximity to fault zones.

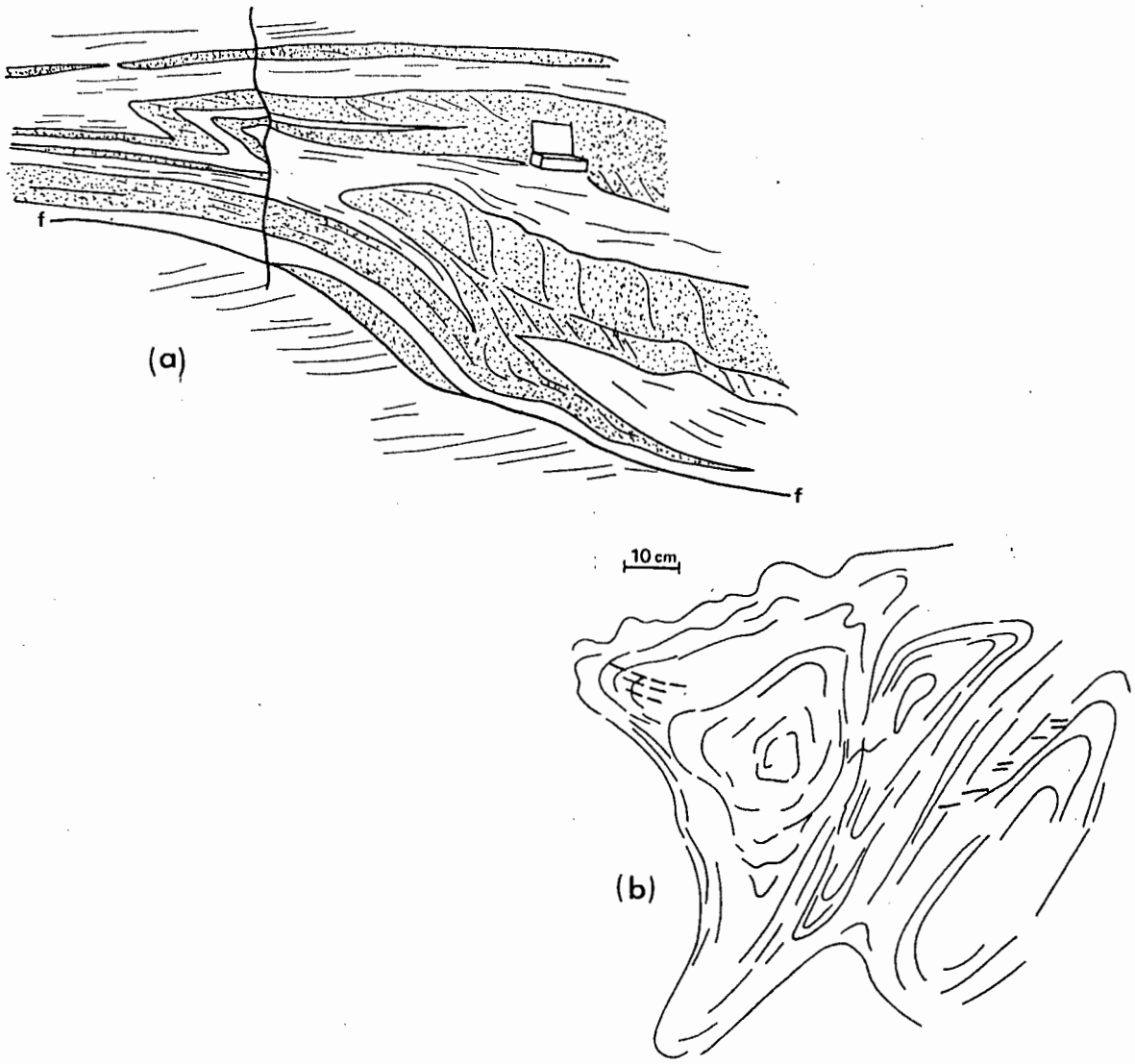

Fig. 21 : Field sketches of F_1 minor folds: (a) Asymmetric fold above a fault (locality 520); (b) Sheath folds (locality 358).

(ii) F_2

F_2 folds, distinguished by their shallow east-dipping axial planes and an "east-over-west" asymmetry, are locally well-developed (Plate 9). They occur in linear zones in the vicinity of major faults, most notably along the Klipneus fault. Their axial traces are sub-parallel to F_1, but they are non-cylindrical with fold axes plunging gently to the NNW or SSE. This non-cylindricity can be mistaken for fold interference from an open transversely trending deformational phase. Interlimb angles vary along strike and they may die out over short distances.

Their fold characteristics are dependent on the orientations of the structures which they superimpose. The expected F_1/F_2 interference patterns is type 3 with "S on Z" interference (fold interference classification of Ramsay, 1967). The dips of the limbs of F_1 folds exert little control on F_2 plunges since the respective fold axes are sub-parallel. The limb dips only affect the location of the axial surfaces and the fold symmetry (Ramsay, op. cit., p. 509).

The shapes of the F_2 folds are very variable (Figs. 22a, 22b) as they depend on factors such as the amounts of shortening, viscosity ratios of the deforming material, and wavelength/ thickness ratios (cf. Biot et al., 1961; Ghosh, 1966; Sherwin & Chapple, 1968; Hudleston, 1973; Hudleston & Stephansson, 1973). If the contrast in viscosity between layers is small, deformation is by layer shortening, and buckle folds rather than kink folds form. Kink folds predominate in alternating layers of high ductility contrast. Layer thickness variations indicate that the folds are usually of class 1c or class 2 type (dip isogon classification method of Ramsay, 1967).

(iii) F_3

A very weak F_3 folding phase with the same NNW structural trend as F_1 and F_2 overprints the F_2 structures. F_3 folds are asymmetrical, non-cylindrical, and concentric (Fig. 23). Interlimb angles vary from open to close and half-wavelengths are in the order of ~0,1-0,5 m. They verge to the west and often occur in strata with westerly dips. Good examples were found in the Hilda and Holgat beds on the eastern limb of the Sendelingsdrif synclinorium, and in the Numees beds on the western limb of the Annisfontein anticlinorium. The style of folding and the downslope vergence direction is indicative of gravity induced folding. Kröner's (1974, 1975) assertion of the importance of this style of deformation may have been based on the examination of well-developed F_3 folds at localities outside the studied area.

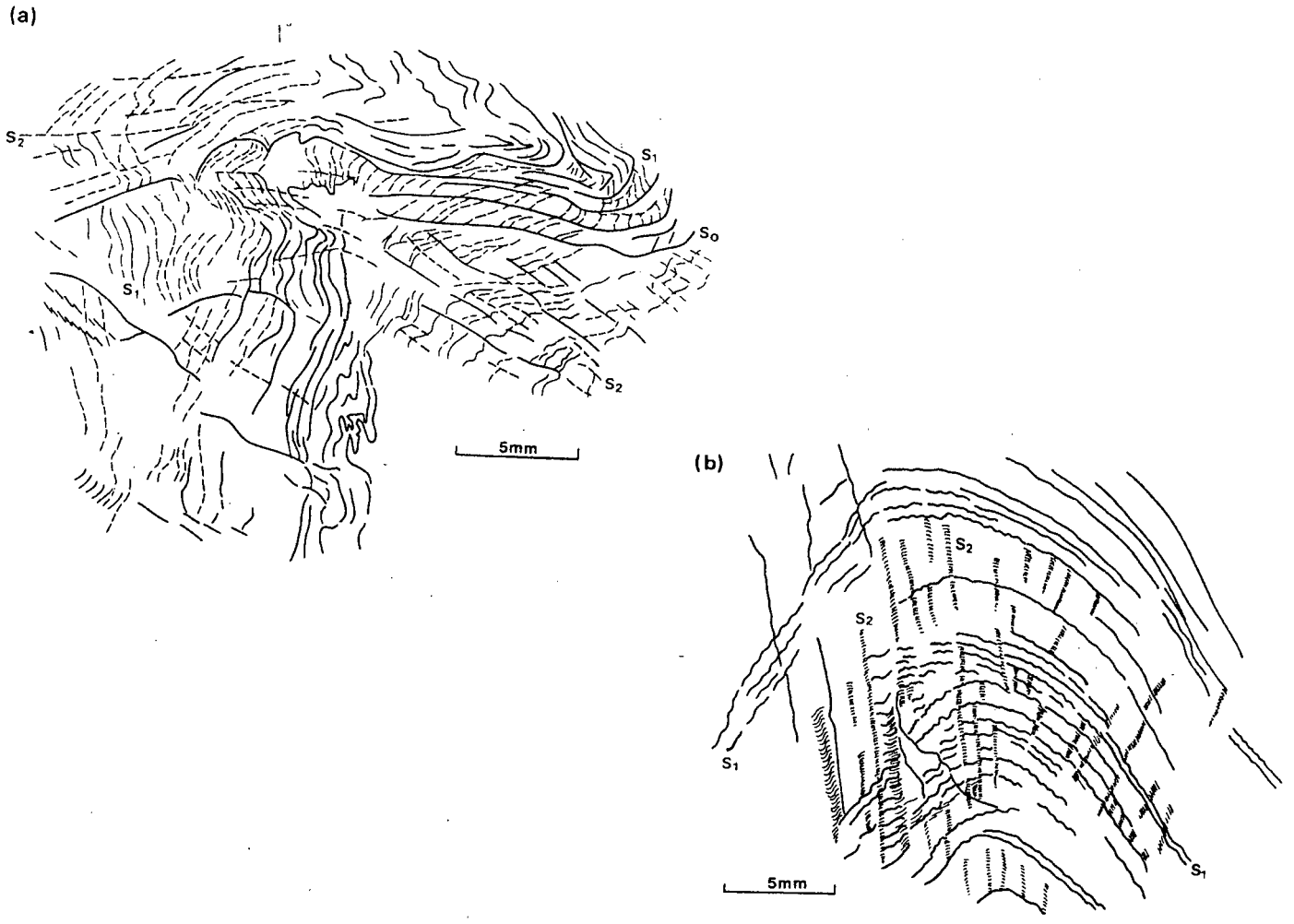

Fig. 22 : Sketches from photomicrographs of F_2 minor folds:
(a) kink folds folding S_0 and S_1. Note that S_2 is slightly affected here by a later event (sample 1523);
(b) buckle fold with fanning S_2 cleavage (sample 597).

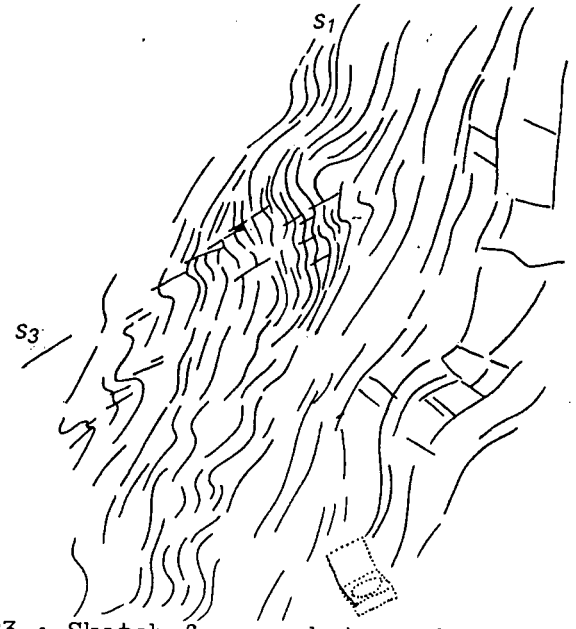

Fig. 23 : Sketch from a photograph of F_3 folds. Viewed to the north.

(iv) F_4

F_4 folds have east-west to northeast-southwest trending axes (Fig. 19 d) and take the form of isolated east-west trending kink folds (Fig. 24a), conjugate reverse kink folds (Fig. 24b; Plate 10), and closely spaced kink bands. The kink bands occupy the limbs of monoclinal warps that are downthrown to the north.

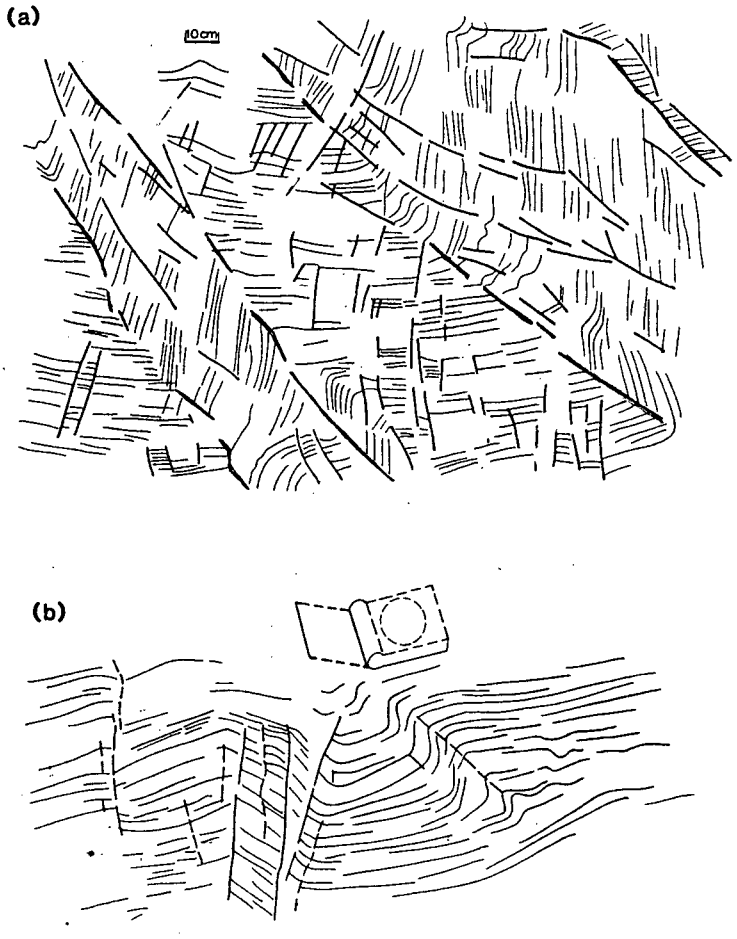

Fig. 24 : Examples of F_4 kink folds.

(c) Cleavages

(i) S_1

S_1 is by far the most penetrative fabric. It has a NNW strike (Fig. 25a) and steepens in an easterly direction asymptotic or sub-parallel to the major faults.

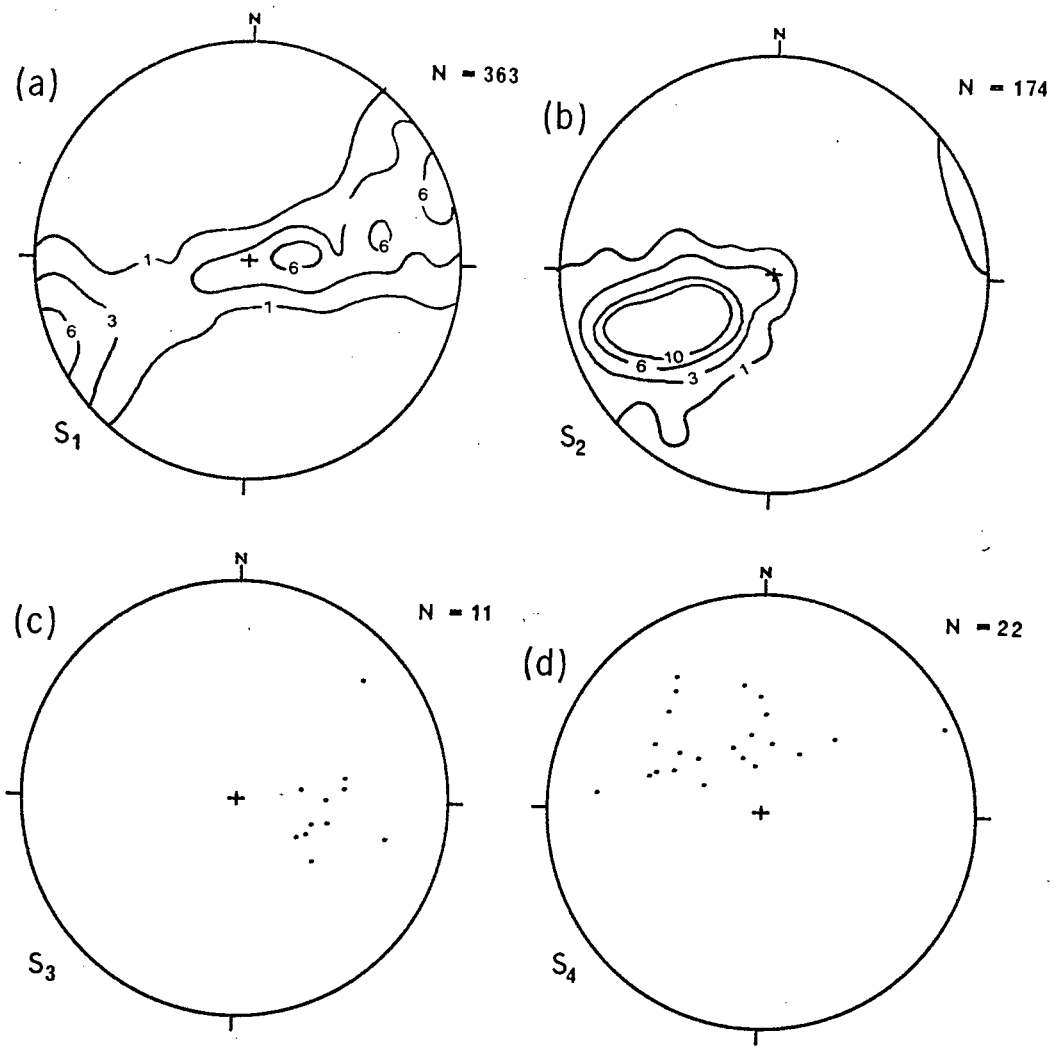

Fig. 25 : Equal-area steronets of poles to planar fabrics associated with D_1-D_4.

The morphology of S_1 is dependent on the host rock-type:

- In greywacke, schist, and phyllite, it takes the form of a continuous slaty cleavage or a disjunctive spaced cleavage (Figs. 26a, 26b) which mimics, refracts, or curves through bedding. The spaced cleavage has a gradational to discrete transition from microlithons to cleavage domains, and cleavage domains are rough and sinuous or anastomosing;

- In mica-poor rudite and arenite, it is defined by the preferred orientation of boulders, pebbles and grains. Pressure solution and microdeformational structures, such as grain indentation, mica beards, quartz overgrowths, undulatory extinction, and subgrain formation are observed. Granoblastic-

polygonal textures are developed in the proximity of shear zones and quartz grains become strongly elongated into lens-shaped blades or ribbons. As the mica content increases a schistosity which flows around competent clasts and grains becomes evident. Competent clasts are generally little deformed, apart from some crosscutting quartz- or calcite-filled fractures, while incompetent clasts are extensively flattened, necked, and boudinaged, and can become poorly distinguishable from the host matrix (Plate 5);

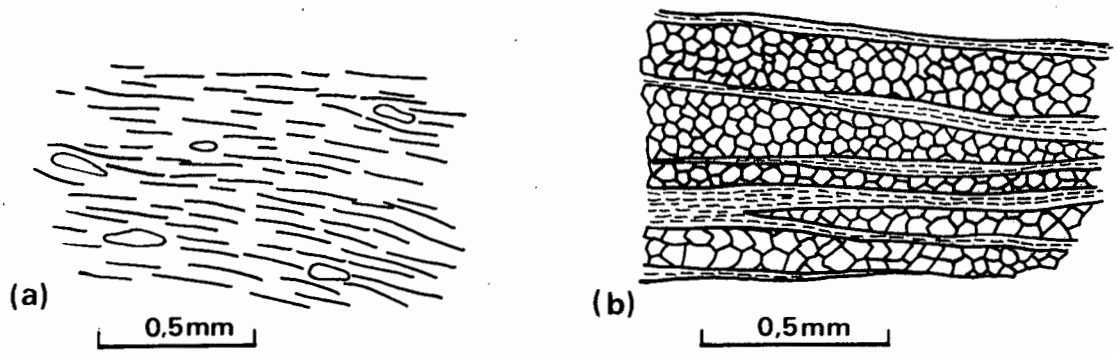

Fig. 26 : Contrasting S_1 fabrics in mica-rich schists: (a) slaty cleavage; (b) disjunctive spaced cleavage.

- Dolomite and marble show little macroscopic evidence for the development of an S_1 foliation, but in thin sections discontinuous, dark, sutured stylolites often parallel a crude alignment of carbonate grains. The stylolites are more closely spaced and straighter in impure carbonates.

In certain instances, two S_1 cleavage trends are observed:

- An anastomosing cleavage may define conjugate or trapezoidal shapes bounding grains or microlithons (Fig. 27a);
- In shear bands, s (schistosité) planes form in the plane of flattening while c (cisaillement, shear) planes form parallel to the plane of maximum shear (Simpson & Schmid, 1983; Fig. 27b). The crystallographic axes of mica grains in the c and s planes have similar orientations;
- A grain alignment representing fine sedimentary laminations may occur within microlithons;
- An earlier cleavage may be overprinted (Fig. 27c). An earlier deformational phase is not necessarily indicated as more that one cleavage may form during overthrusting (cf. Mitra & Elliott, 1980; Mitra & Yonkee, 1985; Marshak & Engelder, 1985). Figure 27c illustrates an early, spaced (S_1a) cleavage overprinted by a continuous (S_1b) cleavage. S_{1a} is not an inherited depositional fabric since its cleavage domains show evidence of selective removal and recrystallization of material, and it is oblique to and cuts across S_0 in the field (Plate 6).

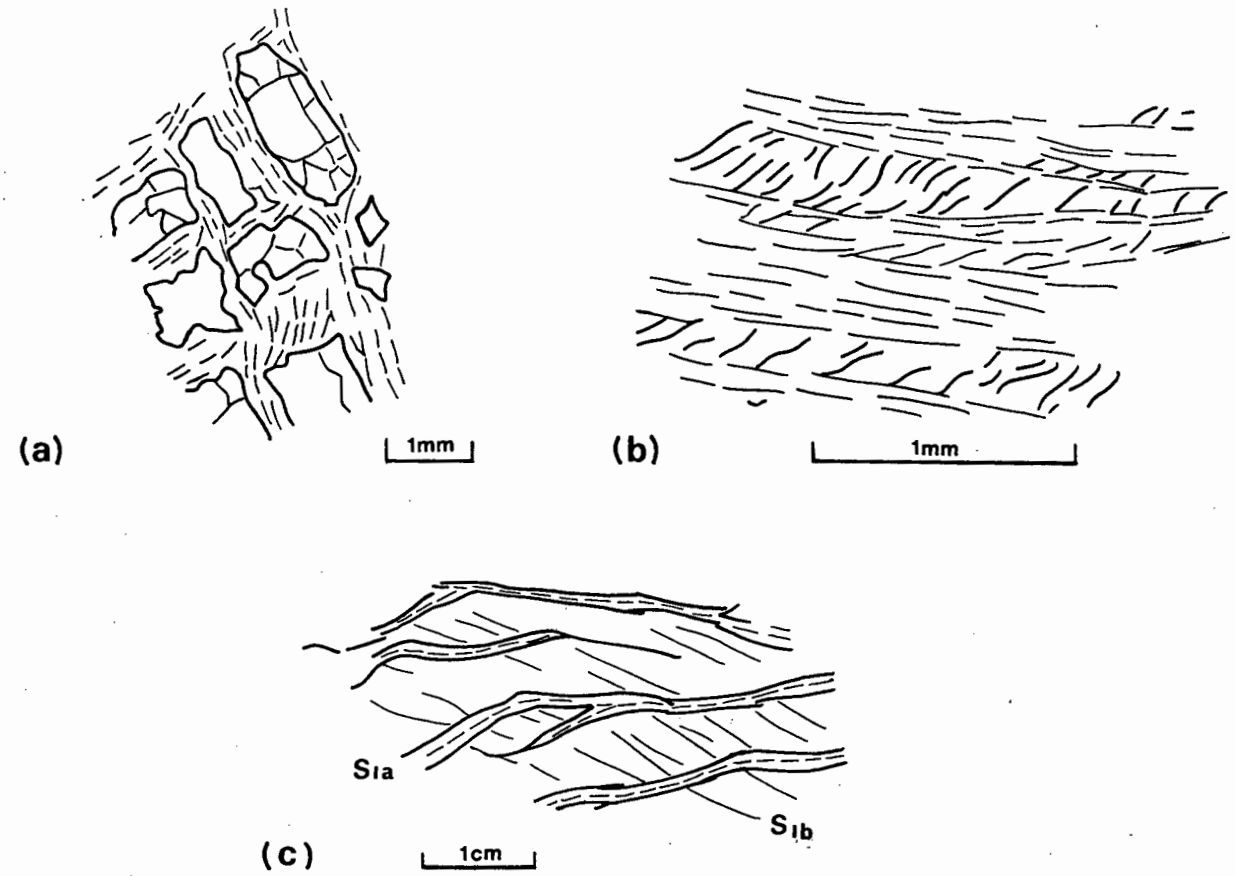

Fig. 27 : Sketches of bimodal S_1 cleavage trends. See text for further details.

(ii) S_2

An axial planar S_2 crenulation cleavage with a shallow ENE dip (mean S_2 = 334/50; Fig. 25b) is often developed in schists and phyllites. Its morphology ranges from an incipient puckering and microfaulting to a zonal cleavage with continuous to discontinuous domain boundaries (Fig. 28). Quartz grains are recrystallized in the hinge regions of microfolds, and sutured and corroded grains and residues of insoluble material occur in the limbs.

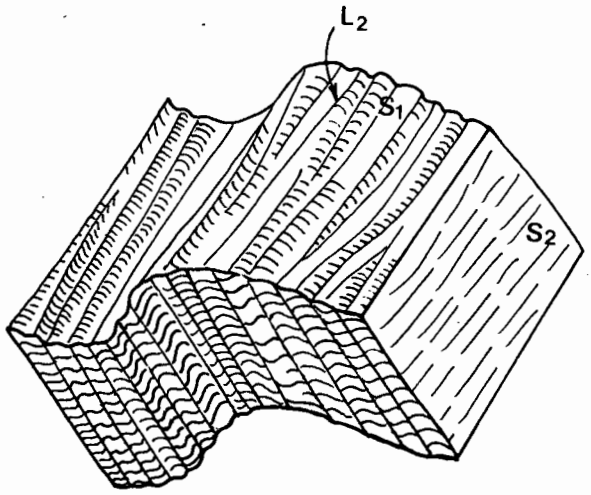

Fig. 28 : D_2 crenulations deforming S_1. Non-penetrative micro-fractures sometimes parallel the microfold hinges. The microfolds usually display westward vergence.

(iii) S_3

An incipient S_3 crenulation cleavage with a rough, sinuous or anastomosing surface is axial planar to the F_3 folds. Some D_3 faults, fractures, kink-bands, and joints with WSW dips and normal displacements occur in the Sendelingsdrif area.

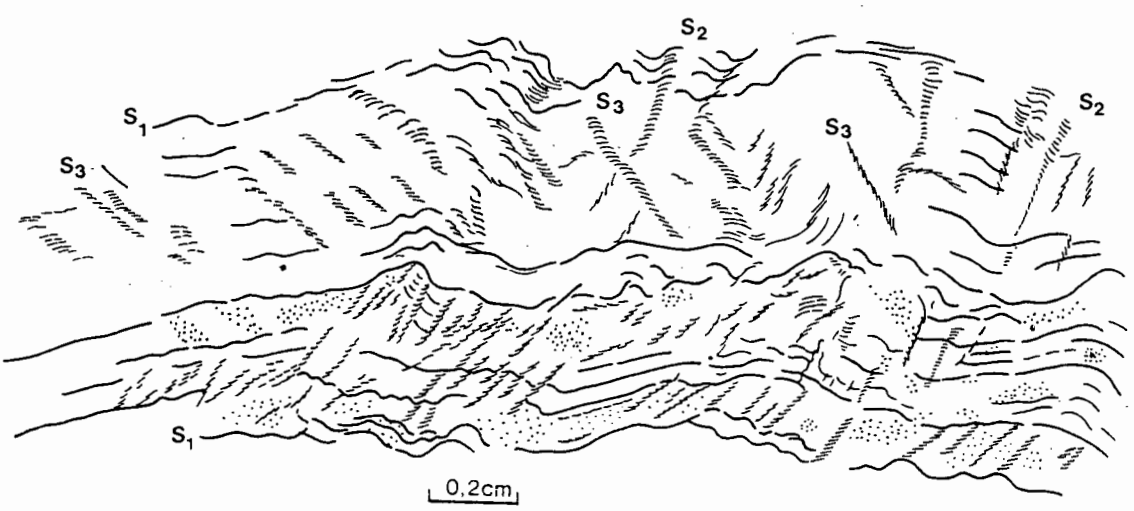

Fig. 29 : Weak S_3 cleavage overprinting S_1 and S_2 (Sample locality 456).

(iv) S_4

An S_4 spaced fracture cleavage obliterates the earlier fabrics for a distance of several hundred metres from the Kuboos pluton contact. S_4 has shallow to moderate south to southeast dips (Fig. 25d).

(d) Linear elements

(i) L_1

Penetrative and non-penetrative L_1 lineations are defined by elongated deformed clasts, tectonic straie on competent clasts, preferred platy mineral orientations, and b_1 fold axes. Mullion structures and slickensided striations oriented parallel to the movement direction occur in mylonitic zones. L_1 lineations have shallow NNW plunges (Fig. 30a) which steepen northwards. The trends become more northerly towards the west (mean L_1 trend and plunge changes from 331/09 in the Helskloof area to 340/13 in the Gorab Peak area).

(ii) L_2

Distinctive L_2 lineations are defined by the hinges of the S_2 crenulations which protrude as anastomosing ridges on S_1 in the finer-grained lithologies (Fig. 28). Where S_1 and S_2 are surfaces of rupture, the rock is broken into long pencils with rectangular or rhombic sections. L_2 lineations have NNW-SSE trends with shallow northerly or southerly plunges (Fig. 30b).

(iii) L_3

L_3 lineations are defined by B_3 axes and the intersections between S_3 and the earlier fabrics. L_3 has similar orientations to L_2 (Fig. 30c).

(iv) L_4

A southward-plunging L_4 stretching or mineral lineation is found along the northern margin of the Kuboos pluton (Fig. 30d).

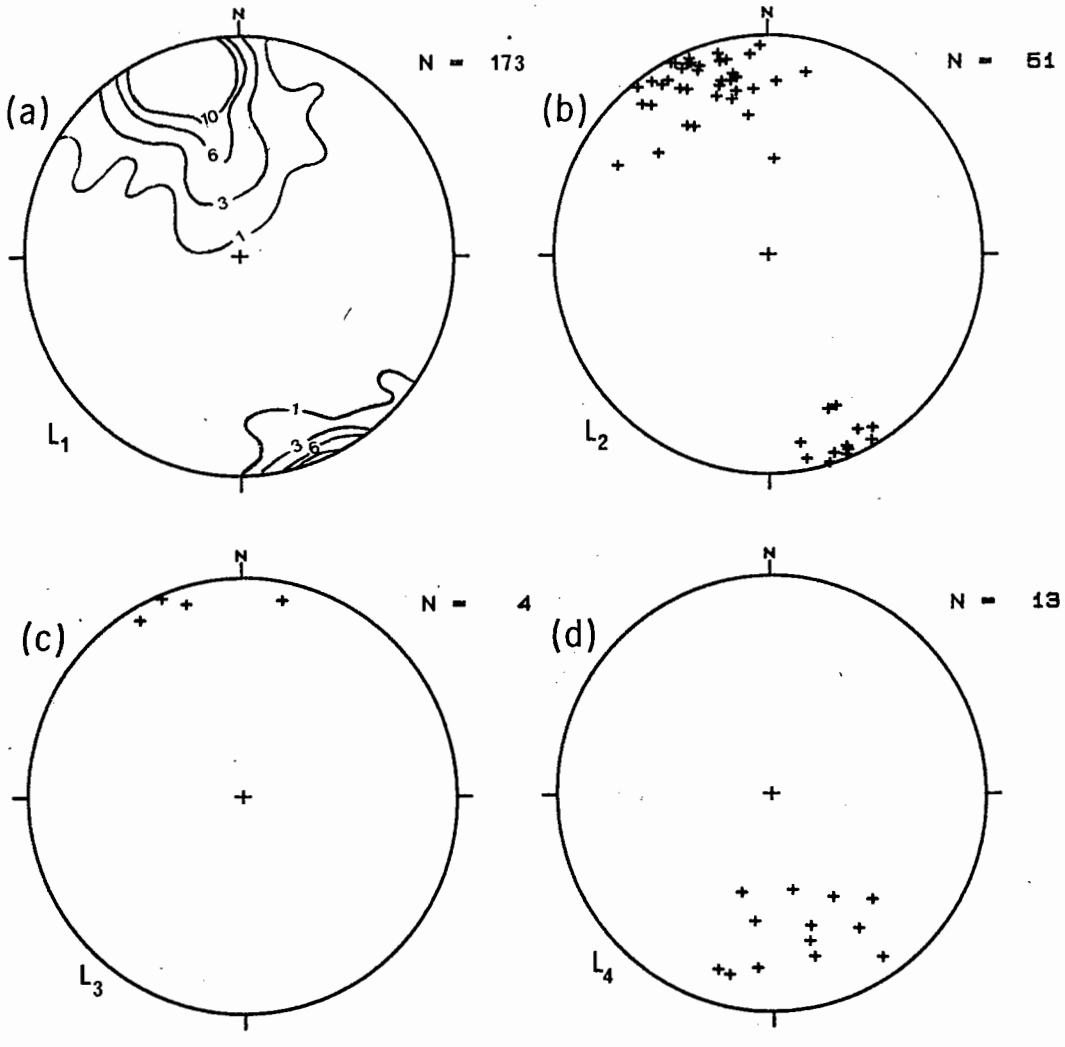

Fig. 30 : Structural orientation data for L_1 - L_4.

3.2.2 Structural domains

In order to describe and interpret the mesoscopic geometry, the area was divided into statistically homogeneous domains, following the method advocated by Turner & Weiss (1963). Each domain is bounded by structural or lithological discontinuities. A graphics-based computer system that provides facilities for statistical processing and plotting of orientation data was developed (Appendix I) and used to define and analyse nine different fabric domains (Fig. 31). A computerized technique for plotting down-plunge projections of orientation data (Charlesworth et al., 1976) was used as an aid in constructing cross-sections of these domains.

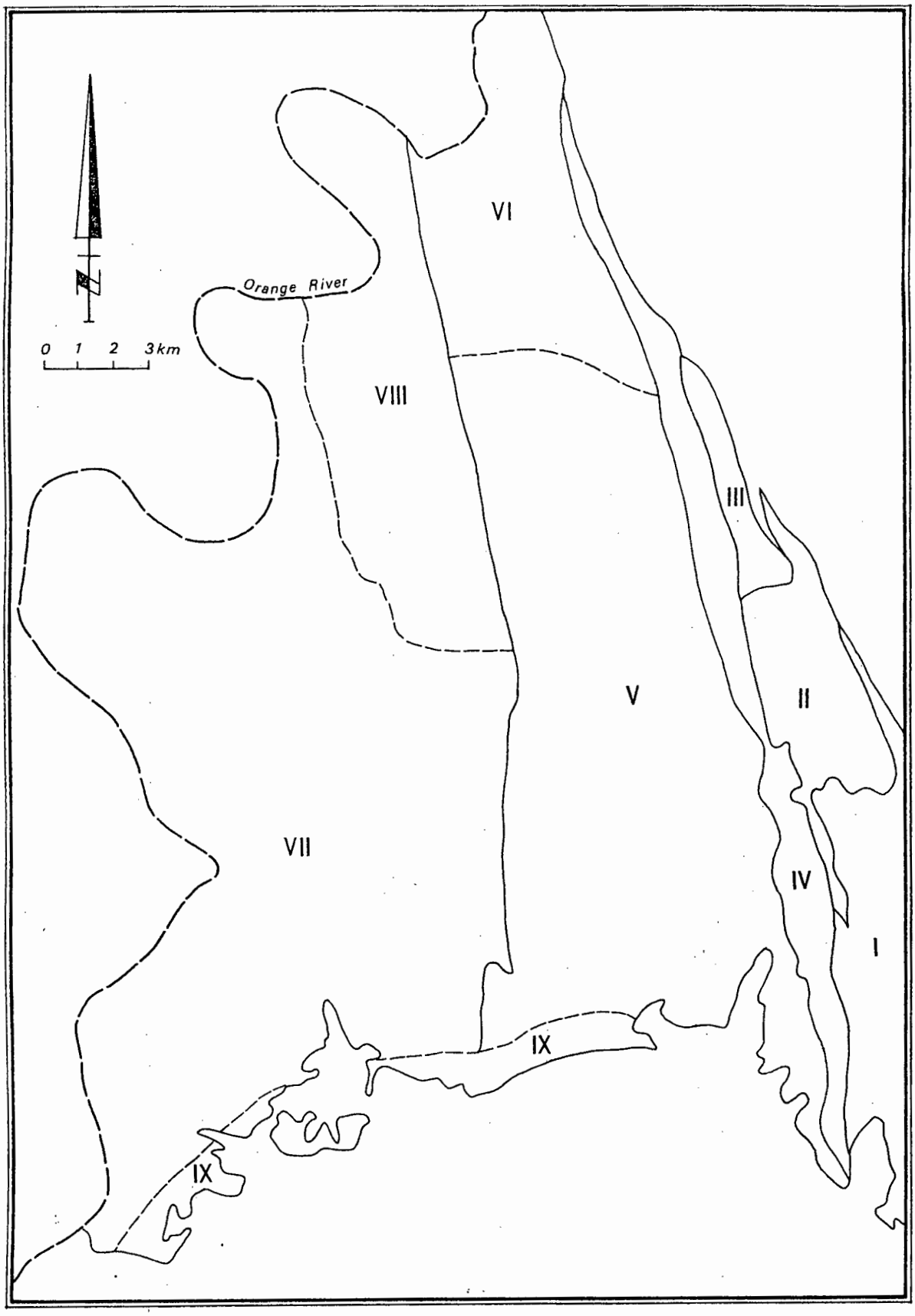

Fig. 31 : Domainal subdivision of the northwestern Richtersveld.

3.2.2.1 Domain I

Domain I, situated south of the Helskloof Pass between the Vandersterrberg and Klipneus faults, is underlain by conglomerate, quartzite, and metavolcanics of the Stinkfontein Sequence.

Mylonitized quartzite and tectonic breccia containing angular blocks of quartzite, gneiss, vein quartz, and quartz-mica schist are present along the basement-Stinkfontein contact. This contact was noted to be a tectonic dislocation by Rogers (1915, p. 84), Joubert (1971, p. 77) and Stowe et al. (1984), although the map of De Villiers & Söhnge (Geological Map of the Richtersveld, Sheet 256, Geological Survey) shows it to be partly unfaulted in the Vandersterrberge. Some of the Gannakouriep dykes, including the main one in the Gannakouriep River valley, maintain their physical continuity across it.

The quartzite within the northern part of the domain is relatively unaffected by faulting as shown by the undisrupted contact with the Kaigas Formation at Helskloof Pass. Further south, thrust faulting phenomena assume increasing importance and have led to thickening and duplication of the local Stinkfontein stratigraphy. A series of fault imbricates repeat a brecciated lava unit in the Bossieshoek valley northeast of the Kuboos pluton .

The domain has a relatively simple internal structure in the north with S_0 and S_1 having moderate to steep dips to the WSW (Figs. 32a, 32b; Table 8). Small-scale folds are rare.

Table 8 : Orientation data statistics for the main fabric elements in domain I derived from orientation tensors. Fabric shape and strength parameters were obtained using the equations of Woodcock (1977, p. 1231-1232, Eqns. 5 and 6). The fabric shape parameter K, where

$$K = \frac{\ln(S_1/S_2)}{\ln(S_2/S_3)}$$

and S_1, S_2, S_3 are normalized eigenvalues, plots in the field $0<K<1$ for distributions with a girdle tendency, and in the field $1<K<\infty$ for cluster distributions. The fabric strength parameter C, where

$$C = \ln(S_1/S_3)$$

has a value C=0 for random distributions, and progressively higher values for increasingly strong preferred orientations (Woodcock, op. cit.).

	S_0	S_1	S_2	L_1	L_2
Vector mean	158/47	160/54	337/43	337/48	332/04
No. of readings	31	23	7	5	4
Fabric shape K	1.46	2.73	1.21	1.02	3.08
Fabric strength	3.43	3.33	4.51	4.93	4.47

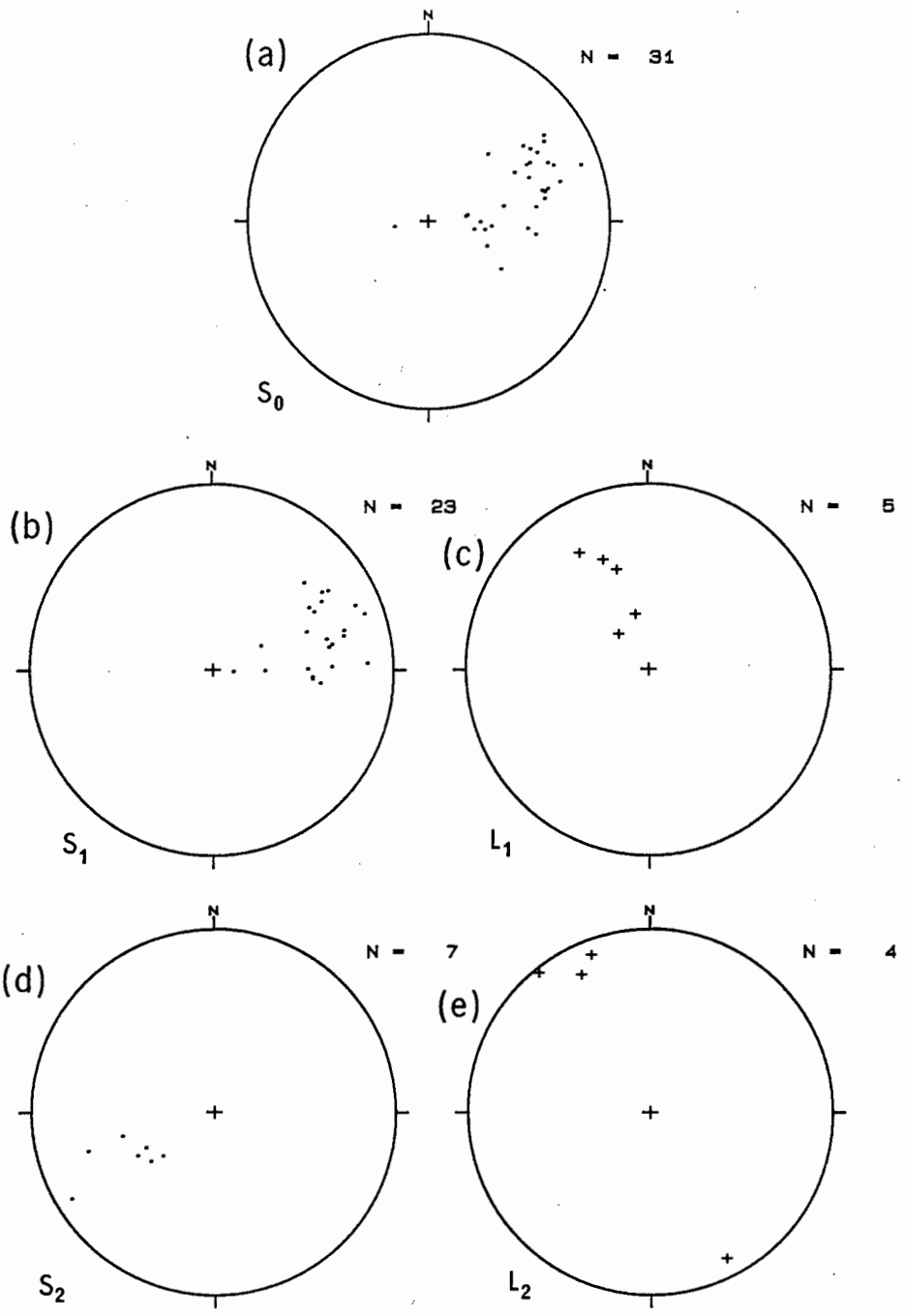

Fig. 32 : Stereonet projections of orientation data for domain I.

3.2.2.2 Domain II

Domain II consists of the Kaigas and Hilda beds in the Helskloof area. It occupies a rectangular area with two tapering branches at either end. Its western and northern margins are defined by the Klipneus, Rio Tinto Camp, Numees, and Vandersterrberg faults, while the eastern margin is bounded by a normal fault contact, the Paradyskloof fault. The unconformity with the underlying Stinkfontein quartzite is exposed in valleys along the southern margin.

The beds are folded into a mesoscopic doubly plunging open syncline and adjacent anticline (Figs. 33a-33c). The synclinal fold axis changes from 319/07 to 154/02 along the axial trace, and the anticline has a northward shoaling axis at 330/10. A thrust fault with a displacement of about 20 m cuts across the axial trace of the syncline before terminating near the Numees summit. The syncline flattens out northwards, and is separated by the failed Numeesberg fault from a smaller syncline that passes into the northern branch of the domain. Some second-order folds that die out upwards are well-exposed in the Helskloof valleys.

The Rio Tinto Camp fault to the west of Numees Prospect duplicates the lava band that is exposed in the Numees valley inlier. A counterpart to the second volcanic unit in the hanging-wall probably occurs below the Kaigas diamictite in the footwall. The Rio Tinto Camp fault dies out into an anticlinal fold at a lateral tip north of Rupping's Prospect.

The poles to S_0 in domain II show a tendency to cluster at two maxima corresponding to the limbs of the major syncline (Fig. 34a). The unconformable relationship between bedding in domains I and II is readily apparent from the respective plots of S_0 (compare Figs. 32a and 34a). S_1 is axial planar to the folds, dipping steeply to the WSW (Fig. 34b). The L_1 fold axes are sub-horizontal (Fig. 34c) because of the control exerted by the flat-lying strata. The L_1 stretching lineations, measured mostly from deformed clasts, have shallower plunges than in the adjacent domains, possibly due to the effects of a dominant pure shear strain on clasts with an initial sub-horizontal primary preferred orientation.

Table 9 : Orientation data statistics for fabrics in domain II. See Table 8 for descriptions of the parameters K and C.

	S_0	S_1	S_2	L_1	L_2
Vector mean	279/04	152/83	328/46	337/02	331/06
No. of readings	135	32	39	44	28
Fabric shape K	0.73	2.60	1.30	7.68	11.79
Fabric strength C	3.08	3.78	4.03	2.34	2.69
Pole to girdle	328/03				

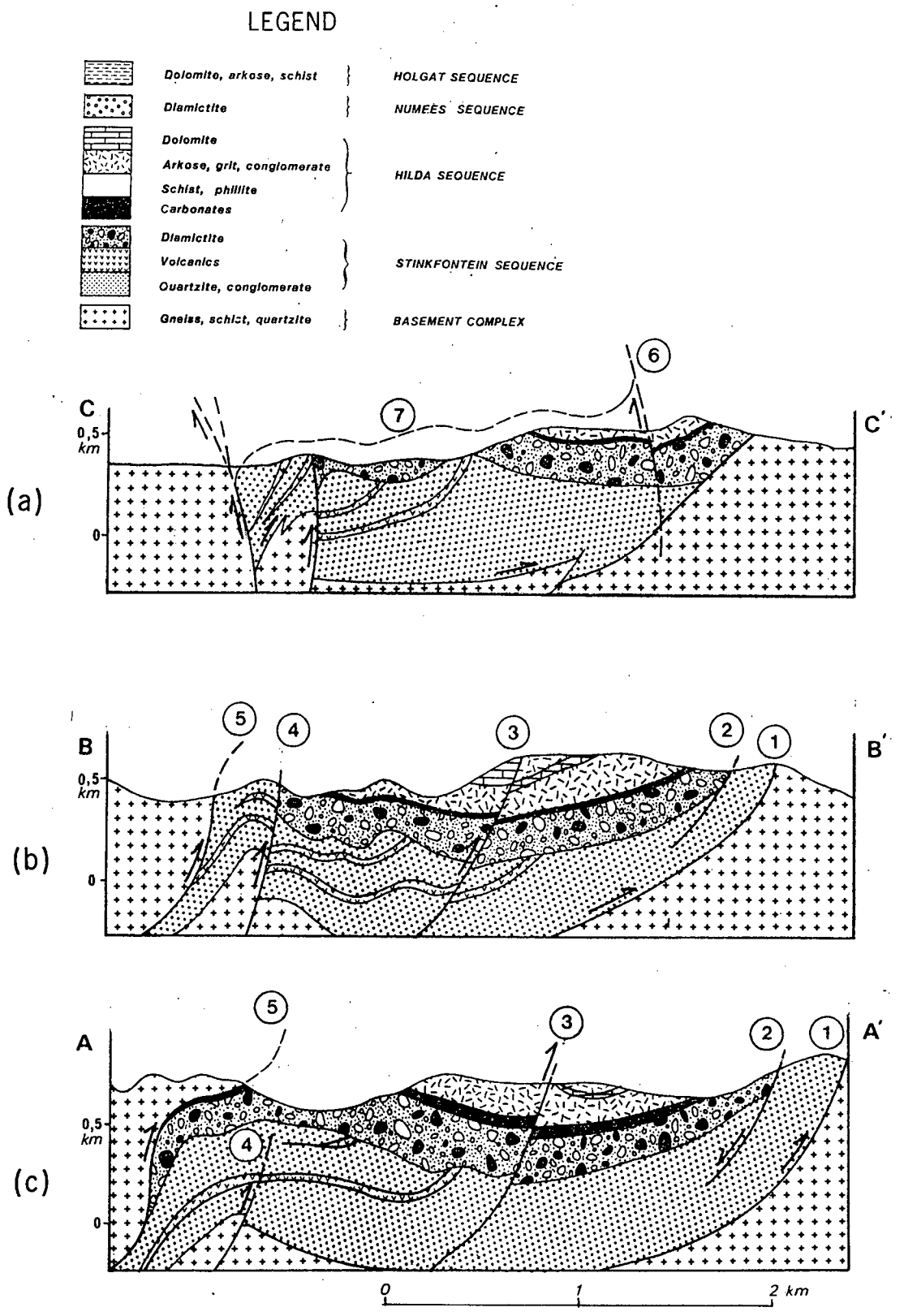

Fig. 33 : Schematic sections at 2 km intervals through the Helskloof area. Section lines are shown in Annexure II. (1) Vandersterrberg fault; (2) Paradyskloof fault; (3) Helskloof fault; (4) Rio Tinto Camp fault; (5) Klipneus fault; (6) Numeesberg fault; (7) Numees fault.

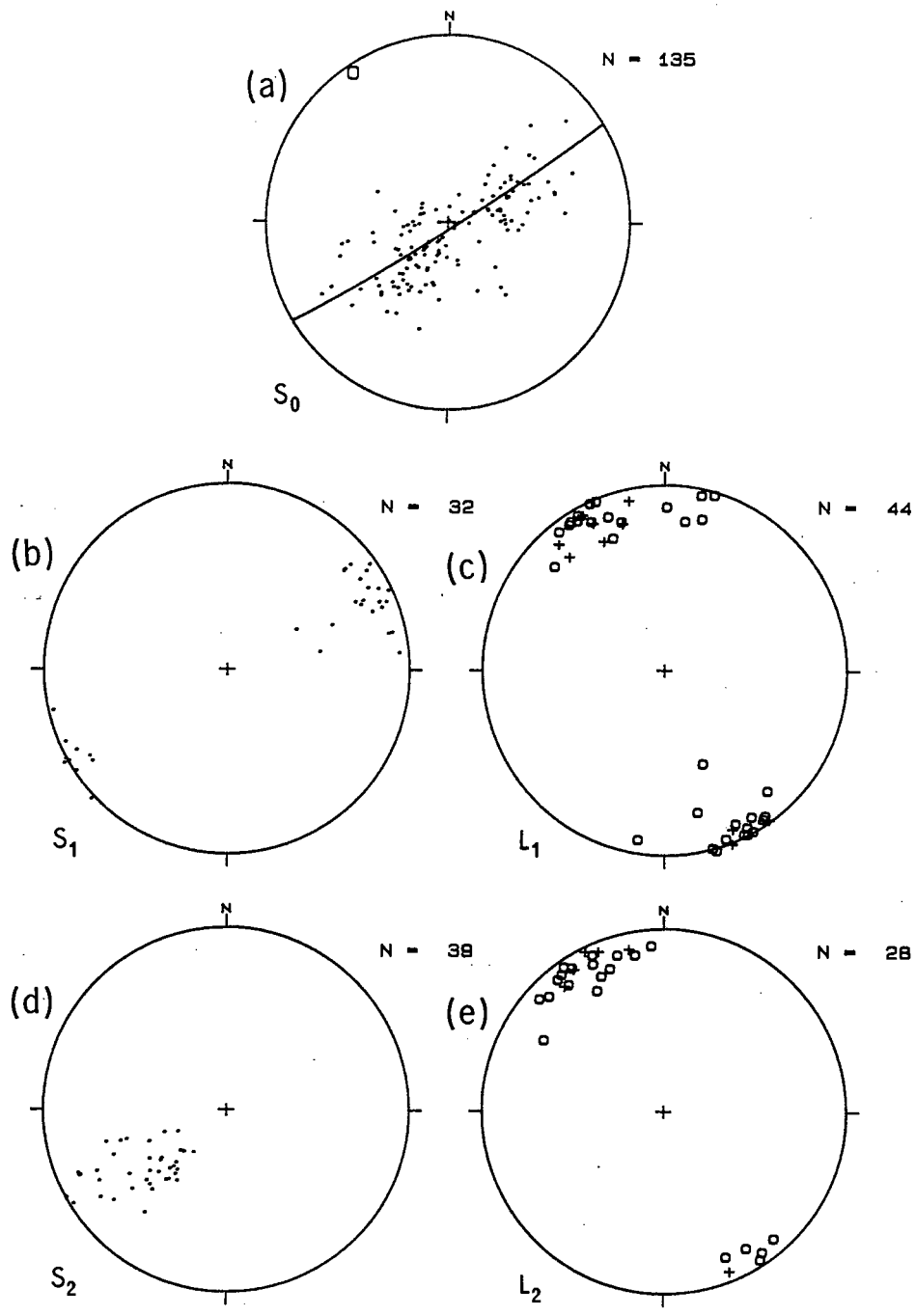

Fig. 34 :Stereonets of fabric elements in domain II.

3.2.2.3 Domain III

Domain III covers the northward continuation of the Stinkfontein quartzite and metavolcanics in the Numeesberge.

The geometry of the faults in this domain can be readily ascertained because of the good relief. Early thrust faults dip in a WSW direction sub-parallel to bedding and imbricate the basement-cover contact (Fig. 35a, 35b). The later faults generally have steep ENE dips and are associated with sinistral wrench movements. They splay into or are cut by east-west striking thrust faults northwest of Kodas Prospect and north of Numees Prospect (the Kodas and Numees cross-faults). The Numees cross-fault, which cuts up-section in a SSE direction, has relayed left-lateral movements from the failed Numeesberg fault to the Klipneus fault. Slip along this cross-fault was sub-parallel to the strike of the Stinkfontein bedding so that the main Numeesberge lava band lies roughly along strike from the one in the Numees Prospect inlier. The NNW-trending faults have been active after the formation of the cross-faults, but later displacements are minimal.

Bedding faces to the west throughout the Numeesberge range. A comparison of the orientation data for domains I and III (Figs. 32, 36 and Tables 8, 10) reveals that S_0 and S_1 in the Stinkfontein quartzites steepen markedly in a northward direction. The fabrics in domain III are locally reoriented into east-west strikes at the cross-faults. L_1 stretching lineations have shallow to steep NNW plunges, and minor F_1 fold axes define a NNW-trending great circle girdle distribution (Fig. 36c). D_2 fabrics are poorly developed in the quartzite.

Table 10 : Orientation data statistics for the main fabric elements in domain III.

	S_0	S_1	S_2	L_1	L_2
Vector mean	152/75	147/89	347/53	337/29	160/03
No. of readings	36	18	5	19	10
Fabric shape K	2.32	2.53	1.08	0.66	2.60
Fabric strength C	3.30	2.95	4.41	2.40	4.64
Pole to girdle				163/79	

3.2.2.4 Domain IV

Domain IV comprises the basement schists, gneisses, and quartzites in the hanging-wall of the Klipneus fault.

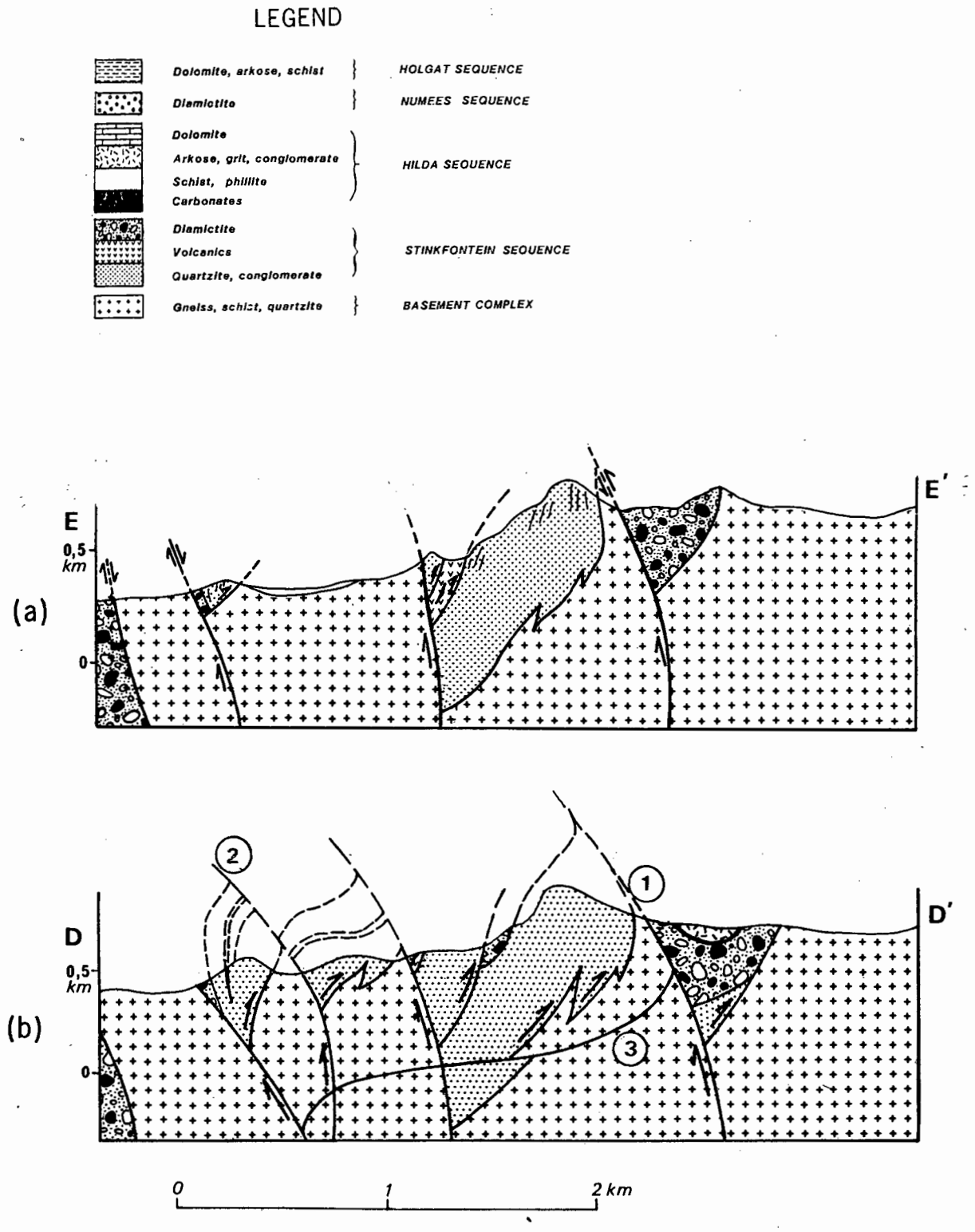

Fig. 35 : Schematic sections through the Numeesberge at 1 km intervals. See Annexure II for the location of the section lines. (1) Numeesberg fault; (2) Klipneus fault; (3) Numees cross-fault.

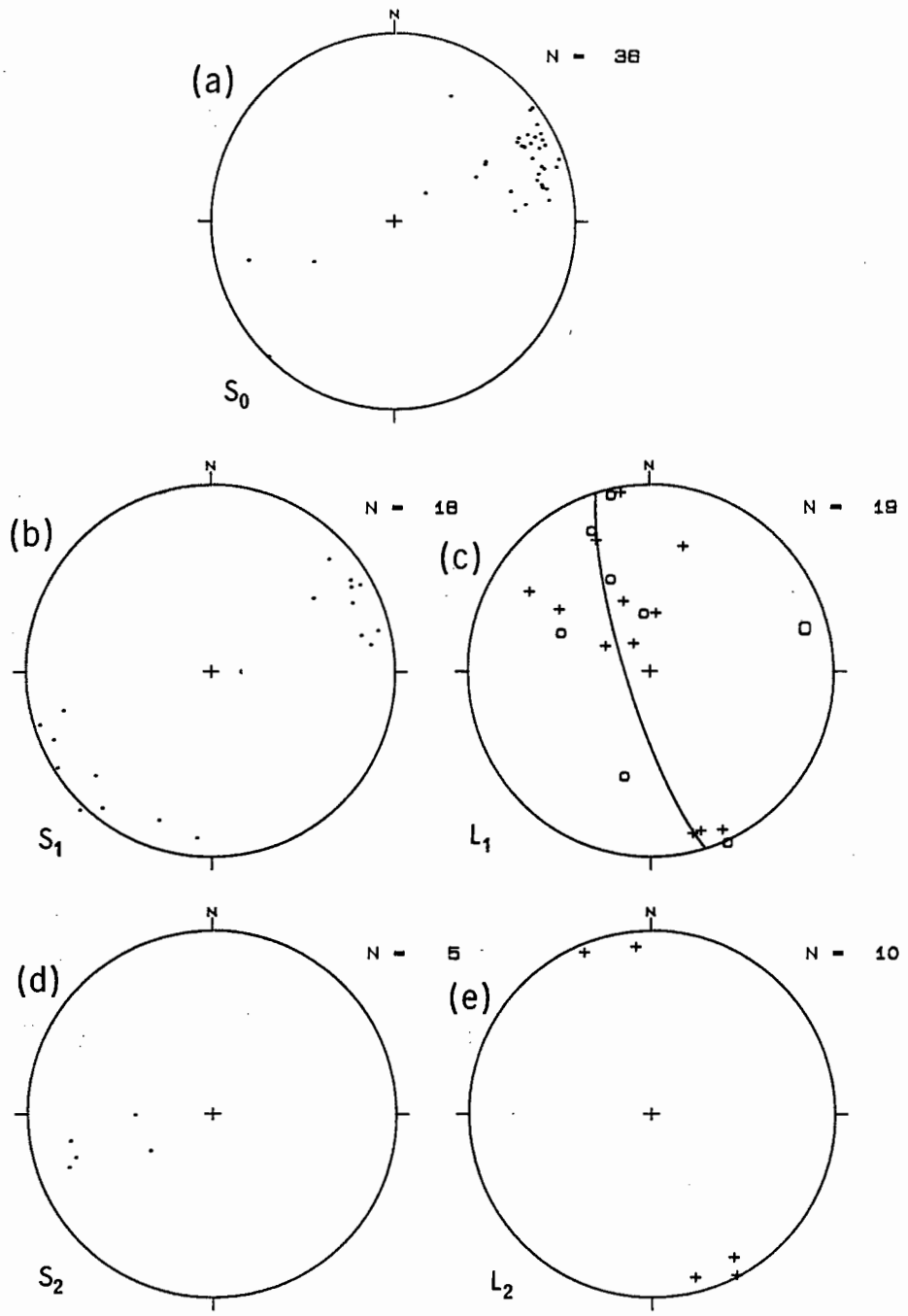

Fig. 36 : Stereonet projections of orientation data for domain III.

The Klipneus fault is a dominant feature in the PNA and can be traced for a distance of over 150 km. It was shown by De Villiers & Söhnge (1959) to continue on the southeastern side of the Kuboos pluton as the Black Hills fault and to join up with the Wildeperderand fault south of Hilda beacon (Geological Map of the Richtersveld, Sheet 256, Geological Survey). On Kröner's (1974) map, the Black Hills fault is shown as a normal fault extending for 5 km southwards from the pluton and as a reverse fault further south, implying rotation about an axis in the Black Hills area. This interpretation is not favoured as basement rocks are exposed along the entire length of the Black Hills fault from Billingham's Prospect to Hilda beacon (Annexure I). The extension of the fault northwards across the Orange River was mapped by McMillan (1968) for a distance of ~20 km in a NNW direction (his Namuskluft fault) and then for another 15 km in a northwest direction.

The fault has a high westerly dip in the southern parts of the study area, shallowing gradually northwards towards Rupping's Prospect. It steepens again rapidly north of the prospect and maintains a sub-vertical or steep easterly dip along the western flank of the Numeesberge. It eventually joins up with the basement-cover fault near Mehlberg.

Domain IV is transected by two major faults. The fault south of Numees Peak duplicates the Rosyntjieberg quartzite and is interpreted as being of Namaqua age (pp. 54, 55). The other fault northwest of the Rio Tinto Camp is of Pan-African age as it emplaces basement granodiorite over a sliver of Stinkfontein quartzite and Kaigas diamictite. It splays from, or is cut off by the Klipneus fault at an unexposed point near the mouth of the Numees valley, and probably joins the Grasvlakte fault on the western side of the Five Sisters ridge.

Intrafolially folded vestiges of an S_1^b cleavage are preserved in the main basement cleavage S_1^n along the southern margin of the granitic body to the east of Swartberg. The granite has acted as a strain shadow, protecting the early fabric from the obliterating effects of later deformations.

S_1^n is difficult to distinguish from S_1, but it can be identified where it is overprinted by later shear cleavages displaying both dextral (S_2^n) and sinistral (S_1) senses of movement. S_1^n is furthermore affected by the F_1-F_4 phases with the result that its poles lie in a great circle girdle (Fig. 37b; Table 11). The associated L_1^n stretching lineation has a more northerly trend and shallower plunge than L_1 (Figs. 37c, 37e).

Table 11 : Orientation data statistics for fabric elements in domain IV.

	S_0	S_1^n	S_1	S_2	L_1^n	L_1	L_2
Vector mean	149/54	155/48	157/61	328/44	178/01	320/52	160/08
No. of readings	8	24	9	12	10	12	8
Fabric shape K	4.82	0.88	3.42	3.44	3.09	1.05	4.48
Fabric strength C	4.71	2.72	3.59	4.48	3.48	3.51	3.32
Pole to girdle		329/07					

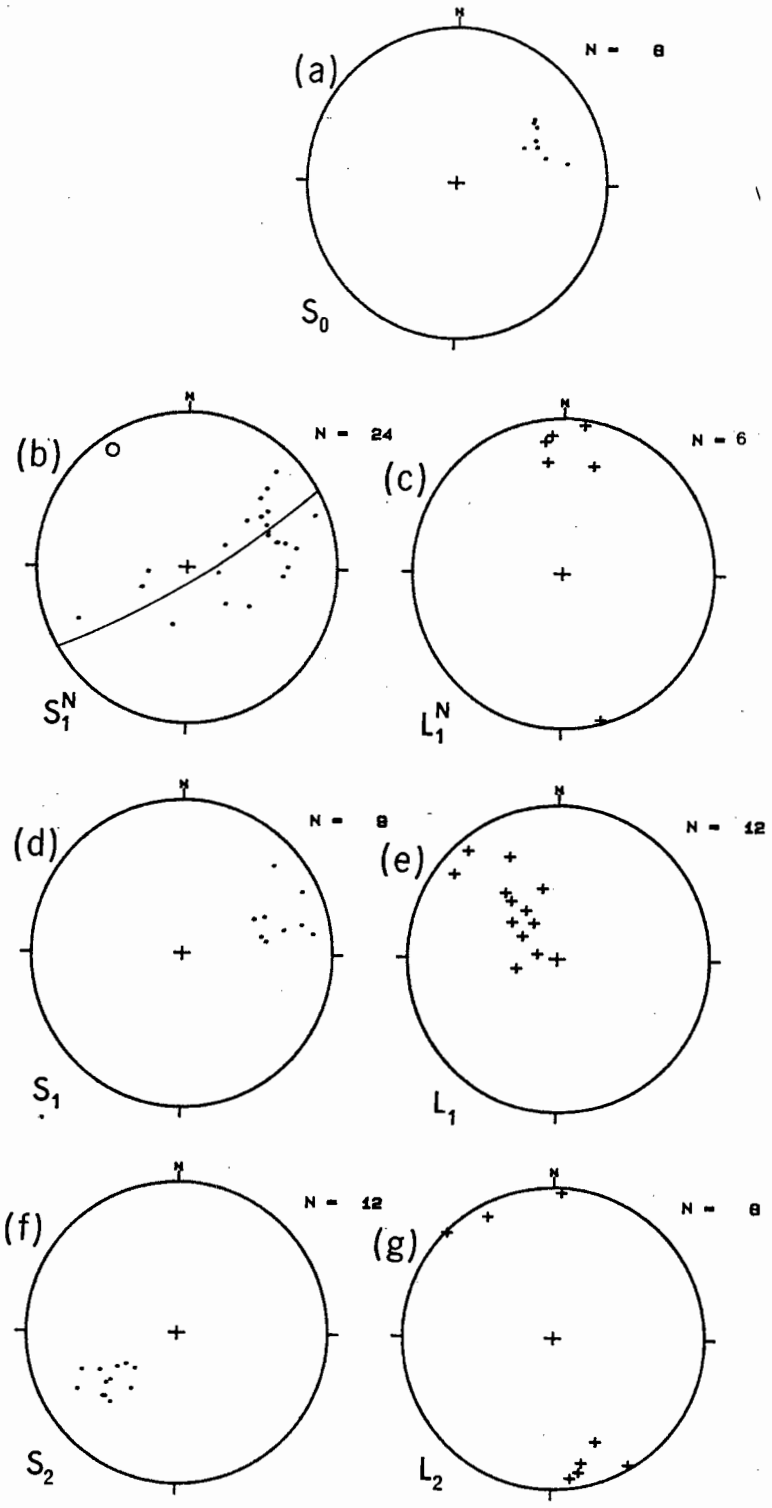

Fig. 37 : Orientation data for domain IV.

3.2.2.5 Domain V

Domain V is underlain by Stinkfontein quartzite, Hilda schist, quartzite, and conglomerate, and Kaigas and Numees diamictite in the southern part of the Klipneus fault hanging-wall. The large-scale structure is that of an east-vergent intraplate fold, the Sendelingsdrif synclinorium, that tightens and steepens in a northward direction (Figs. 38a, 38b).

The Jakkalsberg fault, located along the base of the Numees Sequence dies out southwards near Swartberg. The displacements associated with it appear to be taken up by an isolated splay at a higher stratigraphic level. The importance of tectonic repetition of stratigraphy is generally difficult to assess in this domain because of lateral facies changes in the Hilda and the monotonous nature of the Numees beds.

Minor folds are poorly developed in the southern part of the domain, but become increasingly evident northwards. The calcareous schists at Remhoogte Peak are folded into tight, upright F_1 folds with wavelengths in the order of 10-20 m. The steeply dipping Khubus beds of the Hilda Sequence are warped by open eastwardly inclined F_2 folds, so that the dip directions alternate across axial traces. An F_2 fold west of the Nabab River can be traced northwards to cut the Hilda-Numees contact at Gorab River.

The poles to S_0 lie in a great circle girdle normal to a NNW-plunging B-axis at 335/08 (Fig. 39a; Table 12). The great circle distribution of S_1 (Fig. 39b) is due to the steepening of the foliation in a northerly direction and the effects of the F_2 folding. Its axial planar relationship to the major fold is readily apparent in the hinge zone at Remhoogte Peak. The L_1 lineations have shallow NNW plunges parallel to the axis of the major fold (Fig. 39c).

Table 12 : Orientation data statistics for fabrics in domain V.

	S_0	S_1	S_2	L_1	L_2
Vector mean	156/78	168/58	335/40	344/17	344/11
Number of readings	63	111	47	46	16
Shape parameter K	0.20	0.30	1.27	2.19	1.71
Strength parameter C	2.86	3.10	4.07	4.09	3.66
Pole to best-fit girdle	335/08	343/08			

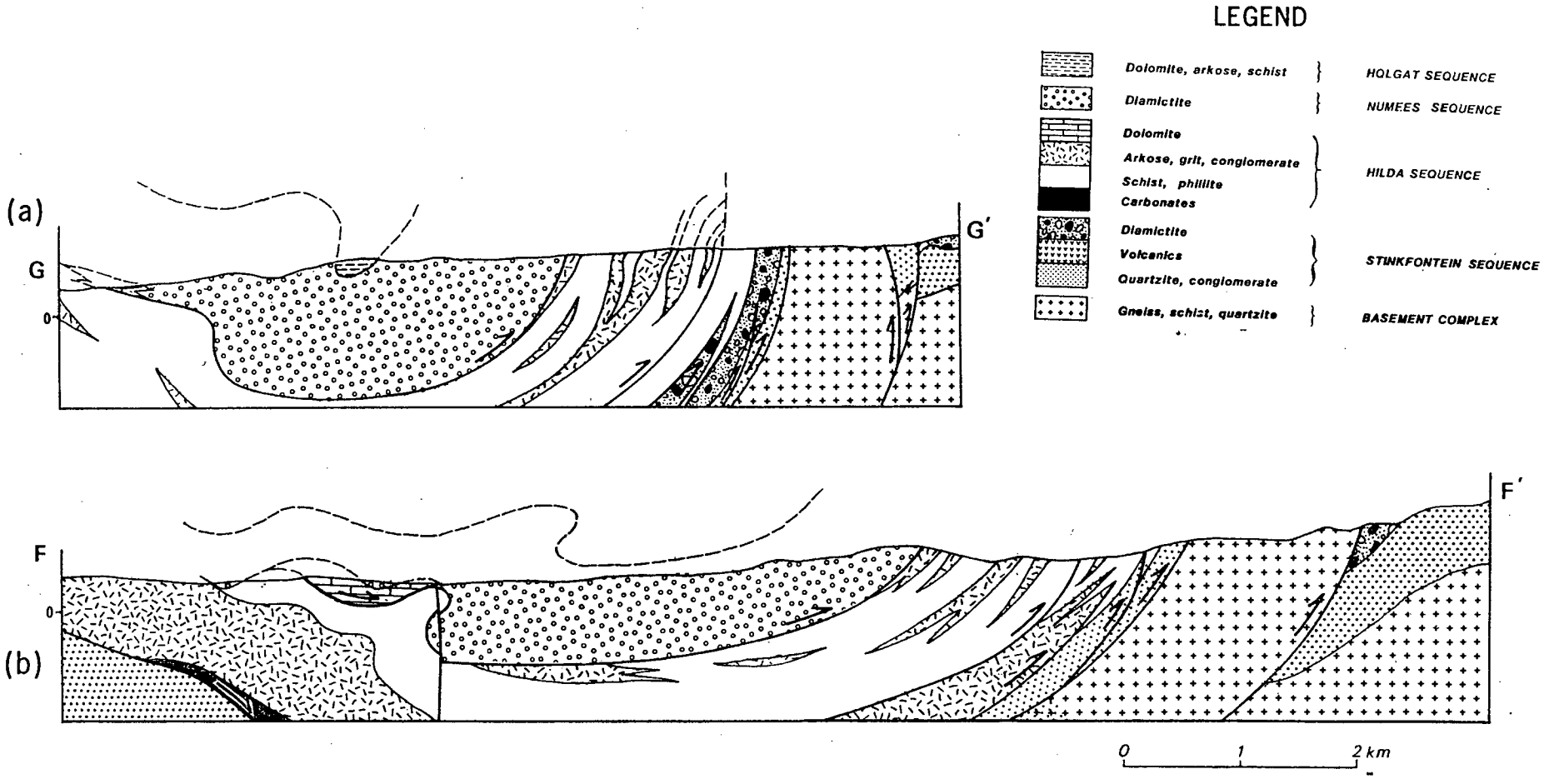

Fig. 38 : Sections through the southern part of the Sendelingsdrif synclinorium. See Annexure II for section lines.

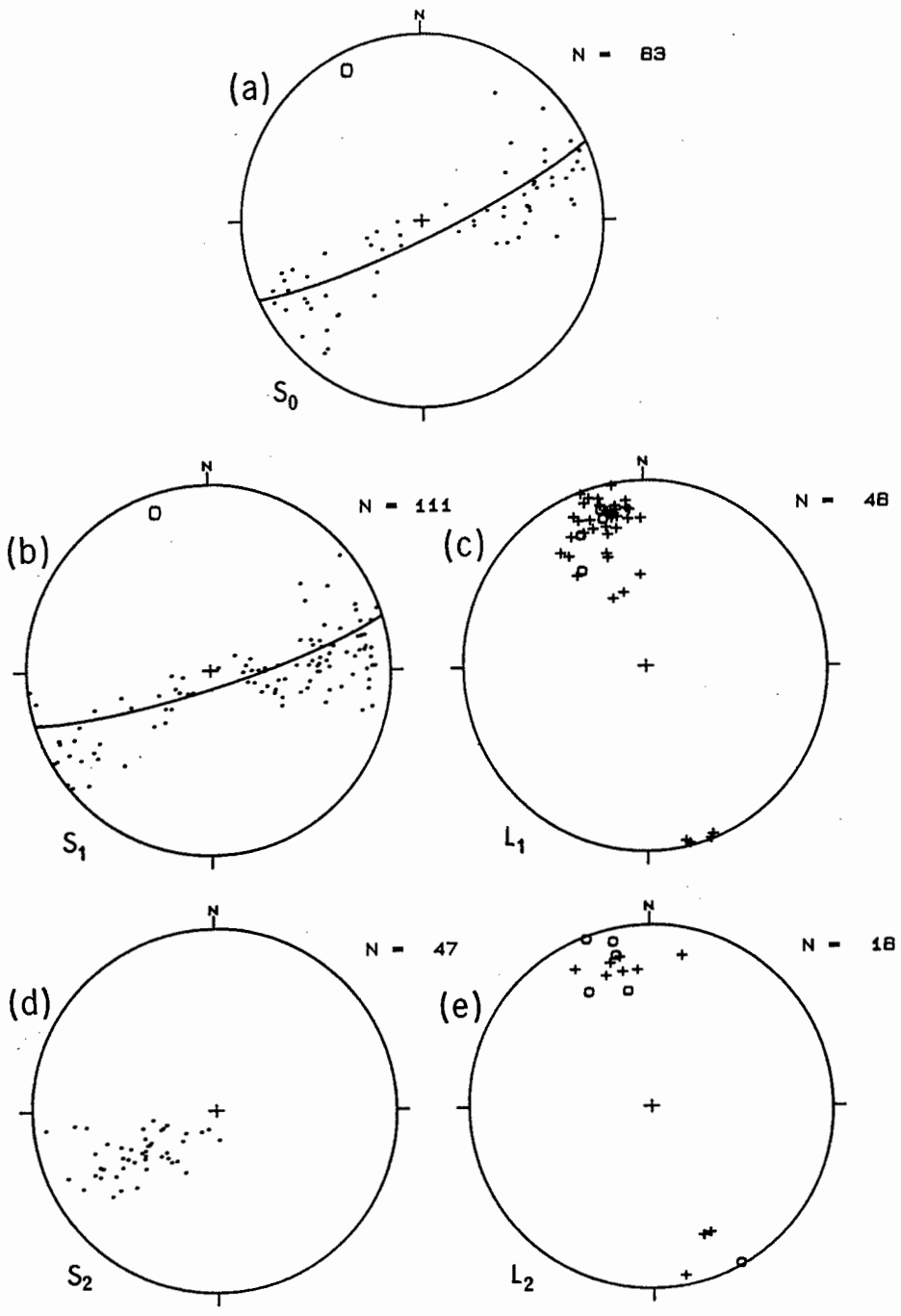

Fig. 39 : Stereonet projections of orientation data readings for domain V.

3.2.2.6 Domain VI

Domain VI is underlain by the Five Sisters dolomite and the Kaigas and Numees diamictite in the Grasvlakte area. It differs from domain V in that both limbs of the Sendelingsdrif fold dip to the east (Fig. 40). The western limb steepens progressively northwards and becomes sub-parallel to the eastern limb at Jakkalsberg. The fold closure is visible on aerial photographs north of the Orange River.

The S_0 and S_1 orientation data reflects the northward steepening of the large-scale structure (Fig. 41; Table 13). L_1 lineations cluster about a maxima with a significantly steeper NNW plunge than for domain V and are markedly oblique to the major fold axis (mean B-axis 160/01), suggesting a shear folding mechanism. The D_2 structures have similar orientations in domains V and VI.

Table 13 : Orientation data statistics for fabric elements in domain VI.

	S_0	S_1	S_2	L_1	L_2
Vector mean	338/84	341/81	331/45	349/41	344/21
Number of readings	43	72	31	54	14
Shape parameter K	2.73	1.86	1.80	1.84	5.60
Strength parameter C	3.00	3.33	3.68	3.21	4.49

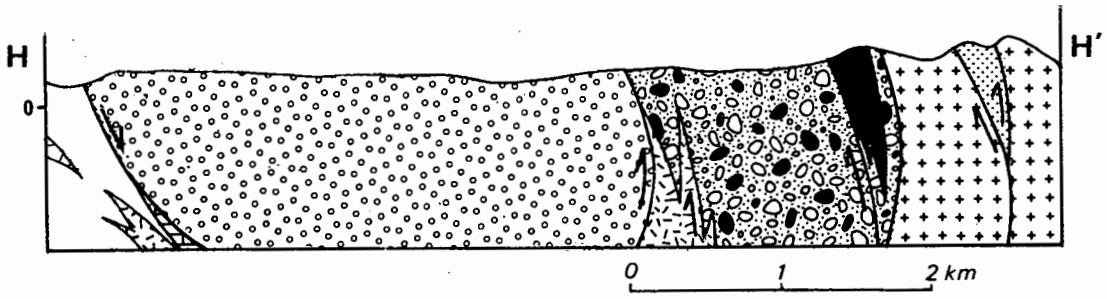

Fig. 40 : Cross-section through the northern part of the Sendelingsdrif synclinorium. Section line is shown in Annexure II.

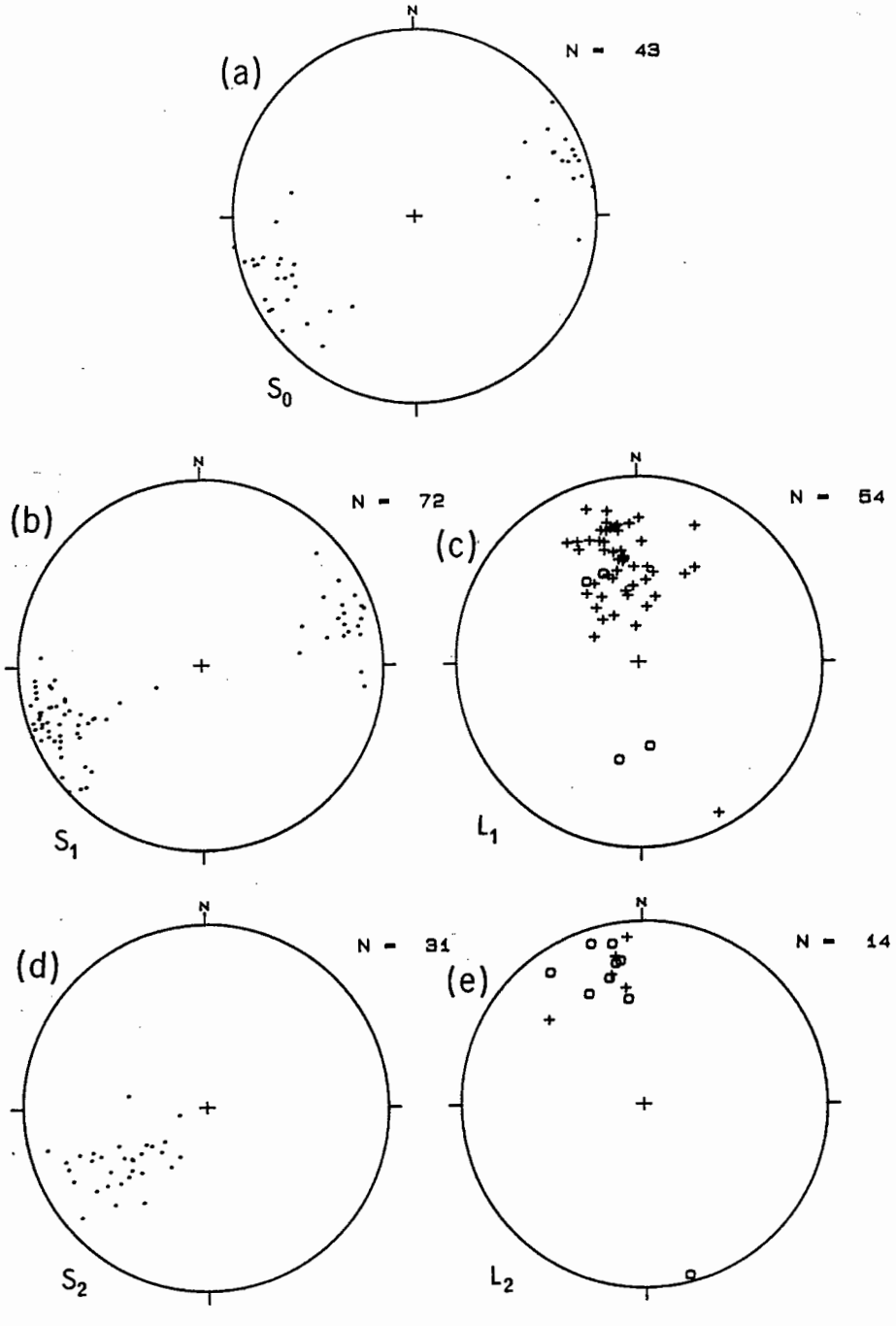

Fig. 41 : Stereonet projections of orientation data readings for domain VI.

3.2.2.7 Domain VII

Domain VII is situated in the western part of the area and makes up most of the Annisfontein anticlinorium. The anticlinorium is a relatively flat-lying open structure with a hinge zone that flattens out and an eastern limb that steepens in a northward direction (Figs. 42a, 42b). A number of fault imbricates repeat the local stratigraphy in the hinge and western limb, and schuppen structures are exposed in the Gorab River valley where the Gorab fault is folded around the anticlinorium. The Gorab fault is cut off by the Annis fault, which thrusts Gumchavib quartzite over Hilda beds in the Wallekraal area. The Hilda sequence has its thickest development and shows the most repetition of stratigraphy at a culmination near Roussouw's Prospect.

S_0 and S_1 planes have very shallow dips, mostly to the WSW (Fig. 43; Table 14). S_1 is sub-parallel to S_0 and not axial planar to it because of the development of the anticlinorium by thrust stacking.

Table 14 : Orientation data statistics for fabrics in domain VII.

	S_0	S_1	S_2	L_1	L_2
Vector mean	159/21	175/10	327/39	340/04	161/01
Number of readings	85	42	7	24	16
Shape parameter K	1.72	0.96	1.44	3.06	2.86
Strength parameter C	3.39	4.34	2.52	3.30	3.96
Pole to best-fit girdle		348/00			

3.2.2.8 Domain VIII

Domain VIII, located within the eastern limb of the Annisfontein fold north of the Gorab River, is defined as a separate domain because of the abundance of minor F_1 and F_2 folds. The open anticline at the Roussouw's Prospect can be traced northwards to Gorab Peak where it becomes the dominant fold (Fig. 44b). It folds the Gorab fault and its eastern flank is cut by the Gumchavib fault to the north (Fig. 44a).

The Gumchavib fault continues northwards across the Orange River towards Gumchavib Peak where it exposes basement rock. The fault cuts the western flank of a major doubly-plunging anticline around which the Pickelhaube fault is folded (Annexure I). The Pickelhaube fault is thus interpreted as the footwall continuation of the Gorab fault. The Pickelhaube fault probably joins up with the Klipneus-Namuskluft fault at depth.

The increased intensity of folding in domain VIII is demonstrated by the great circle girdle distributions of poles to S_0 and S_1 (Figs. 45a, 45b; Table 15). The L_1 lineations, which are mostly sub-horizontal in domain VII, become shallow NNW-plunging in domain VIII (Fig. 45c).

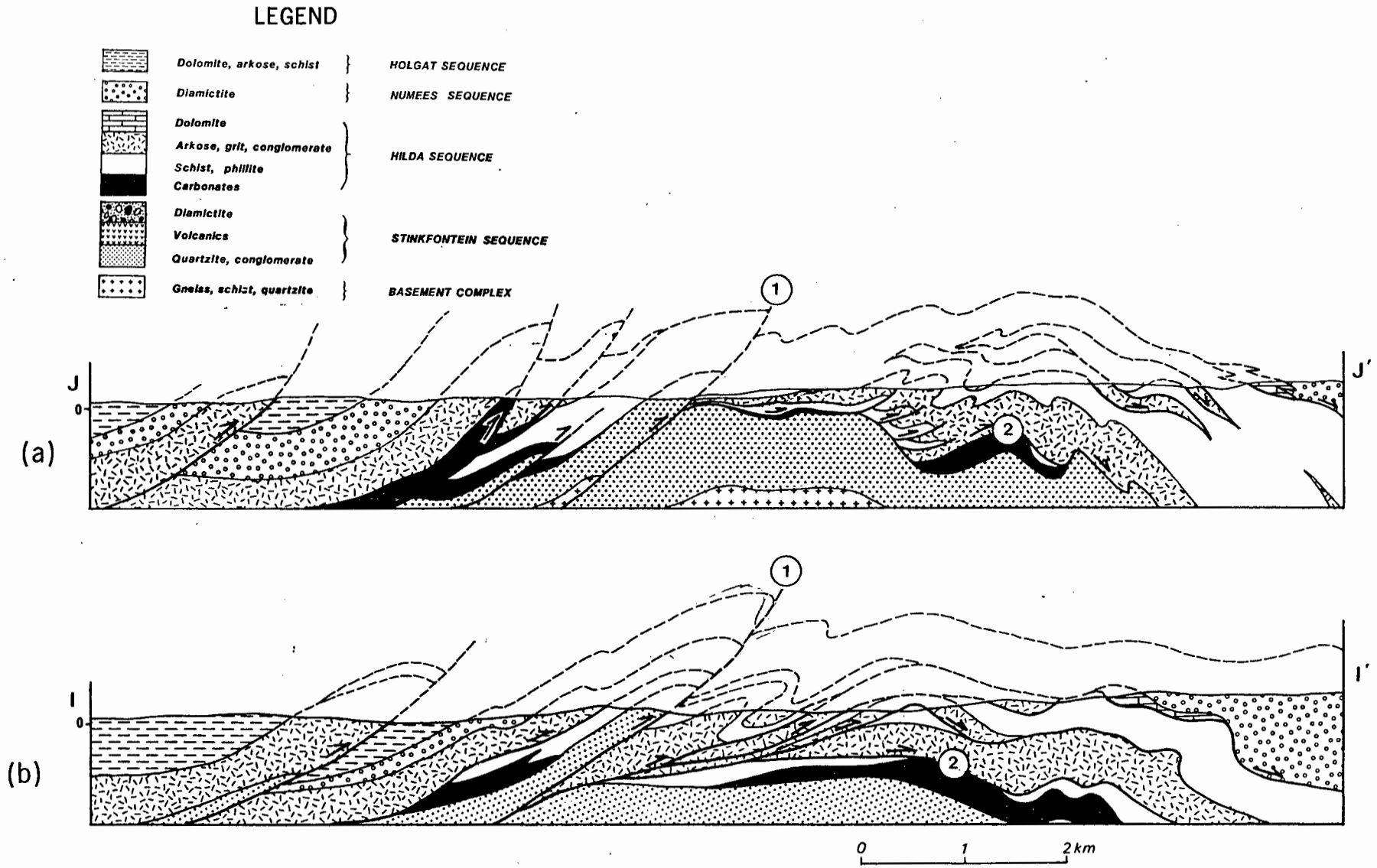

Fig. 42 : Sections through the Annisfontein anticlinorium at 5 km intervals. See Annexure II for the location of section lines. (1) Annis fault; (2) Gorab fault.

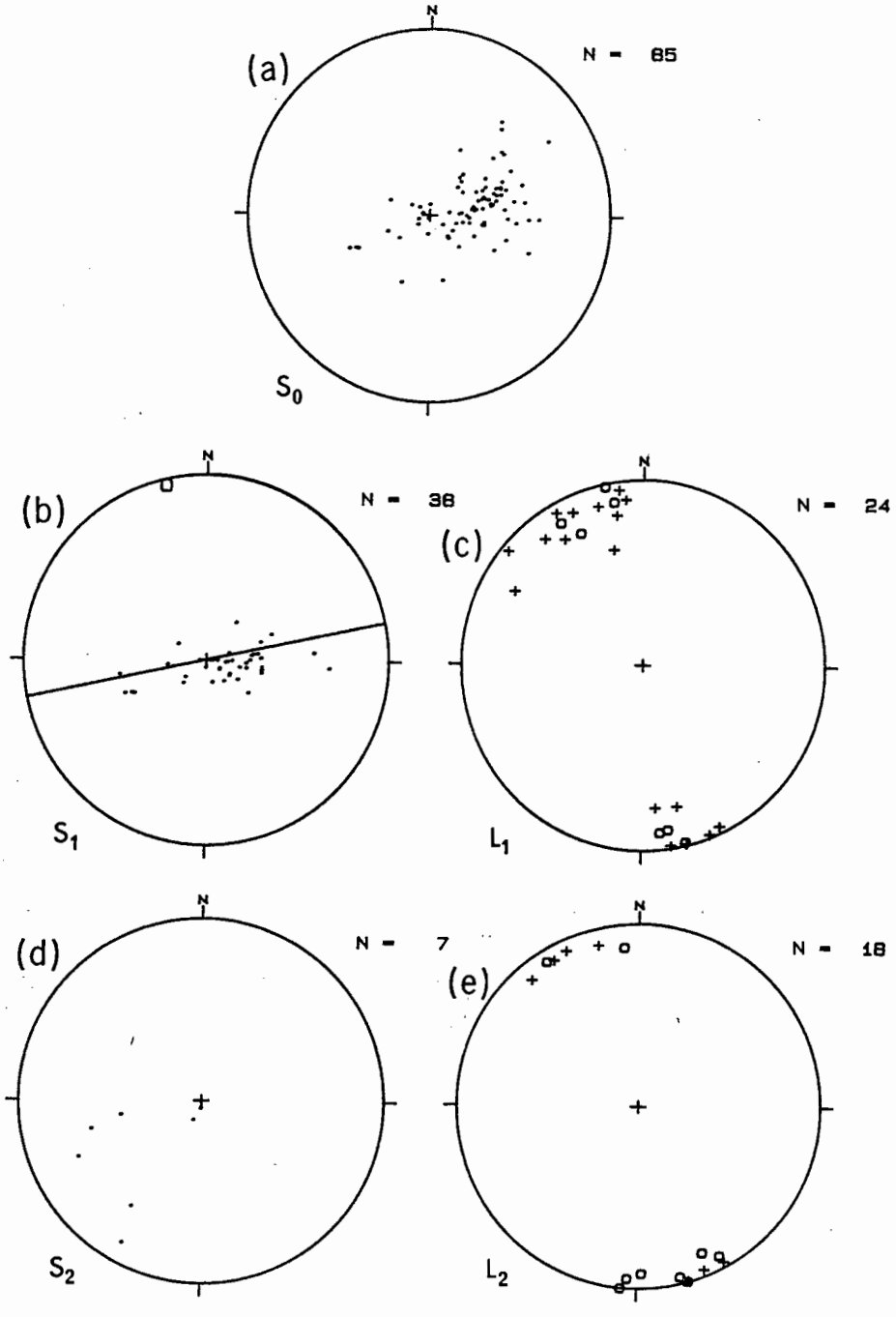

Fig. 43 : Stereonet diagrams of structural data for domain VII.

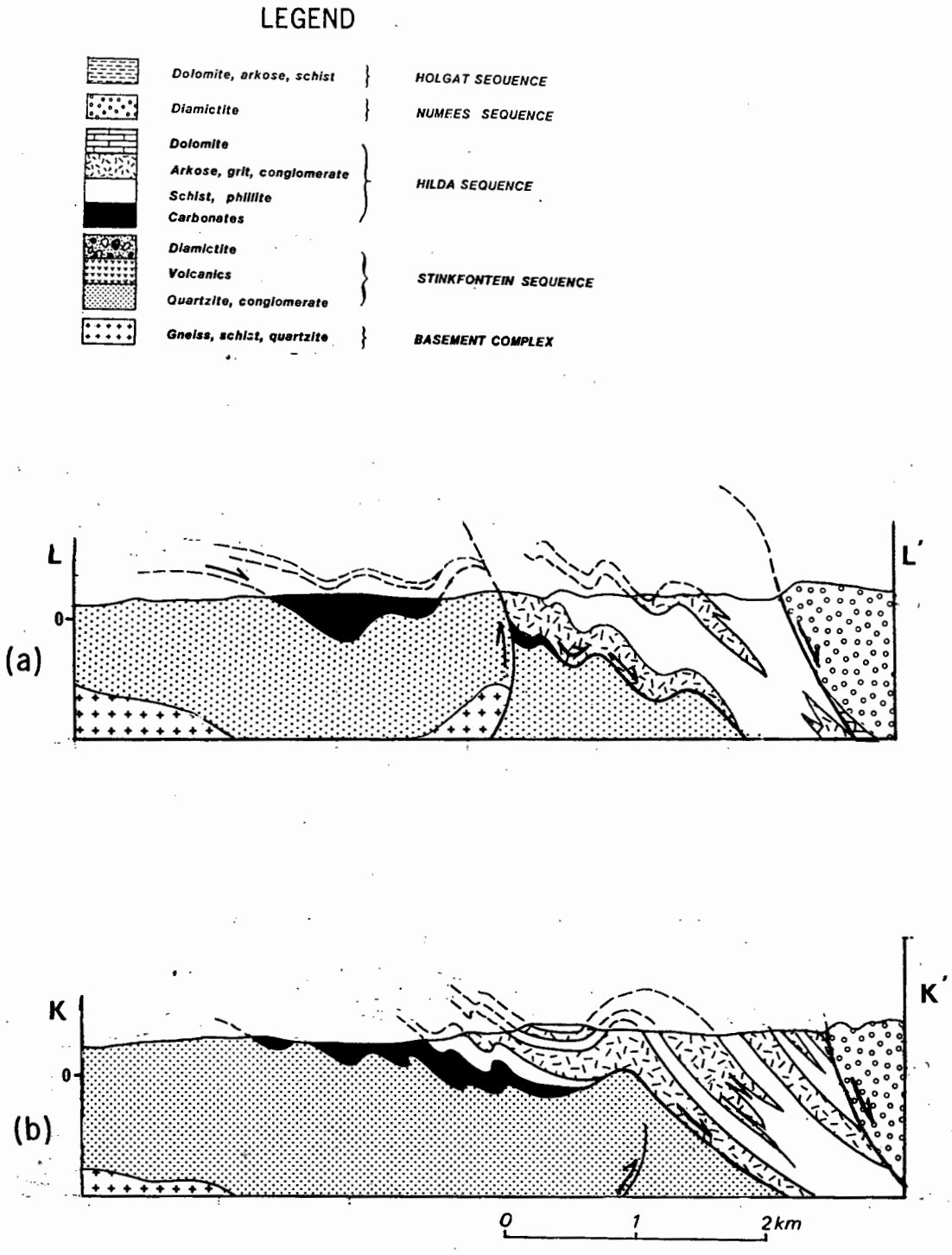

Fig. 44 : Schematic cross-sections showing the Annisfontein fold structure north of the Gorab River. See Annexure II for section lines.

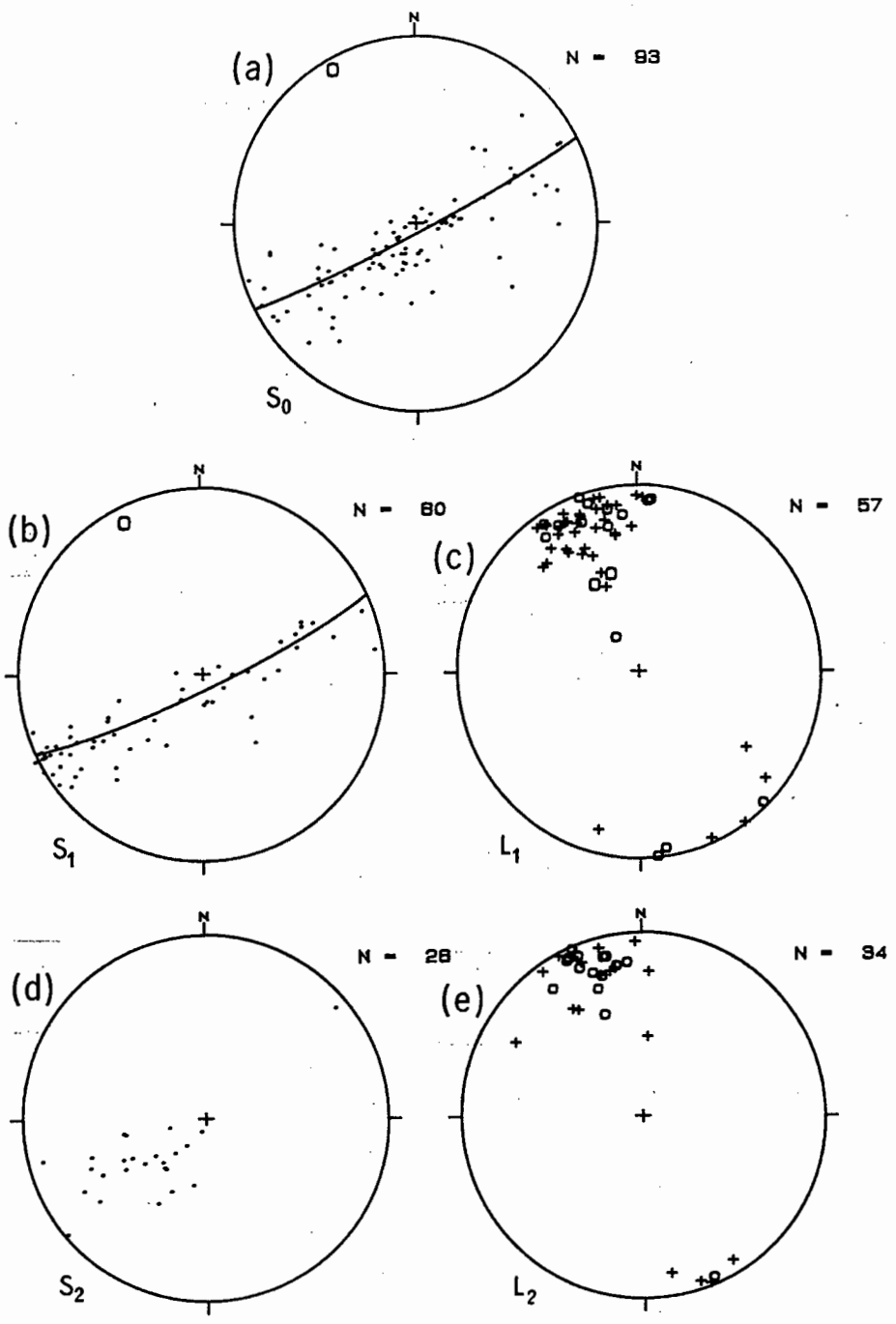

Fig. 45 : Stereonet diagrams of structural data for domain VIII.

The best-fit B_1 axis for the two domains has a northward plunge (331/06), although the anticlinorium has a southerly plunge in map view. This apparent discrepancy between the mesoscopic and macroscopic structures can be attributed to the tightening of the anticlinorium in a northward direction, the northward decrease in topographic elevation, and the down-bending of strata near the Kuboos pluton contact.

Table 15 : Orientation data statistics for fabrics in domain VIII.

	S_0	S_1	S_2	L_1	L_2
Vector mean	316/14	332/66	330/37	340/14	340/11
Number of readings	93	60	26	57	34
Shape parameter K	0.31	0.16	1.22	8.03	4.89
Strength parameter C	3.06	3.50	3.44	2.86	3.35
Pole to best-fit girdle	333/04	335/07			

3.2.2.9 Domain IX

Domain IX covers the narrow zone of plastic deformation in the Kuboos pluton aureole. The pre-existing fabrics have been rotated into parallelism with the pluton contact which dips inward, so that S_0 and S_1 dip to the southeast along its northwestern margin, south in its northern part, and southwest along its northeastern margin. The best-fit distributions to S_0 and S_1 are small circle girdles (Figs. 46a, 46b; Table 16). The more easterly trend of the B-axis to S_0 is due to a sampling bias as many of the S_0 readings were taken from the western part of the domain where bedding is better preserved. L_1 lineations have been rotated to have SSE plunges (Fig. 46 c). The D_2 fabrics have also been reoriented, S_2 being rotated into SSE-ward dips and L_2 having low NNE-ward plunges (Figs. 46d, 46e).

Table 16 : Orientation data statistics for fabrics in domain IX.

	S_0	S_1	S_2	L_1	L_2
Vector mean	062/36	058/36	033/26	163/31	030/12
Number of readings	40	23	6	10	3
Shape parameter K	0.72	0.86	2.33	2.37	1.32
Strength parameter C	2.91	2.93	3.73	3.40	4.37
Pole to best-fit small circle girdle	162/39	176/40			
Half apical angle	78	78			

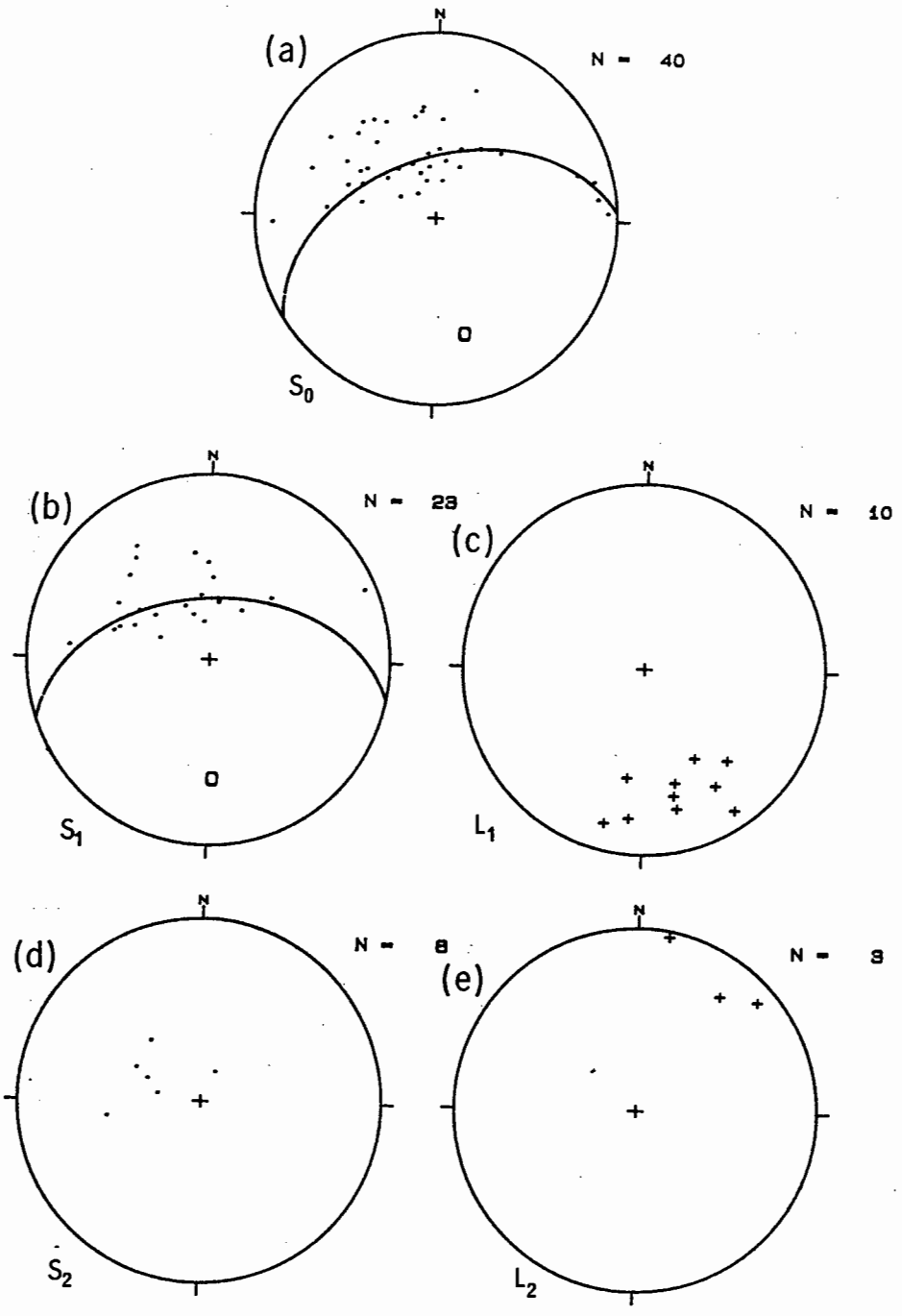

Fig. 46 : Stereonet diagrams for structural data in domain IX.

3.3 Kinematic analysis

Three kinematic phases can be identified from a reconstruction of the translations, rotations, dilations, and distortions associated with the deformational events: a transpressive or convergent wrenching phase, a simple parallel wrenching phase, and a transtensive or divergent wrenching phase.

3.3.1 Transpressive phase

3.3.1.1 Rigid body analysis

The dip directions of the D_1 faults and the sense of vergence of the associated F_1 folds indicate that the transport direction was in a 180° arc about an ENE direction. The l_1 mineral and stretching lineations constrain it to have been towards the southeast or SSE. Left-lateral differential movements are evident from the offset of crosscutting features, drag of bedding, and vergence of shear bands.

The hinges of the F_1 folds are thus sub-parallel or at a low angle to the transport direction, a phenomenon that has been described from field studies in numerous other thrust belts, including the southern Appalachians (Bryant & Reed, 1969) and the Caledonian Belt in Scotland and Scandinavia (Lindström, 1961; Roberts, 1974; Rhodes & Gayer, 1977; Coward & Kim, 1981). Whether the axes form at an angle to the transport direction originally and then rotate into alignment with it, or whether they are sub-parallel to the transport direction throughout their development has not been satisfactorily resolved (Sanderson, 1973; Watkinson & Cobbold, 1981; Jacobson, 1983).

The distances of transport of the faults are poorly constrained because of the paucity of early cross-cutting features. Estimates of contraction from balanced cross-sections (Dahlström, 1969; Price, 1981) are precluded because the majority of the faults are oblique ramps and the plane strain assumption cannot be met (cf. Elliott, 1983).

A strike-slip shift of ~20 km in the adjacent basement is indicated from the 35° sinistral deflection of the Gannakouriep dykes from 210° to 175° over a distance of 26 km as the Gariep Belt is approached. The Klipneus fault displaces the Rosyntjieberg Formation-De Hoop Subgroup contact southwards for a distance of ~11 km from an extrapolated position in the vicinity of Kodas to southeast of Numees Peak, and the De Hoop volcanics-Vioolsdrif granodiorite contact by some 15 km from Sendelingsdrif to Rupping's Prospect. A dip-slip component of at least 4 km is apparent from the thickness of the Klipneus sheet so that the net slip is in the order of 15,5 km. The displacement on the ~230 km Schakalsberg-Marmora fault zone is at least 16 km if the rule that displacement ~0,07 * fault length (Elliott & Johnson, 1980) is followed, and more than 100 km if the bow-and-arrow rule of Elliott (1976a) is applied.

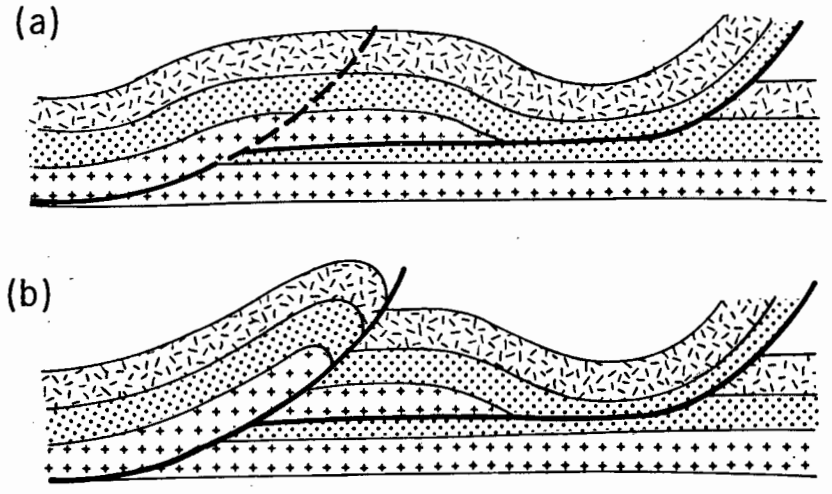

Fig. 48 : (a) A ramp anticline; (b) A compound ramp anticline (after Boyer, 1986, p. 335).

From a comparison of structures in the northwestern Richtersveld with those in the adjoining areas it is evident that there is a systematic along-strike variation in fabric style and orientation that can be attributed to a progressive northward increase in wrench shear strain.

To the south, in the major Eksteenfontein-Dolomite Peaks section, thrust faulting phenomena are dominant (Fig. 49). The stratigraphy is extensively imbricated and the L_1 lineations plunge to the northwest or west, at a moderate to high angle to the F_1 fold hinges. To the north in the Rosh Pinah area, abundant, tight en-echelon folds with steep east-dipping axial planes, a strong L_1 stretching lineation parallel to the strike of bedding, and strike-slip tear faults are consistent with wrench shear deformation.

3.3.1.2 Finite strain analysis

(a) Method and assumptions

A strain determination from deformed clasts in the Kaigas and Numees diamictites and Hilda conglomerate was undertaken to further constrain the kinematic history of the area. Outcrops at suitably spaced intervals with three faces at high angles to each other were located and photographed. Tracings of strain markers were prepared from the photographs, and a developed computer software system (Appendix II) was used to measure the ellipse axial ratios and long axis orientations, determine the two-dimensional finite strains, and combine the two-dimensional data to yield a three-dimensional solution.

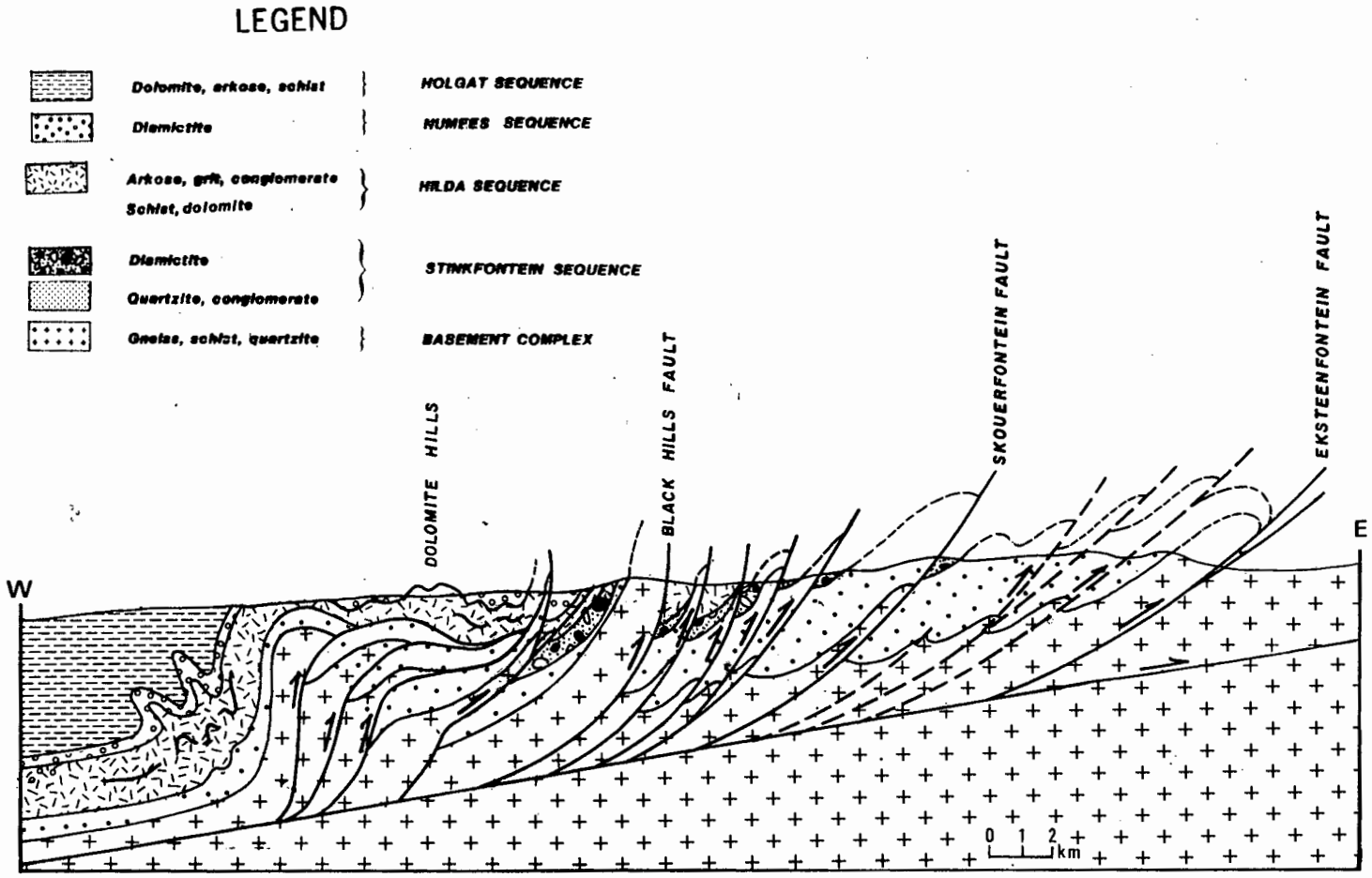

Fig. 49 : Schematic section through the PNA in the central Richtersveld, showing possible subsurface geometry of faults.

Finite strain analysis techniques that use elliptical markers embody a number of assumptions:

- The undeformed markers approximated to ellipsoidal shapes;
- The deformation was homogeneous on the specimen scale;
- No ductility contrast was present between the particles and the matrix;
- The initial fabric was random.

The validity of some of these assumptions is questionable, particularly in the case of the diamictite samples, so that the strain estimates given here should be viewed with caution and regarded as minimum values.

The angular relationships of the strain ellipsoids were compared by plotting stereonet projections of the principal (XY) planes and the maximum principal (X) axes onto a map. The deformational aspects were evaluated by determining and plotting the Flinn k- and d-values. The k-value describes the shape or degree of oblateness or prolateness of the ellipsoid and is defined by:

$$k = \frac{a - 1}{b - 1}$$ (Ramsay, 1967, p. 137)

where a = maximum (X) axis / intermediate (Y) axis
and b = intermediate (Y) axis / minimum (Z) axis of the strain ellipsoid.

For prolate ellipsoids, $\infty > k > 1$, for plane strain ellipsoids, $k = 1$, and for oblate ellipsoids, $1 > k > 0$.

The d-value emphasises the amount of deformation recorded in a strain ellipsoid and is defined by:

$$d = [(a - 1)^2 + (b - 1)^2]^{1/2}$$ (Ramsay & Huber, 1983, p. 202)

(b) Results

The principal planes of the strain ellipsoids are sub-horizontal to the south, becoming steeply dipping to the northeast (Table 17; Fig. 50). The principal X - axes have NNW plunges which steepen northwards. Southward plunges occur in the down-bent strata adjacent to the Kuboos pluton. The average strain ellipsoid has kinematic axes a = 339/27, b = 159/63, c = 066/01.

The ellipsoids have very variable shapes (Fig. 51, 52). Strongly deformed prolate ellipsoids tend to be found in a wide zone in the northern part of the area, while oblate ellipsoids occur to the south and southwest. Highly constricted ellipsoid shapes are located along faults (e.g. sample 579) and in the proximity of the Kuboos pluton.

Table 17 : Finite strain data. Latitudes and longitudes are expressed in degrees, minutes, seconds, and elevations are in metres (A.M.S.L). Rock types are CN- conglomerate or coarse grit, DI- pebbly schist.

Sample no.	latitude	longitude	elevation	strain ratios a	b	k-value	d-value	XY plane	X axis	rock type
308	17 0 32	28 19 39	480	1.223	1.321	.695	.391	340/87	158/16	DI
324	16 53 58	28 18 58	260	2.466	1.619	2.367	1.591	173/25	345/04	DI
336	16 51 44	28 19 10	177	1.253	2.023	.247	1.054	142/14	172/06	CN
353	16 54 11	28 22 14	195	1.628	2.791	.351	1.898	333/15	343/00	DI
362	16 52 53	28 22 21	157	1.867	1.808	1.074	1.185	210/22	344/17	CN
371	16 53 44	28 24 13	120	2.124	1.530	2.120	1.243	156/18	158/02	DI
374	16 54 58	28 23 13	205	2.205	1.337	3.572	1.251	002/12	166/02	DI
386	16 56 49	28 21 11	100	1.340	1.861	.395	.926	335/81	328/16	DI
398	16 59 30	28 26 29	220	2.398	1.085	16.471	1.401	032/84	066/80	CN
417	16 58 25	28 17 45	480	1.258	2.652	.156	1.672	334/80	339/22	DI
421	16 59 26	28 20 10	645	1.754	1.361	2.091	.836	032/35	058/16	DI
429	17 0 14	28 19 53	520	1.306	1.469	.651	.560	011/14	030/04	DI
435	16 57 4	28 18 0	325	1.399	1.253	1.579	.472	322/85	351/56	CN
437	16 56 41	28 18 36	390	1.397	1.482	.825	.624	332/86	336/35	CN
440	16 51 25	28 21 57	100	1.461	2.302	.354	1.381	170/20	242/20	CN
455	16 55 14	28 18 36	380	1.676	1.485	1.392	.832	176/79	348/36	DI
473	16 53 28	28 10 20	480	1.713	1.677	1.054	.983	340/88	342/44	DI
475	16 54 59	28 11 12	130	4.706	1.712	5.205	3.774	147/80	303/67	CN
480	16 52 55	28 11 23	68	2.155	2.547	.747	1.931	348/74	357/27	DI
493	16 55 48	28 15 51	242	2.355	1.063	21.371	1.356	328/72	336/24	CN
497	16 56 16	28 18 50	380	1.397	1.860	.461	.947	332/84	342/55	DI
545	16 51 57	28 13 30	90	1.624	1.145	4.304	.641	324/74	143/03	CN
547	16 52 41	28 14 12	120	2.869	1.817	2.288	2.040	338/53	151/10	CN
548	16 51 53	28 15 14	225	1.674	1.948	.711	1.163	340/45	345/05	CN
550	16 55 33	28 12 4	215	1.556	1.962	.578	1.111	320/70	003/62	CN
551	16 51 22	28 14 7	160	1.652	1.492	1.327	.817	322/79	330/30	CN
554	16 54 16	28 10 14	85	2.219	1.785	1.553	1.450	335/74	350/41	DI
577	16 56 5	28 13 46	240	2.173	2.366	.859	1.801	354/80	009/54	DI
579	16 55 10	28 14 10	175	41.147	2.407	28.528	40.172	335/84	342/48	DI
582	16 56 28	28 15 4	225	2.833	1.275	6.668	1.854	340/78	350/38	DI
584	16 57 22	28 14 55	270	1.393	1.592	.664	.711	168/78	342/24	CN
588	16 53 51	28 11 4	60	6.142	2.466	3.506	5.347	316/70	341/49	DI
589	16 57 3	28 18 51	395	2.162	1.877	1.325	1.456	332/76	341/32	CN

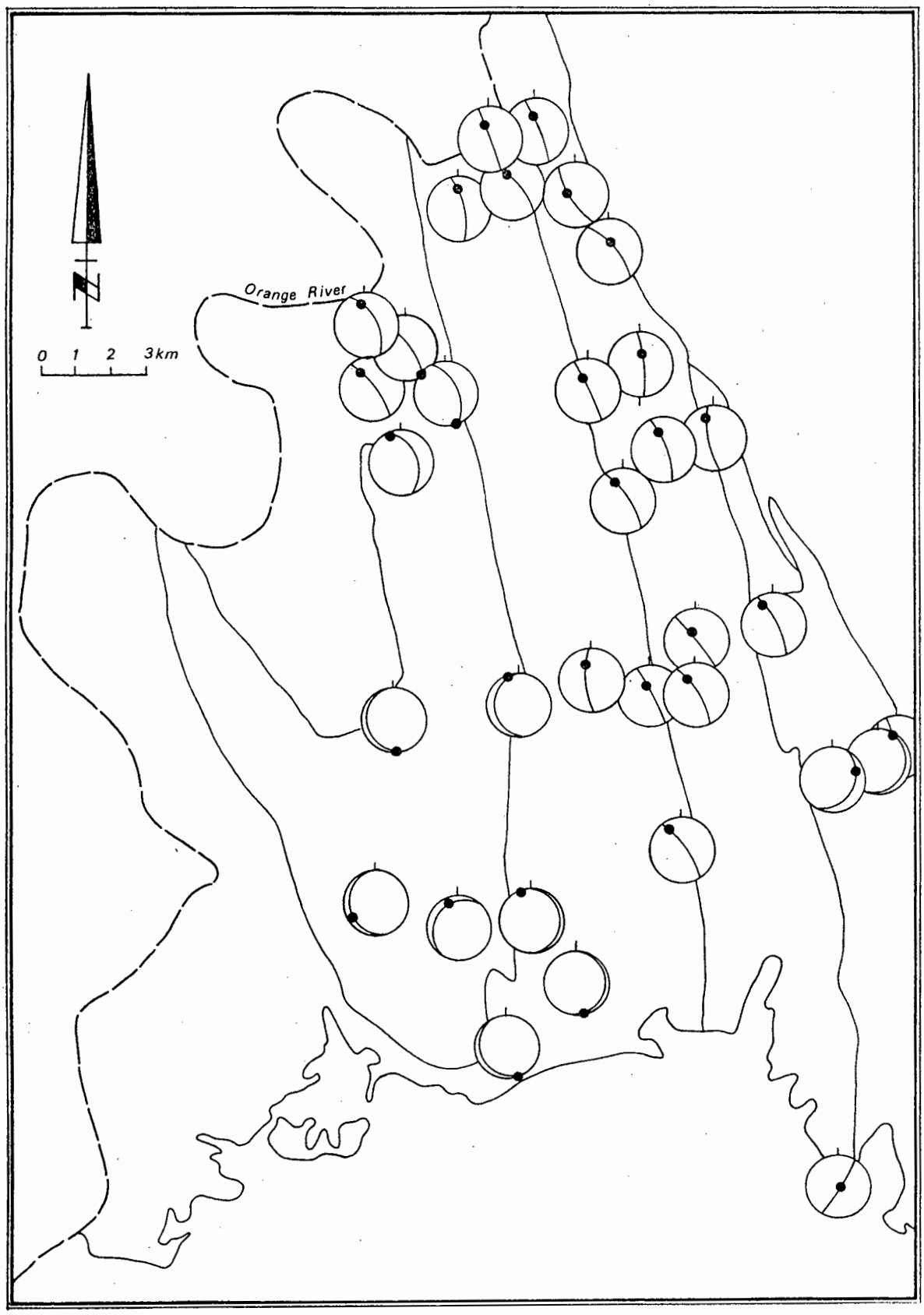

Fig. 50 : Map of the northwestern Richtersveld showing the variation in orientation of the strain ellipsoid.

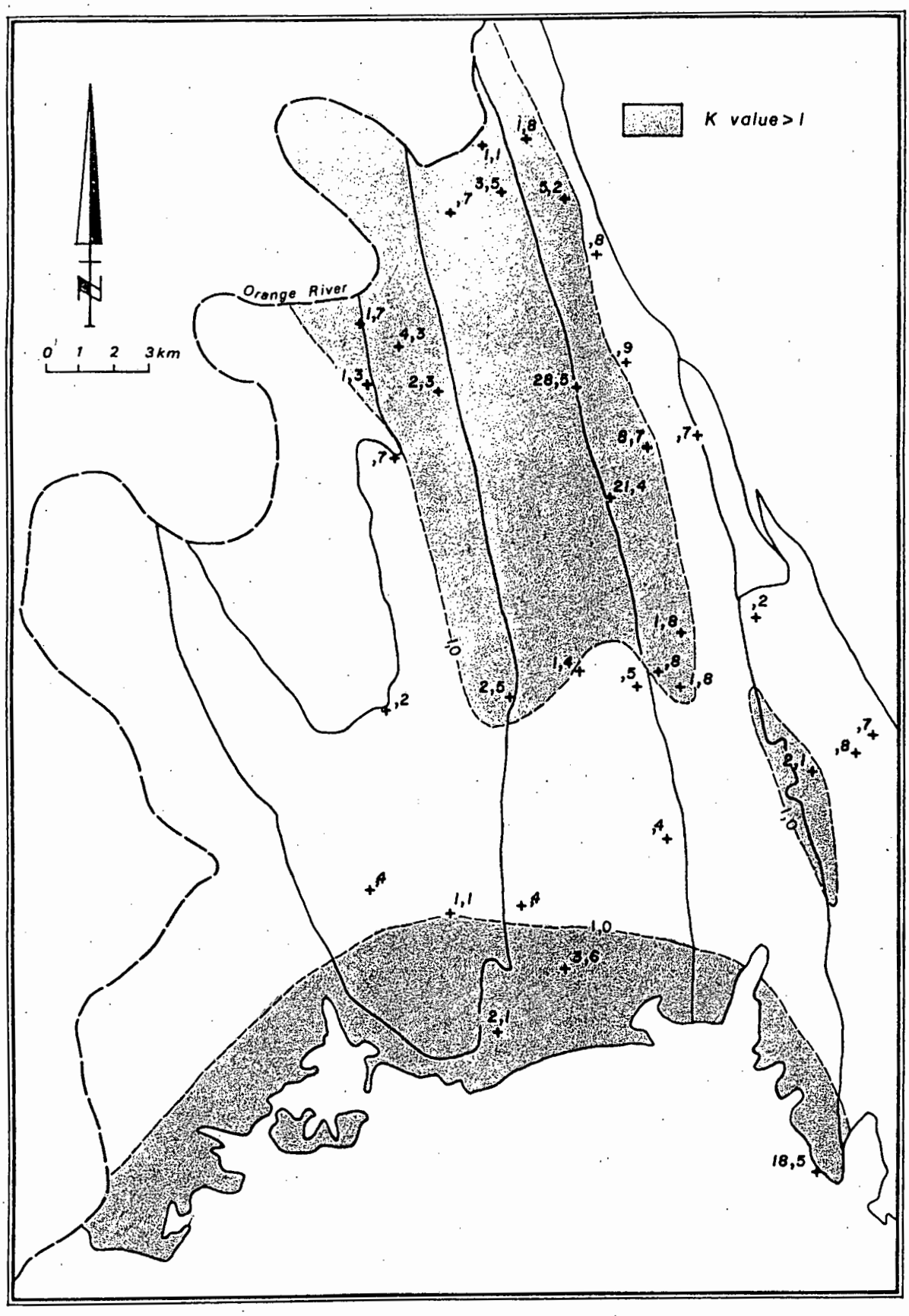

Fig. 51 : Map of the variations in k-values. Prolate ellipsoids (k > 1) are dominant in the shaded areas. See text for further details.

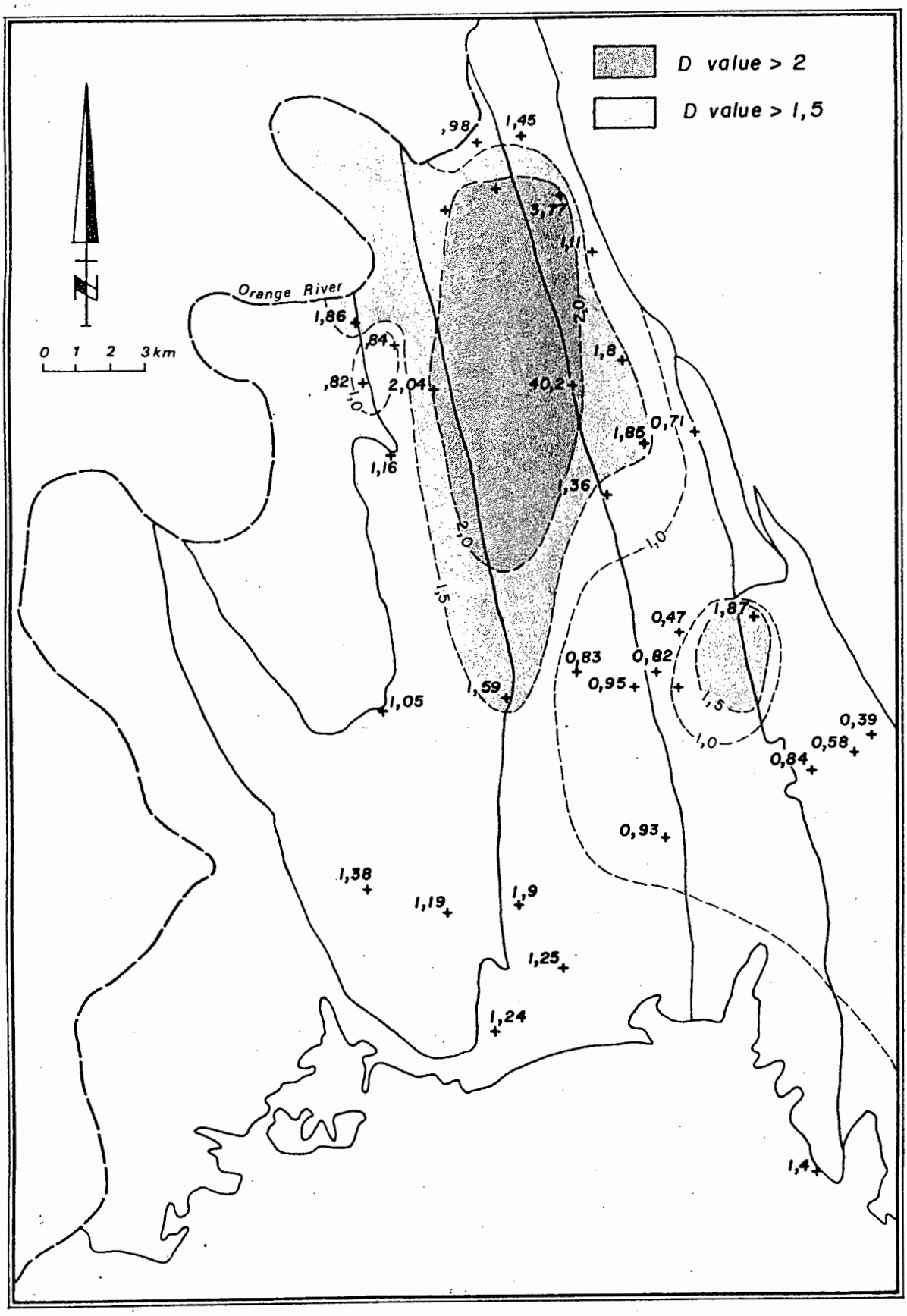

Fig. 52 : Map showing the variations in d-values. The area of high finite strains is shaded. See text for further details.

The total shortening across the PNA due to penetrative strain can be computed by integrating the reciprocal stretch along the Z axis strain trajectory (Cobbold, 1979). The reciprocal stretch $\sqrt{\lambda}'_3$ is plotted against distance and the area under the curve is calculated. The area under the curve equals the original length (L_0) of the strain trajectory. The original length (L_0) and the final deformed length gives the percentage shortening:

$$e_3 = [(L_1 - L_0)/L_0] \times 100.$$

Strain integration of Z trajectories in an an east-west section across the central part of the study area gives an L_0 value of 48.19 over a distance of 25.5 km which is equivalent to an e_3 shortening value of 89 per cent (Fig. 53).

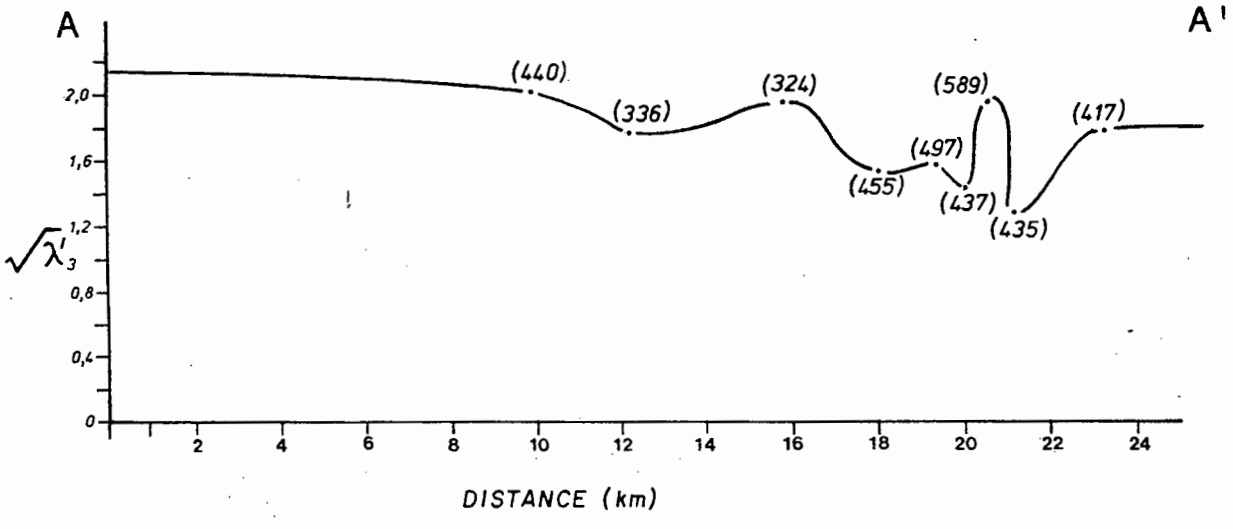

Fig. 53 : Plot of $\sqrt{\lambda}'_3$ versus distance from the Schakalsberg fault. Sample numbers are given in brackets.

(c) Discussion

Davies & Coward (1982) proposed a model of southeast-directed differential movement below a dense overthrust nappe (the Marmora nappe) to account for the arcuate shape of the Gariep Belt. According to theoretical work (Coward & Kim, 1981, Sanderson, 1982; Coward & Potts, 1983), differential movements in a thrust zone (Fig. 54a) produce a variation in the shapes and orientations of the finite strain ellipsoids. At the frontal and rear tips, the rocks suffer the main thrust shear plus longitudinal strain leading to k=1 plane strain ellipsoids. At the lateral edges, wrench shear also produces k=1 ellipsoids. A combination of longitudinal shortening or extension and wrench shear gives rise to oblate and prolate ellipsoids between the frontal and lateral tips, and the lateral and rear tips, respectively (Fig. 54b). The λ_1/λ_3 principal planes, and hence the cleavage, trace out a complex three-dimensional spoon-shaped form.

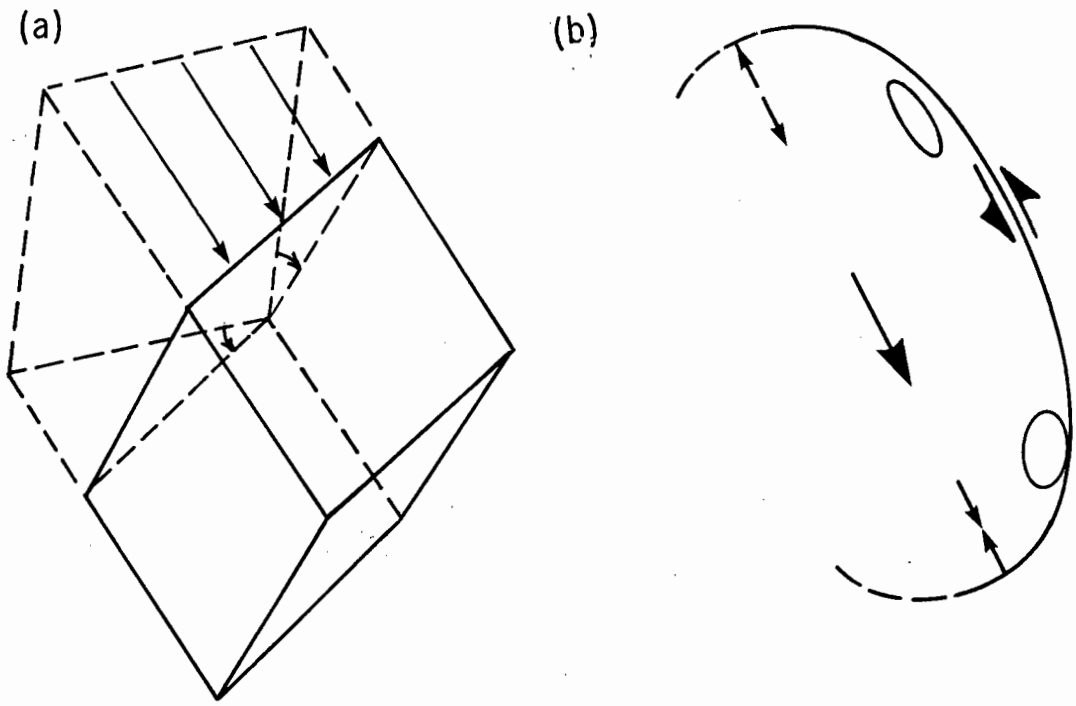

Fig. 54 : (a) Differential movement in a shear zone; (b) Variations in ellipsoid shape resulting from differential movements (after Coward & Potts, 1983).

Because of the southeasterly transport direction, and the swing in structural trend from northwest-southeast in SWA/Namibia to north-south in the central Richtersveld, the study area is situated in the transitional zone between the frontal and lateral edge and a northward increase in the wrench/thrust shear ratio is to be expected (Fig. 55). The $k<1$ oblate shapes in the southern parts of the study area can be related to longitudinal shortening effects, which also caused a shallowing and rotation of the maximum principal axis away from the direction of transport. The presence of prolate ellipsoids in the northern parts is unexpected as extensional flow is not forecast for the transitional zone. Davies & Coward (1982) suggested that the region of extensional flow is situated much further north in the area southeast of Aurusberg in SWA/Namibia. A possible explanation for the prolate strains may be the increase in ductility of the rocks in a northward direction. The southern parts are dominated by competent rocks - granitoids and quartzite in the basement, and quartzite, conglomerate and marble in the cover, while the northern parts are underlain predominantly by ductile schist and gneiss in the basement, and diamictite, schist, and limestone in the cover. The latter rocks would have responded to the deformational stresses by deep folding to produce layer-parallel extension, rather than thrust faulting and layer-normal flattening. Northeast-trending stretching

lineations parallel to the strike of bedding in the coastal outcrops from Cape Voltas to the Holgat River mouth (P. Gresse, pers. commun., 1986) resulted from longitudinal shortening effects in the frontal edge of the nappe.

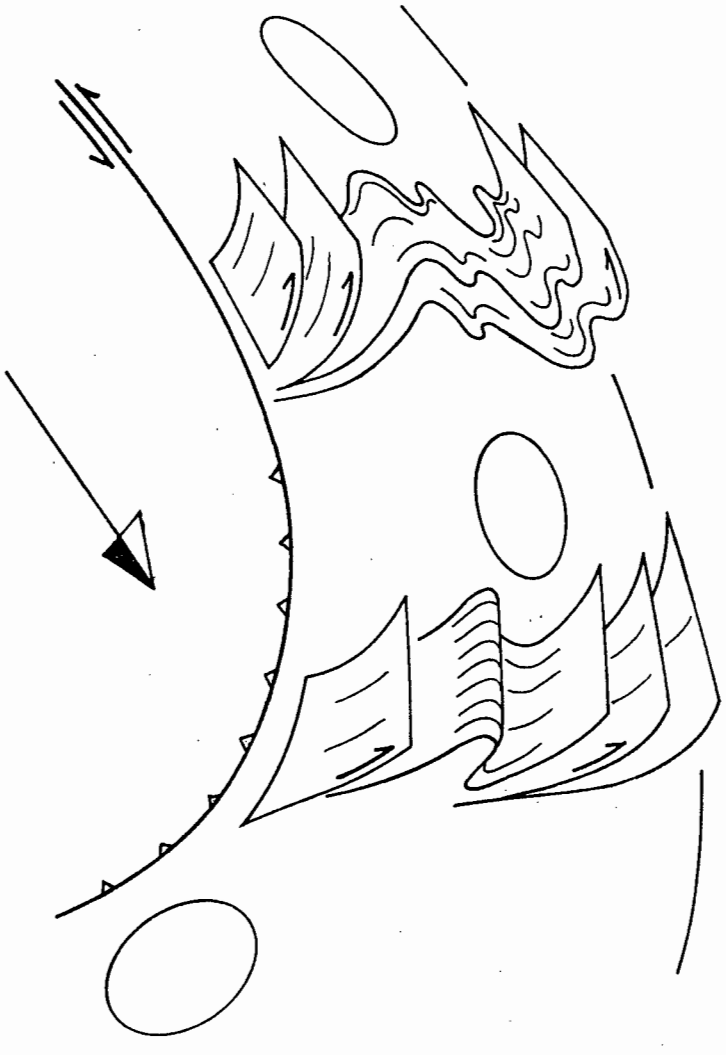

Fig. 55 : Schematic diagram summarizing the structural variations in the central parts of the PNA.

3.3.2 Plane wrenching phase

The transpressive phase was followed by a phase of general sinistral wrenching localized along existing zones of weakness. The wrenching phase is

manifested by the F_2 folds, some late fault structures such as the Numees cross-fault, and tear faults in the Numeesberge and adjacent basement. The F_2 folds were initially diagnosed as backfolds related to a late backfaulting phase because of their sense of asymmetry (Von Veh, 1987a), but have been re-interpreted as wrench-tectonic structures because of their close spatial association with the major fault zones, the absence of backthrusts or any transverse stretching lineations, and their en-echelon arrangement and non-cylindrical shapes.

The geometry of the pre-existing lineations deformed by the folds can yield information about the kinematic a, b, and c axes of the deformational event (Weiss, 1959; Donath & Parker, 1964; Ramsay, 1967). If deformation is by shear folding, producing similar folds, the folded lineations plot on a great circle (Fig. 56a), and the direction of transport lies along the line of intersection of the great circle with the plane of slip (axial plane) of the folds. If folding is by flexural slip, producing concentric folds, the lineations plots on a partial small circle (Fig. 56b) and the transport direction is normal to the fold axis and the axial plane.

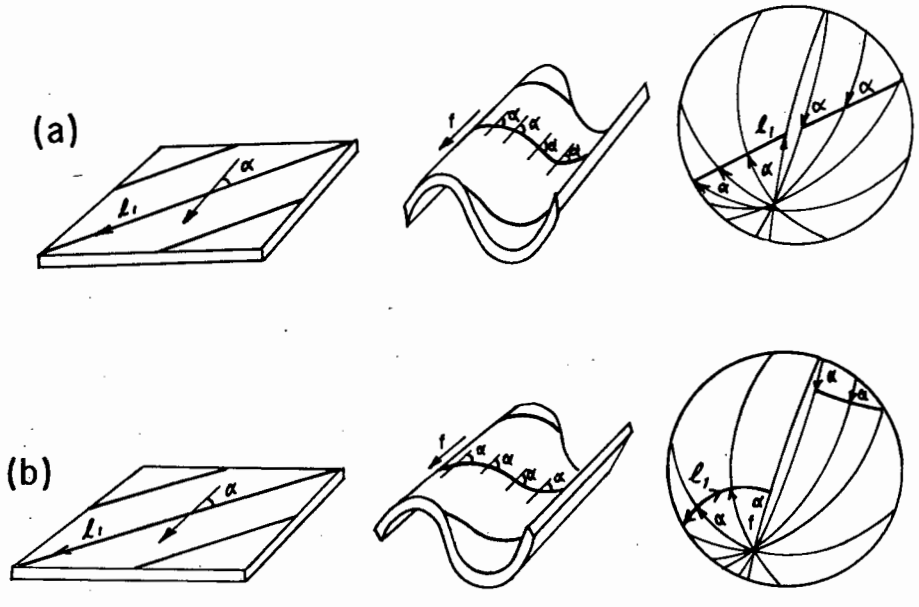

Fig. 56 : Deformation of an earlier lineation by : (a) similar folding; and (b) concentric folding (after Ramsay, 1967, Figs. 8.2, 8.9).

A simple shear folding mechanism can be assumed for the F_2 folds because of the ubiquitous presence of axial planar shear surfaces which crenulate S_0 and S_1. An attempt at estimating the kinematic axes was made by measuring and plotting the change in orientations of l_1 stretching lineations across a number of F_2 folds (Figs. 57a-57c). The technique is of limited use because of the sub-parallelism of L_1 with B_2, although a northward plunging kinematic a axis is suggested in all cases (average **a** = 006/28, **b** lying in the axial plane = 118/38, and **c** is normal to **a** and **b** = 244/40).

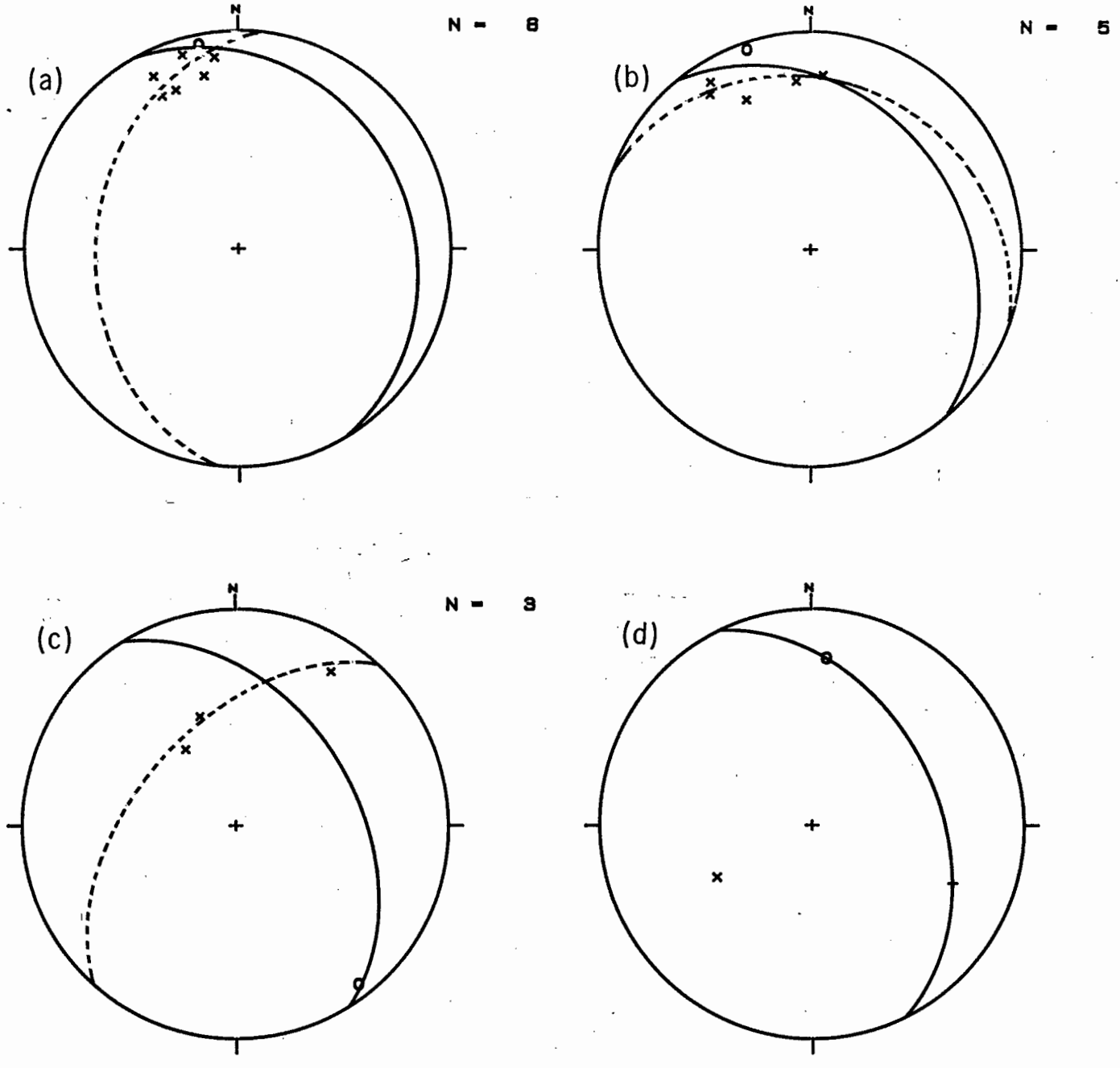

Fig. 57 : Structural data of F_2 folds deforming L_1. Solid great circle - F_2 axial plane; dashed great circle - best-fit plane of L_1 dispersion; o - B_2 axis.
(a) F_2 fold west of Remhoogte (locality 453; intersection lineation a = 356/8); (b) overturned F_2 syncline at the Orange River (locality 511; a = 011/22); (c) anticlinal F_2 fold near Sendelingsdrif (locality 561; a = 012/33); (d) kinematic axes for the D_2 deformation.

The shallow eastward dip of the fold axial planes indicates that the folds nucleated with axial planes normal to the dominant layering (which in the areas of F_2 folding generally has a steep westerly dip) and not parallel to the flattening plane of the finite strain ellipsoid.

3.3.3 Transtensive phase

The geometry of the late (D_3-D_5) structures indicates that they formed during a southeast trending sinistral transtensional phase.

Theoretical and experimental work (Moody & Hill, 1956; Wilcox et al., 1973) has shown that in a classical shear system a number of tectonic elements form at predictable directions (Fig. 58). A set of folds lies along the major axis of the strain ellipse, a conjugate fault set known as Riedel shears forms at low angles (the 'Riedels') and high angles (the 'Riedel conjugates') to the principal shear direction, a normal fault set lies parallel to the minor axis of the strain ellipse, and a reverse fault set lies parallel to the major axis. The Riedel conjugates may be poorly formed or absent. Tensional structures such as normal faults are enhanced if the shear is accompanied by horizontal stretching across the shear plane (Harland, 1971; Sanderson & Marchini, 1984).

A comparison of the observed maxima directions with those expected in a left-lateral wrench system trending at 135° shows reasonably good agreement (Table 18). The Reidel conjugates are poorly represented, although De Villiers & Sönge (1959, p. 171) describe a 30° joint set in the Kuboos granites. The F_3 folds formed at an early stage and the brittle tensional structures dominated during the waning stages during and after the emplacement of the Kuboos pluton. Shearing associated the pluton ascent resulted in prolate strains and local northward-directed structures in the aureole during D_4.

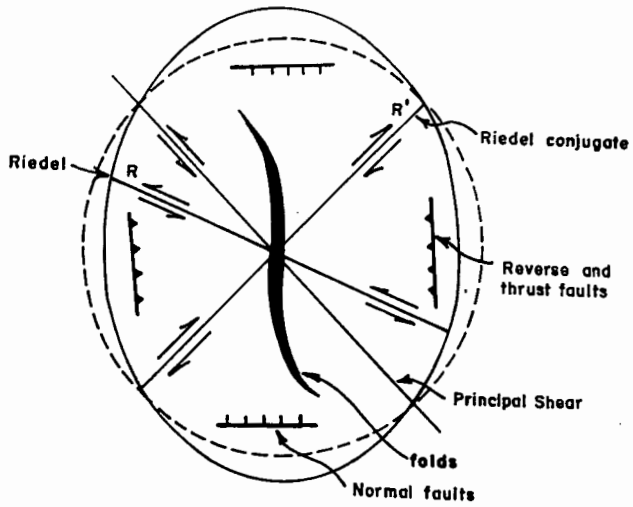

Fig. 58 : Geometric relation of folds and faults in a northwest-southeast trending left-lateral wrench shear system (adapted from Sylvester & Smith, 1976).

Table 18 : Comparison of predicted and observed structural element directions in a sinistral wrench fault system trending 135°.

Element	Expected direction	Observed direction
Main wrench	135°	
Fold axes	345° - 005°	340° - 350°
Riedel	105° - 125°	100° - 130°
Riedel conjugates	045° - 065°	030°
Normal faults	075° - 095°	090° - 100°
Reverse faults	345° - 005°	340° - 350°

The various deformational pulses in the central marginal parts of the PNA are thus interpreted as following each other without discontinuity during a single progressive southeast directed orogenic event, dominated initially by left-lateral transpression but evolving with time to sinistral wrenching and finally to transtension as a result of a gradually changing stress regime.

4 METAMORPHISM

4.1 General aspects

Previous research workers have recognized that the pattern of metamorphism is relatively straight-forward. De Villiers & Söhnge (1959, p. 136) postulated two events affecting their Stinkfontein, Kaigas and Numees Formations: an older dynamic event giving rise to phyllites and chlorite-rich schists, and a younger contact thermal event forming spotted slates and horn-stones. Due to their misinterpretation of intrusive relationships between the grey gneisses and their Gariep System, they inferred an earlier magmatic event affecting the Gariep System. The absence of any large-scale metamorphism associated with it was attributed to the elevated position of the Gariep beds in the depositional basin (op. cit., p. 95). Kröner's (1974, 1975) reinterpretation of the rock relationships invalidated this scheme and only one Barrow-type regional metamorphism, increasing from low grades in the miogeosynclinal shelf sediments to intermediate grades in the eugeosynclinal realm, was recognized.

Phenomena described as "granitization" and "feldspathization" are frequently cited in the older Gariep literature, but are irreconcilable with the ubiquitous low grades of metamorphism. This problem has been largely resolved with the recognition that many of the "granitized" rocks are in fact tectonically emplaced slices of granitic basement. The leucogranite surrounding the Obib water hole and the gneiss and intrusive leucogranite northwest of the Gumchavib trigonometrical beacon were originally interpreted as products of syntectonic isochemical granitization of Gariep metasediments (Martin, 1965, p. 78; McMillan, 1968, p. 159) but a field investigation by Kröner (1974a) proved that they belong to the pre-Gariep basement. Welke et al. (1979) obtained a U-Pb age of 1870±20 Ma for these bodies. Kröner (1974) analysed the highly sheared and "granitized" schists at Hilda beacon and found them to have a chemical composition similar to comparable basement rocks (op. cit., p. 11). Joubert & Kröner's (1972) description of a recrystallized and partially remobilized Stinkfontein outcrop from the southern Richtersveld suggests the presence of an up-faulted slice of basement rock as they state that the "treptomorphism" phenomenon "seems to be restricted to a well-defined large lensoid body within the whole sequence since the gneisses are overlain and underlain by seemingly less metamorphosed beds" (op. cit., p. 53). Isolated and highly sheared granitoid boulders can also be mistaken for local granitization. The gneissose textures reported to be found in association with the granitization appears to refer to the metamorphic differentiation that accompanied D_1, the formation of which is independent of metamorphic grade (Gray, 1977, p. 772). Retrogressive dynamic metamorphism in shear zones can give rise to "augen" porphyroclasts and ribbon structures having a gneissose appearance, particularly if pegmatitic veining is involved.

A microscopic study of the mineral assemblages confirmed that there was only one regional prograde metamorphic event, M_1. It attained greenschist facies grade and culminated in the growth of syn- to post-D_1 biotite porphyroblasts. Retrograde effects occurred during the later phases, with the exception of a localized thermal metamorphic event, M_2, that was associated with the D_4 emplacement of the Kuboos-Rooiberg plutons (Fig. 59).

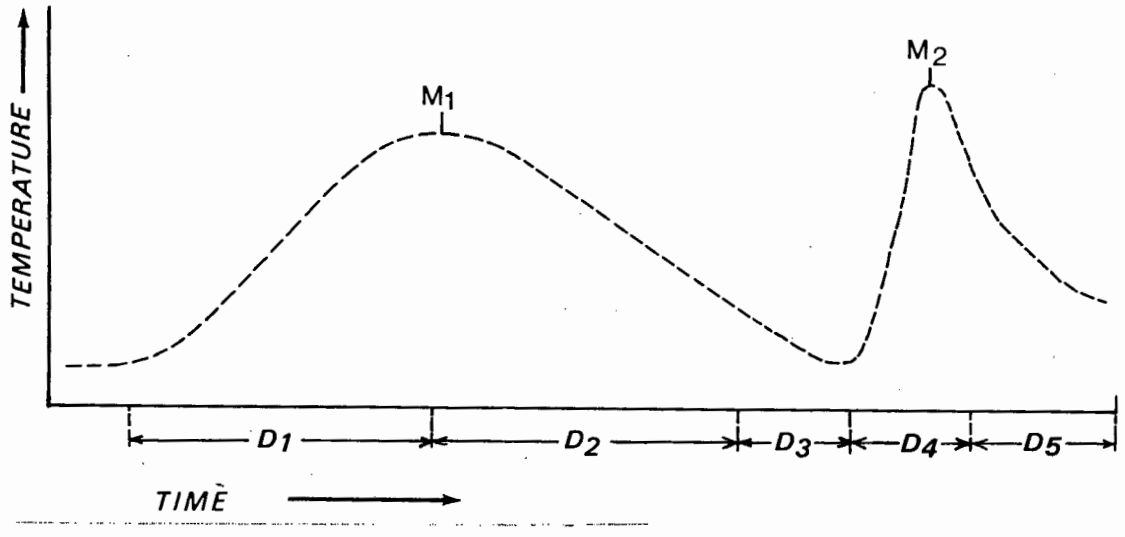

Fig. 59 : Schematic correlation of temperature changes with deformational intensities during the Gariep tectogenesis.

4.2 The regional metamorphic event (M_1)

4.2.1 Mineral paragenesis

The M_1 mineral assemblages are characteristic of the lower to intermediate range (chlorite to biotite zone) of the greenschist facies. In metapelites the mineral paragenesis is:

muscovite - chlorite - quartz - albite ± biotite ± calcite ± epidote.

The chlorite is of both prograde and retrograde origin. Calcite and epidote are relatively minor constituents and accessory minerals are apatite, zircon, sphene and oxide minerals. In the more arenaceous rocks the assemblage is usually restricted to:

quartz - muscovite ± feldspar ± biotite.

Much of the feldspar is of detrital origin and includes plagioclase, microcline and perthite. In marbles, the paragenesis is:

calcite - dolomite ± quartz ± talc ± muscovite ± chlorite.

The marbles are usually very pure, consisting almost entirely of calcite - dolomite. In greenschists (Grootderm volcanics, Stinkfontein lava), the assemblage is:

albite - chlorite - calcite - actinolite - epidote - opaques ± biotite.

4.2.2 Temperatures

No evidence was found to support Kröner's (1974, p. 101) assertion of a westward progression of M_1 temperatures from the quartz-albite-muscovite-chlorite subfacies to the quartz-albite-epidote-biotite subfacies of the greenschist facies and possibly into the andalusite-cordierite-muscovite subfacies of the amphibolite facies. The sericitized cordierite which he cites from calcareous schists in the Holgat River (reported by De Villiers & Söhnge, 1959, p. 57) is probably related to M_2 because of its proximity to the Rooibank pluton and the association of cordierite with the contact metamorphism. Although McMillan (1968, p. 158-163) recorded minerals in the Obib and Gumchavib area indicative of local intermediate grades: blue-green hornblende, plagioclase with an oligoclase-andesine composition, and almandine garnet, his descriptions are centred around the granitization problem there, so that they may have been observed in samples collected from basement schists and gneisses. Only low grade minerals were reported in petrographic descriptions of the footwall and ore rocks of the Rosh Pinah Mine (Page & Kindl, 1978). Many metapelitic samples collected during this study from the western "eugeosynclinal" parts contain no biotite or only biotite with a pale green-orange colour indicative of low grades. Biotite does not occur in the Grootderm volcanics along the Orange River (Dr. D. Waters, pers. commun., 1984). M_1 temperatures are thus assumed to have been consistently low across the area and possibly not in excess of ~450°.

4.2.3 Pressures

In contrast to the temperatures, the pressures appear to have been reasonably high and to have increased in a westerly direction. High pressure minerals (glaucophane and other Na-amphiboles) were reported by Beetz (1926, pp. 199, 202) and Kröner (1974, p. 101) from the central parts of the Gariep Belt at or near the contact between the Grootderm volcanics and underlying greywacke. These minerals do however require the co-existence of jadeite or lawsonite to

prove high pressure conditions (Fyfe & Turner, 1966, p. 361). From a comparison study of the b_0 spacing of white micas, Ritter (1980, p. 202) found suggestions of increasing celadonite content from basement to cover. He reports a mean b_0 -value of 9,0464 for his Gariep samples. This is a typical value for intermediate pressure Barrovian-type metamorphism (Sassi & Scolari, 1974), although Miyashiro & Shido (1984) have shown that muscovites with a high celadonite content can form under a variety of pressure conditions. Pressure conditions probably corresponded to those in the Southern Marginal Zone of the Damara Orogen, estimated by Hartmann et al. (1983) to be ~6-7 kb.

4.2.4 Relationship to D_1

Information about the relative timing between growth of metamorphic minerals and deformation events can be inferred from the study of microstructural relationships between porphyroblasts and matrix (e.g. MacQueen & Powell, 1977; Vernon, 1978). Porphyroblasts often contain inclusions with a preferred alignment representing the trend of a pre-existing foliation. Temporal relationships are elucidated from the relationships between the internal (S_i) and external (S_e) s-surfaces, and between porphyroblast margins and S_e. The following criteria indicate that the M_1 biotite porphyroblasts grew after D_1, but before D_2:

- Their long axes orientations are usually randomly arranged with respect to S_e (S_1). Some parallelism may occur due to mimetic growth;
- S_1 is not deflected around the porphyroblasts;
- The internal trails are continuous with S_1 and have a consistent relationship to the porphyroblast margins (Fig. 60). The S_i trace out microfolds only when the margins are deformed by the same microfolds;
- The porphyroblasts are fractured, bent, folded and internally strained by D_2 (e.g. samples 342, 436, 441, 528, 597). They fracture when the (001) mica orientation is normal to S_2, but fold when it is subparallel to S_2;
- S_2 deflects around, truncates or passes through the porphyroblasts;
- The porphyroblasts may be partially or totally retrograded to chlorite. Chloritization occurs preferentially along defects related to D_2.

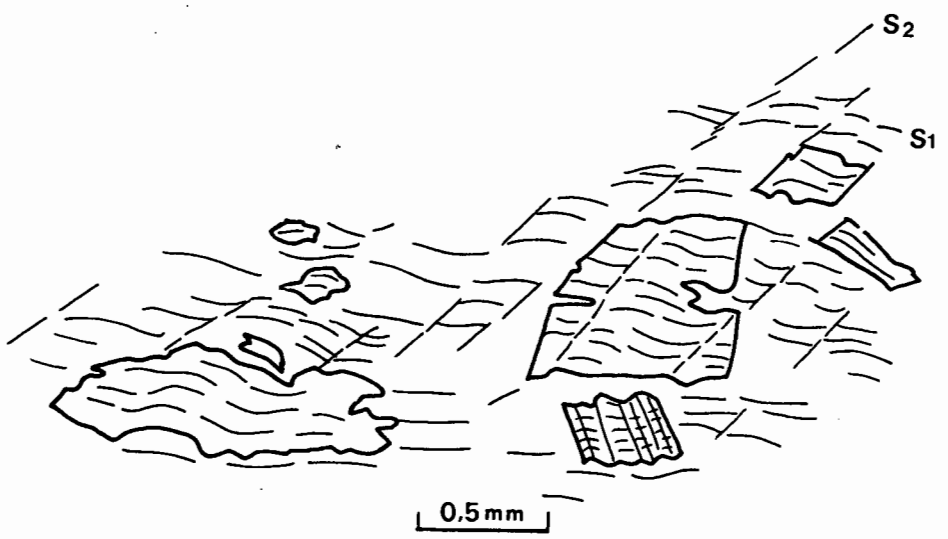

Fig. 60 : Sketch of M_1 biotite porphyroblasts (sample 436) showing typical post-kinematic relationships.

4.3 The contact metamorphic event (M_2)

4.3.1 Characterization

Recrystallization effects associated with an M_2 thermal event are observed in thin-sectioned samples from localities in proximity to the Kuboos pluton. The pluton is a composite body, consisting of a small eccentrically situated core of syenite and quartz syenite near Ploegberg, surrounded by a younger, inner medium-grained granite, and an outer mass of coarse porphyritic granite (Söhnge & De Villiers, 1948). It is only partly exposed, but an almost perfectly circular margin with a diameter of ~27 km is apparent from aeromagnetic data (open file sheet 2816BB, Geological Survey). Its northern margin dips inwards but it is steep-sided elsewhere.

The contact aureole can be subdivided into two zones on a textural basis:

4.3.1.1 Outer spotted zone

The first visible M_2 effects are small (0,5-1,0 mm) chlorite and muscovite spots in pelites and greywackes, occurring as far north as Remhoogte (locality

619). They gradually increase in size and density and undergo a change in composition. Large (5,0 -30,0 mm), closely spaced porphyroblasts of biotite, cordierite, and andalusite produce a nodular texture from a distance of up to 4 km from the contact. The cordierite porphyroblasts may display a zoned alteration from a sericitic core to a chloritic rim. The porphyroblasts are normally partly to totally retrogressed.

4.3.1.2 Inner hornfels zone

Extensive recrystallization occurs in a zone of plastic deformation extending up to several 100 m from the contact. In pelitic hornfels and metagreywacke, progressive dehydration has given rise to the paragenesis:

cordierite - andalusite - biotite - Ca plagioclase - quartz - opaques.

Muscovite, chlorite and chloritoid are present in small amounts as retrogressive products of cordierite. The introduction of Ca during late-stage metasomatism is evidenced by epidote and tremolite grains and spherulitic carbonate in quartz veins (sample 458). The iron-amphibole grunerite occurs in association with the Numees iron formation at the Dabie River outlier (sample 357).

In marbles and calc-silicates, the assemblage:

dolomite - calcite - diopside - anorthite - epidote

with accessory sphene and apatite is found (sample 401). Tremolite needles were observed in some of the dolomites in the central Richtersveld.

4.3.2 Timing

The following microstructural features suggest that the M_2 porphyroblasts grew after D_1 and D_2:

- They are randomly oriented with respect to the S_1 and S_2 fabrics;
- They contain trains of folded S_i in continuity with S_e, although their margins are not deformed (Fig. 61; samples 466, 632);
- There is little optical evidence for internal strain in the porphyroblasts. Some minor undulatory extinction and bending and fracturing of grains (samples 393, 396) can be attributed to the late transtensive phase. The amphiboles occur as radiating aggregates and rosettes indicating post-tectonic growth (sample 357).

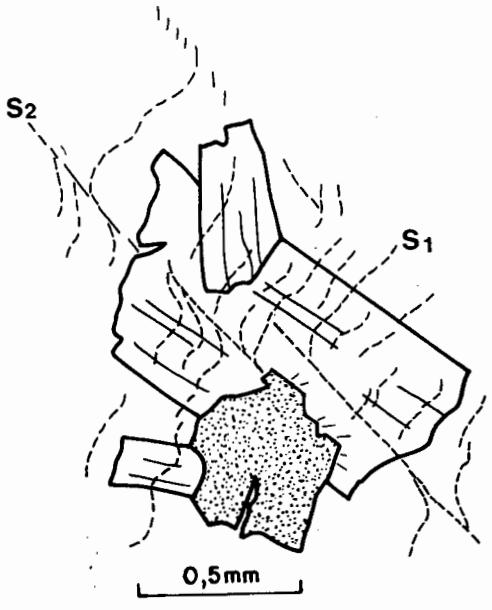

Fig. 61 : Microfolds in M_2 muscovite porphyroblasts indicative of their relative timing of growth (sample 632).

5 CONCLUSIONS

5.1 Geodynamic synthesis

There is a growing consensus of opinion that plate tectonic processes of some sort were active by the Late Precambrian, and played a role in the development of the Pan-African orogenic belt system. This uniformitarian belief is based on the recognition of criteria indicating subduction and collision of continental margins and island arcs, such as ophiolitic mafic assemblages and melanges, high pressure metamorphism, paired metamorphic belts, and asymmetric calc-alkaline magmatism. Plate tectonic models have been proposed for the Pharusian Belt in the central Sahara (Caby et al., 1977; Bertrand & Caby, 1978; Black et al., 1979; Engel et al., 1980), the Arabian-Nubian shield and its extension into the Mozambique Belt (Greenwood et al., 1976; Gass, 1977, 1978), and the intracrustal arm of the Damara Orogen (Hartnady, 1973; Blaine, 1977; Kasch, 1979; Barnes & Sawyer, 1980).

Although evidence for plate tectonic processes is less abundant in the Gariep Belt, a collisional mechanism can be inferred from the intense thrusting of the continental margin sediments, the high-pressure metamorphism, and the presence of basic and ultrabasic igneous rocks in the Grootderm Suite. Widespread calc-alkaline magmatism and high-temperature metamorphic assemblages are observed in its geological counterpart in southeast Brazil and Uruguay, the Ribeiro Belt (Porada, 1979; Bernasconi,1983).

Models relating the development of the Gariep Belt to the growth and closure of a Pan-African ocean (the "Adamaster Ocean"; Hartnady et al., 1985) have been proposed by several workers, particularly in the context of the evolution of the Damara Belt (Kröner, 1974, 1975; Hartnady, 1978; Kasch, 1983, 1983a; Davies & Coward, 1982; Porada, 1983). The Gariep Belt and its extensions are generally regarded as recording the development of an ocean of substantial width, with the northeast trending Damara Belt forming as an aulacogen or failed rift. Thereafter, consumption of oceanic lithosphere culminated in the collision of the Kalahari craton with the Congo craton, and the African cratons with a subduction complex fronting a South American craton (Martin & Porada, 1977; Porada, 1979, 1983; Martin, 1983; Miller, 1983).

A weakness of the models is that they are based for the most part on detailed studies in the Damara Belt, and generalizations are made about relationships in the Gariep Belt, a complex area in which little field data is available. In the following account, some of the shortcomings of the current models are analysed, and an attempt is made to identify how the observed relationships in the study area contribute to a better understanding of the various stages of the geodynamic evolution of the Gariep Belt.

5.1.1 Oceanic opening

An Atlantic-type passive continental margin evolution for the Gariep sediments is evidenced by the progression from an early coarse terrigenous clastic phase (Stinkfontein Sequence), to a platform carbonate and continental shelf clastic phase (Hilda Sequence), to a deep-water clastic phase (Holgat Sequence).

The exceptional maturity of the basal Lekkersing quartzites and the upward transition to increasingly immature Vredefontein arenites suggests that continental separation was preceded by a protracted period of stretching and thinning of the subjacent crust causing gradual epierogenic subsidence (Fig 62a). The sporadic carbonates along the basal contact at Eksteenfontein overlie the Stinkfontein so that no small, disconnected basins filled with evaporites on the pre-Stinkfontein erosional surface are envisaged (cf. Ritter, 1980, pp. 200, 202). The early stages of rifting were accompanied by dextral transtensional movement in the basement, producing north-east to NNE-trending shears (D_2^n), and some syn-sedimentary gravity deformational structures in the cover. Crustal attenuation eventually resulted in a major rupturing event, recorded by the unconformity at the base of the Kaigas diamictite. The immature and laterally variable Kaigas sediments were rapidly deposited into restricted grabens bounded by listric and block faults (Fig. 62b). In the Rosh Pinah area, the crust responded to the extensional stresses by deep faulting, with voluminous outpouring of alkaline acid volcanics, tuffs, and agglomerates.

The rifting stage was followed by a sea-floor spreading stage when the continental margin cooled and subsided as it moved away from a spreading centre (Fig. 62c). Quiet carbonate shelf conditions prevailed during Hilda times in southern SWA/Namibia and the central Richtersveld, but in the northern Richtersveld coarse clastics were still being shed into the basin. The absence of a regional break-up unconformity separating the rift deposits from drifting stage deposits indicates that the rifting was unaccompanied by doming (cf. Miller, 1987). A period of tectonic instability with probable glacial activity followed, and the unconformably overlying Numees diamictite and ferruginous sediments were deposited in a continental slope environment (Fig. 62d). With continued subsidence, the deeper-water Holgat quartzite, schist, and carbonates were lain down in a distal, slope or basin environment (Fig. 62e). The uplifted hinterland region to the east was largely eroded away by this time and the shallow water Kuiseb and lower Schwarzrand clastics and carbonates transgressed onto the adjoining craton. Some molasse material from an approaching orogenic front may have been incorporated in the distal parts of the depositional basin.

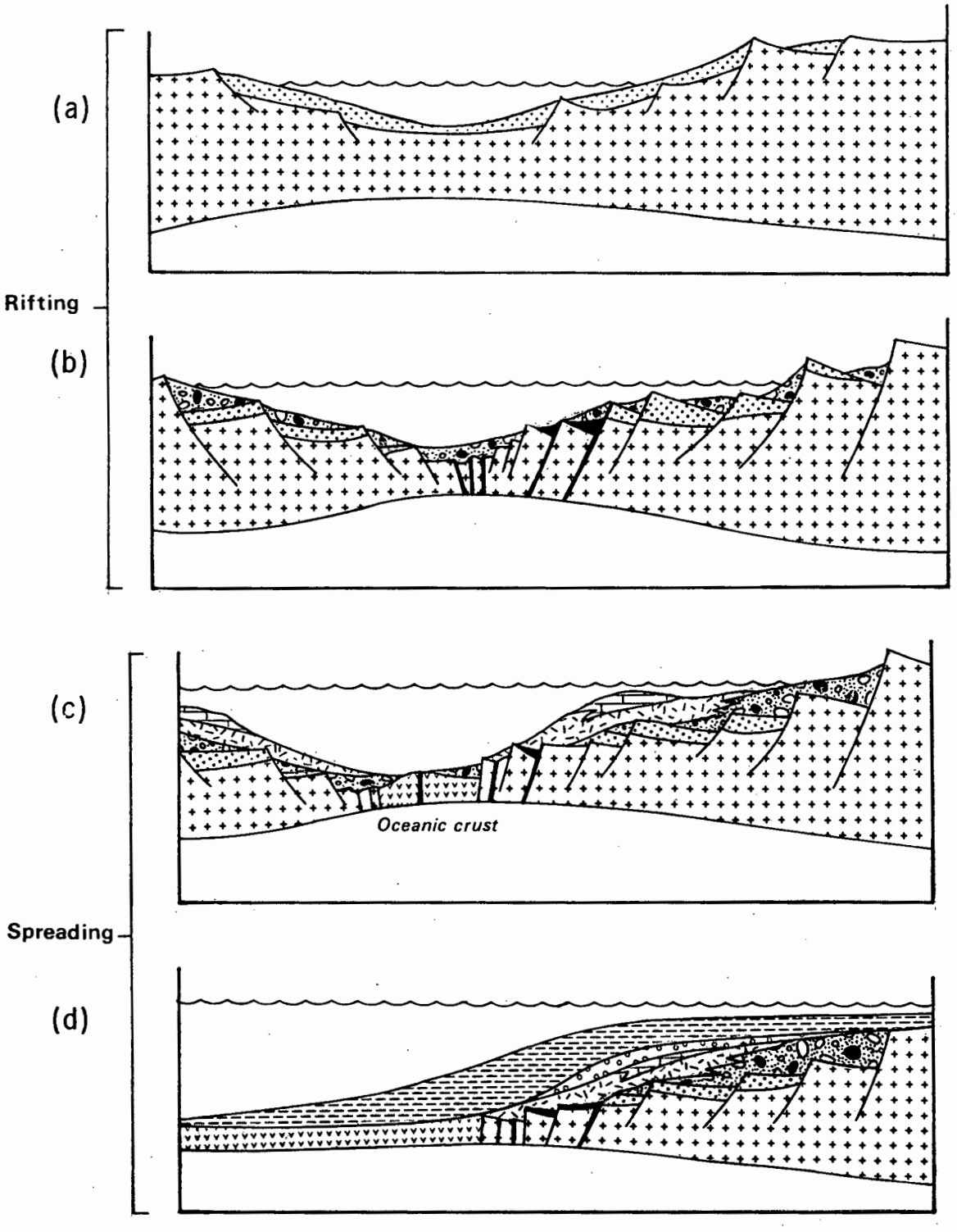

Fig. 62 : Schematic sections showing the rifting and spreading stages of Gariep evolution.

5.1.2. Oceanic closure and collision

The geodynamic models that have been proposed for the Gariep Orogeny generally relate its deformation to final closure of the northeast-trending "intracrustal" branch of the Damara Orogen, because of the coincident transport vector for the final phase of deformation in the southern Damara Belt. Davies & Coward (1982) for example envisaged the emplacement of a thick dense mass of basic-volcanic rocks to the southeast during its closure. Because of gravitational instabilities, the mass collapsed and spreading initiated imbricate faulting in the previously undeformed foreland sediments (Fig. 63). Kasch (1981, 1983) visualized the continuation of subduction of oceanic material along a coastal extension of the Damara Belt after collision of the Kalahari and Congo cratons. The pre-Gariep subduction complex rotated relative to the Damara Belt prior to its collision in the Gariep Belt (Figs. 64a-64c).

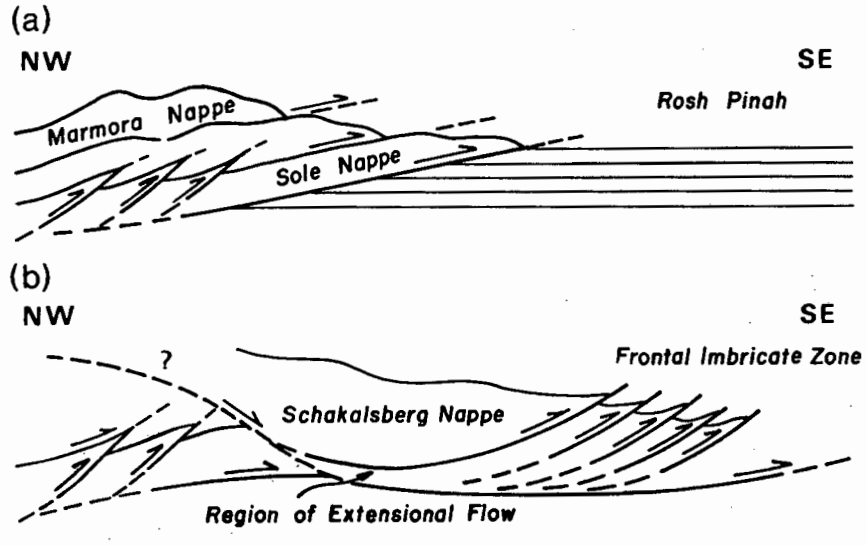

Fig. 63 : Cross-sections showing the gravitational collapse model of Davies & Coward (1982).

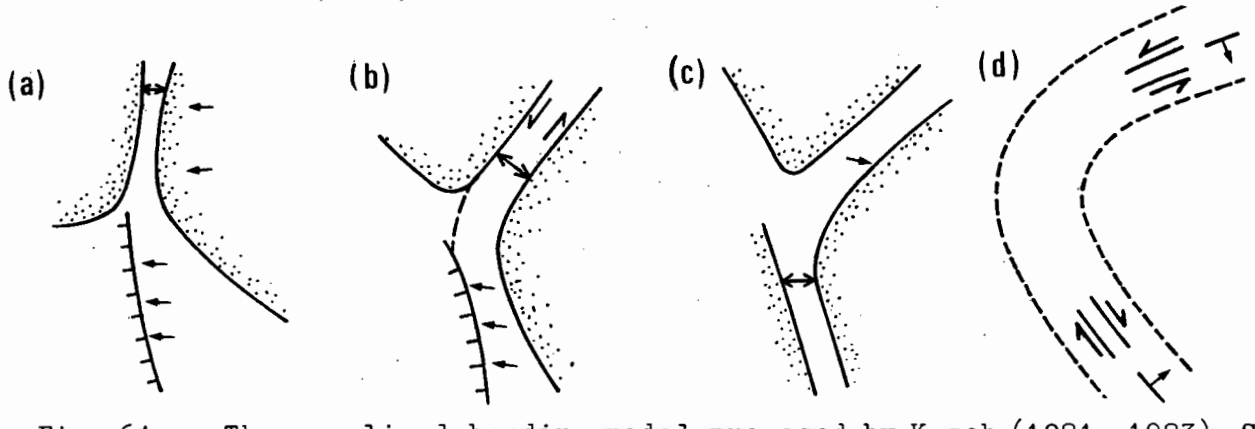

Fig. 64 : The oroclinal bending model proposed by Kasch (1981, 1983). See text for details.

There is some evidence to suggest that the Gariep paroxysm did not result from the final closure of the Damara Belt, but rather predated it:

- The main phases of Gariep deformation predate the ~550-525 Ma emplacement of the Kuboos pluton (cf. De Villiers & Burger, 1967; Allsopp et al., 1979), whereas the deformation in the Southern Front and Southern Marginal Front of the Damara Belt occurred between 540 and 523 Ma (Miller, 1983, p. 507), and the final gravity-induced emplacement of the Naukluft Nappe Complex onto deformed Nama only ended between 495 and 480 Ma (op. cit., p. 509).

- Kasch (1983, p. 231) cited the coarsening upwards of the Schwarzrand Subgroup in the northern Zaris basin and the appearance of a western provenance area only in the upper Schwarzrand beds (Germs, 1972, 1974) as evidence for later Gariep tectonism. Germs (1983, p. 100) has however suggested that the sedimentological response to the major uplift of the Damaran orogenesis is represented by the Nomtsas unconformity in the upper Schwarzrand, and that the molasse-like deposits of the overlying Fish River Subgroup represent the material that was shed from the uplifted regions into the foreland basin. Since his palaeocurrent maps (op. cit., Figs. 11 and 13) clearly illustrate a change from a western to a northern source area during deposition of the Fish River Subgroup, the Gariep uplift would appear to predate that of the southern parts of the Damara Belt.

If a dense, basic mass had originally been obducted along the southern margin of the Damara Belt, as proposed by Davies & Coward (1982), then a decrease in the intensity of deformation would be expected in the southern Richtersveld in parts of the foreland well removed from the spreading mass. The Pan-African deformation front can however be traced southwards into a region of brittle fracture of high-grade basement rocks along the western margin of the Namaqua Province (the "West Coast Zone" of Stowe et al., 1984). Furthermore, the model can not account for the fact that the Gariep rocks were subjected to a prolonged history of sinistral movement subsequent to the overthrusting.

The oroclinal bending model of Kasch (1981, 1983) offers an explanation for sinistral shearing in the Damara Belt, but it is discounted by the absence of dextral shear zones in the Gariep Belt (as predicted in Fig. 64d) and by the lack of evidence for large bending strains in the basement rocks of the Kalahari craton.

The recent recognition of southeast-directed transport vectors along other parts of the Pan-African belt system along the west coast of Southern Africa (e.g. Hälbich et al., 1987), including the northern coastal branch of the Damara Orogen (Guj, 1970; Coward, 1983; Miller, 1983), the Nama correlatives in the Vanrhynsdorp area (Gresse, 1987), and the Malmesbury Group rocks in the southwestern Cape (Hartnady, 1973; Von Veh, 1983), leads to the conclusion that the Gariepian orogeny resulted from oblique southward closure of the NNW-SSE trending proto-Atlantic ocean, rather than of the intracrustal branch.

The possible configuration of a subduction zone leading up to its collision with the northwestern corner of the Kalahari craton is shown in Figs. 65a, 65b. According to this model, the rate of its southward migration exceeded the rate of closure in the Damara Belt so that the Kalahari craton arrived at the consuming arc while the main deformational pulse was still proceeding in the central parts of the Damara Belt. The leading edge of the subduction zone, consisting of ophiolitic material from an accretionary prism (the Grootderm Suite) and part of a Chilean-type forearc basin (the Oranjemund Suite) was obducted in a south-east to SSE direction across the passive margin of the craton (Fig. 65c; cf. Kröner, 1979; Smith & Hartnady, 1984). It acquired its arcuate shape because of gravitational forces resisting displacements up the west-dipping continental slope. The eastern part of the arc will have become sutured while overriding continued to the west for some distance. An analogous present-day example is the southern Lesser Antilles arc which is colliding in an ESE direction with the northeastern continental South America (Speed, 1985).

Overriding caused detachment and folding of the PNA foreland sediments, with transport at a very oblique angle to the trend of the belt. Thickening of the crust upset the geothermal profile and produced low T, high P Barrovian metamorphism. The M_1 porphyroblasts are post-tectonic with respect to D_1 since pressures decreased during isostatic readjustment while temperatures continued to increase at depth due to the upward convection of heat (cf. England & Richardson, 1977; England & Thompson, 1984). Loading of the lithosphere caused flexuring and subsidence of the Nama basin ahead of the deformation front, resulting in deposition of the upper Schwarzrand and lower Fish River molasse (Germs, 1983).

The subduction zone continued its southward migration in a direction roughly parallel to the western margin of the Kalahari craton, but because the obducted Marmora Terrane had become sutured to the PNA, a major left-lateral transform fault developed in an off-shore position at or near the interface between the continental and oceanic lithosphere (Fig. 65d). Some left-lateral wrench and transtensional structures developed in the adjacent, presently exposed parts of the Gariep Belt. The Pan-African evolution of the region ended with the emplacement of the Kuboos-Bremen line of plutons, prior to, or during the final closure of the Damara Belt.

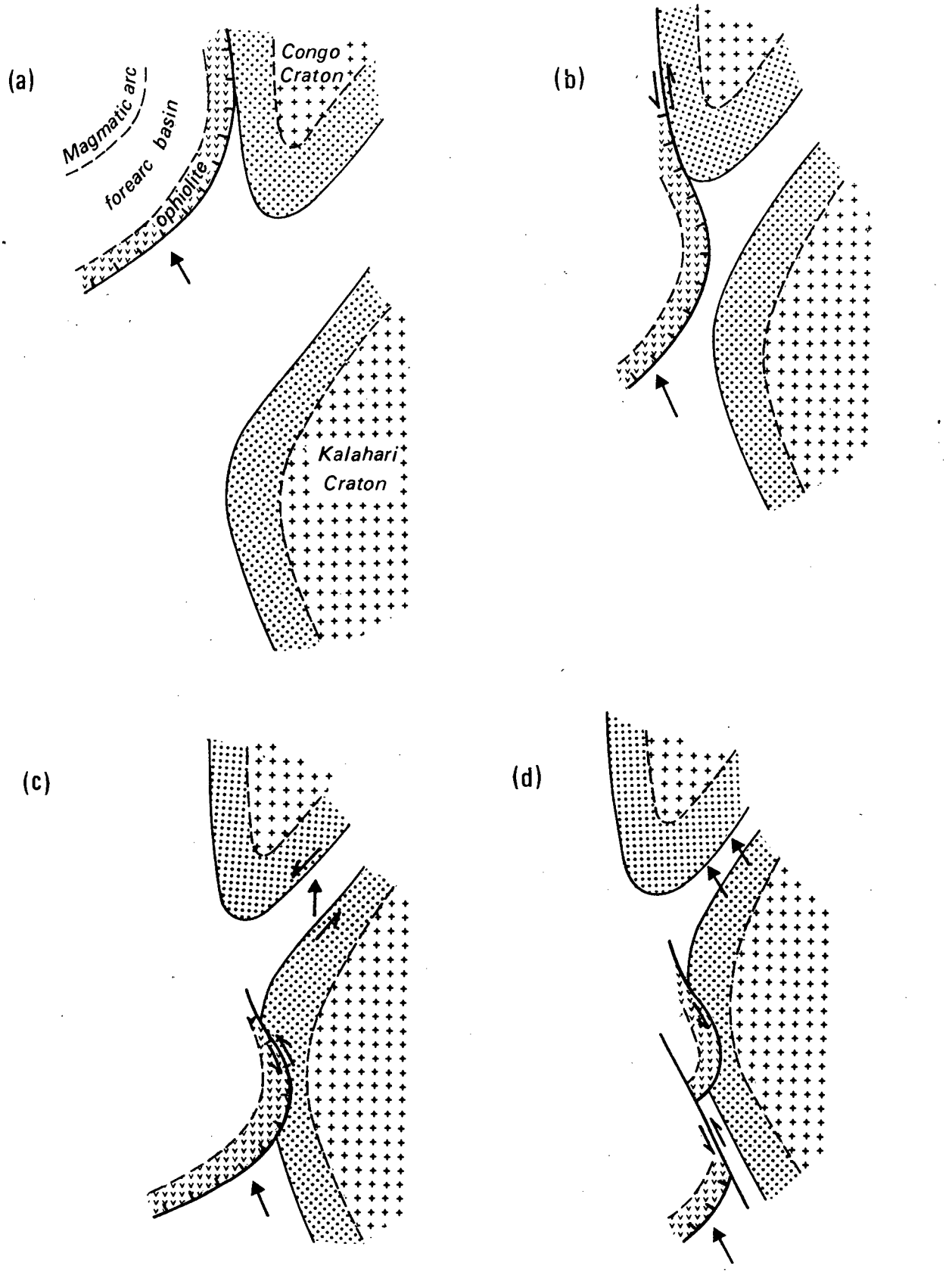

Fig. 65 : Schematic model showing successive configurations of a coastal subduction zone that could have led to the development of the Gariep arc.

5.2 Summary

5.2.1 Stratigraphy

(i) The Port Nolloth Assemblage in the central marginal parts of the Gariep Belt is a westward-younging passive continental margin succession, resting with a faulted contact on older crystalline basement;

(ii) The basal Stinkfontein Sequence is composed of clastic sediments which become finer-grained upwards and away from a main depocentre in the central Richtersveld. It is subdivided into four formations. To the east, the Lekkersing Formation, consisting of quartz arenite, grit and orthoconglomerate of proximal fluvial origin, interfingers with and is overlain by distal fluvial deposits and minor volcanics of the Vredefontein Formation. The Vredefontein is overlain with a mainly discordant contact by discontinuous debris flow deposits of the Kaigas Formation. The diamictitic beds around Numees Prospect and those in the immediate hanging-wall of the Klipneus fault are correlated with the Kaigas on lithological and structural grounds. To the west, in the deeper, submerged parts of the basin, shallow marine clastics and carbonates of the Gumchavib Formation were deposited;

(iii) Overlying the Stinkfontein with a a complex contact relationship is the carbonate-bearing Hilda Sequence, which should include the upper Helskloof and upper Kaigas beds. The Hilda is made up of three lithofacies units. The lower and upper dolomitic units, the Pickelhaube and Dabie River Formations, were laid down at moderate to shallow water depths in a carbonate platform environment. The middle Wallekraal Formation consists of laterally discontinuous conglomerates, grits, quartzites and schists which were deposited as submarine fans from a northeasterly source;

(iv) The Numees Sequence, which incorporates the Bloeddrif, Goms, and Eksteenfontein diamictites, rests unconformably on the Hilda. A lower Jakkalsberg Formation, consisting of banded iron formation and ferruginous quartzite of probable volcanic origin, is intercalated with and overlain by unbedded glaciogenic diamictite of the Sendelingsdrif Formation;

(v) The Holgat Sequence overlies the Numees and is probably a time-equivalent of the lowermost Nama Group. The sequence is made up of wackes, schists, and carbonates that were deposited in a slope or basin environment. Some of the immature, clastic material may have been derived as molasse from the advancing Pan-African deformation front.

5.2.2 Structure

(i) Faulting in the Armmanshoek-Omsberge area in the adjacent basement is equated to backthrusting of the Vioolsdrif granitoids in the southern Richtersveld over the Rosyntjieberg Formation, Orange River Group, during the Kibaran Namaqua Orogeny;

(ii) The basement rocks were subjected to a phase of dextral shearing in a north to NNE direction prior to deposition of the Stinkfontein sediments;

(iii) Syn-sedimentary gravity tectonics has played a relatively minor role in shaping the Pan-African structures;

(iv) At least five Pan-African deformational phases were recognized on the basis of overprinting relationships, structural styles and orientations (Table 19);

(v) Most of the major folds and faults formed during the D_1 overthrusting event. Leading-edge folds (e.g. the Eksteenfontein syncline), intraplate folds (the Sendelingsdrif synclinorium), and trailing-edge ramp anticlines (the Annisfontein anticlinorium) are represented;

(vi) The fabric styles and orientations associated with D_1 vary systematically along the strike of the Gariep Belt because of a northward increase in the wrench shear/thrust shear ratio. The stratigraphy is extensively imbricated by low-angle thrust faults in the southern Richtersveld, while strike-slip tear faults and tight upright shear folds become important in southern SWA/Namibia;

(vii) The transport direction during D_1 as determined from stretching lineations was to the southeast or SSE. A sinistral offset of ~15 km is apparent for the basement-involved Klipneus fault, but displacements on other faults are poorly constrained. Finite strain ellipsoids change from weakly deformed, sub-horizontal oblate shapes in the south and southwest to strongly stretched, NNW-plunging prolate shapes to the northeast because of differential movements during overthrusting;

(viii) The D_2 backfolds are interpreted as sinistral wrench tectonic structures on the basis of the geometry of pre-existing lineations deformed by the folds and the absence of transverse lineations. A few SSE-directed frontal thrusts, including the Numees cross-fault, are associated with this event;

(ix) The style and geometry of the late (D_3 and D_5) structures suggests that they formed during south-east trending sinistral transtensional shear which was active until after the emplacement of the Kuboos-Bremen Line of intrusives. Some D_4 compressional structures occur in the pluton aureoles.

Event	Faults, dykes, etc.	Folds	Associated cleavage	Associated lineation
D_1	Numerous NNW-SSE trending thrust faults; faults steepen north-eastwards.	i) Asymmetric, open to isoclinal F_1 folds with NNW-SSE axes and eastward vergeance; ii) Sheath folds with NNW-trending axes.	Penetrative S_1 schistosity striking NNW-SSE, at a low angle sub-parallel to S_0 in the west but steepening eastwards.	Strong NNW-plunging L_1 stretching lineation; steepens northeastwards.
D_2	-	Abundant non-cylindrical, close F_2 folds with NNW-trending axes and westward vergeance.	Shallow to moderate ENE-dipping S_2 crenulation cleavage often developed.	Sub-horizontal to shallow NNW-plunging L_2 mineral lineation.
D_3	Minor NNW-SSE trending normal faults.	Rare open small-scale F_3 gravity folds. Axes strike NNW-SSE.	Incipient axial planar S_3 cleavage, westward inclined.	-
D_4	Reverse faults. Trends mimic Kuboos pluton contact.	F_4 kink folds, conjugate folds, and box folds with E-W to WNW trending axes.	Strong S_4 schistosity in the pluton aureole.	S-plunging L_4 mineral lineation along pluton margin.
D_5	ESE-WNW striking normal faults, dykes, veins, fractures, joints.	-	Local S_5 fracture cleavage parallel to faults.	Sub-vertical L_5 slickensiding.

Table 19 : Summary of structural features associated with the Pan-African deformational events.

5.2.3 Metamorphism

(i) A microscopic study of mineral assemblages and microtextures indicated the existence of only one regional high-P prograde metamorphic event, M_1, which reached greenschist facies grade, and peaked between D_1 and D_2. No variations in P/T conditions are apparent across or along the marginal part of the Gariep Belt;

(ii) M_2 was a localized thermal metamorphic episode that postdated D_1 and D_2 and is associated with the late intrusive bodies.

5.2.4 Geodynamics

(i) The stratigraphic, structural and metamorphic evidence is consistent with a plate tectonic model involving the growth and closure of a Pan-African Atlantic Ocean;

(ii) The rifting stage of passive margin development (~900-720 Ma) commenced with ductile crustal stretching, causing gradual subsidence and the growth of a clastic sedimentary basin. The crust eventually ruptured producing basaltic dyke intrusions, alkali magmatism, volcanic extrusions and immature rift sedimentation. The change to a sea-floor spreading stage (~720 - 650 Ma) was gradual, and transgressive carbonate-rich sediments were laid down into the subsiding basin;

(iii) Oceanic convergence culminated in oblique collision of the continental margin with a subduction complex and the southeastward obduction of a sheet of ophiolitic material over the west-facing passive margin sediments (~650-580 Ma). Models relating this event to the final closure of the Damara Belt are discounted by the geochronological, sedimentological and structural data;

(iv) The continued SSE-ward migration of the uncollided part of the subduction complex parallel to the western margin of the Kalahari craton caused late strike-slip wrenching in the collisional foreland and transform faulting in the unexposed hinterland during the final stages of the Pan-African orogeny (~580-480 Ma).

REFERENCES CITED

Ahrendt, H., Hunziker, J.C., and Weber, K., 1978. Age and degree of metamorphism and time of nappe emplacement along the southern margin of the Damara Orogen/Namibia (SW Africa). Geol. Rdsch., 67, 719-742.

Alexander, Capt., J.E., 1838. An Expedition of Discovery into the Interior of Africa, London, (2 Vols.).

Allsopp, H.L., Köstlin, E.O., Welke, H.J., Burger, A.J., Kröner, A., and Blignault, H.J., 1979. Rb-Sr and U-Pb geochronology of Late Precambrian-Early Palaeozoic igneous activity in the Richtersveld (South Africa) and southern South West Africa. Trans. geol. Soc. S. Afr., 82, 185-204.

Barnes, S.J., and Sawyer, E.W., 1980. An alternative model for the Damara Mobile Belt. Ocean crust subduction and continental convergence. Precambr. Res., 13, 297-336.

Beck, M., Cox, A., and Jones, D.L., 1980. Penrose Conference report - Mesozoic and Cenozoic microplate tectonics of western North America. Geology, 8, 454-456.

Beetz, W., 1926. Die Konkip- und Namaformation. In: Kaiser, E. (Ed.) Die Diamantenwuste Sudwest-Afrikas. D. Reimer Verlag, Berlin, 92-122.

Bernasconi, A., 1983. Geological comparison of Precambrian and early Paleozoic terrains between the southern west coast of Africa and the southeast coast of South America. Precambr. Res., 23, 9-31.

Bertrand, J.M., 1976. Granitoids and deformation sequence in the Goodhouse-Henkries area. A new interpretation of the relationship between rocks in the Vioolsdrif-Goodhouse area and the Namaqualand and Bushmanland gneisses. A. Rep. Precambr. Res. Unit, Univ. Cape Town, 13, 61-70.

Bertrand, J.M., and Caby, R., 1978. Geodynamic evolution of the Pan-African orogenic belt: A new interpretation of the Hoggar Shield (Algerian Sahara). Geol. Rdsch., 67, 357-383.

Biot, M.A., Ode, H., and de Roever, W.L., 1961. Experimental verification of the folding of stratified viscoelastic media. Bull. geol. Soc. Am., 72, 1621-1632.

Black, R., Caby, R., Moussine-Pouchkine, A., Bayer, R., Bertrand, J.M., Boullier, A.M., Fabre, J., and Lesquer, A., 1979. Evidence for late Precambrian plate tectonics in West Africa. Nature, 278, 223-226.

Blaine, J.L., 1977. Tectonic evolution of the Waldau Ridge structure and the Okahandja Lineament in part of the central Damara Orogen, west of Okahandja, South West Africa. Trans. geol. Soc. S. Afr., 82, 329-333.

Blignault, H.J., 1974. Aspects of the Richtersveld Province: In: Kröner, A. (Ed.) Contributions to the Precambrian geology of Southern Africa. Bull. Precambr. Res. Unit, Univ. Cape Town, 15, 49-56.

Blignault, H.J., 1977. Structural-metamorphic imprint on part of the Namaqua Mobile Belt in South West Africa. Bull. Precambr. Res. Unit, Univ. Cape Town, 23, 197pp.

Booth, P.W.K., 1987. The relationship between the Richtersveld and Bushmanland Subprovinces in the Namaqualand coastal belt. In: Hartnady, C.J.H. (Ed.) Proceedings and Abstracts of the Alex. L. du Toit Golden Jubilee Conference on Tectonostratigraphic Terrane Analysis. Precambr. Res. Unit, Univ. Cape Town, 34-35.

Botha, J., 1986. Bergwoestyn van die Richtersveld. Custos, 15, 12-19.

Boyer, S.E., 1986. Styles of folding within thrust sheets: examples from the Appalachian and Rocky Mountains of the U.S.A. and Canada. J. Struct. Geol., 8, 325-340.

Boyer, S.E., and Elliott, D., 1982. Thrust systems. Bull. Am. Ass. Petrol. Geologists, 66, 1196-1230.

Breitkopf, J.H., and Maiden, K.J., 1986. A volcanogenic exhalative iron formation in the Southern Margin Zone of the Damara Orogen. Commun. geol. Surv. S.W.A./Namibia, 2, 131-144.

Bryant, B., and Reed, J.C., 1969. Significance of lineation and minor folds near major thrust faults in the southern Appalachians and the British and Norwegian Caledonides. Geol. Mag., 106, 412-429.

Burger, A.J., and Coertze, F.J., 1973. Radiometric age measurements on rocks from Southern Africa to the end of 1971. Bull. geol. Surv. S. Afr., 58, 46pp.

Butler, R.W.H., 1982. The terminology of structures in thrust belts. J. Struct. Geol., 4, 239-245.

Butler, R.W.H., 1985. Thrust tectonics: a personal view. Geol. Mag., 122, 223-232.

Butler, R.W.H., 1987. Thrust sequences. J. Struct. Geol., 9, 619-634.

Butler, R.W.H., and Coward, M.P., 1984. Geological constraints, deep geology and structural evolution of the NW Scottish Caledonides. Tectonophysics, 3, 347-365.

Caby, R., Dostal, J., and Dupuy, L., 1977. Upper Proterozoic volcanic greywackes from northwestern Hoggar (Algeria) - geology and geochemistry. Precambr. Res., 5, 283-297.

Charlesworth, H.A.K., Langenberg, C.W., and Ramsden, J., 1976. Determining axes, axial planes and sections of macroscopic folds using computer-based methods. Can. J. Earth Sci., 13, 54-65.

Clifford, T.N., 1967. The Damaran episode in the Upper Proterozoic-Lower Palaeozoic structural history of Southern Africa. Spec. Pap. geol. Soc. Am., 92, 100pp.

Cobbold, P.R., 1979. Removal of finite deformation using strain trajectories. J. Struct. Geol., 1, 67-72.

Corvinus, G., and Hendey, Q.B., 1978. A new Miocene vertebrate locality at Arrisdrift in SWA (Namibia). Neues Jb. Geol. Palaont. Mn., 4, 193-205.

Coward, M.P., 1980. The Caledonian thrust and shear zones of NW Scotland. J. Struct. Geol., 2, 11-17.

Coward, M.P., 1983. The tectonic history of the Damara Belt. In: Miller R. McG. (Ed.) Evolution of the Damara orogen, South West Africa/Namibia. Spec. Publ. geol. Soc. S. Afr., 11, 409-429.

Coward, M.P., and Kim, J.H., 1981. Strain within thrust sheets. In: McClay, K., and Price, N.J. (Eds.) Thrust and Nappe Tectonics. Spec. Publs. geol. Soc. Lond., 9, 275-292.

Coward, M.P., and Potts, G.J., 1983. Complex strain patterns at the frontal and lateral tips to shear zones and thrust zones. J. Struct. Geol., 5 383-399.

Crowell, J.C.,1983. The recognition of ancient glaciations: Bull. geol. Soc. Am. Mem., 161, 279-288.

Dahlström, C.D.A., 1969. Balanced cross-sections. Can. J. Earth Sci., 6, 743-757.

Davies, C., and Coward, M.P., 1982. The structural evolution of the Gariep Arc in southern Namibia. Precambr. Res., 17, 173-198.

De Villiers, J., 1945. The age of the Numees tillite relative to the Nama System. Trans. geol. Soc. S. Afr., 48, 135-142.

De Villiers, J., 1968. A. Rep. Precambr. Res. Unit, Univ. Cape Town, 6, 36pp.

De Villiers, J., and Burger, A.J., 1967. Note on the minimum age of certain granites from the Richtersveld area. Ann. geol. Surv. S. Afr., 6, 83-84.

De Villiers, J., and Söhnge, P.G., 1959. The geology of the Richtersveld. Mem. geol. Surv. Dep. Min. S. Afr., 48, 295pp.

Donath, F.A., and Parker, R.B., 1964. Folds and Folding. Bull. geol. Soc. Am., 75, 45-62.

Dorr, J.V.N., 1973. Iron Formation in South America. Econ. Geol., 68, 1005-1022.

Dreimanis, A., and Schluchter, C., 1985. Field criteria for the recognition of till or tillite. Palaeogeogr., Palaeoclimatol., Palaeoecol., 51, 7-14.

Dunn, E.J., 1872. On the country traversed by the "Gold Prospecting Expedition" Namaqualand. Cape of Good Hope Parl. Rep., G 21, Cape Town.

Dunnet, D., and Siddans, A.W.B., 1971. Non-random sedimentary fabrics and their modification by strain. Tectonophysics, 12, 307-325.

Eisbacher, G.H., 1978. Re-definition and subdivision of the Rapitan Group, Mackenzie Mountains. Pap. geol. Surv. Can., 77-35, 21pp.

Elliott, D., 1976. The motion of thrust sheets. J. Geophys. Res., 81, 949-963.

Elliott, D., 1976 a. The energy balance and deformation mechanisms of thrust sheets. Phil. Trans. R. Soc., A273, 289-319.

Elliott, D., 1983. The construction of balanced cross sections. J. Struct. Geol., 5, 101-102.

Elliott, D., and Johnson, M.R.W., 1980. Structural evolution in the northern part of the Moine thrust belt, NW Scotland. Trans. R. Soc. Edinburgh: Earth Sciences, 71, 69-96.

Engel, A.E.J., Dixon, T.H., and Stern, R.J., 1980. Late Precambrian evolution of Afro-Arabian crust from ocean arc to craton. Bull. geol. Soc. Am., 91, 199-206.

England, P.C., and Richardson, S.W., 1977. The influence of erosion on the mineral facies of rocks from different metamorphic environments. J. geol. Soc. Lond., 134, 201-213.

England, P.C., and Thompson, A.B., 1984. Pressure temperature time paths of regional metamorphism. I. Heat transfer during the evolution of regions of thickened continental crust. J. Petrol., 25, 894-928.

Flint, R.F., Sanders, J.E., and Rodgers, J., 1960. Diamictite, a substitute term for symmite. Bull. geol. Soc. Amer., 71, 1809.

Fyfe, W.S., and Turner, F.J., 1966. Reappraisal of the concept of metamorphic facies. Beit. Mineral. Petrog., 12, 354-364.

Gass, I.G., 1977. The evolution of the Pan-African crystalline basement in NE Africa and Arabia. J. geol. Soc. Lond., 134, 129-138.

Gass, I.G., 1978. Evolutionary model for the Pan-African crystalline basement (abs.) Precambr. Res., 6, A23.

Gendzwill, D.J., and Stauffer, M.R., 1981. Analysis of triaxial ellipsoids: their shapes, plane sections, and plane projections. Math. Geol., 13, 135-150.

Germs, G.J.B., 1972. The stratigraphy and paleontology of the Lower Nama Group, South West Africa. Bull. Precambr. Res. Unit, Univ.Cape Town, 12, 250pp.

Germs, G.J.B., 1974. The Nama Group in South West Africa and its relationship to the Pan-African geosyncline. J. Geol., 82, 301-307.

Germs, G.J.B., 1983. Implications of a sedimentary facies and depositional environmental analysis of the Nama Group in South West Africa/Namibia. In: Miller, R. McG. (Ed.) Evolution of the Damara orogen, South West Africa/Namibia. Spec. Publ. geol. Soc. S. Afr., 11, 409-429.

Germs, G.J.B., Knoll, A.H., and Vida, G., 1986. Latest Proterozoic microfossils from the Nama Group, Namibia (South West Africa). Precambr. Res., 32, 45-62.

Ghosh, S.K., 1966. Experimental tests of buckling folds in relation to strain ellipsoid in simple shear deformation. Tectonophysics, 3, 169-185.

Gray, D.R., 1977. Morphological classification of crenulation cleavage. J. Geology, 85, 229-235.

Greenwood, W.R., Hadley, D.G., Anderson, R.E., Fleck, R.J., and Schmidt, D.L., 1976. Late Proterozoic cratonization in southwestern Saudi Arabia. Phil. Trans. Roy. Soc. London, A230, 517-527.

Gresse, P.G., 1987. The Vanrhynsdorp foreland thrust-fold belt in southern Namaqualand. In: Hartnady, C.J.H. (Ed.) Proceedings and Abstracts of the Alex. L. du Toit Golden Jubilee Conference on Tectonostratigraphic Terrane Analysis. Precambr. Res. Unit, Univ. Cape Town, 34-35.

Gross, G.A., 1973. The depositional environment of principal types of Precambrian iron-formation. In: Genesis of Precambrian Iron and Manganese Deposits. Proc. Kiev. Symp. UNESCO Earth Sciences, 9, 15-21.

Guj, P., 1970. The Damara mobile belt in the south-western Kaokaveld, South West Africa. Bull. Precambr. Res. Unit, Univ. Cape Town, 18, 168pp.

Hälbich, I.W., Gresse, P.G., Freyer, E.E., and Horstmann, U., 1987. Evidence for oblique southward subduction along the west coast of Southern Africa in Pan-African times. In: Hartnady, C.J.H. (Ed.) Proceedings and

Abstracts of the Alex. L. du Toit Golden Jubilee Conference on Tectonostratigraphic Terrane Analysis. Precambr. Res. Unit, Univ. Cape Town, 36.

Hambrey, M.J., and Harland, W.B., 1985. The Late Proterozoic Glacial Era. Palaeogeogr., Palaeoclimatol., Palaeoecol., 51, 255-272.

Harland, W.B., 1971. Tectonic transpression in Caledonian Spitzbergen. Geol. Mag., 108, 27-42.

Harland, W.B., 1983. The Proterozoic glacial record. In: Medaris, L.G., Byers, C.W., Michelson, D.M., and Shanks, W.C. (Eds.) Proterozoic geology. Bull. geol. Soc Am. Mem., 161, 279-288.

Hartmann, O., Hoffer, E., and Haack, U., 1983. Regional metamorphism in the Damara orogen: Interaction of crustal motion and heat transfer. Spec. Publ. geol. Soc. S. Afr., 11, 233-241.

Hartnady, C.J.H., 1973. A new model for the Damaran Orogeny. Unpubl. rep., Annex. to IGP Res. Project proposal of the Precam. Res. Unit, Univ. Cape Town.

Hartnady, C.J.H., 1978. The Structural Geology of the Naukluft Nappe Complex and its relationship to the Damara Orogenic Belt, S.W.A/Namibia. Unpubl. Ph.D. thesis, Univ. Cape Town.

Hartnady, C.J.H., 1978 a. An appraisal of research trends in Pan-African terrains and the PRU's role in South African sciences. A. Rep. Precambr. Res. Unit, Univ. Cape Town, 14&15, 145-150.

Hartnady, C.J.H., 1983. Structural geology in the PRU. A. Rep. Precambr. Res. Unit, 18-20, 52-75.

Hartnady, C.J.H., Joubert, P., and Stowe, C., 1985. Proterozoic crustal evolution in southwestern Africa. Episodes, **8**, 236-244.

Hartnady, C.J.H., and Vajner, V., 1975. Formulation of a tectonic data-base. In: GEOKONGRES 75: Mineralisation in Metamorphic Terranes. Abstr. Geocongr. 75, geol. Soc. S. Afr., 50-53.

Hartnady, C.J.H., von Veh, M.W., and Booth, P.W.K., 1984. Excursion A (Tectonic Option) In: Conference on Middle to Late Proterozoic lithosphere evolution. Excursion Guidebook Precambr. Res. Unit, Univ. Cape Town, 1-63.

Haughton, S.H., 1961. Discussion of "The Gariep System" by J. de Villiers. Publ. C.C.T.A. 80, 89.

Haughton, S.H., 1963. Stratigraphic history of Africa south of the Sahara. Oliver and Boyd, Edinburgh, 365pp.

Hendey, Q.B., 1978. Preliminary report on the Miocene vertebrates from Arrisdrift. Ann. S. Afr. Mus., 76, 1-41.

Henry, G., Stanistreet, I.G., and Maiden, K.J., 1986. Preliminary results of a sedimentological study of the Chuos Formation in the Central Zone of the Damara Orogen: evidence for mass flow processes and glacial activity. Commun. geol. Surv. S.W.A./Namibia, 2, 75-92.

Hobbs, B.E., Means, W.D., and Williams, P.F., 1976. An Outline of Structural Geology. J. Wiley & Sones, New York, 571pp.

Hoffman, K.H., 1983. Lithostratigraphy and facies of the Swakop Group of the Southern Damara Belt, S.W.A/Namibia. In: Miller R. McG. (Ed.) Evolution of the Damara orogen, South West Africa/Namibia. Spec. Publ. geol. Soc. S. Afr., 11, 409-429.

Horstmann, U.E., 1987. Die metamorphische Entwicklung im Damara Orogen, Sudwest Afrika/Namibia, abgeleitet aus K/Ar-Datierungen an detritischen Hellglimmern aus Molassesedimenten der Nama Group. Gottinger Arb. Geol. Palaont., 32, 78-86.

Hossack, J.R., 1983. A cross-section through the Scandinavian Caledonides constructed with the aid of branch-line maps. J. Struct. Geol., 5, 103-111.

Hudleston, P.J., 1973. Fold morphology and some geometrical implications of theories of fold development. Tectonophysics, 16, 1-46.

Hudleston P.J., and Stephansson, O., 1973. Layer shortening and fold shape development in the buckling of single layers. Tectonophysics, 17, 299-321.

Jacobson, C.E., 1983. Structural geology of the Pelona Schist and Vincent thrust, San Gabriel Mountains, California. Bull. geol. Soc. Am., 94, 753-767.

Jamison, W.R., 1987. Geometric analysis of fold development in overthrust terranes. J. Struct. Geol., 9, 207-219.

Joubert, P., 1971. The regional tectonism of the gneisses of part of Namaqualand. Bull. Precambr. Res. Unit, Univ. Cape Town, 10, 220pp.

Joubert, P., and Kröner, A., 1972. The Stinkfontein Formation south of the Richtersveld. Trans. geol. Soc. S. Afr., 75, 47-54.

Joubert, P., Hartnady, C.J.H., and von Veh, M.W., 1986. The geology of the Alexander Bay area. Explanation of Sheet 2816 (Scale 1 : 250 000), Open file rep. geol. Surv. Dep. Min., 28pp.

Kaiser, E., 1926. Die Eruptivgesteine der Chloritschieferstufe, der Konkip- und der Namaformation und die Amphibolitisierung in diesn Stufen. In: Kaiser, E. (Ed.) Die Diamantenwuste Sudwest-Afrikas.D. Reimer Verlag, Berlin, 190-208.

Kalkani, E.C., and von Frese, R.R.D., 1980. Computer construction of equal-angle fabric diagrams and program comparisons. Computers and Geosciences, 6, 279-288.

Kasch, K.W., 1979. A continental collision model for the tectono-thermal evolution of the (southern) Damara Belt. A. Rep. Precambr. Res. Unit, Univ. Cape Town, 16, 101-107.

Kasch, K.W., 1981. The structural geology, metamorphic petrology and tectonothermal evolution of the southern Damara belt around Omitara, SWA/Namibia. Bull. Precambr. Res. Unit, Univ. Cape Town, 27, 333pp.

Kasch, K.W., 1983. Tectonothermal evolution of the southern Damara Orogen. In: Miller, R. McG. (Ed.) Evolution of the Damara Orogen, South West Africa/Namibia. Spec. Publ. geol. Soc. S. Afr., 11, 255-265.

Kasch, K.W., 1983a. Continental collision, suture progradation and thermal relaxation: A plate tectonic model for the Damara Orogen. In: Miller, R. McG. (Ed.) Evolution of the Damara Orogen, South West Africa/Namibia. Spec. Publ. geol. Soc. S. Afr., 11, 423-430.

Kimberly, M.M., 1978. Paleaoenvironmental classification of iron formations. Econ. Geol., 73, 215-229.

Knetsch, G., 1937. Ubersicht uber die Geologie des sudlichen Lüderitzlandes. Geol. Rdsch., 28, 208-223.

Kröner, A., 1972. Preliminary resume of the geology of the Gariep geosyncline in the Orange River area. In: De Villiers, J. (Ed.) A. Rep. Precambr. Res. Unit, Univ. Cape Town, 7-9, 51-57.

Kröner, A., 1974. The Gariep Group, Part I: Late Precambrian formations in the western Richtersveld, northern Cape Province. Bull. Precambr. Res. Unit, Univ. Cape Town, 13, 115pp.

Kröner, A., 1974a. Reports on research activities - The Gariep Group. A. Rep. Precambr. Res. Unit, Univ. Cape Town, 10-11, 73-74.

Kröner, A., 1975. Late Precambrian formations in the western Richtersveld, northern Cape Province. Trans. R. Soc. S. Afr., 41, 375-433.

Kröner, A., 1977. Non-synchroneity of late Precambrian glaciations in Africa. J. Geol., 85, 289-300.

Kröner, A., 1977a. The Sinclair aulacogen - a Late Proterozoic volcano-sedimentary association along the Namib Desert of southern Namibia. Abstr. Colloq. Afr. Geol. Goettingen, 9, 83.

Kröner, A., 1979. Pan-African mobile belts as evidence for a transitional tectonic regime from intraplate orogeny to plate margin orogeny. In: Al-Shanti, A. (Ed.) Evolution and mineralization of the Arabian-Nubian Shield. Pergamon Press, Oxford, 21-27.

Kröner A., and Blignault, H.S., 1976. Towards a definition of some tectonic and igneous provinces in western South Africa and southern South West Africa. Trans. geol. Soc. S. Afr., 79, 232-238.

Kröner, A., and Germs, G.J.B., 1971. A re-interpretation of the Numees-Nama contact at Aussenkjer, South West Africa. Trans. geol. Soc. S. Afr., 74, 69-74.

Kröner, A., and Hawkesworth, C.J., 1977. Late Pan-African emplacement ages for Rossing alaskitic granite (Damara belt) and Rooi Lepel bostonite (Gariep belt) in Namibia and their significance for the timing of metamorphic events. A. Rep. res. Inst. Afr. Geol., Univ. Leeds, 20, 14-17.

Kröner, A., and Jackson, M.P.A., 1974. Geological reconnaissance of the coast between Lüderitz and Marble Point, South West Africa. Bull. Precambr. Res. Unit, Univ. Cape Town, 15, 79-103.

Kröner A., McWilliams, M.O., Germs, G.J.B., Reid, A.B. and Schalk, K.E.L., 1980. Paleomagnetism of late-Precambrian mixtite-bearing formations. Am. J. Sci., 280, 942-968.

Kröner, A., and Rankama, R., 1972. Late Precambrian sedimentary rocks in southern Africa: a compilation with definitions and correlations. Bull. Precambr. Res. Unit, Univ. Cape Town, 11, 37pp.

Kröner, A., and Welin, E., 1973. Evidence for a +500 my old thermal episode in southern South-West Africa. Earth Planet Sc. Lett., 21, 149-152.

Kruger, J.K., 1979. Structures and textures in till indicating subglacial deposition. Boreas, 8, 323-340.

Kruger, J.K., and Marcussen, I., 1976. Lodgement till and flow till; a discussion; Boreas, 5, 61-64.

Lagarde, J.L., and Michard, A., 1986. Stretching normal to the regional thrust displacement in a thrust-wrench shear zone, Rehamna Massif, Morocco. J. Struct. Geol., 8, 483-492.

Lindström, M., 1961. Beziehungen zwischen Klein faltenuergenzen und andern Gefugemerkmalen in den Kaledoniden Skandinaviens. Geol. Rdsch., 51, 144-180.

Lisle, R.J., 1977. Estimation of the tectonic strain ratio from the mean shape of deformed elliptical markers. Geologie Mijnb., 56, 140-144.

Loudon, T.V., Wheeler, J.F., and Andrew, K.P., 1980. Affine transformations for digitized spatial data in geology. Computers and Geosciences, 6, 397-412.

MacQueen, J.A., and Powell, D., 1977. Relations between deformation and garnet growth in the Moine rocks of W. Scotland. Bull. geol. Soc. Am., 88, 235-240.

Mancktelow, N.S., 1981. A least-squares method for determining the best-fit point maximum, great circle, and small circle to non-directional orientation data. Math. Geol., 13, 507-521.

Marshak, S., and Engelder, T., 1985. Development of cleavage in limestones of a fold-thrust belt in eastern New York. J. Struct. Geol., 7, 345-359.

Martin, H., 1965. Precambrian geology of South West Africa and Namaqualand. Rustica Press, Wynberg, Cape Province, 159pp.

Martin, H., 1983. Alternative geodynamic models for the Damara Orogeny. A critical discussion. In: Martin, H., and Eder, F.W. (Eds.) Intracontinental Fold Belts. Springer-Verlag, Berlin, 913-945.

Martin, H., and Porada, H., 1977. The intracratonic branch of the Damara orogen in South West Africa. I. Discussion of geodynamic models. Precambr. Res., 5, 311-388.

Martin, H., Porada, H., and Wallister, O.H., 1985. Mixtite deposits of the Damara sequence, Namibia, problems of interpretation. Palaeogeogr., Paleoclimatol., Palaeoecol., 51, 159-196.

McKee, E.D., 1982. The Supai Goup of Grand Canyon, Prof. Pap. U.S. geol Surv., 1173, 504pp.

McMillan, M.D., 1965. Preliminary report on the geology of the lower Fish River area, South West Africa. In: De Villiers, J. (Ed.) A. Rep. Precambr. Res. Unit, Univ. Cape Town, 3, 5-16.

McMillan, M.D., 1968 . The geology of the Witputs-Sendelingsdrif area. Bull. Precambr. Res. Unit, Univ. Cape Town, 4, 177pp.

Middlemost, E.A.K., 1964. Petrology of the plutonic and dyke-rocks of the south-eastern Richtersveld. Trans. geol. Soc. S. Afr., 67, 227-261.

Middlemost, E.A.K., 1966. The genesis of the Stinkfontein Formation. Trans. geol. Soc. S. Afr., 69, 87-98.

Miller, J.M.G., 1987. Palaeotectonic and stratigraphic implications of the Kingston Peak - Noonday contact in the Panamint Range, Eastern California. J. Geol., 95, 75-86.

Miller, R. McG., 1983. A geodynamic model for the Damara Belt. In: Miller, R. McG. (Ed.) Evolution of the Damara Orogen, South West Africa/Namibia. Spec. Publ. geol. Soc. S. Afr., 11, 431-515.

Mitra, G and Elliott, D., 1980. Deformation of basement in the Blue Ridge and the development of the South Mountain cleavage. In: Wones, D.R. (Ed.) The Caledonides of the USA. Virginia Polytech. Inst. Mem. geol. Soc. Sci., 2, 167-177.

Mitra G. and Yonkee, W.A., 1985. Relationship of spaced cleavage to folds and thrusts in the Idaho-Utah-Wyoming thrust belt. J. StructGeol., 7, 361-373.

Miyashiro A. and Shido, F., 1984. Tschermak substitution in low- and middle-grade pelitic schists. J. Petrology., 2, 449-487.

Moody, J.D., and Hill, M.J., 1956. Wrench-fault tectonics. Bull. geol. Soc. Am., 67, 1207-1246.

Onstott, T.C., Hargraves, R.B., and Reid, D.L., 1986. Constraints on the tectonic evolution of the Namaqua Province III: paleomagnetic and $^{40}Ar/^{39}Ar$ results from the Gannakouriep dyke swarm. Trans. geol. Soc. S. Afr., 89, 171-183.

Ovenshine, A.T. 1970. Identification of ice-rafted deposits; Bull. geol. Soc. Am., 81, 891-894.

Page, D.C., and Watson, M.D., 1976. The Pb-Zn deposit of Rosh Pinah Mine, South West Africa. Econ. Geol., 71, 306-327.

Page, D.C., and Kindl, S., 1978. The Zinc-Lead-Copper deposits of the Rosh Pinah Mine, South West Africa. Unpubl. Rep., IMCOR Zinc(Pty.) Ltd., Rosh Pinah, 17pp.

Peach, C.J., and Lisle, R.J., 1979. A Fortran IV program for the analysis of tectonic strain using deformed elliptical markers. Computers and Geosciences, 5, 325-334.

Porada, H., 1979. The Damara-Ribeira orogen of the Pan-African/Brasiliano Cycle in Namibia and Brazil as interpreted in terms of continental collision. Tectonophysics, 57, 237-265.

Porada, H., 1983. Geodynamic model for the geosynclinal development of the Damara Orogen, Namibia/South West Africa. In: Martin, H., and Eder, F.W., (Eds.) Intracontinental Fold Belts. Springer-Verlag, Berlin, 503-542.

Price, R.A., 1981. The Cordilleran foreland thrust and fold belt in the southern Canadian Rocky Mountains. In: McClay, K., and Price, R.A. (Eds.) Thrust and Nappe Tectonics. Spec. Publs. geol. Soc. Lond., 9, 427-448.

Price, R.A., 1986. The southeastern Canadian Cordillera: thrust faulting, tectonic wedging, and delamination of the lithosphere. J. Struct. Geol., 8, 239-254.

Ramsay, J.G., 1967. Folding and Fracturing of Rocks. McGraw-Hill, New York, 568pp.

Ramsay, J.G., and Huber, M.I., 1983. The Techniques of modern Structural Geology. Vol. 1: Strain Analysis. Academic Press, London, 307pp.

Reid, D.L., 1977. Geochemistry of Precambrian igneous rocks in the Lower Orange River Region. Bull. Precambr. Res. Unit, Univ. Cape Town, 22, 397pp.

Reid, D.L., 1979. Age relationships within the Mid-Proterozoic Vioolsdrif batholith, lower Orange River Region. Trans. geol. Soc. S. Afr., 82, 305-311.

Reid,D.L., 1979a.The Late Precambrian Gannakouriep mafic dyke swarm, lower Orange River region. Geol. Soc. S. Afr., 18th Congr. Abstracts, 1, 286-285.

Reid, D.L., 1979b. Basic-ultrabasic complexes within the Vioolsdrif batholith, lower Orange River region. Geol. Soc. S. Afr., 18th Congr. Abstracts, 1, 282-285.

Reid, D.L., 1982. Age relationships within the Vioolsdrif batholith, lower Orange River region. II. A two stage emplacement history and the extent of Kibaran overprinting. Trans. geol. Soc. S. Afr., **85**, 105-110.

Rhodes, S., and Gayer, R.A., 1977. Non-cylindrical folds, linear structures in the X direction and mylonite developed during translation of the Caledonian Kalak Nappe Complex of Finnmark. Geol. Mag., 114, 329-341.

Ritter, U., 1978. The southwestern Richtersveld between Eksteenfontein and Klein Helskloof, its relationship to Gariep metamorphism and tectonism and to the Namaqua Metamorphic Complex. A. Rep. Precambr. Res. Unit, Univ. Cape Town, 14 & 15.

Ritter, U., 1980. The Precambrian evolution of the Eastern Richtersveld. Bull. Precambr. Res. Unit, Univ. Cape Town, 26, 276pp.

Roberts, J.L., 1974. The structure of the Dalradian rocks in the SW Highlands of Scotland. J. geol. Soc. Lond., 130, 93-124.

Rogers, A.W., 1915. The geology of part of Namaqualand. Trans. geol. Soc. S. Afr., 18, 72-101.

Rogers, A.W., 1929. The Ventersdorp System. In Steinmann, G., and Wilckens, O. (Eds.) Handbuch der Regionalen Geologie, Bd. VII, (7 Abt.), The Union of South Africa, Carl Winters Universitatsbuchhandlungen, Heidelberg.

Salomon, K.B., 1978. An efficient point-in-polygon algorithm. Computers and Geosciences, 4, 173-178.

Sanderson, D.J., 1973. The development of fold axes oblique to the regional trend. Tectonophysics, 16, 55-70.

Sanderson, D.J., 1982. Models of strain paths and strain fields within nappes and thrust sheets. Tectonophysics, 88, 201-233.

Sanderson, D.J., and Marchini, W.R.D., 1984. Transpression. J. Struct. Geol., 6, 449-458.

Sassi, F.P., and Scolari, A., 1974. The b_0 value of the potassic white micas as a barometric indicator in low-grade metamorphism of pelitic schists. Contr. Miner. Petrol., 45, 143-152.

Schemerhorn, I.J.G., 1974. Late Precambrian mixtites: glacial and/or nonglacial? Am. J. Sc., 274, 673-824.

Sherwin, J.A., and Chapple, W.M., 1968. Wavelengths of single layer folds: A comparison between theory and observation. Am. J. Sci., 266, 167-179.

Shimamoto, T., and Ikeda, Y., 1976. A simple algebraic method for strain estimation from deformed elliptical objects. I. Basic theory. Tectonophysics, 36, 315-337.

Shimron, A.E., 1987. Proterozoic orogenesis and crustal evolution in the Richtersveld Subprovince. A. Rep. Precambr. Res. Unit, Univ. Cape Town, 21-23, 58-66.

Simpson, C., and Schmid, S.M., 1983. An evaluation of criteria to deduce the sense of movement in sheared rocks. Bull. geol. Soc. Am., 94, 1281-1288.

Smith, H.S., and Hartnady, C.J.H., 1984. Geochemistry of Grootderm Formation lavas: Indication of tectonic environment of extrusion (Abs.). Precambr. Res. Unit, Univ. Cape Town, 21st A. Conf., 20-21.

Söhnge, P. G., and de Villiers, J., 1946. Resume of the geology of the Richtersveld and the eastern Sperrgebiet. Trans. geol. Soc. S. Afr., 49, 263-276.

Söhnge, P. G., and de Villiers, J., 1948. The Kuboos Pluton and its associated line of intrusives. Trans. geol. Soc. S. Afr., 51, 1-31.

South African Committee for Stratigraphy (SACS), 1977. South African Code of stratigraphic terminology and nomenclature. Trans. geol. Soc. S. Afr., 20, 22pp.

South African Committee for Stratigraphy (SACS), 1980. The Gariep Complex. In: Kent, L.E. (Comp.) Stratigraphy of Southern Africa. I. Lithostratigraphy of the Republic of South Africa, South West Africa /Namibia, and the Republics of Bophuthswana, Transkei and Venda. Handbk. geol. Surv. Dep. Min. S. Afr., 8, 690pp.

Speed, R.C., 1985. Cenozoic collision of the Lesser Antilles Arc and continental South America and the origin of the El Pilar fault. Tectonics, 4, 41-69.

Stowe, C.W., Hartnady, C.J., and Joubert, P., 1984. Proterozoic tectonic provinces of Southern Africa. (Abs). Precambr. Res., 25, 229-231.

Suppe, J., 1983. Geometry and kinematics of fault-bend folding. Am. J. Sci., 283, 648-721.

Suppe, J., and Medwedeff, D.A., 1984. Fault-propagation folding. Abs. Progm. geol. Soc. Am., 16, 670.

Sylvester, A.G., and Smith, R.R., 1976. Tectonic transpression and basement-controlled deformation in the San Andreas fault zone, Salton Trough, California. In: Sylvester, A.G. (Ed.). Wrench Fault Tectonics. AAPG Reprint Series, 28, 173-194.

Tankard, A.J., Eriksson, K.A., Hobday, D.K., Hunter, D.R., Minter, W.E.L., 1982. Crustal evolution of Southern Africa. Springer Verlag, New York, 480pp.

Theart, H.F.J., 1980. The geology of the Precambrian terrane in parts of western Namaqualand. Bull. Precambr. Res. Unit, Univ. Cape Town, 30, 103pp.

Turner, F.J., and Weiss, L.E., 1963. Structural analysis of metamorphic tectonites. McGraw-Hill, New York, 545pp.

Van Biljon, S., 1939. The Kuboos batholith in Namaqualand, South Africa. Trans. geol. Soc. S. Afr., 42, 123-219.

Van Vuuren, C.J.J., 1986. Regional setting and structure of the Rosh Pinah Zinc-Lead deposit, South West Africa/Namibia. In: Anhaeusser, C.R., and Maske, S. (Eds.) Mineral Deposits of Southern Africa. Vol II. Geol. Soc. S. Afr., Johannesburg, 1593-1607.

Vernon,R.H., 1978. Porphyroblast-matrix microstructural relationships in deformed metamorphic rocks. Geol. Rdsch., 67, 288-305.

Visser, J.N.J., 1983. The problems of recognizing ancient subaqueous debris flow deposits in glacial sequences. Trans. geol. Soc. S. Afr., 86, 127-136.

Von Veh, M.W., 1980. Development of systems for digitizer and computer in the study of structural fabrics, and their application to selected samples from the Malmesbury Group. Unpubl. B.Sc. (Hons.) thesis, Univ. Cape Town, 37pp.

Von Veh, M.W., 1983. Aspects of sedimentation, structure and tectonic evolution in the Tygerberg Terrane, Southwestern Cape Province. Bull. Precambr. Res. Unit, Univ. Cape Town, 32, 88pp.

Von Veh, M.W., 1987. A profile across the Gariep Belt. In: Hartnady, C.J.H. (Ed.) The Richtersveld Excursion of the Tectonostratigraphic Terrane Analysis Conference. Precambr. Res. Unit, Univ. Cape Town, 15-32.

Von Veh, M.W., 1987a. Stratigraphy and structure of the Port Nolloth Terrane, Gariep Belt. A. Rep. Precambr. Res. Unit, Univ. Cape Town, 21-23.

Von Veh, M.W., 1987b. GASTRA-3: An interactive computer packagefor the analysis of finite strains from elliptical markers. A. Rep. Precambr. Res. Unit, Univ. Cape Town, 21-23, 48-54.

Von Veh, M.W., and Hartnady, C.J.H., 1986. RPHIN - A Fortran 77 program for acquiring axial ratios, long axis orientations and centroid positions of elliptical strain markers. Computers and Geosciences, 12, 339-347.

Von Veh, M.W., and Shimron, A.E., 1987. Tectonostratigraphic subdivision of the northern Richtersveld. In: Hartnady, C.J.H. (Ed.) Proceedings and Abstracts of the Alex. L. du Toit Golden Jubilee Conference on Tectonostratigraphic Terrane Analysis. Precambr. Res. Unit, Univ. Cape Town, 32.

Watkinson, A.J., and Cobbold, P.R., 1981. Axial directions of folds in rocks with linear/planar fabrics. J. Struct. Geol., 3, 211-217.

Weiss, L.E., 1959. Geometry of superposed folding. Bull. geol. Soc. Am., 70, 91-106.

Welke, H.J., Burger, A.J., Corner, B., Kröner, A., and Blignault, H.J., 1979. U-Pb and Rb-Sr age determinations on middle Proterozoic rocks from the Lower Orange river area, South West Africa. Trans. geol. Soc. S. Afr., 82, 205-214.

Whitten, E.H.T., 1969. Trends in computer applications in structural geology. In: Merriam, D.F. (Ed.) Computer applications in structural geology: an international symposium. Plenum Press, New York, 233-249.

Whitten, E.H.T., 1981. Trends in computer applications in structural geology: 1969 -1979. In: Merriam, D.F. (Ed.) Computer applications in the Earth Sciences: An update of the 70's: Plenum Press, New York, 323-368.

Wilcox, R.E., Harding, T.P., and Seely, D.R., 1973. Basic wrench tectonics. Bull. Am. Ass. Petrol. Geol., 57, 74-96.

Williams, G.D., and Chapman, T.J., 1983. Strains developed in the hangingwall of thrusts due to their slip/propagation rate; a dislocation model. J. Struct. Geol., 5, 563-571.

Williams, P.F., 1985. Correlation in multiply deformed terrains. J. Struct. Geol., 7, 269-285.

Woodcock, N.H., 1977. Specification of fabric shapes using an eigenvalue method. Bull. geol. Soc. Am., 88, 1231-1236.

Wyley, A.W., 1857. Report upon the mineral and geological structure of south Namaqualand and the adjoining mineral districts. Cape of Good Hope Parl. Rep., G 36, Cape Town.

Yeo, G., 1978. Iron-Formation in the Rapitan Group, Mackenzie Mountains, Yukon and Northwest Territories. Econ. Geol. Ser., Dept. of Northern Affairs Mineral Industry Rep., Northwest Territories, 5, 170-175.

Young, G.M., 1976. Iron-Formation and Glaciogenic rocks of the Rapitan Group, Northwest Territories, Canada. Precambr. Res., 3, 137-158.

Young, G.M., 1982. The Late Proterozoic Tindir Group, east-central Alaska - Evolution of a continental margin. Bull. geol. Soc. Am., 93, 759-783.

APPENDIX I

A computerized system for structural domain analysis

In order to capture, store, retrieve, and process the structural data obtained during the present study, a computer system, named G/ASTRA-1 (Graphics-based Advanced Structural and Strain Analysis Package - Component 1) was designed. G/ASTRA-1 evolved from an existing computer-based structural analysis package, the PRUDE system (Hartnady & Vajner, 1975; Hartnady, 1978). It has a similar structure to PRUDE and many of the PRUDE modules were used in its development. Although PRUDE contained routines for stereographic projection plotting, data-site map plotting, and statistical analysis of orientation data, it had shortcomings as a tool for domainal analysis. The range of data extraction and graphical procedures that it allowed for was limited and significant prior knowledge was required for its efficient operation. Being operational on the University of Cape Town Sperry Univac 1100, processing was generally done in batch mode and the "turn-around" time was slow.

The G/ASTRA-1 system was designed for use on a dedicated Hewlett-Packard work-station containing a graphics terminal, digitizer, and drafting and graphics plotters, so that user interaction with the computer could be significantly improved. Data handling and retrieval capabilities were enhanced through use of a commercial (Hewlett-Packard IMAGE/1000) database management system, and several new graphics modules were incorporated for plotting a variety of stereonets, maps, and cross-sections.

I.1 System design

The design of the system allows for collected field data to be entered into temporary input files and validated before being stored in a database. Data for subareas of interest are then extracted from the database, written to temporary output files, and analysed until the user is satisfied with the results. This process is illustrated by means of a flow chart (Fig. I.1):

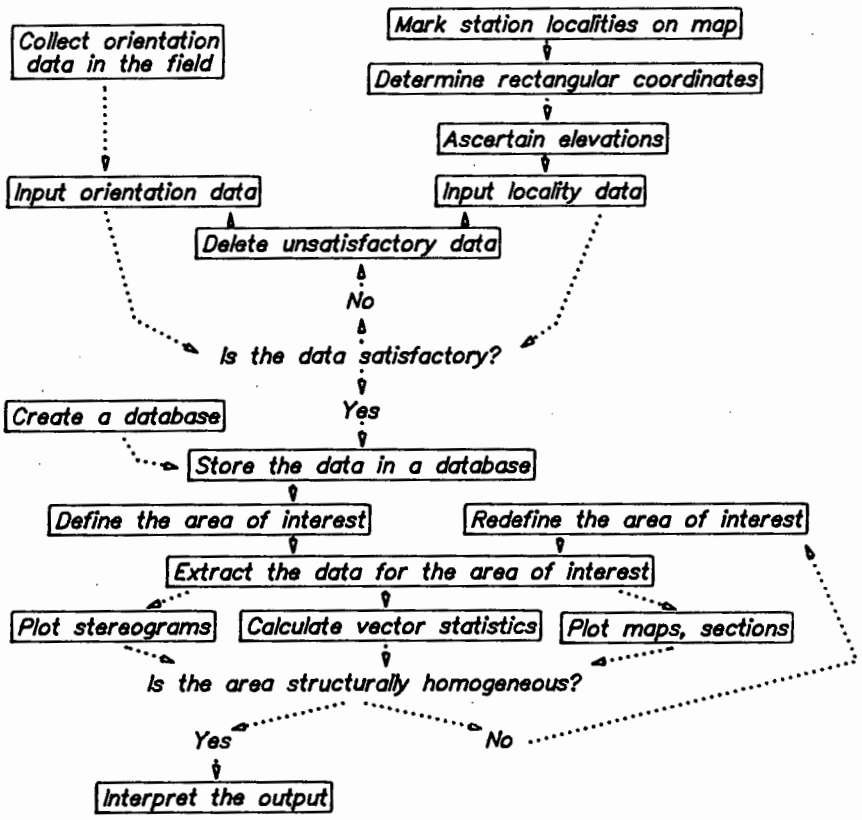

Fig. I.1 : Flow diagram illustrating the operational system supporting G/ASTRA-1.

A controlling program, ASTR1, presents the operator with the available options and activates requested program modules (Fig. I.2). Its design allows for by-passing or repeated scheduling of any of the available options, so that the user is not restricted to the operational system shown above. The database entry and extraction procedures can, for example, be entirely by-passed.

Fig.I.2 : Flow chart of the ASTR1 program showing names of scheduled modules.

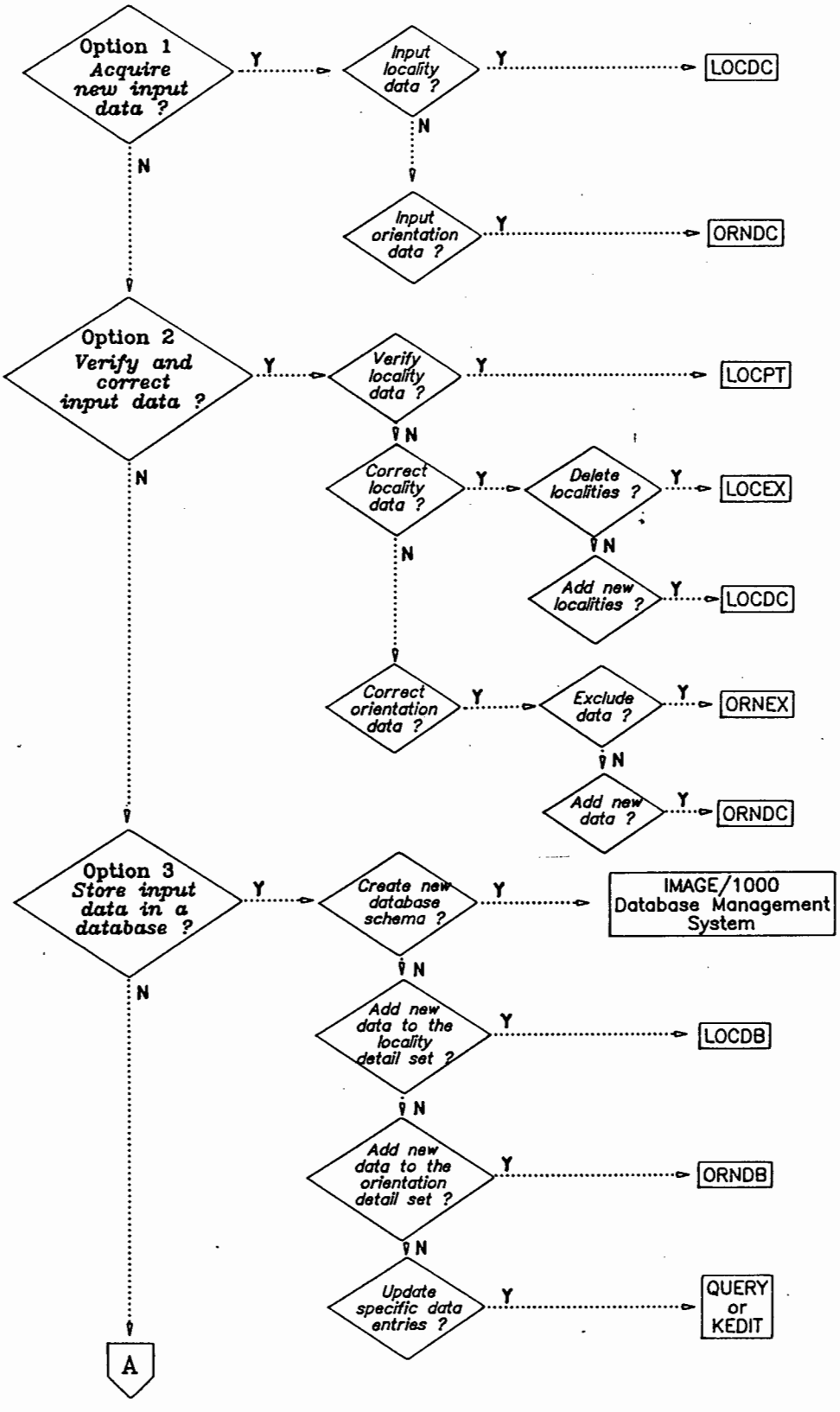

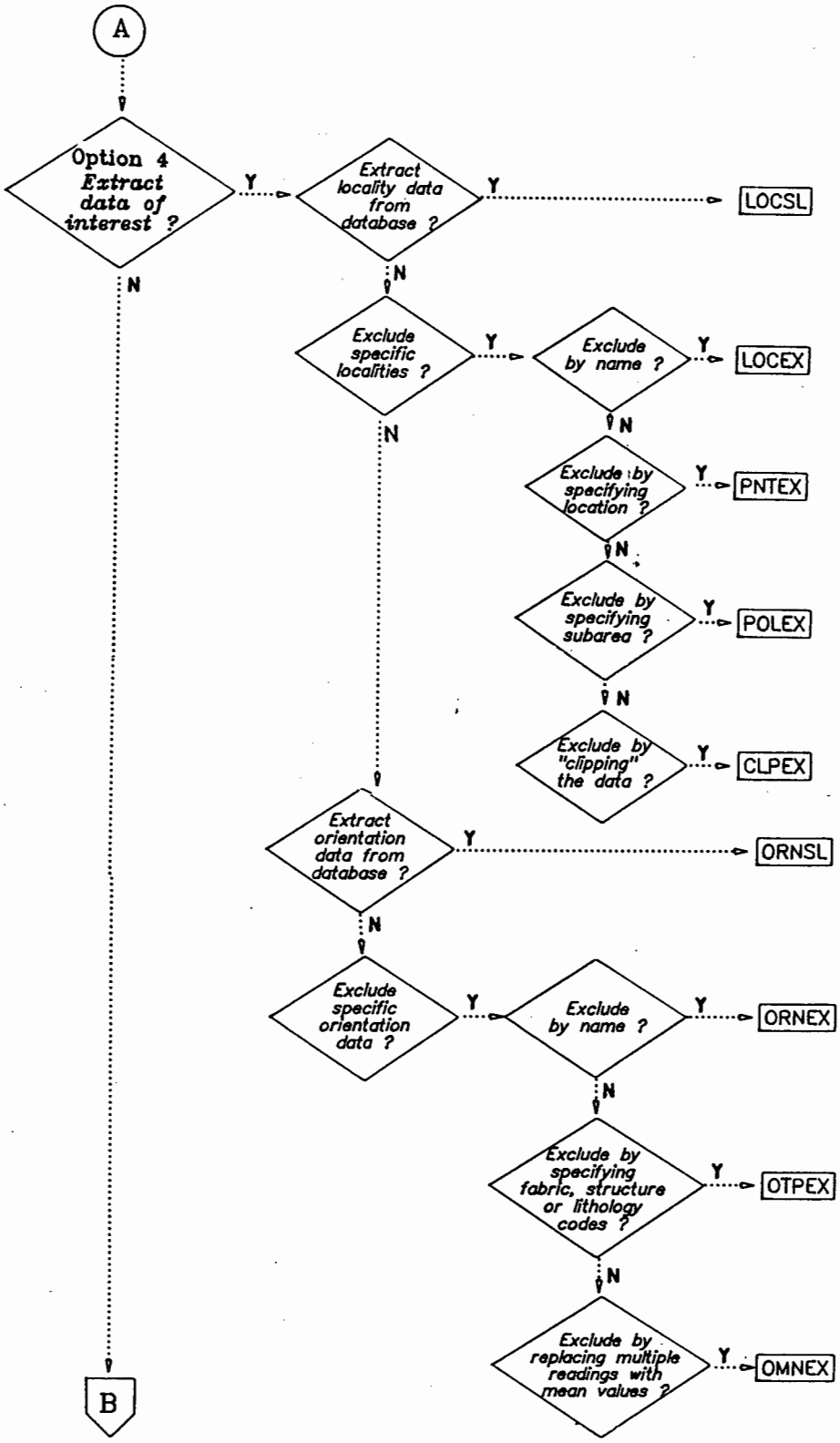
A
Option 4 Extract data of interest ?
Y
N
Extract locality data from database ?
Y
LOCSL
N
Exclude specific localities ?
Y
Exclude by name ?
Y
LOCEX
N
Exclude by specifying location ?
Y
PNTEX
N
Exclude by specifying subarea ?
Y
POLEX
N
Exclude by "clipping" the data ?
Y
CLPEX
N
Extract orientation data from database ?
Y
ORNSL
N
Exclude specific orientation data ?
Y
Exclude by name ?
Y
ORNEX
N
Exclude by specifying fabric, structure or lithology codes ?
Y
OTPEX
N
Exclude by replacing multiple readings with mean values ?
Y
OMNEX
B

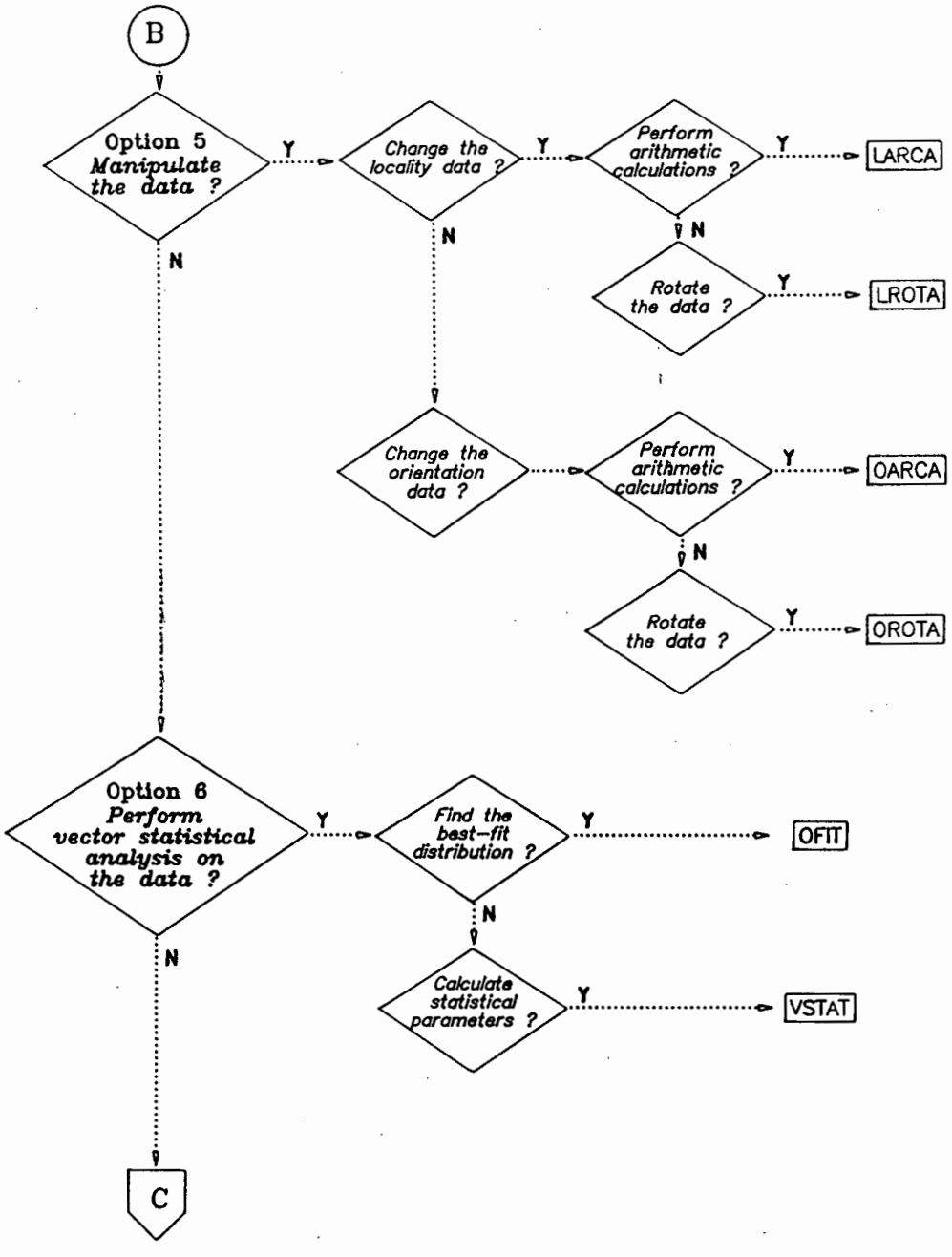
B
Option 5
Manipulate the data ?
Y
Change the locality data ?
Y
Perform arithmetic calculations ?
Y
LARCA
N
N
Rotate the data ?
Y
LROTA
N
Change the orientation data ?
Perform arithmetic calculations ?
Y
OARCA
N
Rotate the data ?
Y
OROTA
Option 6
Perform vector statistical analysis on the data ?
Y
Find the best-fit distribution ?
Y
OFIT
N
N
Calculate statistical parameters ?
Y
VSTAT
C

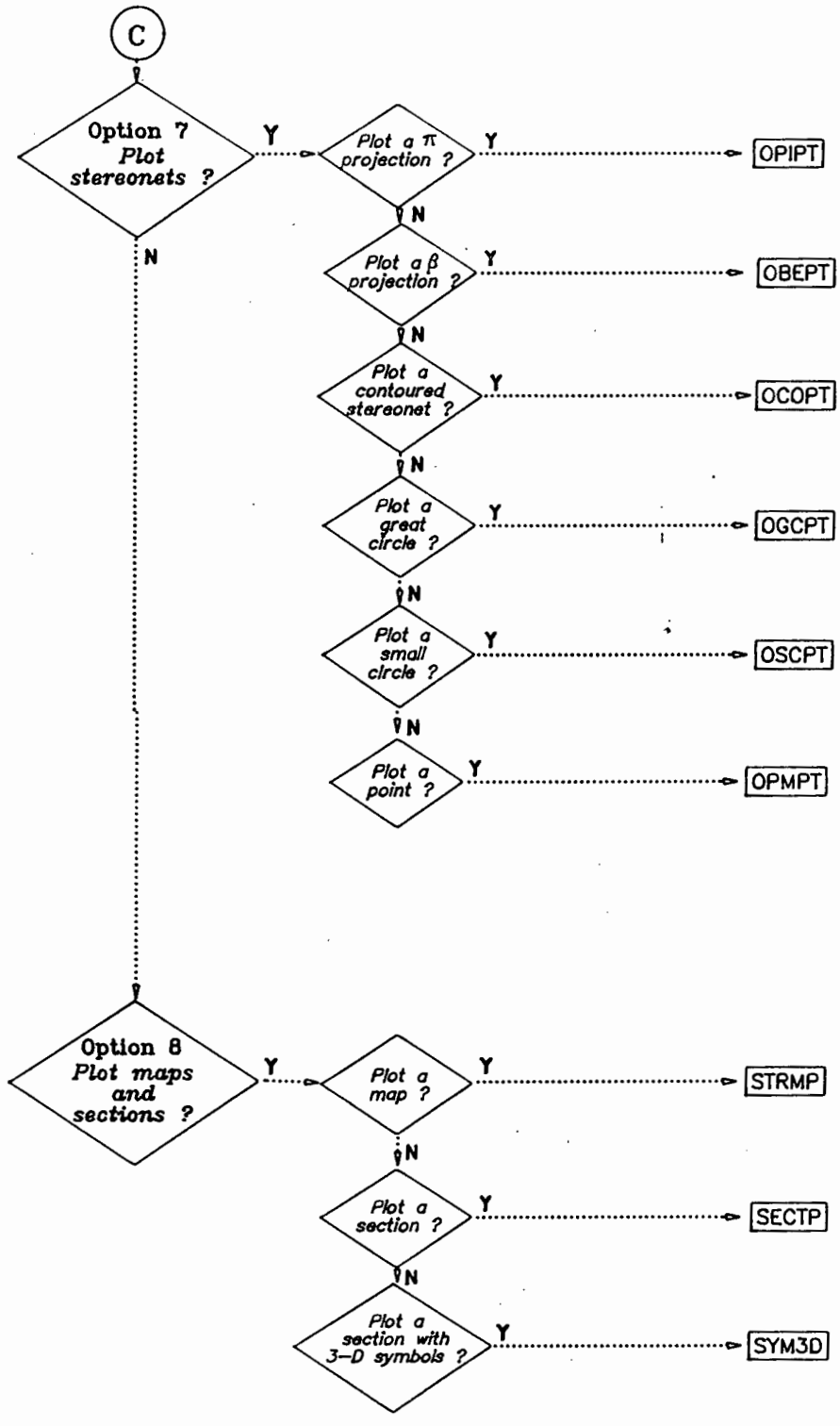
C
Option 7 Plot stereonets ?
Y
N
Plot a π projection ?
Y
OPIPT
N
Plot a β projection ?
Y
OBEPT
N
Plot a contoured stereonet ?
Y
OCOPT
N
Plot a great circle ?
Y
OGCPT
N
Plot a small circle ?
Y
OSCPT
N
Plot a point ?
Y
OPMPT
Option 8 Plot maps and sections ?
Y
Plot a map ?
Y
STRMP
N
Plot a section ?
Y
SECTP
N
Plot a section with 3-D symbols ?
Y
SYM3D

I.2 **Module descriptions**

The function of each of the modules shown in Fig. I.2. is described below. The author(s) or source of the coding is given in brackets after the module name.

Option 1 : Data capture

LOCDC (Von Veh; Loudon et al., 1980) : the location data input module captures three items of information for each location on a map: a station identification number, a pair of map reference coordinates, and a topographic elevation. This information is written to a temporary locality input disc file in a list-directed format (Table I.1).

Table I.1 : Example of a locality data set obtained from LOCDC. Order of variables is : x - coordinate, y - coordinate, elevation, identification number.

```
14356.33 4132.37 241.3 245
16235.74 3623.58 347.2 246
15243.90 3391.23 323.8 247
12934.71 4327.08 290.4 248
14904.46 3981.31 308.1 249
```

The map reference coordinates are obtained through use of a digitizing table. The digitized table coordinates are transformed into map coordinates and corrected for map distortions using routines described by Loudon et al. (1980). Elevation data can be captured interactively or determined from a previously prepared grid of elevation values. Grids are generated by a data contouring package, SACLANT, operational on the University of Cape Town UNIVAC 1100/81 Series.

ORNDC (Mr. C. Steyl, PRU) : captures the following items of information for each orientation data reading: a station identification number, an azimuth and inclination value, a fabric element code, a structure type code, and a rock type code. The data is entered using a data collection form (Fig. I.3) and transmitted to a temporary orientation input file (Table I.2). Readings are submitted in the form of trend/plunge for linear structural elements, and as strike/dip (right-handed down-dip rule) or dip direction/dip for planar fabric elements.

ORIENTATION DATA COLLECTION FORM

AZIMUTH	I	___	Azimuth refers to trend,strike or dip direction
INCLINATION	I	__	Inclination refers to plunge or dip
LOCALITY	I	____	Locality refers to station identification number
FABRIC	A	____	Fabric refers to the fabric element code
STRUCTURE	A	____	Structure refers to the structure type code
LITHOLOGY	A	____	Lithology refers to the rock type code

Fig. I.3 : Input form for collection of orientation data.The underscored spaces represent the unprotected fields into which the data is input. The data is of integer (I) or alphanumeric (A) type.

Table I.2 : Example of an orientation data set obtained from ORNDC. Order of variables is : azimuth, inclination, locality, fabric code, structure type code, lithology code.

319	55	244	S0	BED	SSTN
243	12	244	L1	FAX	SSTN
339	44	245	S0	BED	LMST
322	53	246	S1N	AXCL	MXTT
347	26	246	S2	CRCL	MXTT

The orientation data is verified at the stage of data entry. Errors that are checked for include: (i) azimuth and inclination input data is of integer type; (ii) azimuth readings are in the range 0^{o}-360^{o}; (iii) inclination readings are in the range 0^{o}-90^{o}; and (iv) fabric element, structure, and rock type codes are of alphanumeric type.

Option 2 : Data verification

LOCPT (Von Veh) : plots maps of station locations at any scale to enable locality data verification (Fig. I.4). Station identification numbers or station elevations can be plotted adjacent to the location markers. Potential sources of error for the locality data include faulty digitization of calibration points, incorrect entry of map coordinates of the calibration points, inaccurate digitization of locations, mistyped entry of station identification numbers, and misread or mistyped station elevations.

LOCEX (Von Veh) : removes erroneous data from the locality data file.

ORNEX (Von Veh) : removes erroneous data from the orientation data file.

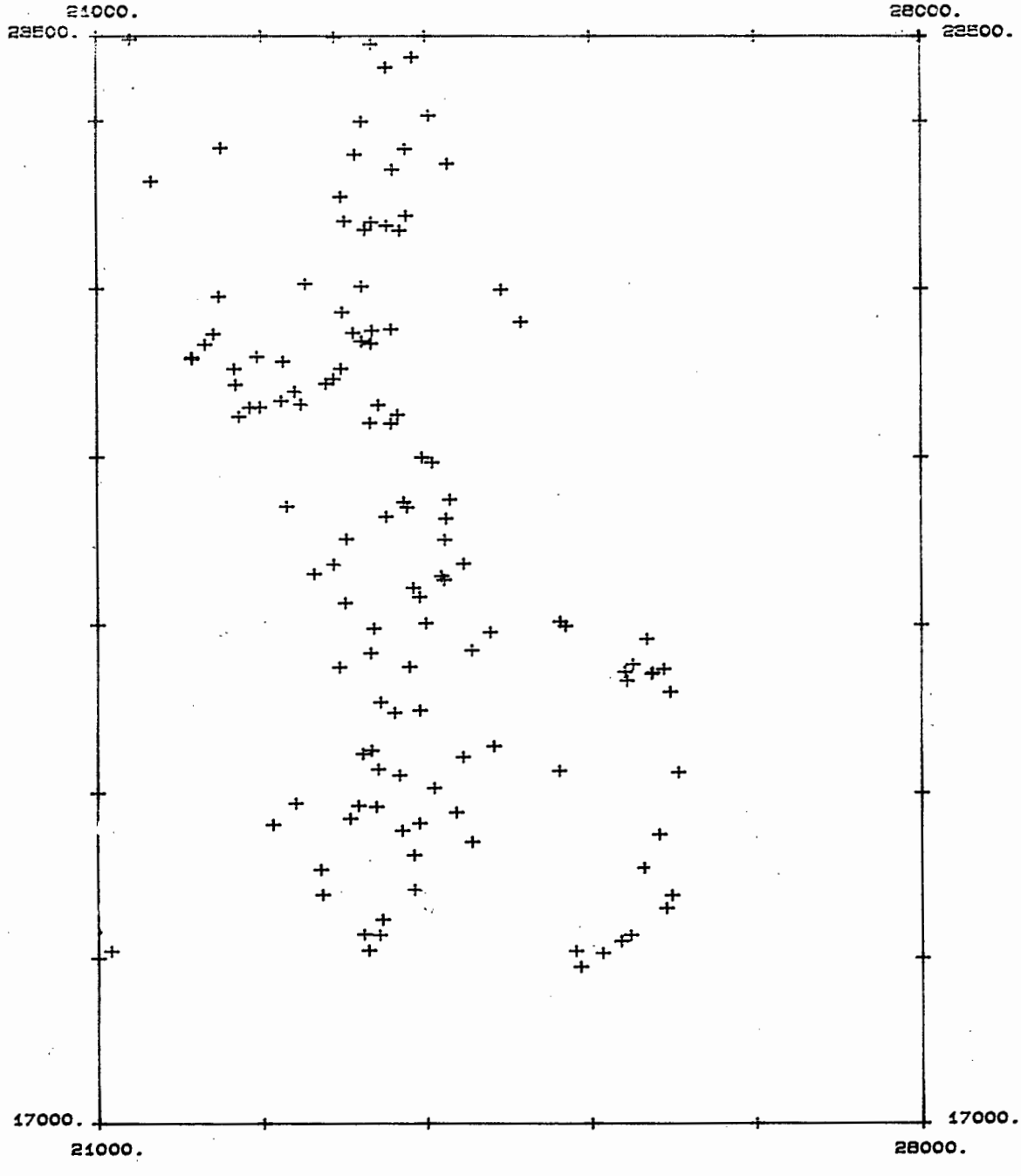

Scale 1: 40000.

HELSKLOOF AREA STATION LOCATIONS

Fig. I.4 : Plot of station locations produced by LOCPT (location numbers omitted).

Option 3 : Data storage

The IMAGE/1000 data-base management system was used to provide the archival storage medium. IMAGE/1000 uses a simple network structure to consolidate individual data files into a single, interrelated database (see Hewlett-Packard IMAGE/1000 92069A Data Base Management Systems Reference Manual). The network consists of master data sets connected by data paths to detail data sets. Master data sets can stand alone and contain information relating to a uniquely identifiable entity (manual master sets), or they can serve as a link to the detail data sets (automatic master sets). Automatic master sets contain only a single linking data item, the key item. The detail sets comprise entities of related data items.

The structural database was designed so as to distinguish between the entities of user's project information, location data, and orientation data. The following attributes of these entities were considered to be essential or potentially useful:

Entity	Data items
Project data:	Project code, geologist, date, area, map references, map origin for coordinates, descriptions of the fabric, structure and rock type codes used, and data collection method.
Location data:	Station number, map coordinates, station elevation
Orientation data:	Station number, azimuth, inclination, fabric type, structure, and rock type codes

Since the project information entity is uniquely identifiable and is not generally altered during data updates, it was designated as a manual master set. The link between the location and orientation data is through the station identification number, so that this key item forms an automatic master set. The relationships between the sets is illustrated in Fig. I.5.

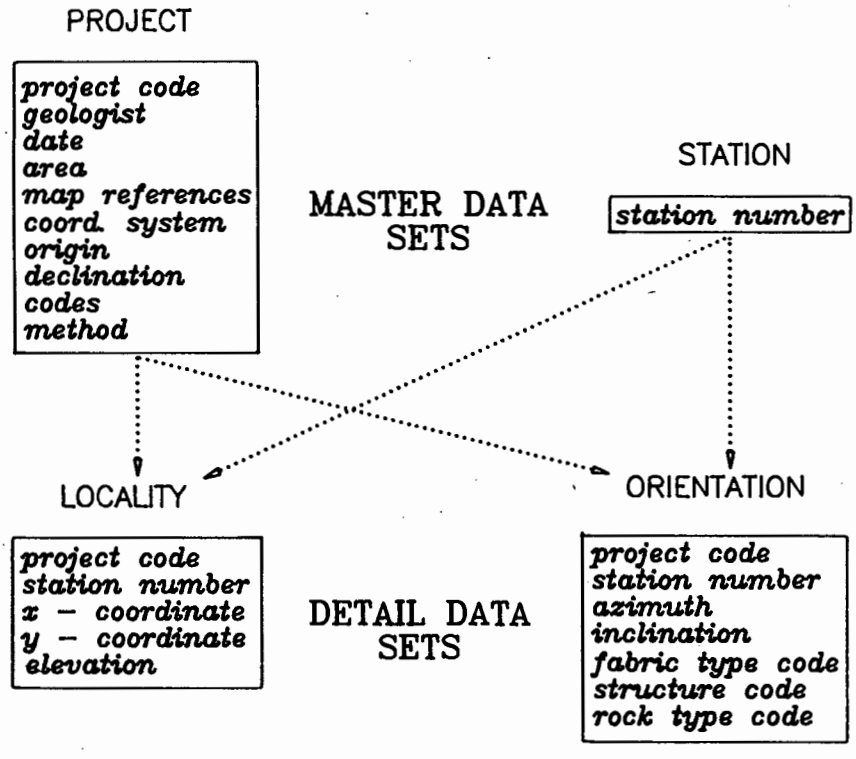

Fig. I.5 : Set relationships of the database.

The PROJECT master set must contain an entry with the correct project number before any locality or orientation data items are added for a particular station. A station number entry is however automatically added to the STATION master set when a detail entry is added to the LOCALITY or ORIENTATION detail sets, unless it already exists in the STATION set. Similarly a station number entry is automatically deleted if no data items are associated with that station.

IMAGE/1000 processes a description or schema of the database and creates the data files in which the database elements are stored. Applications modules gain access to the database through calls to IMAGE library subroutines. The database is generally created at the start of a project, at which stage the data items in the PROJECT master set are also entered (Fig. I.6):

Project code: 001 Geologist : M. W. von Veh Date : May, 1985
Area : Central portion of the Port Nolloth Terrane, Gariep Belt
Map references : 2816BB Sendelingsdrif, 2816BD Khubus, 2817AC Vandersterrberg
Coordinate system : Gauss conformal projection
Origin Latitude : 16° 45' E Longitude : 28° 30' S
Magnetic declination : 21° 6' W of TN (1972) decreasing 3' annually
Fabric element codes : SO - Sedimentary layering
S1 - Early foliation etc.
Structure type codes : CREC - Crenulation cleavage
FAX - Fold axes etc.
Lithology codes : QSST - Quartzitic sandstone
CNGL - Conglomerate etc.
Data collection method : COCLA magnetic stratum compass

Fig.I.6 : Example of the data item information in the PROJECT master set.

The modules scheduled by the data storage option are:

LOCDB (Steyl) : reads records from the temporary locality file and writes them into the database.

ORNDB (Steyl) : dumps records from the temporary orientation file into the database.

QUERY (IMAGE/1000) : provides access to the data in the database. It can be used to modify or delete data values, retrieve data that meets selection criteria or print information about selected data.

KEDIT (HP1000 User's Group) : an alternative more "user-friendly" utility for editing the database.

Option 4 : Data extraction

LOCSL (Steyl) : extracts the locality data contained within a specified rectangular area from the database and writes the data to a temporary locality file.

PNTEX (Von Veh) : excludes data from a locality file on the basis of digitized coordinate values.

POLEX (Salomon, 1978; Von Veh) : excludes data lying outside the boundary of a digitized subarea. A "point-in-polygon" algorithm is used to determine whether a point is interior to a polygonal boundary.

CLPEX (Von Veh) : excludes data lying beyond specified distances from a plane of section. Distances from the data station to the "hither" and "yon" planes is found through simultaneous linear equations.

ORNSL (Steyl) : retrieves the orientation data linked to the subset of localities from the orientation detail set of the database and writes the data to a temporary orientation disc file.

ORNEX (Von Veh) : excludes data associated with specified stations from the orientation file.

OTPEX (Von Veh) : excludes data associated with particular fabric element, structure type, or lithology type codes from the orientation file.

OMNEX (Prof. H.A.K. Charlesworth, University of Alberta) : excludes multiple readings by replacing them with a mean orientation value.

Option 5 : Data manipulation

LARCA (Von Veh) : performs arithmetic operations on the locality data, e.g. to redefine the map origin or to convert from one map reference frame or scale to another.

LROTA (University of Alberta) : rotates space coordinates about a given point.

OARCA (Von Veh) : performs arithmetical functions on the orientation data, e.g. to correct for magnetic declination.

OROTA (University of Alberta) : rotates orientation data about a given point.

Option 6 : Orientation data analysis

OFIT (Dr. N.S. Mancktelow, Max Planck Institute) : determines a "best-fit" plane (great circle or girdle), cone (small circle) and/or point maximum by minimizing the sum of the squares of the angular residuals (Mancktelow, 1981).

OVSTA (Dr. C.J.H. Hartnady, PRU) : determines a best-fit great circle or point maxima from the eigenvectors or "moments of inertia" of the data set. Mancktelow (1981) suggests that the OFIT method is appropriate for geological distributions with moderate scatter. OVSTA also computes Woodcock's (1977) fabric shape and strength parameters and the Lisle-Hossack fabric strength parameter (Lisle, 1977).

Option 7 : Stereonet plotting

OPIPT (Von Veh) : constructs lower hemisphere equal-area stereonets of lineations or poles to planes. The operator selects plotting symbols from the alphanumeric character set (Fig.I.7a). The position of the stereonet on the plotter and its diameter can be specified. The primitive circle and the plot title can be omitted to allow for the overlay of diagrams.

OBEPT (Von Veh) : draws a stereonet diagram of the planar data.

OGCPT (Von Veh) : draws a user-defined great circle arc on a stereonet.

OSCPT(Von Veh) : draws a user-defined small circle on a stereonet.

OPMPT (Von Veh) : plots user-defined points on a stereonet.

OCOPT (Kalkani & Von Frese, 1980) : performs density contouring and plotting of the fabric data (Fig.I.7 b). The module uses a spherical grid, of user-defined size (1^{o}, 2^{o}, 3^{o}, 5^{o}, 6^{o}, or 9^{o}) to determine population densities. The contour interval can be specified.

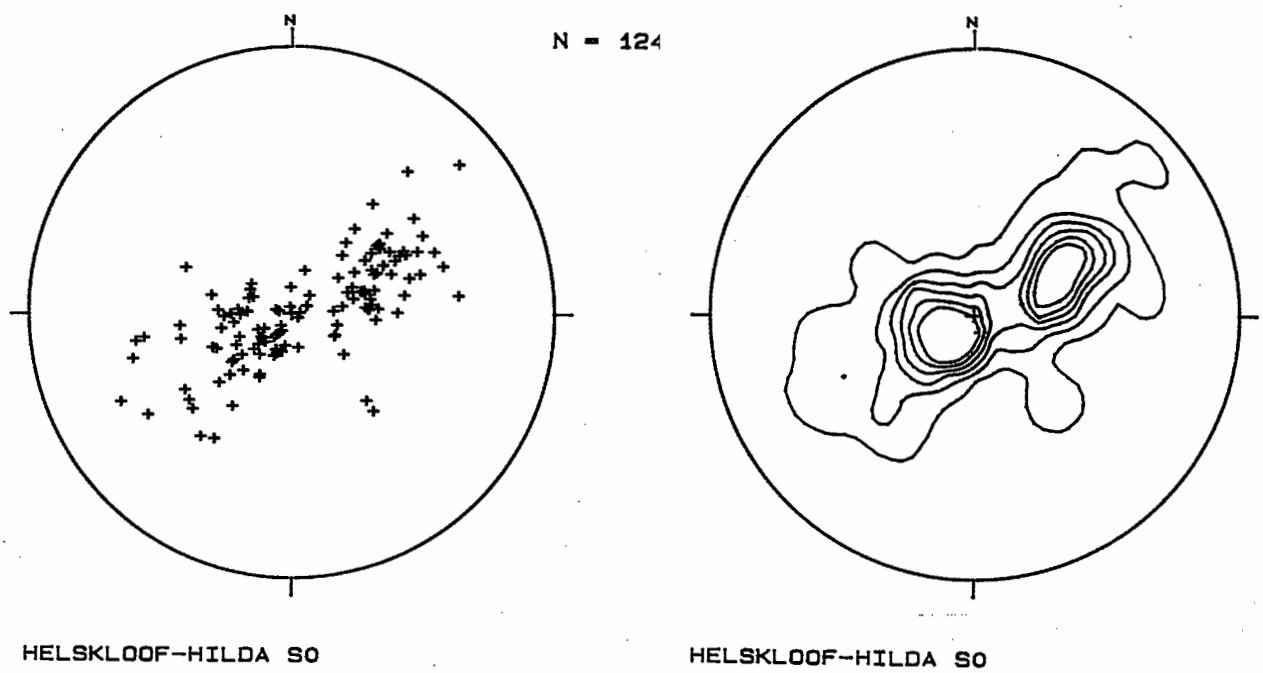

Fig.I.7 : Examples of the plots produced by OPIPT and OCOPT. Contours in Fig. I.7b are at 2 per cent intervals.

Option 8 : Map and section plotting

STRMP (Von Veh) : plots orientation data information onto an annotated map. The axes are labelled with tic marks at user defined intervals. The orientation data symbols can be plotted with or without plunge or dip values adjacent to symbols. The plunge and dip values can be represented by setting the lengths of the lineation symbols proportional to the plunges and the number of dip direction tic marks proportional to the dips (Fig. I.8). Alphanumeric identification characters may be plotted adjacent to the symbols.

SECTP (University of Alberta) : computes and plots down-plunge sections (Charlesworth et al., 1976). The sections are constructed by projecting planar orientation data parallel to the fold axis onto a specified plane of section. The pitch of the trace of the data on the plane of section is represented by a short line (Fig. I.9a). For data to be correctly projected, the folding must be shown to be cylindrical (option 6). Composite profiles over an area consisting of several cylindrical subareas can be constructed by rotating the subareas (using LROTA and OROTA) so that they all have a constant direction of projection.

SYM3D (Von Veh) : is a modified version of SECTP in which the planar orientation data is represented on down-plunge projections as small three-dimensional 'platelets' (Fig. I.9b). This facility is useful for assessing the degree of cylindricality of individual stations.

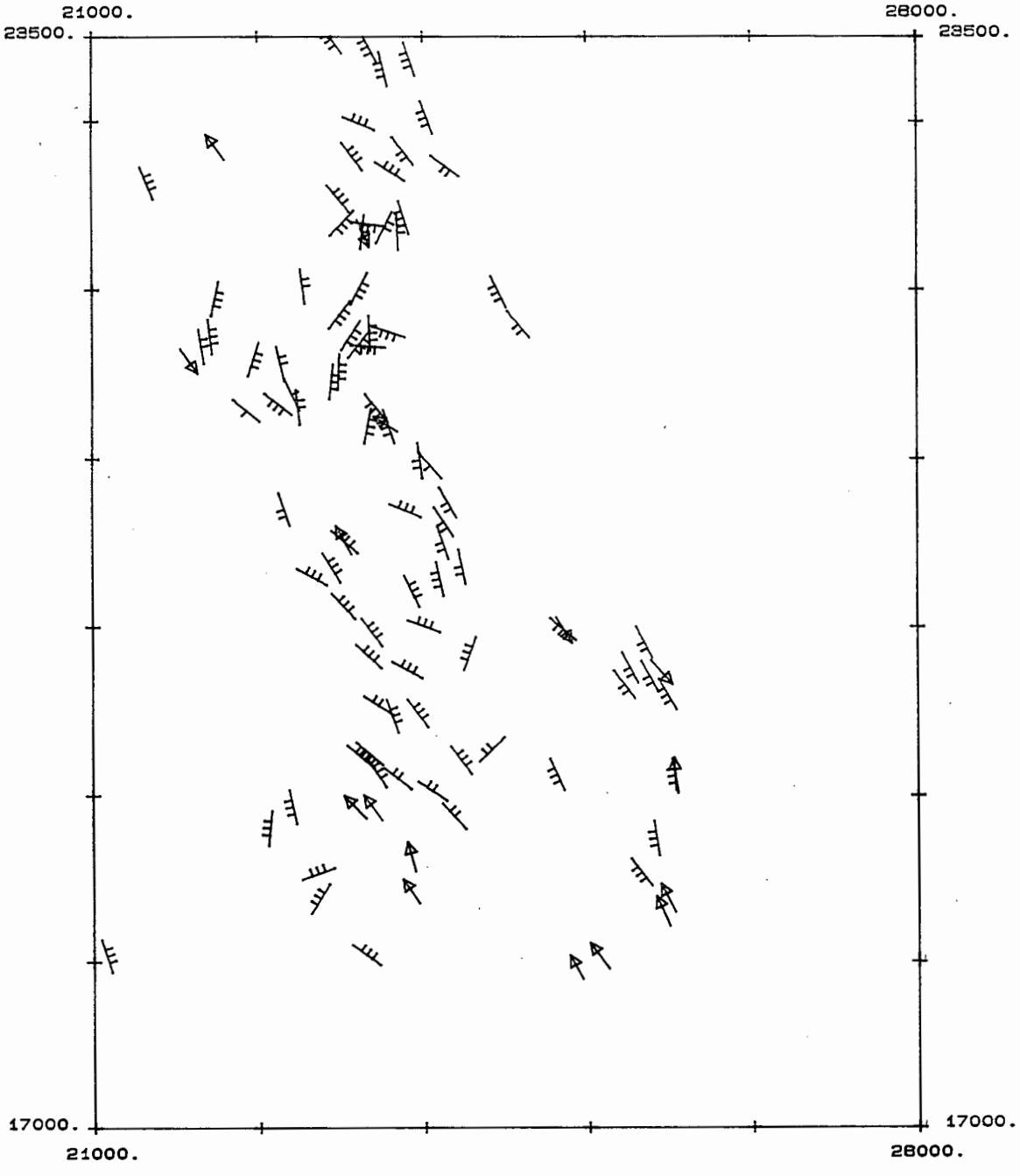

Scale 1: 40000.

HELSKLOOF AREA STRUCTURE

Fig. I.8 : Example of a structure map produced by STRMP (dip values excluded).

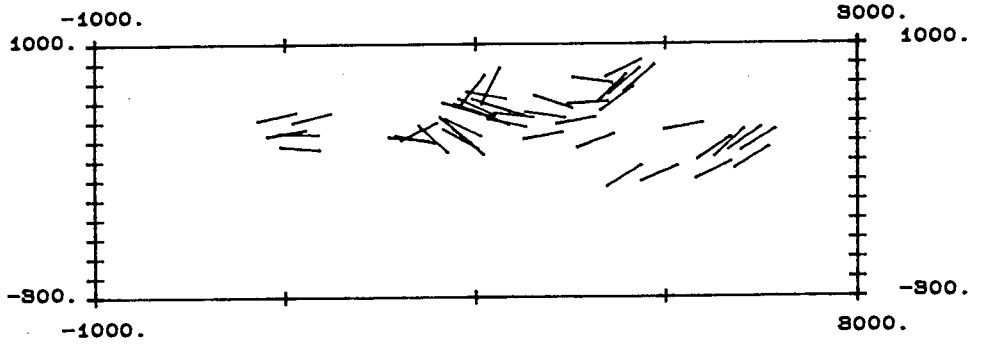

(a)

Scale 1: 40000.

HELSKLOOF AREA STRUCTURE

Direction of view : 880/10.
Profile passes through point : 22000. 18000.
Fold axis trend/ plunge : 880/10.

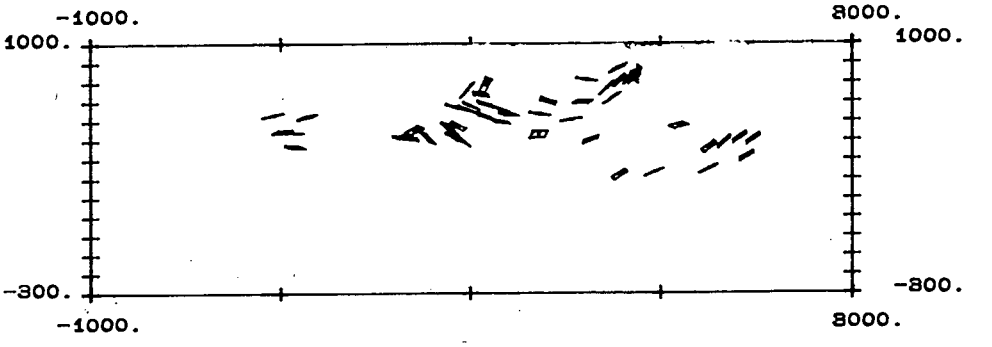

(b)

Scale 1: 40000.

HELSKLOOF AREA STRUCTURE

Direction of view : 880/10.
Profile passes through point : 22000. 18000. 0.
Fold axis trend/ plunge : 880/10.

Fig. I.9 : Examples of structure sections produced by SECTP and SYM3D.

I.3 Map and section enhancements

A number of modules were written to draw geological features on the structural maps and sections. A file containing coordinate and elevation data of geological boundaries in the entire field area is initially prepared and the data for the subarea of interest can then be extracted and plotted when required. A controlling program, ASTR2, schedules the following options:

Option 1 : Data capture

GEODC (Von Veh) : uses a digitizing table to input geological map features (Table I.3). The distance between digitized points can be specified to suit the required accuracy and available storage capacity. The routines used for bringing the coordinates into a frame of reference that is internal to the map is described on p. 150. Elevations can be input interactively or determined from a grid of topographic elevations.

Table I.3 : Example of the output from GEODC. The first record contains a description of the digitized map feature. Order of variables is : x and y map reference coordinates, topographic elevation, pen up/pen down status code, and pen colour code.

```
Kaigas/Helskloof-Hilda contact
22725.   21427.   675.  03
22780.   21422.   665.  13
22804.   21326.   650.  13
22793    21242.   635.  13
22727.   21204.   620.  13
22752    21034.   625.  13  etc.
```

Option 2 : Data selection

SCOEX (Von Veh) : excludes digitized features associated with a particular pen colour code prior to plotting.

SPOEX (Salomon, 1978; Von Veh) : excludes digitized features that lies outside a specified polygonal subarea.

SCLEX (Von Veh) : excludes data situated beyond specified distances from a plane of section.

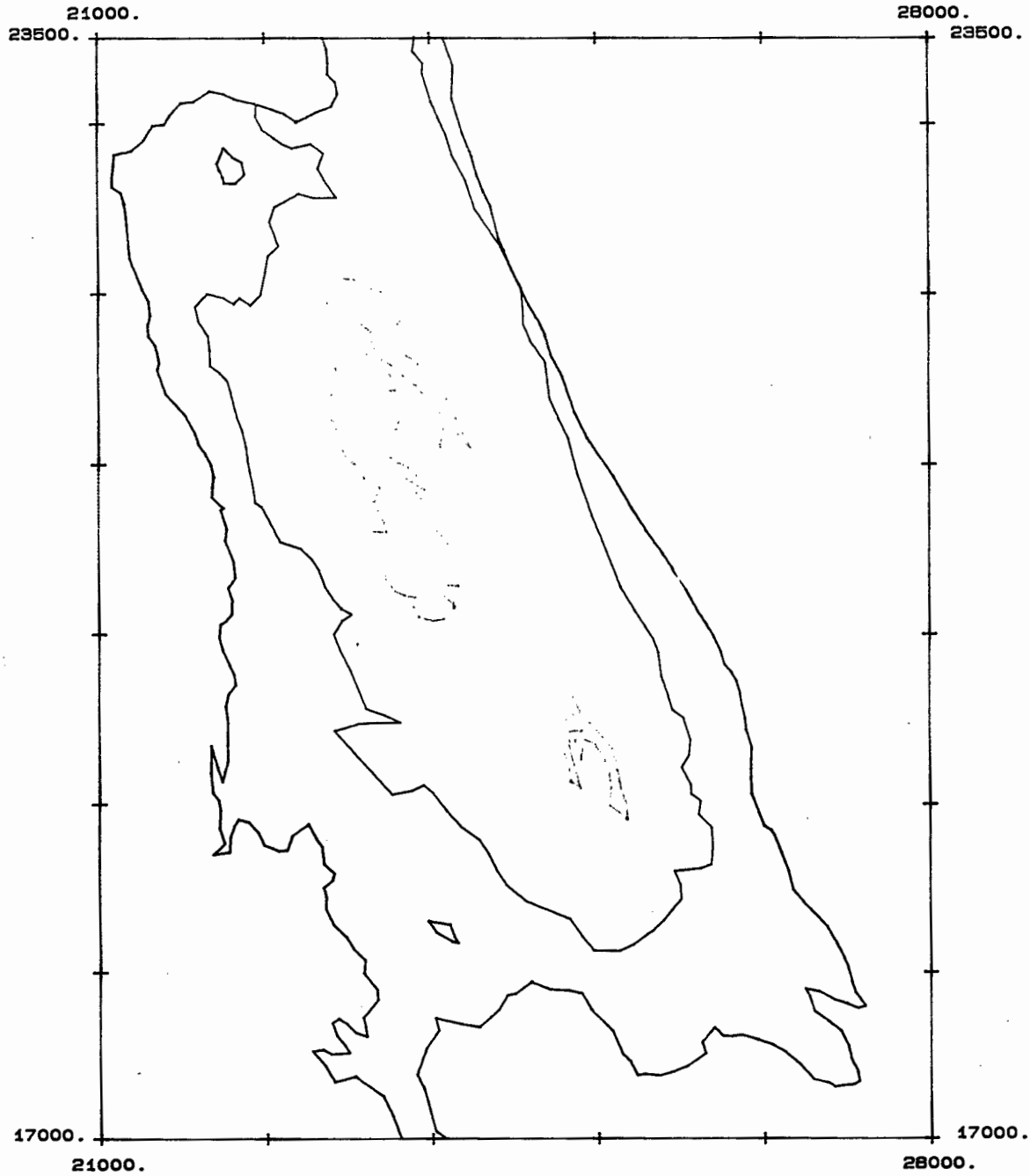

Scale 1: 40000.

HELSKLOOF AREA GEOLOGICAL CONTACTS

Fig. I.10 : Example of a map plot produced by GEOPT.

Option 3 : Data manipulation

LARCA (Von Veh) : performs arithmetical operations on the coordinate data.

LROCA (University of Alberta) : rotates the coordinate data about a point.

Option 5 : Map and section plotting

GEOPT (Von Veh) : plots a map of the digitized data with annotated axes at any required scale (Fig. I.10).

SDPPT (Von Veh) : projects the digitized data parallel to a given direction onto a specified section plane (Fig. I.11; adapted from SECTP, p. 158).

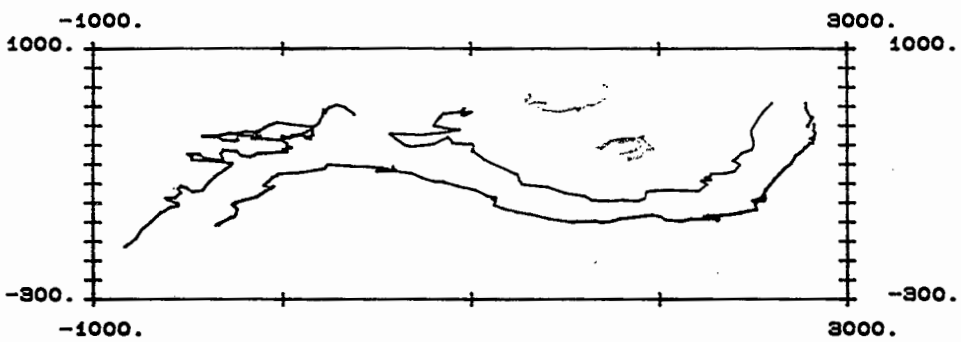

Scale 1: 40000.

HELSKLOOF AREA GEOLOGICAL CONTACTS

Direction of view : 330/10.
Profile passes through point : 22000. 18000.
Fold axis trend/ plunge : 330/10.

Fig.I.11 : Example of a profile plot drawn by SDPPT.

APPENDIX II

A computerized system for finite strain analysis

A computer-based system was developed to undertake finite strain determinations from deformed elliptical markers (see pp. 97-106). The system offers facilities for digitizing strain markers to yield axial ratio/long axis orientation (Rf/Ø) data, calculating average strain ellipses, computing a three-dimensional ellipsoid, and plotting the results (Von Veh, 1987b). It produces most of the frequently-used diagrams for strain analysis in a publishable form. A controlling program, ASTR3, allows the user to select from one of the following options:

1. Acquire new Rf/Ø data from the population of ellipses in a plane section;
2. Determine an average ellipse;
3. Plot average ellipse data results, long axes orientations and Rf/Ø diagrams;
4. Combine the ellipse data to yield the strain ellipsoid;
5. Plot strain ellipsoid results on a Flinn, Ramsay or Hsü diagram and principal axes orientations on a stereonet.

A choice of techniques or plots is available within some of the options (Fig. II.1):

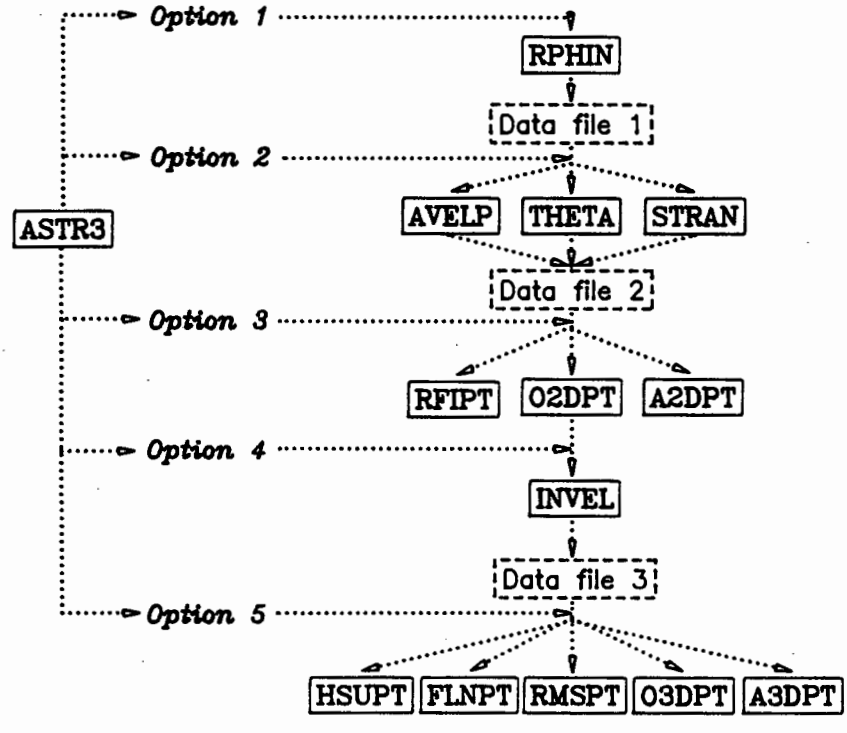

Fig. II.1 : Module interrelationships for G/ASTRA-3. See text for descriptions of the the module functions.

Option 1 : Data acquisition

Prior to running ASTR3, the user must prepare photographs/tracings of three non-parallel plane sections with known orientations. The end-points of the long and short axis of each ellipse have to be located for the population of ellipses in the three sections, and the cleavage and bedding traces, if present, must be marked (Fig. II.2).

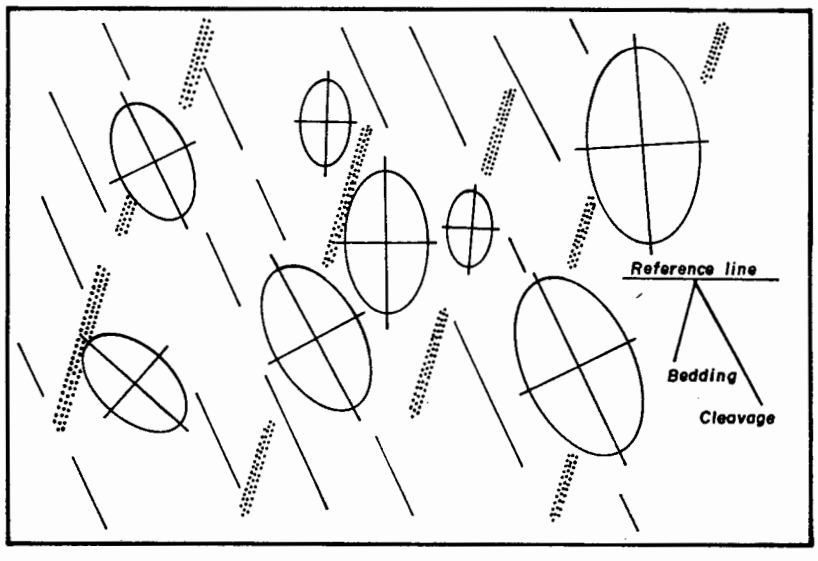

Fig. II.2 : Example of a tracing of a plane section prepared for strain analysis.

RPHIN (Von Veh & Hartnady, 1986) : captures the input data required for strain analysis. The coordinates of two points on the specimen coordinate axis are digitized to define a reference line to which all subsequent data is referred. The end-points of the long and short axes for each ellipse are digitized and the ellipse axial ratios, long axes orientations, lengths, and centroid positions are calculated. The data is checked for ellipticity and if found to be acceptable is written to a disc file (Table II.1).

Table II.1 : Example of the output from RPHIN

```
Sample 315 :  Conglomerate                          (Sample identification)
    25376.        17225.        265.                (Mapcoordinates and elevation)
134 2    272.2     144.6     331.0    75.           (Number of samples, face number,
                                                      cleavage trace, bedding trace,
                                                      section dip direction and dip)
  1.88    -23.2    16.24     8.60   163.77   89.04  (Axial ratio, long axis
  1.40    -42.9     7.45     5.32   130.19  102.77   orientation, ellipse length,
etc.                                                  ellipse width, X- and Y-
                                                      axes centroid positions)
```

Option 2 : Ellipse strain determinations

To calculate an average ellipse for each plane section, the user has a choice of three methods. The output in each case consists of an average ellipse ratio, a mean long axis orientation, and associated errors, for each of the three sections.

AVELP (Dr. N. Odling, PRU) : uses a method developed by Shimamoto & Ikeda (1976) in which the average ellipse is defined by the arithmetic mean of the tensor components of the population of ellipses.

THETA (Peach & Lisle, 1979) : utilizes the "Theta-curve" method of Lisle (1977); a median Ø direction is determined and after "unstraining" the markers perpendicular to this direction, the undeformed orientations are grouped into classes. A statistical χ^2 test is applied to test whether the marker orientations are random. This procedure is repeated with incrementally changed reciprocal strain ratios and the lowest χ^2 value is taken as the strain ratio.

STRAN (Dunnet & Siddans, 1971) : determines an average ellipse for elliptical particles with a primary planar or semi-planar fabric by examining the degree of symmetry of the Rf/Ø plot. If the plot is symmetric, no primary fabric is indicated and one of the above methods is used. If the plot is asymmetric about the cleavage trace, the data is progressively unstrained and the plot symmetry is re-examined after every small increment. In the case where the unstrained fabric was bedding-symmetric, the strain ratio is taken to represent the stage where the orientation of the vector mean of the Ø values becomes equal to the bedding trace. For imbricate initial fabrics, the strain ratio is found by maximizing the symmetry of the Rf/Ø diagram (Dunnet & Siddans, op. cit.).

Option 3 : Ellipse strain data output

RFIPT (Von Veh) : plots a scatter diagram of ellipse axial ratios versus long axis orientations (Rf/Ø plot). Rf/Ø "onion" curves for the appropriate strain ratio and varying initial ellipse ratios can be superimposed.

O2DPT (Von Veh) : draws a stereonet diagram showing the orientations of the plane sections and the pitches of the ellipse long axes in the planes.

A2DPT (Von Veh) : draws the plots of RFIPT and O2DPT plus other relevant information onto one plot (Fig. II.3).

Option 4 : Strain ellipsoid calculation

INVEL (Gendzwill & Stauffer, 1981) : combines the three sections to yield a strain ellipsoid solution. The module uses errors to adjust the observed ellipses so that they are exact solutions of the nearest true ellipsoid, whose dimensions are then found by solving a system of linear equations.

Option 5 : Strain ellipsoid output

HSUPT (Von Veh) : draws an Hsü diagram (Lode's Parameter (V) vs. the natural logarithmic strain (Es)). An option is available for drawing lines of percentage shortening on the plot.

FLNPT (Von Veh) : draws a Flinn diagram (a vs. b Flinn parameters).

RMSPT (Von Veh) : draws a 'Ramsay' diagram (ln a vs. ln b).

O3DPT (Von Veh) : draws a stereonet of the strain axes orientations.

A3DPT (Von Veh) : draws the above-mentioned three diagrams plus other relevant information onto one diagram (Fig. II.4).

SAMPLE : TEST SAMPLE. FIVE SISTERS OOLITIC DOL. 28/04/84

Grid reference : X = 34126. Y = -5237. Elev. : 624.

	Face 1	Face 2	Face 3
Face orientation (Dip dir./dip)	240/30	130/80	20/60
Long axis pitch	44	132	28
Standard error	1.020	2.150	14.010
Strain ratio	1.64	1.68	1.18
Standard error	.210	.240	.170

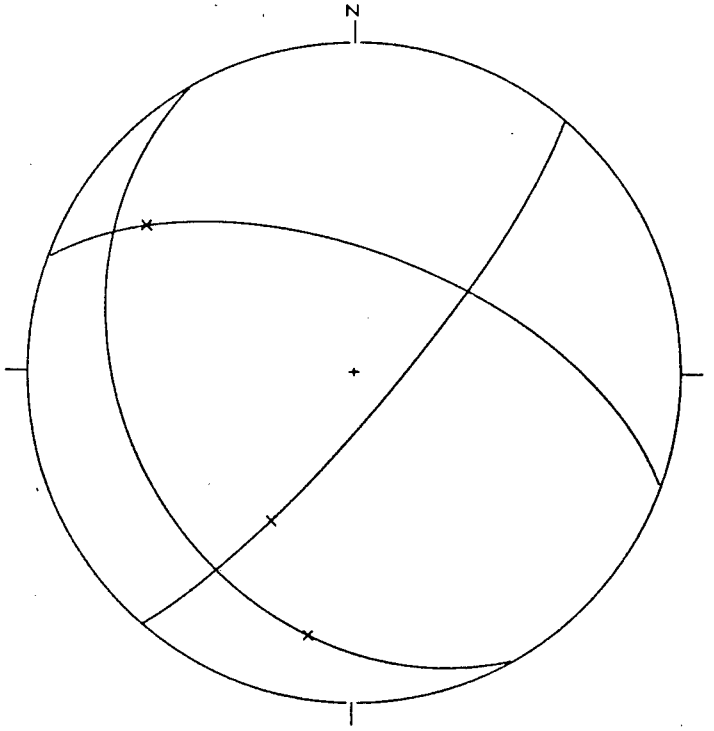

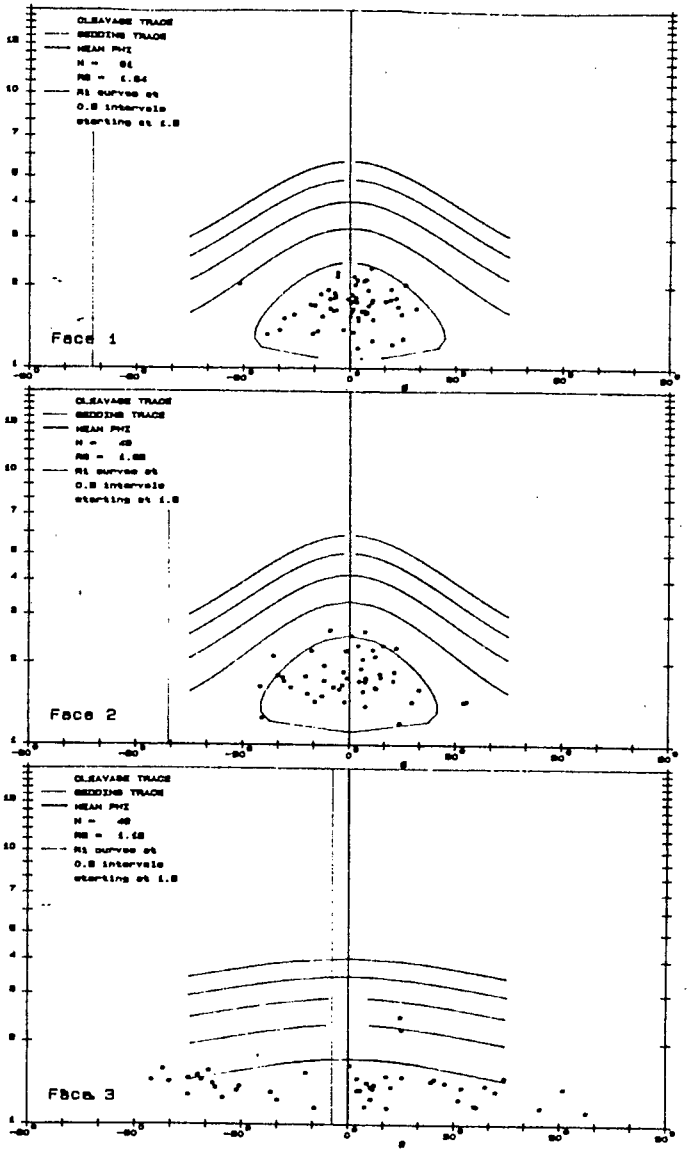

Fig.II.3 : Example of a plot obtained from A2DPT.

SAMPLE : TEST SAMPLE. FIVE SISTERS OOLITIC DOL. 28/04/84

Grid reference : X = 34128. Y = -5237. Elevation : 824.

	max.	int.	min.
Semi axes (S1, S2, S3)	1.993	1.138	1.000
Principal natural strains (E1, E2, E3)	.690	.130	0.000
Quadratic elongations (λ1, λ2, λ3)	3.972	1.298	1.000
Percentage elongations (+X%, +Y%, -Z%)	199.3	113.8	100.0
Principal axes orientations (Tr/Plu)	295/38	178/32	59/38

Strain intensity factor (γ_o) = .733

Natural logarithmic strain (Es) = .741 Lode's parameter (V) = -.624

Flinn parameters K = 5.418, a = 1.750, b = 1.138; ln a = .560; ln b = .130

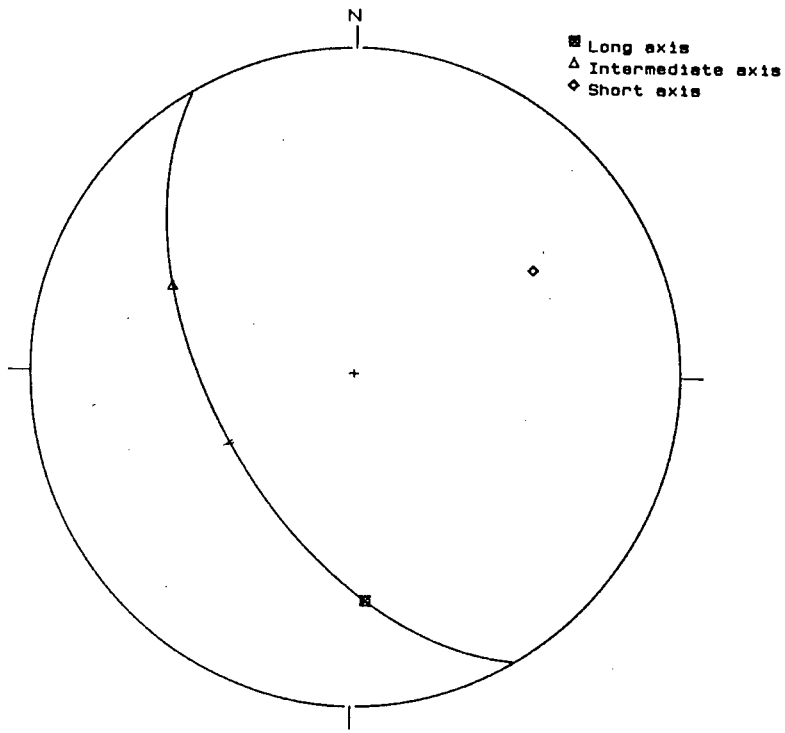

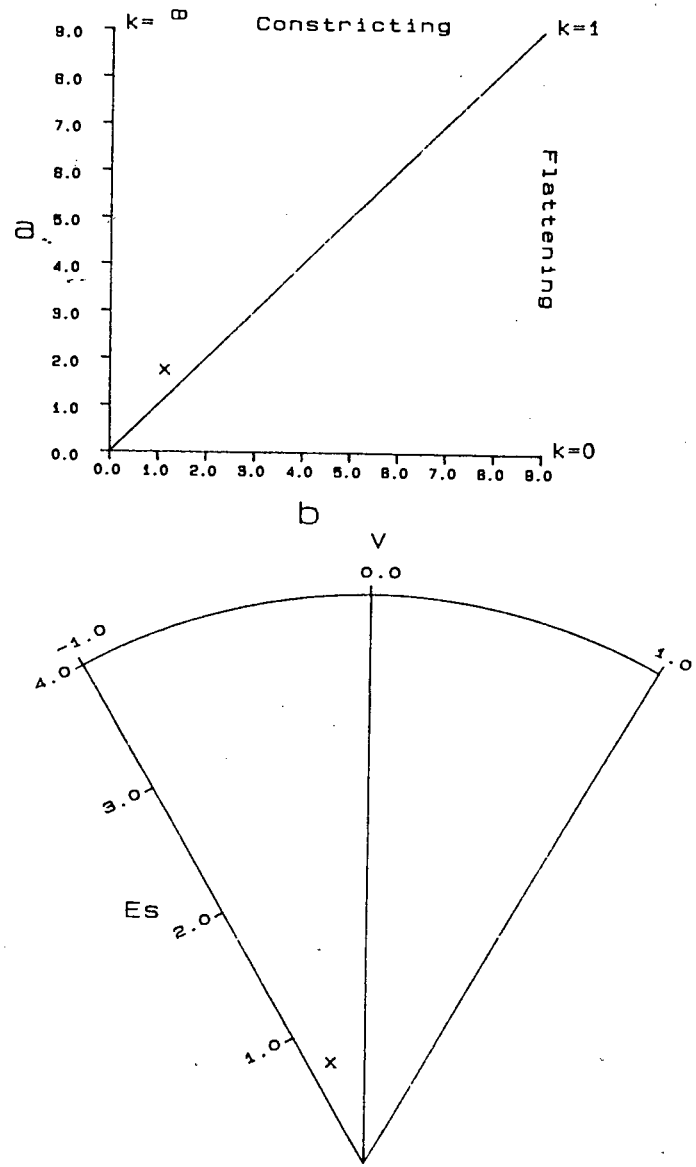

Fig. II.4 : Example of a plot obtained from A3DPT.

PLATES

Plate 1 : Unconformity between Stinkfontein quartzite and Kaigas pebbly schist at an inlier near Helskloof Pass.

Plate 2 : Unconformity (dashed) between folded Hilda quartzite and Numees iron formation and diamictite, 5 km south of Jakkalsberg.

Plate 3 : Minor thrust fault (dashed) displaying a lateral ramp in the Hilda Sequence, 2 km ENE of Auchas Peak.

Plate 4 : Large-scale recumbent F_1 fold with sub-horizontal axial planar S_1 cleavage, 2 km north of Wallekraal prospect in the Gorab River valley, view to the south.

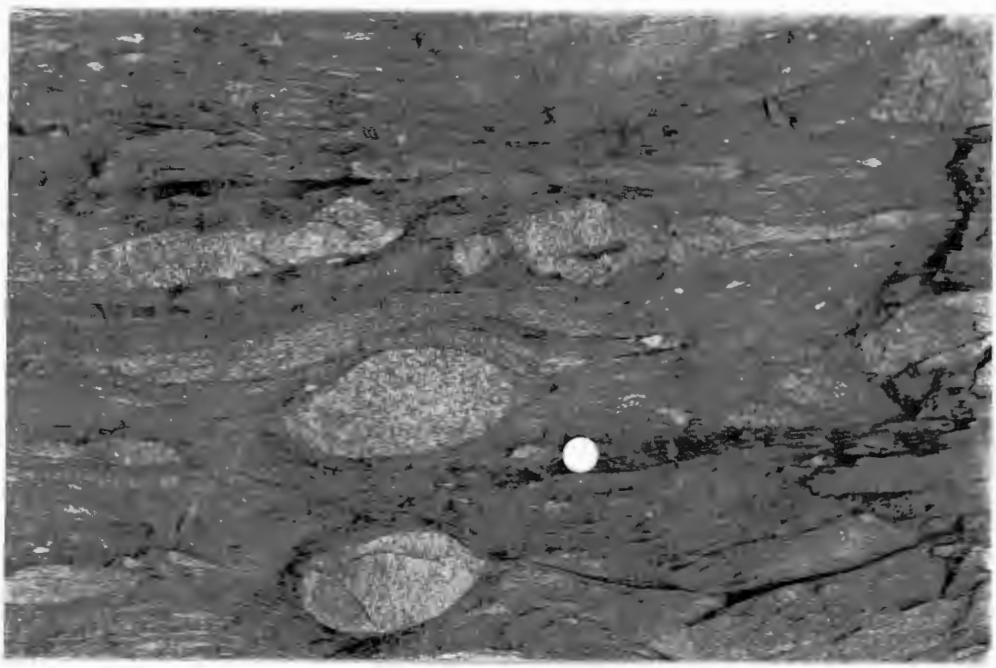

Plate 5 : Foliated Kodas-Kaigas diamictite showing difference in degree of flattening strain between competant and incompetant clasts. Locality is 2,5 km west of Kodas Prospect. Coin diameter = 3 cm.

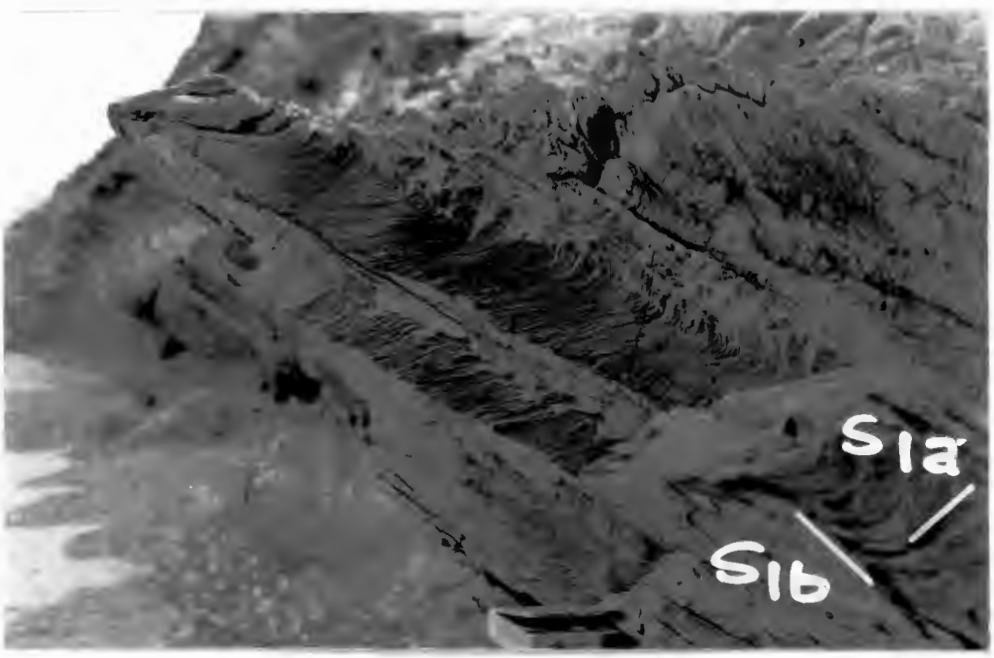

Plate 6 : Rare example of two 'S_1' cleavages in a graded Holgat wacke. A bedding-parallel (S_{1b}) fracture cleavage is deforming an earlier (S_{1a}) foliation, Sanddrif area. Viewed towards the SSE.

Plate 7 : F_1 sheath fold folded by a close F_2 fold, 5 km north of Gorab Peak on the banks of the Orange River.

Plate 8 : Asymmetrical F_1 fold overprinted by an S_2 cleavage, 2 km southwest of Jakkalsberg. View to the NNW.

Plate 9 : Typical overturned F_2 fold. Locality: 3,5 km NNE of Gorab Peak. Viewed to the north.

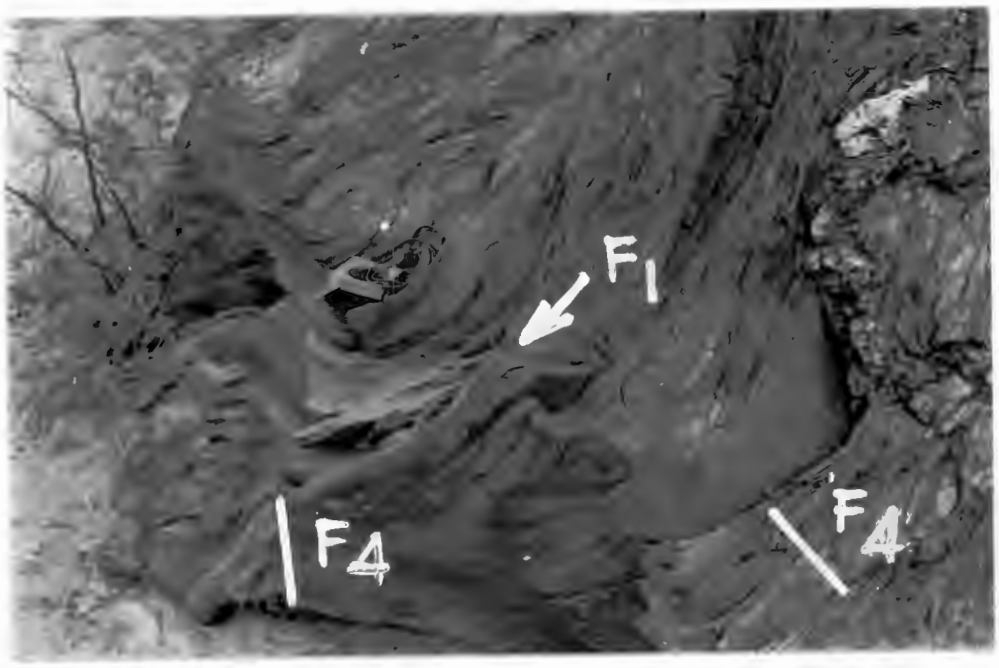

Plate 10 : Recumbent F_1 fold refolded by a conjugate F_4 fold, 2,5 km NNE of Gorab Peak. View to the WNW.